

THE UNIVERSITY OF HULL

**HIERARCHICALLY STRUCTURED COMPOSITES AND
POROUS MATERIALS**

being a Thesis submitted for the Degree of Doctor of Philosophy
in the University of Hull

by

Benjamin Robert Thompson

MChem (University of Hull)

September 2017

Acknowledgements

I would first like to thank my academic supervisors, Prof. Vesselin N. Paunov and Dr. Tommy S. Horozov for their help, support and guidance during my PhD project. Their continuous encouragement has been instrumental for my development into a confident and independent researcher. I would also like to thank my industrial supervisor, Prof. Simeon D. Stoyanov for his interest and ideas during this project.

Thanks also go to the Engineering and Physical Sciences Research Council (EPSRC) and Unilever (Vlaardingen, The Netherlands) for financial support in sponsoring this project.

I appreciate the help from Dr. Qin Qin of The Acoustics Research Centre at The University of Hull, who was always ready to offer advice during the acoustics experiments (Chapter 4). Furthermore, I am grateful to Brogan Taylor for help obtaining the experimental data used to determine the sound transmission loss during her undergraduate MChem research project.

I would also like to thank the people who have made my time here enjoyable: Jamie, Anupam, Jevan, Bobby, Khaled, Ana Maria and Connor.

Finally, I would like to thank my family who provided support and encouragement during all of my time in education.

Publications and presentations

The work contained within this thesis has given rise to the following publications and presentations:

1. Stimulus responsive soap-hydrogel bead composites for controlled dissolution and release of actives, B. R. Thompson, M. Rutkevicius, T. S. Horozov, S. D. Stoyanov, and V. N. Paunov, *in preparation*.
2. Hierarchically porous composites fabricated by hydrogel templating and viscous trapping techniques, B. R. Thompson, T. S. Horozov, S. D. Stoyanov and V. N. Paunov, *Mater Des.*, 2018, **5**, 384-393.
3. Sound transmission loss of hierarchically porous composites produced by hydrogel templating and viscous trapping techniques, B. R. Thompson, B. L. Taylor, Q. Qin, S. D. Stoyanov, T. S. Horozov and V. N. Paunov, *Mater. Chem. Front.*, 2017, **1**, 2627-2637.
4. An ultra-melt resistant hydrogel from food grade carbohydrates, B. R. Thompson, T. S. Horozov, S. D. Stoyanov and V. N. Paunov, *RSC Adv.*, 2017, **7**, 45535-45544.
5. Structuring and calorie control of bakery products by templating batter with ultra melt-resistant food-grade hydrogel beads, B. R. Thompson, T. S. Horozov, S. D. Stoyanov and V. N. Paunov, *Food Funct.*, 2017, **8**, 2967-2973.
6. Oral presentation: “Microstructure, mechanical and thermal insulating properties of hierarchically porous composites fabricated by hydrogel templating and viscous trapping techniques”, UK Colloids 2017, July 2017, Manchester, UK.

Abstract

This thesis develops a hydrogel bead templating technique for the preparation of hierarchically structured composites and porous materials. This method involves using slurries of hydrogel beads with different size distributions as templates. Mixing hydrogel beads with a scaffolding material and then allowing the scaffold to harden, followed by drying of the composite leaves pores in the place of the hydrogel beads. These pores reflect the size and shape of the templates used and the porosity reflects the volume percentage of hydrogel bead slurry mixed with the scaffolding material. A viscous trapping technique has been developed which utilises the viscosity of methylcellulose to stop sedimentation of the scaffold particles during network formation. Both of these methods are attractive due to being cheap, non-toxic and they use food grade materials which allows their use in a multitude of applications.

Porous and hierarchically porous gypsum composites have been prepared using both hydrogel bead templating and viscous trapping techniques, or a combination of the two. The level of control over the final microstructure of the dried composites offered by these techniques allowed for a systematic investigation of their thermal and mechanical properties as a function of the pore size, porosity and hierarchical microstructure. It has been shown that the thermal conductivity decreases linearly with increasing porosity, however it was not dependent on the pore sizes that were investigated here. The mechanical properties, however, were significantly different. The porous composites produced with either small hydrogel beads (100 μm) or methylcellulose solution had approximately twice the compressional strength and Young's modulus compared to the ones produced with large hydrogel beads (600 μm).

The sound insulating properties of porous and hierarchically porous gypsum composites have also been investigated. With increasing porosity, the sound transmission loss decreases, as expected. At constant porosity, it is shown that the composites with large pores perform significantly better than the ones with small pores in the frequency range of 75-2000 Hz. At higher frequencies (>2400 Hz) the composites with smaller pores begin to perform better. The material's microstructure has been studied in an attempt to explain this effect.

The hydrogel templating technique can be used to prepare composite materials if the drying step is not performed. Hydrogel beads have been incorporated into a soap matrix. The dissolution rate of these composites as a function of hydrogel bead size and volume percentage of hydrogel beads incorporated within the soap matrix has been investigated. It has been shown that the dissolution rate can be increased by increasing the volume percentage of hydrogel beads used during composite preparation but it is independent on their size distribution. Finally, three methods of controlling the release rate of encapsulated species from these soap-hydrogel bead composites have been shown. The first method involved varying the size distribution of the hydrogel beads incorporated within the soap matrix. The second involved changing the concentration of the gelling polymer and the final method required co-encapsulation of an oppositely charged polyelectrolyte.

A binary hydrogel system has been developed and its rheological and thermal properties have been investigated. It consists of agar and methylcellulose and shows significantly improved rheological properties at high temperatures compared to agar alone. The storage modulus of the two component hydrogel shows a maximum at 55 °C which was explained by a sol-gel phase transition of methylcellulose, evidence of which was seen during differential scanning calorimetry measurements. After exposure of this binary hydrogel to high temperatures above the melting point of agar alone (> 120 °C), it maintains its structure. This suggests it could be used for high temperature templating or structuring of food products.

The melt-resistant binary hydrogel was used for the preparation of pancake-hydrogel composites using hydrogel bead templating. Mixing slurry of hydrogel beads of this composition with pancake batter, followed by preparation at high temperatures produced pancakes with hydrogel beads incorporated within. Bomb calorimetry measurements showed that the caloric density could be reduced by a controlled amount by varying the volume percentage of hydrogel beads used during preparation of the composites. This method could be applied to other food products such as biscuits, waffles and breakfast bars. Furthermore, there is scope for development of this method by the encapsulation of flavour enhancing or nutritionally beneficial ingredients within the hydrogel beads.

Contents

1. Introduction.....	1
1.1. Hierarchically porous materials.....	1
1.1.1. Methods of production	5
1.1.1.1. Surfactant templating.....	5
1.1.1.2. Breath figures.....	7
1.1.1.3. Freeze drying	8
1.1.1.4. Colloidal crystal templating.....	9
1.1.1.5. Biological templating.....	10
1.1.1.6. Emulsion templating.....	10
1.1.1.7. Polymer templating.....	11
1.1.2. Applications of hierarchically porous materials	13
1.1.2.1. Catalysis.....	13
1.1.2.2. Energy storage, usage and conversion of hierarchically porous materials	15
1.1.2.3. Separation applications	16
1.1.2.4. Adsorption of pollutants	17
1.1.2.5. Sensors	20
1.1.2.6. Biomaterials	21
1.1.3. Outlook.....	23
1.2. Hydrogels	23
1.2.1. Agar-agar.....	25
1.2.2. Methylcellulose (MC)	28
1.3. Gypsum	29
1.4. Presentation of this thesis	31
1.5. References	33
2. Experimental	42

2.1. Materials	42
2.1.1. Hydrocolloids	42
2.1.2. Matrix materials	42
2.1.2.1. Gypsum	42
2.1.2.2. Soap base	42
2.1.2.3. Bakery ingredients for pancake batter	43
2.1.3. Water	43
2.1.4. Solvents	43
2.1.5. Other chemicals	43
2.2. Characterisation equipment	43
2.2.1. Microscopy	43
2.2.1.1. Optical microscopy	43
2.2.1.2. Scanning electron microscopy	44
2.2.1.3. Cryogenic scanning electron microscopy	44
2.2.2. Measurement of thermal conductivity	44
2.2.3. Acoustical analysis	46
2.2.4. Dissolution rates	48
2.2.5. UV-vis	48
2.2.6. Release rates from soap-hydrogel composites	48
2.2.7. Rheology	49
2.2.8. Calorimetry	49
2.2.8.1. Differential scanning calorimetry	49
2.2.8.2. Bomb calorimetry	50
2.2.9. Temperature stability	50
2.2.9.1. High temperature	50
2.2.9.2. Low temperature	51
2.2.10. Mechanical properties	51

2.2.11.	X-ray diffraction.....	51
2.3.	Methods.....	52
2.3.1.	Preparation of starting materials.....	52
2.3.1.1.	Agar hydrogel.....	52
2.3.1.2.	Methylcellulose solution.....	52
2.3.1.3.	Agar-methylcellulose hydrogel.....	52
2.3.1.4.	Gypsum slurry.....	53
2.3.1.5.	Molten soap base.....	53
2.3.1.6.	Pancake batter.....	53
2.3.2.	Preparation of hydrogel beads.....	53
2.3.2.1.	Agar hydrogel beads.....	53
2.3.2.2.	Agar-methylcellulose hydrogel beads.....	55
2.3.3.	Hydrogel bead templating to formulate porous gypsum composites...55	
2.3.4.	Dual templating with two size hydrogel beads for production of hierarchically porous gypsum composites.....	56
2.3.5.	Viscous trapping to produce porous gypsum composites.....	57
2.3.6.	Hierarchically porous gypsum composites from a combined viscous trapping and hydrogel bead templating method.....	58
2.3.7.	Formulation of soap-hydrogel composites.....	61
2.3.8.	Pancake-hydrogel composites.....	62
2.4.	References.....	63
3.	Microstructure, mechanical and thermal insulating properties of hierarchically porous gypsum composites fabricated by hydrogel templating and viscous trapping techniques.....	64
3.1.	Introduction.....	65
3.2.	Results.....	67
3.2.1.	Hydrogel bead size analysis.....	67
3.2.2.	Porosity and volume reduction of the composites.....	68

3.2.3.	Thermal conductivity of porous gypsum composites	72
3.2.4.	Mechanical properties	79
3.2.5.	Microstructure analysis	86
3.3.	Conclusions	94
3.4.	References	96
4.	Sound transmission loss of hierarchically porous composites produced by hydrogel templating and viscous trapping techniques	98
4.1.	Introduction	98
4.2.	Results	100
4.2.1.	Size distributions of hydrogel beads	100
4.2.2.	Porous gypsum composites	103
4.2.3.	Acoustic properties of the porous composites	105
4.2.4.	Mechanical properties	112
4.2.5.	Microstructure analysis	115
4.3.	Conclusions	117
4.4.	References	120
5.	Pressure responsive soap-hydrogel bead composites for controlled dissolution and release rate of actives	122
5.1.	Introduction	123
5.2.	Results	125
5.2.1.	Hydrogel bead size analysis	125
5.2.2.	Dissolution rate of the soap-hydrogel composites	126
5.2.3.	Controlling the release rate of active species from the soap-hydrogel composites.....	128
5.2.3.1.	Role of hydrogel bead size on the release rate of berberine	128
5.2.3.2.	Role of agar concentration on the release rate of berberine	129
5.2.3.3.	Effect of polyelectrolyte co-encapsulation on the release rate of methylene blue	131

5.2.4.	Mechanical properties of soap-hydrogel composites.....	133
5.2.	Conclusions	135
5.3.	References	137
6.	An ultra melt-resistant hydrogel from food grade carbohydrates	139
6.1.	Introduction	139
6.2.	Results	141
6.2.1.	Rheological properties of agar-MC hydrogels.....	141
6.2.2.	Uniaxial compression.....	146
6.2.3.	DSC measurement.....	148
6.2.4.	Thermal stability	149
6.2.5.	Hydrogel microstructure analysis	152
6.2.6.	X-ray diffraction analysis.....	159
6.3.	Conclusions	159
6.4.	References	161
7.	Structuring and calorie control of bakery products by templating batter with ultra melt-resistant food-grade hydrogel beads.....	164
7.1.	Introduction	164
7.2.	Results	166
7.2.1.	Rheology and microstructure of agar-MC hydrogel	166
7.2.2.	Hydrogel bead size analysis	169
7.2.3.	Formulation of pancake-hydrogel composites	171
7.2.4.	Caloric density of pancake-hydrogel composites	176
7.3.	Conclusions	180
7.4.	References	182
8.	Summary of the thesis.....	184
8.1.	Future work	188
8.2.	References	190

List of abbreviations

AA	Ascorbic acid
AIBN	Azobisisobutyronitrile
BBR	Berberine
BF	Breath figure
CMC	Critical micelle concentration
Cryo-SEM	Cryogenic scanning electron microscopy
Cryo-TEM	Cryogenic transmission electron microscopy
CV	Crystal violet
DA	Dopamine
DCM	Dichloromethane
DMF	<i>N,N</i> -dimethylformamide
DS	Degree of substitution
DSC	Differential scanning calorimetry
DVB	Divinylbenzene
FCC	Face centred cubic
FTIR	Fourier transform infra-red
HF	Hydrogen fluoride
HIPE	High internal phase emulsion
HTAB	Hexadecyltrimethyl ammonium bromide
LB	Large beads
LbL	Layer-by-layer
MB	Methylene blue
mBMSC	Mouse bone mesenchymal stem cells
MC	Methylcellulose
MOF	metal organic framework
ORR	Oxygen reduction reaction
OTS	Octadecyltrimethoxysilane
PCL	Poly(ϵ -caprolactone)
PE	Petroleum ether
PLLA	Poly(L-lactic acid)
PMMA	Poly(methyl methacrylate)

PS	Polystyrene
PSS	Poly(sodium-4-styrenesulfonate)
PU	Polyurethane
PVC	Poly(vinyl chloride)
SANS	Small angle neutron scattering
SB	Small beads
SEM	Scanning electron microscopy
STL	Sound transmission loss
THF	Tetrahydrofuran
TOPO	Trioctylphosphine oxide
UA	Uric acid
UV-vis	Ultraviolet-visible
VPP	Vapour phase polymerisation
WHO	World health organisation
XPS	X-ray photoelectron spectroscopy
XRD	X-ray diffraction
ZIF	Zeolitic imidazolate framework

1. Introduction

The aim of this thesis is to further develop the hydrogel bead templating technique for the preparation of hierarchically porous and composite materials.¹ Through the use of a combination of hydrogel bead slurries of different size distributions, hierarchically porous materials with tuneable porosity, pore sizes and ratio of different sized pores at constant porosity were prepared. From here, the aim was to investigate if it was possible to tune various physical properties (mechanical, thermal, acoustical) of the produced hierarchically porous materials by controlling the porosity, pore size and microstructure at constant porosity.

This chapter introduces hierarchically structured and porous materials and reviews the literature on the current methods of their fabrication using a variety of templating techniques. This is followed by a review on the applications of hierarchically structured and porous materials. As there have been multiple reviews already,²⁻¹² only recent applications have been discussed. This is followed by a discussion of hydrogels; in particular agar-agar and methylcellulose (MC) as they were used extensively during this research project. The reader will find a section introducing gypsum in the next section which was used as a scaffold throughout Chapters 3-4. Finally, the structure of the thesis is described.

1.1. Hierarchically porous materials

Porous materials are classified as micro-, meso- or macroporous if their pore diameter is < 2 nm, 2-50 nm or > 50 nm, respectively.¹³ Hierarchically porous materials are porous materials that contain pores on multiple length scales. This could be a combination of micro-mesopores, micro-macropores, meso-macropores or two different length scale of the same type pores i.e. macro-macro with 100 nm and 100 μ m pore diameters. Furthermore, tri-modal pore size distribution has also been demonstrated (micro-meso-macro).¹⁴

Another type of hierarchical porosity is where the porosity is graded i.e. a continuous increase or decrease in pore width along one direction. Such materials have been exploited for their enhanced sound absorbing properties when the pore size decreases

along the direction of sound wave propagation. These types of porous structures have a steady increase in resistance to airflow due to a decrease in pore size.¹⁵

There are many different types of pores, of which the most well-known are open and closed pores. IUPAC have classified pores according to their availability to an external fluid, with the help of Figure 1.1.

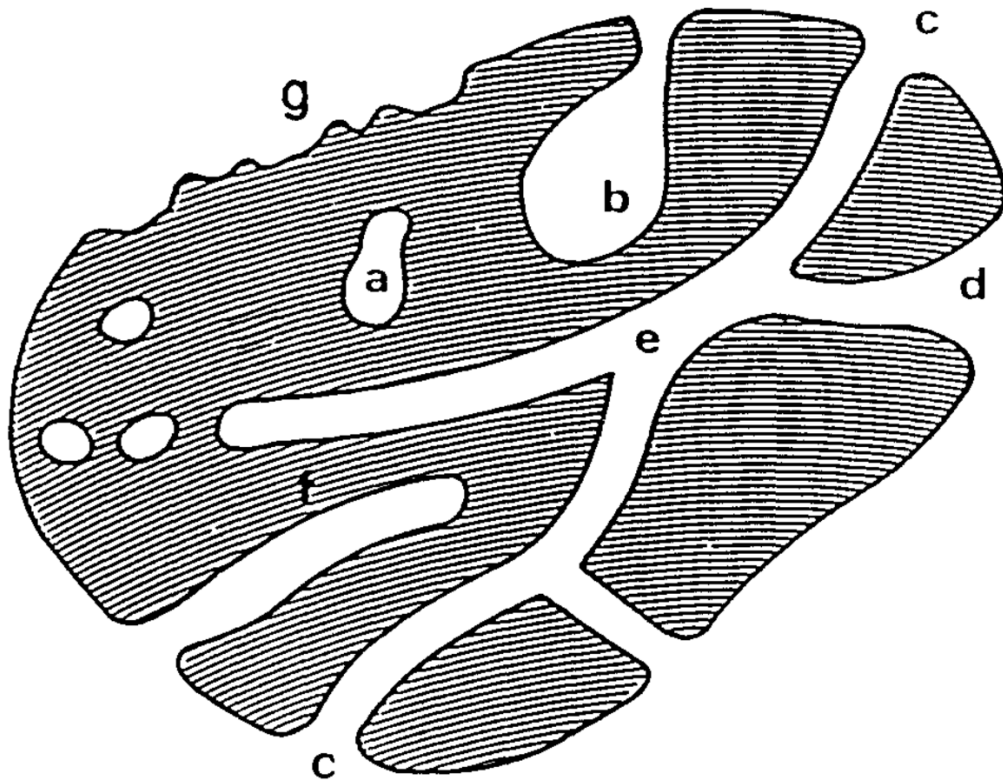


Figure 1.1. Schematic cross section of a porous material. (a) shows a closed pore, (b) shows an open ink-bottle shaped open pore, (c) shows a through open pore, (d) shows a funnel shaped open pore, (e) is an open pore, (f) is a dead-end open pore and (g) shows the surface roughness which can be classed as a pore if it is deeper than it is wide. Reproduced from IUPAC[©] 1994, reference 13.

From Figure 1.1, (a) shows a closed pore i.e. a pore that is isolated from neighbouring pores. The pores represented by (b) – (f) show open pores as they are open to the surface of the material. These can be classified as through pores (e) or dead-end pores (b) and (f). Further classification can be done from the pore shape; they can be cylindrical (through open (e) or dead-end open (f)). They can also be ink-bottle shaped

(b) or funnel shaped (d). Finally, (g) shows the roughness of the surface of the material. This can be classed as a type of pore if the depth is greater than the width.

A significant amount of research is being performed on materials with structural hierarchy because of their immense potential in a large amount of applications. The combination of a large surface area due to micropores and easier mass transport due to the presence of meso- or macropores can lead to materials with superior properties to those with a single pore size distribution.¹⁶

Biological materials (i.e. wood, bone or grass) produced through long-term evolution to be optimal for their purpose are often found to be hierarchically structured.¹⁷ Many of these materials have an astounding efficiency, which is believed to be due to a functional adaptation of all levels of the hierarchical structure. Figure 1.2 shows an overview of hierarchically structured materials from nature.¹⁸ Hierarchical structuring of porous materials can mimic natural materials in an attempt to obtain optimal structures and can lead to novel materials with the possibility of the functionalisation of each level of porosity.

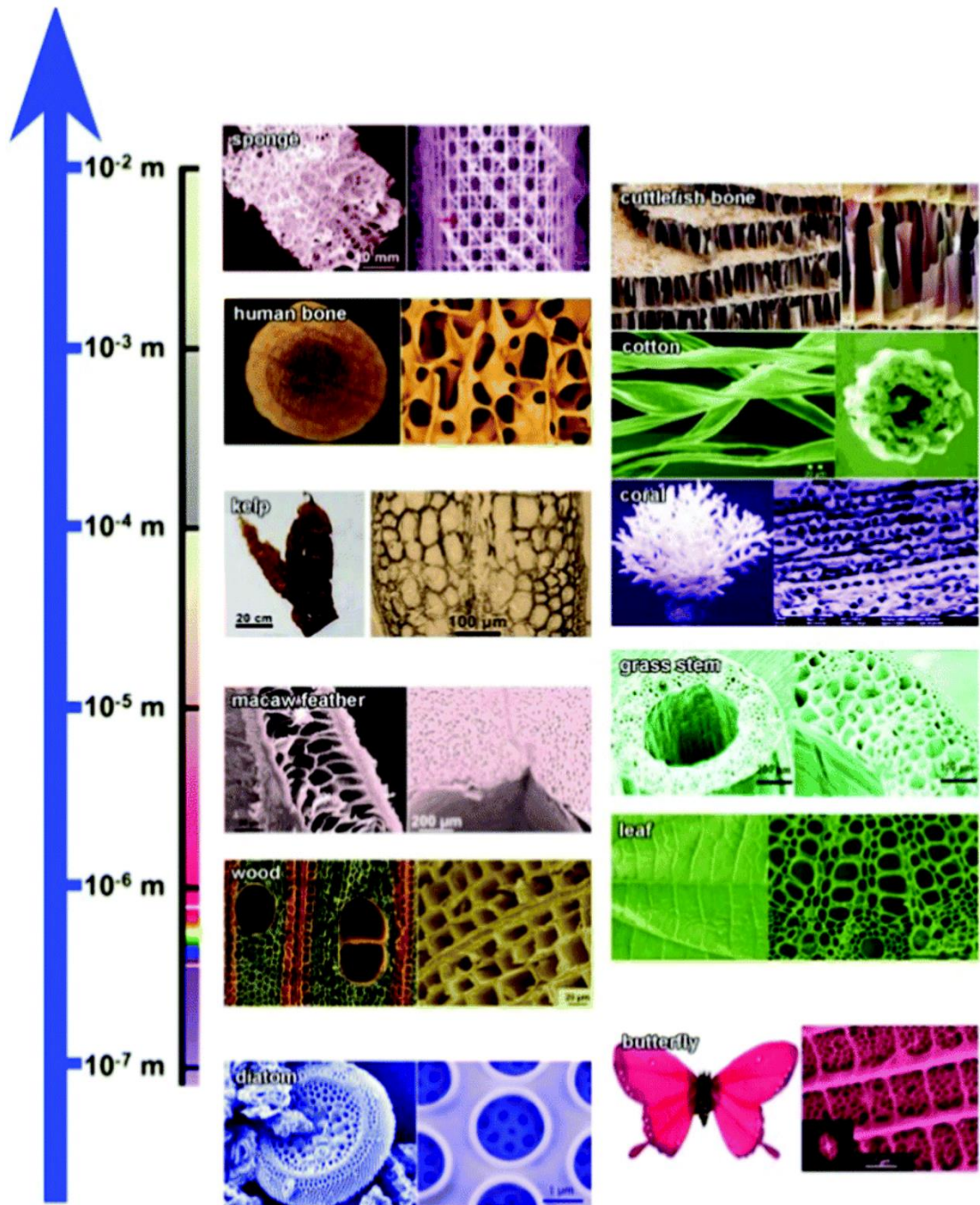


Figure 1.2. Overview of hierarchically structured materials found in nature. From bottom to top: diatom, butterfly, wood, leaf, macaw feather, grass stem, kelp, coral, cotton, human bone, cuttlefish bone and sponge. Reproduced from Reference 18. Copyright 2011, Wiley-VCH.

1.1.1. Methods of production

Whilst there are many techniques to produce hierarchically porous materials, it is difficult to classify them into separate sections as they are commonly a combination of multiple techniques. However, the next part of this brief review will aim to review some of the widely used methods to synthesise materials with multimodal porosity. It concentrates on templating methods as these have been employed extensively in this thesis. A thorough review on preparation methods can be found elsewhere.¹⁰

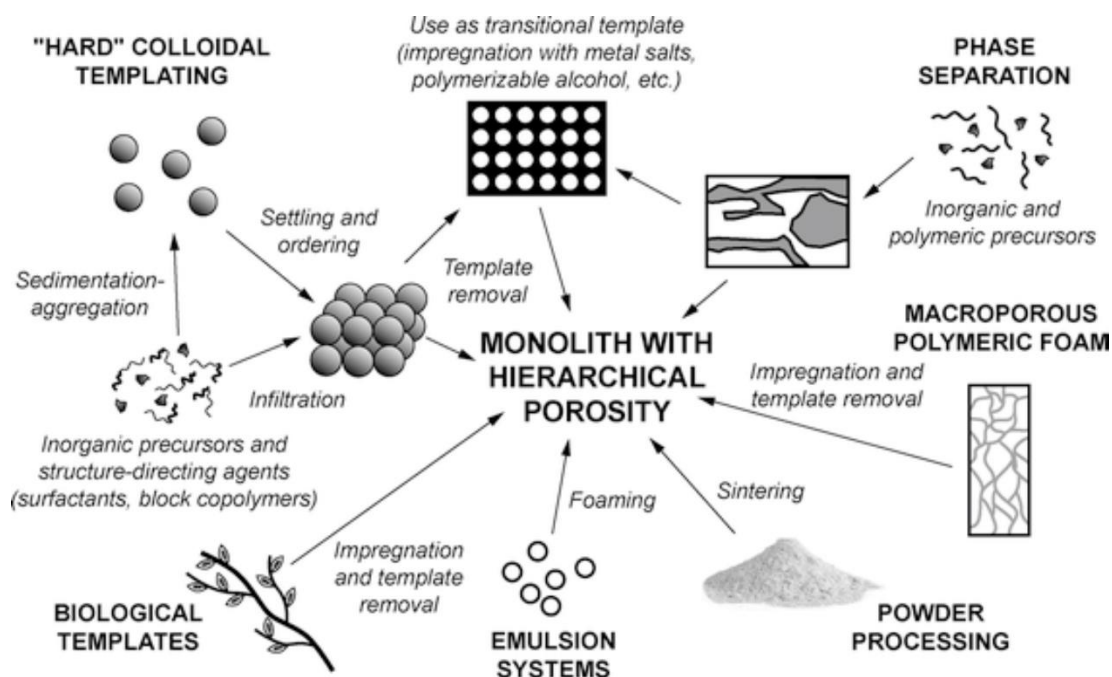


Figure 1.3. Overview of some of the current methods for production of hierarchically porous materials.¹⁹ Reproduced from *J. Mater. Sci.*, Fabrication of ceramic components with hierarchical porosity, **45**, 2010, 5425-5455, P. Colombo, C. Vakifahmetoglu, S. Costacurta with permission of Springer. (Reference 19).

1.1.1.1. Surfactant templating

Some of the early techniques to produce materials with hierarchically porous structures involved the use of surfactant templates. Through careful control of the phase separation of two surfactants dissolved in an aqueous medium, it is possible to use these assemblies to fabricate a hierarchically structured material. The choice of surfactants is of utmost importance as their interaction determines whether they can be used to introduce hierarchical porosity. Figure 1.4 shows possible outcomes of mixing two different surfactants in solution.²⁰

The self-assembly of the surfactants into micellar structures will occur at concentrations above the critical micelle concentration (CMC). This takes place to lower the free energy of the system by reducing the contact between the hydrophobic hydrocarbon regions and the surrounding water.²¹ Whilst this method seems simple, mixing of micelles is the issue holding it back, with no current examples of using a three surfactant system as a template to produce a material with a trimodal mesoporous structure. This approach is limited by the availability of data for phase diagrams of mixed surfactant systems.

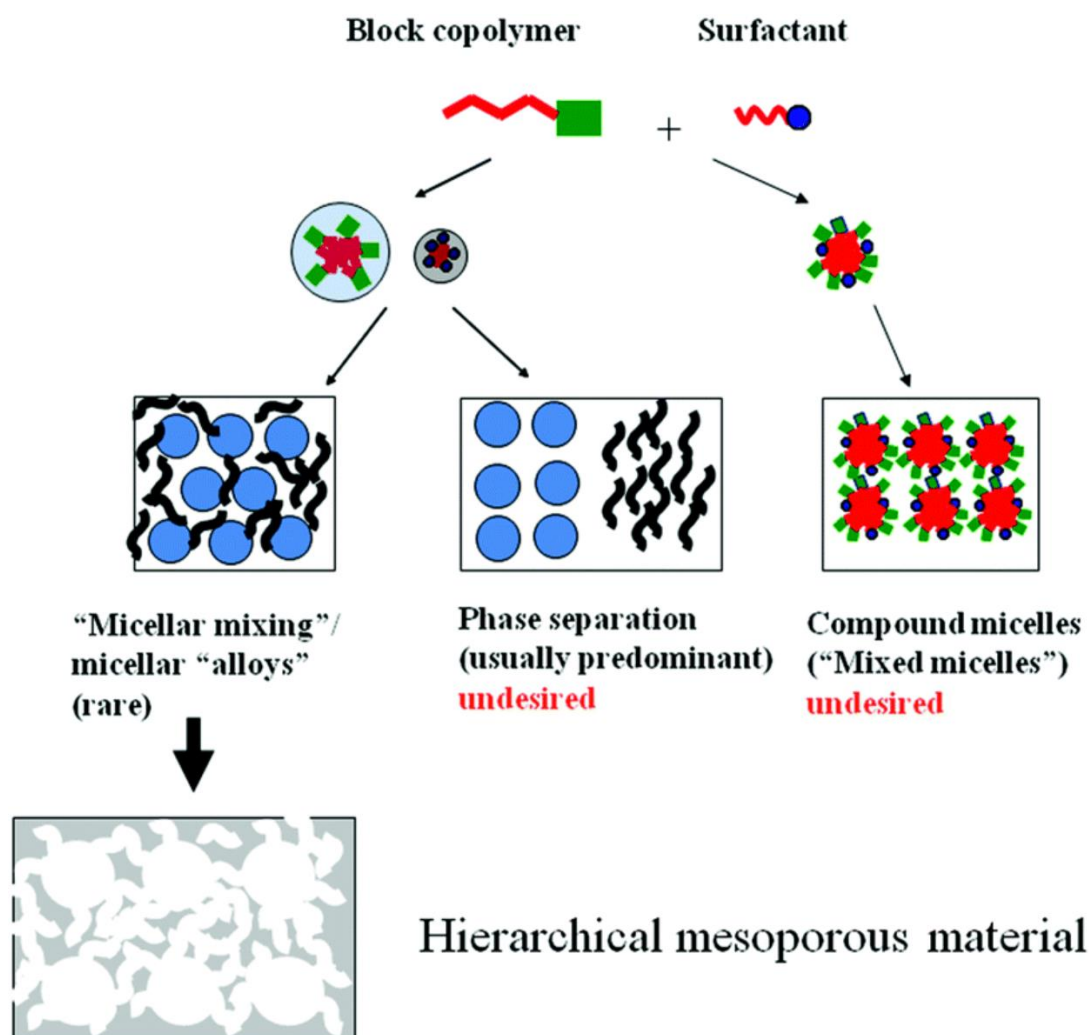


Figure 1.4. Schematic illustration of the various ways of co-templating of two surfactants (block copolymer and a low molecular weight surfactant) for use as templates. The block copolymer consists of a long straight polymer chain (red) and a branched polymer (green) and the surfactant has a hydrophobic chain (red) and hydrophobic head (blue) Reproduced from Reference 20. Copyright 2011, Wiley-VCH.

If trimodal porosity is required, a combination of surfactant templating and another technique to introduce porosity on a different length scale would be needed. One group utilised a block copolymer surfactant, an ionic liquid surfactant and polystyrene (PS) microspheres as templates to produce a material with hierarchical porosity with pores on three different length scales.²²

1.1.1.2. Breath figures

The fog that forms when water vapour condenses upon contact with a cold surface is known as a breath figure (BF). An everyday example that led to its name is breath on a window. These were first utilised for the preparation of structured films in 1994.²³ The general procedure is encouraged by evaporation of the solvent of a polymer solution. The process of evaporative cooling causes water droplets to condense on the surface into a well ordered hexagonal array which is stabilised by the polymer in solution. If the solvent has a higher density than water, the droplets will only structure the surface. Conversely, if the solvent is less dense than water, the droplets will propagate through the polymer solution and introduce porosity upon drying.¹⁰ This method is attractive due to using water as the template and due to the possibility of tuning the pore size by control of the preparation conditions. Whilst the preparation methods of materials structured by BFs are fairly simple, the theory behind them is not, due to complex mass and heat transfer mechanisms. A thorough review on BFs can be found elsewhere.²⁴

BFs have been used to prepare hierarchically structured films. One method involved addition of trioctylphospine oxide (TOPO) ligand stabilised CdSe nanoparticles to a PS in chloroform solution. It was evaporated at room temperature and 80% humidity. The drying of the water droplets produced pores that were decorated with CdSe nanoparticles trapped at the polymer-air interface, resulting in a hierarchically structured PS film.²⁵

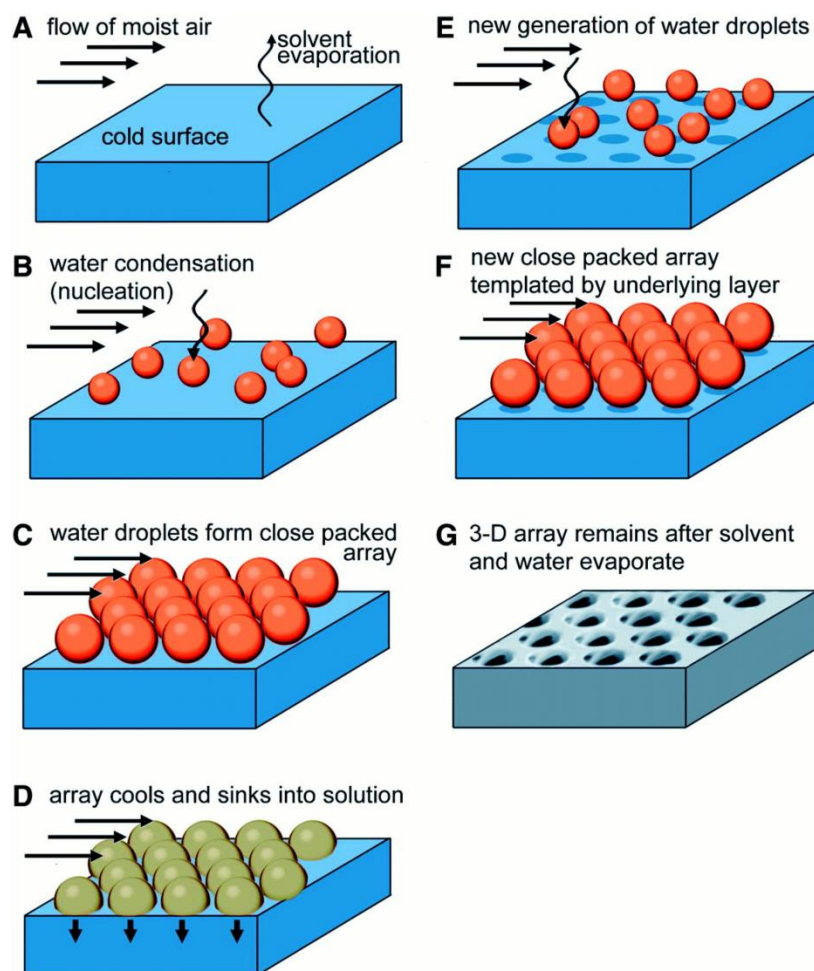


Figure 1.5. Schematic of using BF templating to produce a 3D porous material.²⁶ From M. Srinivasarao, D. Collings, A. Philips and S. Patel, *Science*, 2001, **292**, 79–83. Reprinted with permission from AAAS. (Reference 26).

1.1.1.3. Freeze drying

Freeze drying is the process of freezing a solution, usually in liquid nitrogen, then removing the frozen solvent by sublimation at a pressure and temperature below its triple point.²⁷ This process has been exploited for the preparation of porous and hierarchically porous materials and is known as ice-templating.¹⁰ The porous structure can be varied by controlling the freezing rate, initial freezing temperature, solution concentration and direction of freezing.^{27,28} A binary colloid system has been ice templated to obtain a hierarchically structured material. It involved the dispersion of submicron size silica (SiO_2) particles into a SiO_2 sol. After subsequent gelation and freeze-drying, a hierarchically structured material was obtained.²⁹

This technique has many advantages, the first being the use of environmentally friendly water ice as the pore inducing template. It can also be applied to many types of materials and can be used for biological applications. Thorough reviews on ice templating, also known as freeze-casting, can be found elsewhere.^{27,30}

1.1.1.4. Colloidal crystal templating

A colloidal crystal contains a large number of monodisperse colloidal particles arranged in a three-dimensional uniform array.³¹ The most common colloidal crystal structure is the face centred cubic (FCC), however there are reports of other lattice geometries.^{32,33} These colloidal crystals can be used as sacrificial hard templates to introduce well-ordered and monodisperse pores into materials. A general technique, described in 1997, was the preparation of a PS latex solution and then allowing it to form a crystal structure on a membrane due to sedimentation. It was subsequently soaked with hexadecyltrimethylammonium bromide (HTAB) solution to hydrophobise the latex particles which would induce polymerisation of a SiO₂ sol. The excess HTAB was removed by washing with water which was followed by infiltration of the colloidal crystal with a SiO₂ sol. This was left to gel, dried under vacuum and finally the latex particles were removed by heating to 450 °C for four hours to obtain a porous SiO₂ monolith.³⁴ This method can be further developed by using two different sized latex particles,³⁵ or combined with other methods to introduce porosity such as surfactant templating or zeolites to prepare hierarchically porous materials.^{36,37}

Velev *et al.* have utilised this method to obtain hierarchically porous gold by preparing a solution of PS latex particles and gold nanoparticles. They were allowed to sediment on a membrane where the PS formed a colloidal crystal structure and the gold nanoparticles were within the interstitial holes. PS was removed by heating, thus yielding macroporous gold. However, if acid or trichloromethane was used to remove the PS, hierarchically meso-macroporous gold was obtained.³⁸

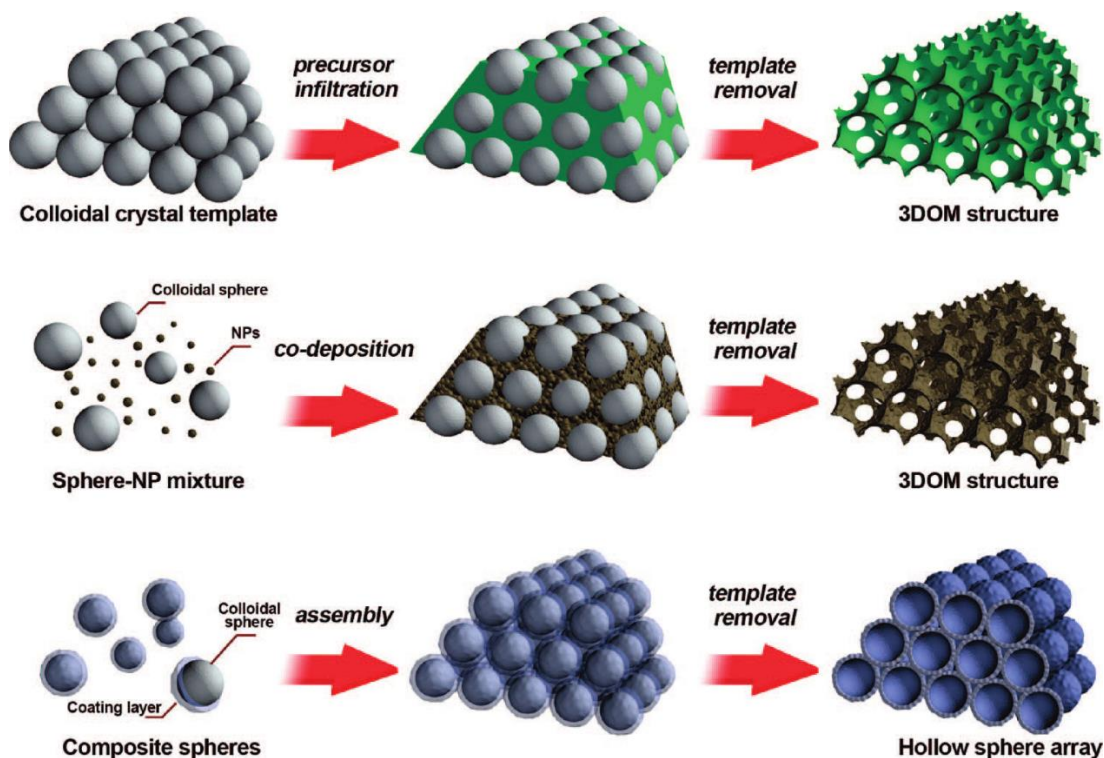


Figure 1.6. Three different schematics showing examples of colloidal crystal templating. Reprinted with permission from A. Stein, F. Li and N. R. Denny, *Chem. Mater.*, 2008, **20**, 649–666. Copyright 2008 American Chemical Society. (Reference 32).

1.1.1.5. Biological templating

Another templating technique that has been used involves the use of natural plants as templates. This is a clever approach as hierarchically porous structures in nature have pores that are well ordered and have a small pore size distribution. A SiO_2 sol was prepared and mixed with various parts of plant structure which had various types of porosities. Pith was used that had pores that decreased in size from edge to centre, while xylem has hierarchical porosity and epidermis had a single level of porosity. Upon drying and calcination of the sol, the SiO_2 monolith had a porous structure that represented the template used.³⁹

1.1.1.6. Emulsion templating

Emulsion templating is an effective and widely used technique for preparing porous materials. Mixing two immiscible liquids, i.e. water and oil, in the presence of a

surfactant⁴⁰ or colloidal particles^{41,42} results in a dispersed phase of droplets within a continuous phase. Generally, the continuous phase is solidified around the dispersed droplets which are subsequently removed by solvent evaporation. Solidification of the continuous phase can be done by inclusion of a functionalisable monomer and an initiator to the continuous phase. After preparation of the emulsion, the continuous phase can then be polymerised.

High internal phase emulsions (HIPEs), emulsions with a volume fraction of the dispersed phase greater than 0.74, have been employed as templates for preparation of hierarchically porous materials. Through control of the preparation conditions, it is possible to obtain bimodal droplet sizes which leads to a hierarchical pore size distribution. A study has shown that low surfactant concentrations and short homogenisation times leads to polydisperse water droplets. They prepared a HIPE of aqueous CaCl₂ solution dispersed in a continuous phase consisting of styrene, divinylbenzene (DVB), Hypermer 2296 surfactant and azobisisobutyronitrile (AIBN, a free radical initiator). After preparation, it was immediately polymerised by heating to 70 °C for 24 hours. Finally, it was dried in a vacuum oven to obtain a hierarchically porous polyHIPE.⁴³ There are many other examples of the use of polyHIPEs to obtain hierarchically porous materials.^{44,45}

1.1.1.7. Polymer templating

Hierarchically structured polymers can be employed as sacrificial templates for the production of porous materials. The mixing of such structures with a scaffold material, followed by the subsequent removal of the template can yield materials with a hierarchical structure that reflects the initial microstructure of the templates.

Monodisperse PS latex particles can be prepared with a variety of sizes and surface functionalities. One study showed how combining two different size PS particles to prepare hierarchically structured PS templates could be utilised to prepare a porous material with two different monodisperse pore sizes. They functionalised the surface of small PS particles (80 nm diameter) with NH₂ groups and large PS particles (1.5 µm diameter) with COOH groups. The small PS particles assembled around the surface of the large PS particles when they were mixed together (small in excess) due to electrostatic interactions. A coupling reaction was used to fix them in place. They

were then mixed with a SiO₂ sol, followed by drying and then removal of the templates by heating to 540 °C for three hours. This obtained a hierarchically porous material with a raspberry-like internal structure imparted by the template.⁴⁶

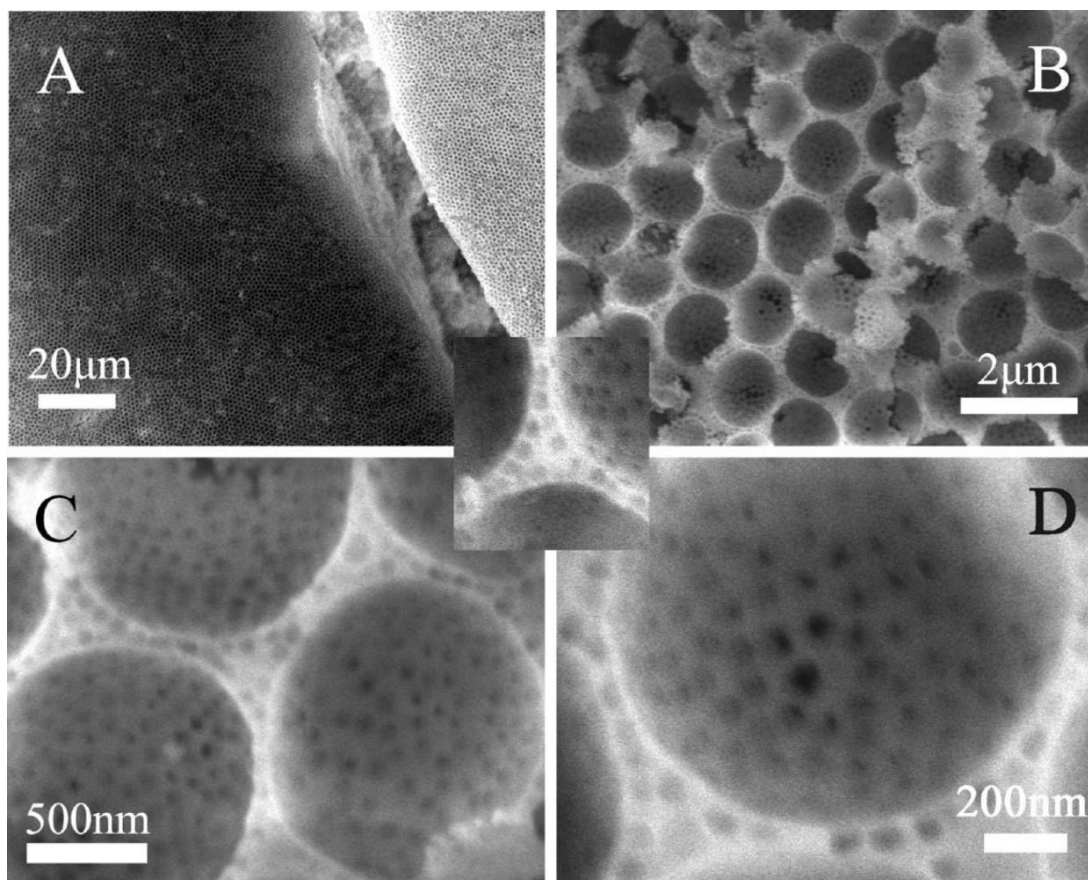


Figure 1.7. Hierarchically porous SiO₂ produced using raspberry-like PS particles. Reprinted with permission from B. Zhao and M. M. Collinson, *Chem. Mater.*, 2010, **22**, 4312–4319. Copyright 2010 American Chemical Society. (Reference 46).

Another way polymer templating can be used to produce hierarchically porous materials is through the infiltration of a polymer gel network by nanoparticles. It has been demonstrated by Fe₃O₄ nanoparticles infiltrating into poly(acrylic acid). Upon removal of the organic polymer by heating in air, the nanoparticle structure was left intact and formed a hierarchically porous material.⁴⁷

1.1.2. Applications of hierarchically porous materials

The next section will review how hierarchically porous materials have been utilised for specific applications in recent years.

1.1.2.1. Catalysis

A large proportion of research into materials with hierarchical porosity goes into their applications in catalysis. With catalytic processes being involved in more than 20% of all industrial processes, it is highly worthwhile to develop more efficient catalysts.¹¹ Hierarchically porous materials are well suited for this role due to their high surface area due to the presence of micropores, leading to an abundance of active sites. Furthermore, macropores provide easier mass transport through the material due to lower pressure drops i.e. a reduction in frictional forces compared to meso- or micropores.⁴⁸

Through careful design of hierarchically structured materials, it is possible to prepare catalysts for oxygen reduction reactions (ORRs) that do not contain precious metals, yet have a comparable or superior activity to them. ORRs are very important reactions that occur at a cathode and determine the performance of fuel cells and metal-air batteries.⁴⁹ Metal organic frameworks (MOFs) have been investigated as precursors to produce porous carbon-based catalysts for ORRs. This technique allows for controllable porous structural characteristics by changing one or both of the central metal ion and the bridging electron donating molecules. Furthermore, it allows for doping of the final product by the inclusion of heteroatoms within the organic linkers. MOFs have been used to produce porous carbon-based materials previously, however their ORR activity was lower than current commercial catalysts. This is assumed to be due to low specific surface area, a microporous structure or poor electrical conductivity, or a combination of these.⁵⁰

Zeolitic imidazolate frameworks (ZIFs) are a subclass of MOF and a combination of two ZIFs have been used to produce a hierarchically porous cobalt and nitrogen co-doped carbon-based electrocatalyst. Core-shell materials with a ZIF-8 (zinc-based) core and a ZIF-67 (cobalt-based) shell were produced using a ZIF-8 seed mediated growth of ZIF-67 crystals.⁵¹ Briefly, ZIF-67 crystals were grown on ZIF-8 seeds and then they were heated at 950 °C for two hours in an argon atmosphere to produce

cobalt and nitrogen co-doped hierarchically porous carbon nanopolyhedra. This was then investigated for its ORR activity and was found to be superior to a commercial platinum-based catalyst. Furthermore, they show higher durability and methanol tolerance when compared to the Pt catalysts.⁵⁰

Another hierarchically porous catalyst has been developed for ORRs. PS and anhydrous FeCl₃ were added to *N,N*-dimethylformamide (DMF) and stirred until a red solution was formed. This was then electrospun into fibres. After subsequent drying of these fibres, they were subjected to vapour phase polymerisation (VPP) with pyrrole for 12 hours. Following this, the fibres were heated at 900 °C for two hours in a nitrogen atmosphere. The inactive iron particles were then removed by acid leaching and then another identical heat treatment was performed and hierarchically porous iron and nitrogen doped carbon nanofibres were obtained. These were used to assemble a zinc-air battery which showed a higher power density and increased long-term stability when compared to a zinc-air battery produced using a commercial platinum catalyst.⁵²

Significant efforts have been made towards development of heterogeneous catalysts.⁵³ Stable surfaces have been shown to be unfavourable for catalysis whereas surfaces with defects or surfaces with high interfacial energy are more favourable.⁵⁴ Because of this, working with polymorphs of a material is an attractive method to tune catalytic activity. For oxidation of CO with an Au/TiO₂ catalyst, using a brookite TiO₂ polymorph instead of the anatase polymorph, complete oxidation occurs at significantly lower temperatures.⁵⁵ Alumina (Al₂O₃) is another common material used in catalytic processes.^{56,57} It is desirable due to being cheap, resistant to thermal and chemical treatment and has a high melting point.⁵⁸ Alongside the thermodynamically stable α -Al₂O₃, there is also γ -Al₂O₃ which has a spinel structure with vacancies in the cation lattice.⁵⁹ It contains many Lewis acid sites on the surface which are employed in many catalytic processes.⁵⁹⁻⁶¹ One study has produced an aerogel structure consisting of γ -Al₂O₃. They reacted the volatile precursor trimethylaluminium (AlMe₃) with oxygen at a high temperature and in the gaseous phase. This obtained the kinetic product γ -Al₂O₃ instead of the thermodynamic product α -Al₂O₃. It formed an aerogel-like structure with an interconnected micro-meso-macroporous network and its catalytic activity was investigated by using the dehydration of hexanol to 1-hexene as

a model reaction. The γ -Al₂O₃ aerogel was far superior (91% conversion) to commercial γ -Al₂O₃ catalysts (29.5% conversion) and also showed a better selectivity.

1.1.2.2. Energy storage, usage and conversion of hierarchically porous materials

All fossil fuel reserves are estimated to be used up by the year 2112⁶² and their use brings with it multiple issues such as pollution, global warming and climate change. Development of materials for more efficient energy storage, usage and conversion is a step towards combating these issues.

Lithium ion batteries have been a staple in the market of portable electronic devices for many years as their high energy density and durable cycle life makes them desirable. However LiCoO₂, the cathode material, is toxic, expensive and has lower specific capacity than the anode.^{63,64} Lately, lithium based phosphates have attracted a significant amount of attention as cathode materials.^{65,66} A recent hierarchically porous, lithium based phosphate that was produced was a composite of Li₃V₂(PO₄)₃ and carbon (LVP-HPC). It was produced as shown in Figure 1.8.



Figure 1.8. Schematic of the production of LVP-HPC. Reproduced from Y. Cheng, W. Zhou, K. Feng, H. Zhang, X. Li and H. Zhang, *RSC Adv.*, 2017, **7**, 38415–38423 – Published by the Royal Society of Chemistry. (Reference 64).

This was then investigated for its suitability as an electrode and it was found to be robust, retaining 96% of its capacity after 800 cycles whereas the same material

without the hierarchical structure retained only 81%. Furthermore, it exhibited high rate performance. These attributes have been explained by lower charge transfer resistance, increased diffusion rates of Li^+ and an interconnected, hierarchically porous structure with a large surface area.

1.1.2.3. Separation applications

Contamination of water as a by-product of human activity has been recognised as a serious environmental issue.^{67,68} Waste products from industrial processes which contain water immiscible oily compounds are common pollutants which has led to the investigation of materials that are efficient for separation of oil from water.

Superhydrophobic porous sponges with hierarchical structure have been produced by BF lithography and nanoparticle templating on an already macroporous polyurethane (PU) sponge. Poly(methyl methacrylate) (PMMA) and octadecyl-functionalised SiO_2 nanoparticles were mixed with a volatile solvent (THF). The PU sponge was soaked in this solution, followed by evaporation of THF in a moist environment. Due to water having a lower density than PMMA, the BF technique introduced surface roughness rather than porosity to the PMMA after evaporation of the water. The octadecyl-functionalised (hydrophobic) SiO_2 nanoparticles created a secondary roughness on the nanoscale. This hierarchical structure imparted superhydrophobicity which could be utilised for separation of oil and water and had very high oil absorption capacity (15 – 28 times its own weight). Furthermore, it was stable up to at least 115 °C and showed no significant reduction in absorption capacity after ten cycles (cleaned with purified oil or ethanol between each cycle). A final functionalisation of this hierarchically structured sponge was done by inclusion of magnetic nanoparticles in the initial formulation. Iron oxide nanoparticles were coated with SiO_2 which were again hydrophobically modified by functionalisation with octadecyl units. This allowed for manual targeting of oil pollutant through the use of a magnet. The sponge could also be cut into smaller pieces, increasing the area of contact between oil and sponge, then easily recovered using a magnet.⁶⁹

Another study has shown the fabrication of a hierarchically porous titanium membrane by growth of TiO_2 nanotubes on macroporous titanium via anodisation at 35 V with an aqueous hydrogen fluoride (HF) electrolyte. Drying of the membrane at 450 °C

obtained the anatase polymorph of TiO_2 . Measurements showed that this membrane was superhydrophilic in air and superoleophobic whilst underwater and was efficient for separation of oil and water. The catalytic properties of anatase TiO_2 were exploited as a further functionality of the membrane. Methylene blue (MB) was used as a model pollutant and whilst the aqueous MB solution passed through the membrane, it was irradiated with UV light. A flow-through photocatalysis device was constructed which allowed investigation of the number of cycles and size of the macropores on the degradation of the MB. It was seen that the size of the macropores had a significant effect on the photocatalytic degradation of MB, with the membrane with the smallest macropores having an 84.5% reduction in MB concentration in the filtrate after four cycles. On the other hand, the membrane with the largest macropores had only a 27% reduction in MB concentration after four cycles. Finally, it was shown that after contamination of the membrane with the model pollutant octadecyltrimethoxysilane (OTS), the membrane could regain its functionality after irradiation with UV light.⁷⁰

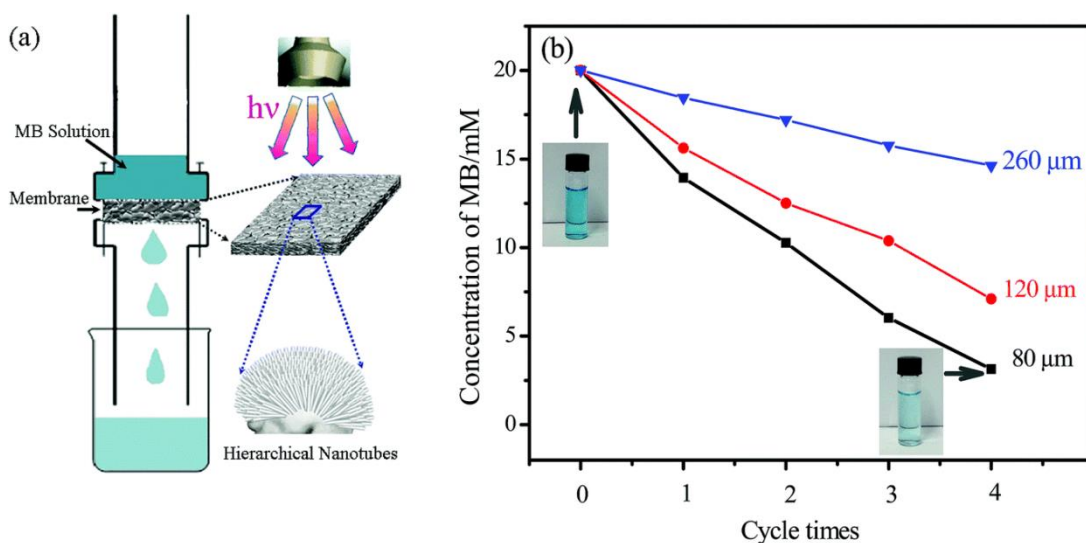


Figure 1.9. The flow-through photocatalysis set up can be seen in (a) and the reduction in MB concentration as a function of macropore size and number of cycles can be seen in (b). Reproduced from reference 70 with permission of The Royal Society of Chemistry.

1.1.2.4. Adsorption of pollutants

Environmental pollution is becoming a serious issue due to the rate at which large amounts of waste chemicals are being produced. The pollution of water with materials

such as dyes and heavy metal ions can easily lead to them being taken in by the human body through consumption of contaminated water. Hierarchically porous materials are widely used for the sorption of harmful pollutants from the environment.⁹

Pollution of water with arsenic has become a worldwide issue and is hazardous to ecosystems and public health alike through accumulation in food chains. Materials such as active carbon, metal oxides, zeolites etc. have been investigated for their adsorption of As(III) and As(V), however they have shown unsuitable uptake ability and low removal efficiencies.⁷¹⁻⁷³ Iron-based materials have shown great promise for removal of arsenic by demonstrating enhanced capturing ability and a selective affinity for arsenic anions.⁷⁴ A hierarchically porous, functionalised carbon-based foam has been prepared and investigated for its arsenic removal ability. It was fabricated by a pyrolysis method with melamine foam as the starting material. The first step was heating at 700 °C for two hours, followed by hydrothermal treatment with nitric acid (3 M) at 120 °C for one hour. This hydrothermal treatment was done to impart hydrophilicity and maximise the presence of oxygen-containing functional groups. It was then washed and dried at 60 °C. The growth of β -FeOOH nanorods on the carbon foam was done by a further hydrothermal treatment. The foam was soaked in an aqueous solution of FeCl₃, NaNO₃, HCl and acetonitrile for one hour, followed by heating to 100 °C four hours. After washing and vacuum drying at 60 °C, the hierarchically porous carbon foam functionalised with β -FeOOH nanorods was obtained.⁷⁵

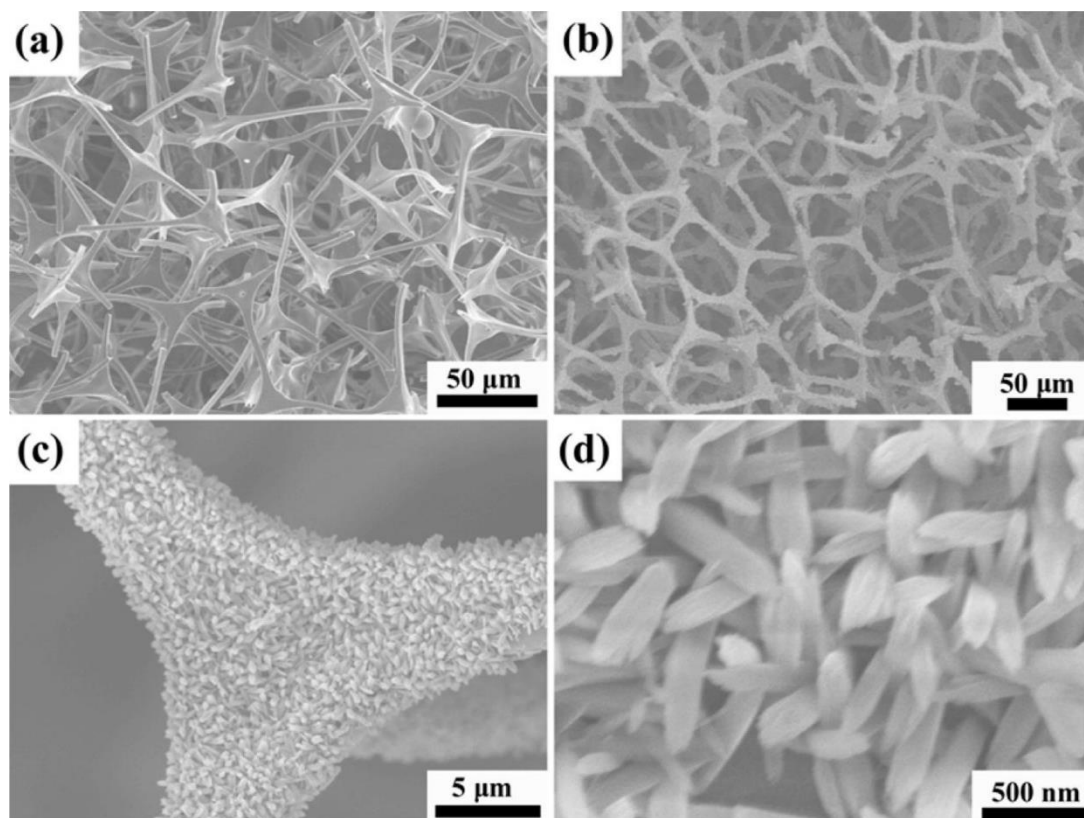


Figure 1.10. The carbon foam before the growth on β -FeOOH nanorods is shown in (a). (b) – (d) show the carbon foam with β -FeOOH nanorods grown directly onto the surface at different magnifications. Adapted with permission from X. Ge, Y. Ma, X. Song, G. Wang, H. Zhang, Y. Zhang and H. Zhao, *ACS Appl. Mater. Interfaces*, 2017, **9**, 13480–13490. Copyright 2017, American Chemical Society. (Reference 75).

Upon investigating its ability to remove arsenic from water, it was found that it could reduce the concentration of a 10 ppm solution to less than 10 ppb which is the acceptable standard for drinking water set by the World Health Organisation (WHO). Through the use of Fourier transform infrared spectroscopy (FTIR) and x-ray photoelectron spectroscopy (XPS), they revealed the adsorption mechanism to be formation of As-O-Fe bonds and the replacement of hydroxyl radicals with H_2AsO_3^- and H_2AsO_4^- . The abundance of active sites due to the high surface area of the nanorods and the efficient mass transport due to the macroporous foam backbone leads to high adsorption of arsenic species.

One group utilised a microwave assisted hydrothermal method to produce hierarchically porous γ - Al_2O_3 from an aqueous solution of $\text{KAl}(\text{SO}_4)_2 \cdot 12\text{H}_2\text{O}$ and urea, followed by calcination at 600 °C. It was found to have smaller pore sizes and

increased surface area when compared to the same material produced using a regular hydrothermal method. Both materials were tested for their ability to adsorb Cu^{2+} ions and the one produced using the microwave assisted method performed better, demonstrating approximately a 20% reduction in concentration of Cu^{2+} compared to approximately 6.5% reduction. Furthermore, it showed a quicker rate of adsorption.⁷⁶

An interesting technique to fabricate hierarchically porous hydrogels involved exploitation of the well-known fermentation process that occurs when yeast and sugar are in water. A pre-polymer solution was mixed with a solution of yeast and sugar in a sealed container and then polymerised. The production of CO_2 bubbles occurred and they were trapped within the already porous hydrogel matrix, obtaining a hierarchical structure that could be controlled by varying the concentrations of yeast and sugar. The produced hierarchically porous hydrogels showed increased swelling capacity and swelling rates as well as increased absorption of crystal violet (CV) dye, when compared to hydrogels produced without yeast and sugar.⁷⁷

1.1.2.5. Sensors

Development of sensors with rapid response times and low detection limits is essential for environmental monitoring, control of chemical processes and for occupational health and safety.

Due to the widespread use of organic liquids in many industrial processes, efforts must be made into the detection and subsequent automated intervention of solvent leaks. One study demonstrated the fabrication of a conductive polymer composite on a porous PU foam using a layer-by-layer (LbL) technique. The foam was dipped in a chitosan solution (positively charged) then the excess was removed, followed by dipping in a negatively charged solution of carbon black, cellulose nanocrystals and natural rubber. This was repeated for a number of times to obtain materials with different layer thicknesses and finally dried at 80 °C for six hours. It was tested for its detection ability using petroleum ether (PE) as a model organic liquid by connecting the produced material to two electrodes and monitoring its current signal over time before and after adding PE. The current signal showed a sharp decrease after addition of PE, with a response time of 0.05 – 0.15 s. The speed of the response was dependent on the thickness of the conductivity polymer composite on the PU foam, controlled by

the number of LbL coatings. These response times are ~3 orders of magnitude faster than current state of the art sensors and are currently the fastest recorded in the literature. The rapid response of these composites has been attributed to the hierarchical structure, as when they were compared to bulk conductive polymer composites they were far superior. Furthermore, when organic liquids come into contact with the polymer coating, it causes swelling which blocks the micropores. Therefore, this material is not only an efficient sensor, it can also block solvent leaks upon their detection.⁷⁸

Other work has developed a nitrogen doped hierarchically porous carbon that is an efficient sensor of uric acid (UA), dopamine (DA) and ascorbic acid (AA) in a 0.1 M PBS solution at physiological pH (7.4). These analytes were chosen as they play important roles in maintaining the functions of human metabolism, the central nervous system and the circulatory system.⁷⁹ Its production began with a solvothermal treatment of aqueous ammonia solution, $\text{Zn}(\text{NO}_3)_2 \cdot 6\text{H}_2\text{O}$, water, ethanol and 3-aminophenol at 100 °C for 24 hours. This yielded a resin which was washed and then subjected to two heat treatments; one at 550 °C followed by one at 1200 °C. After cooling, a 3D nitrogen doped hierarchically porous carbon was obtained. A glassy carbon electrode was then coated with this hierarchically structured material and tested for its ability to detect UA, DA and AA. Cyclic voltammetry demonstrated three separate, distinguishable anodic peaks representing UA, DA and AA and square wave voltammetry allowed for simultaneous detection and quantification of these analytes. It was suggested that the hierarchical structure, alongside an abundance of various functional groups was the reason this was possible.⁸⁰

1.1.2.6. Biomaterials

Introducing hierarchical porosity into materials for medical purposes has attracted much attention lately due to each level of porosity being functionalised to facilitate separate biological processes. For example, when preparing bioactive glasses for bone repair engineering, an interconnected macroporous network is a necessity as it allows for cell proliferation whilst ensuring effective mass transport between the growing tissue and surrounding media.⁸¹ Furthermore, a mesoporous network is desired due to being effective for drug release.⁸² A hierarchically porous bioactive glass was prepared

by first mixing commercial milk, SiO₂ nanoparticles and water in various ratios and then freeze-drying. Subsequent annealing at different temperatures between 600-800 °C in an air atmosphere yielded hierarchically porous bioactive glasses. Upon immersing the samples that were annealed at 600 °C in a simulated body fluid at 37 °C, hydroxyapatite began to form.⁸³

Bioactive glasses have also been shown to promote angiogenesis which is critical for wound healing due to oxygen and nutrient demands during the process.⁸⁴ One group has combined electrospinning and pulsed laser deposition to produce a hierarchically structured bioactive glass which showed significantly increased wound healing abilities and re-epithelialisation when compared to materials without the hierarchical structure.⁸⁵

Fabrication of biocompatible and biodegradable materials for scaffolds should be performed with an aim to have a biodegradation rate similar to the rate of remodelling.⁸⁶ A water-in-oil HIPE stabilised by hydrophobic SiO₂ nanoparticles (h-SiO₂) was formulated that had a viscosity suitable for 3D printing. Water was added to a solution of poly(L-lactic acid) (PLLA) and poly(ε-caprolactone) (PCL) in dichloromethane (DCM) that contained h-SiO₂ nanoparticles. The final volume fraction of the dispersed water phase was 0.75. Through careful control of the pressure used during the 3D printing stage, the HIPE was stable to deformation and coalescence whilst being printed into a hierarchically structured scaffold which became porous after solvent evaporation. These biocompatible scaffolds were tested for their drug release kinetics, showing that the release rate of an anti-inflammatory drug was sufficient for combating inflammation in the early period of implantation. The mechanism of drug release was investigated by fitting different kinetic models to the drug release profiles. It was shown that the Hixson-Crowell model was the most appropriate which describes a mechanism of drug erosion.⁸⁷ This model assumes spherical particles (that stay intact and spherical during dissolution) in perfect sink conditions i.e. no significant change in concentration of dissolved substance over time. It takes into account the change in surface area during dissolution. The model is:⁸⁸

$$\sqrt[3]{M_t} = \sqrt[3]{M_0} - kt \quad (1.1)$$

Where M_t and M_0 are the mass of the particle of interest at time $t = 0$ and at time t , respectively and k is a constant. Finally, cell culture studies showed that the scaffold

allowed for adhesion and proliferation of mouse bone mesenchymal stem cells (mBMSCs) which demonstrates their excellent biocompatibility.⁸⁹

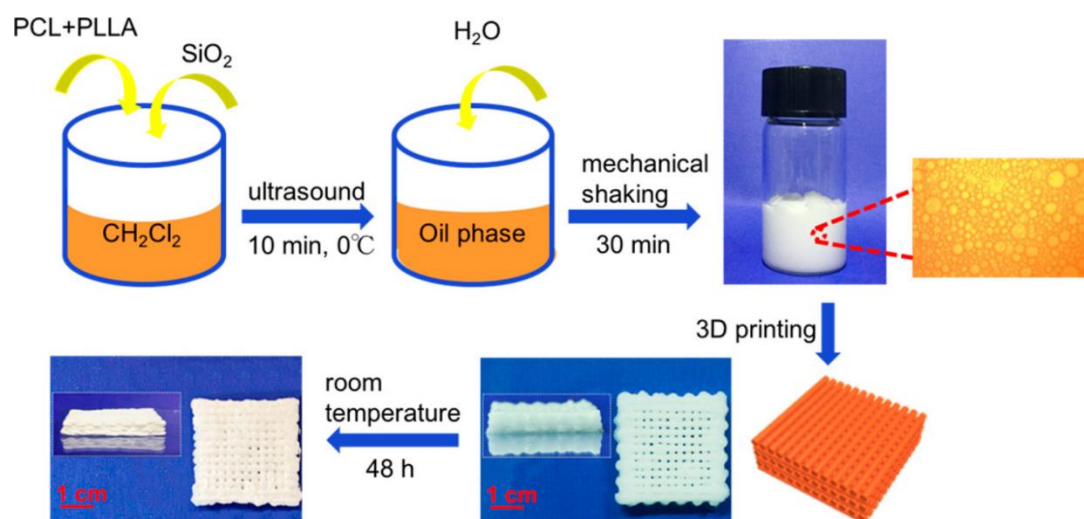


Figure 1.11. Schematic to show the formulation of a hierarchically porous biocompatible scaffold by 3D printing of a HIPE. Reprinted with permission from T. Yang, Y. Hu, C. Wang and B. P. Binks, *ACS Appl. Mater. Interfaces*, 2017, **9**, 22950–22958. Copyright 2017, American Chemical Society. (Reference 89).

1.1.3. Outlook

There are an abundance of methods in the literature that can be used for the preparation of hierarchically porous and structured materials. Furthermore, combinations of techniques can be employed to create structures on multiple length scales. They can be rationally designed for specific applications and functionalisation on each level of hierarchical structure is possible. Future efforts should be directed at increasing the level of control over the ratio of different pore structures within the material i.e. vary the volume percentage of micropores and macropores at a constant porosity with an aim to fine-tune material properties.

1.2. Hydrogels

In this thesis, hydrogels and hydrogel beads are used as templates. These are polymers that when mixed with water, under certain conditions, can assemble into a polymer network with trapped water inside the hydrogel matrix to form a gel. There have been

many different definitions given for gels. The famous polymer chemist, Flory, gave the definition of a gel as a material that “has a continuous structure with macroscopic dimensions that is permanent on the time scale of an analytical experiment and is solid-like in its rheological properties”.⁹⁰ More recently, the generally used definition is that a gel has a substantial amount of liquid present and solid-like rheological properties. For a material to be classed as having solid-like properties, it must have a storage modulus that is considerably larger than its loss modulus. Furthermore, the material’s storage modulus must exhibit a plateau in a time scale in the order of seconds.⁹¹ The storage modulus is the elastic response of the material under deformation and describes its ability to store potential energy that will then be released when the force acting upon it is removed. Energy dissipation in the form of heat upon deformation is associated with the loss modulus i.e. a viscous response of the material.

Polymers used to make hydrogels can be sourced from many different materials. Some examples of polymer sources are trees (cellulose), plants (starch, pectin, cellulose), seeds (guar gum, locust bean gum, tara gum), red seaweeds (agar, carrageenan) and there are also microbial hydrocolloids (xanthan gum, gellan gum, dextran).⁹²

Hydrocolloids are very important in the food industry, with them often being used to modify the structure of food products or as stabilisers. They can be used in high concentrations i.e. a gel for structure modification, or low concentrations as a viscosity modifier. An example of hydrocolloids being used in the food industry is guar gum and xanthan gum used in low fat mayonnaise as fat replacers where they increase the viscosity of the continuous phase, leading to a slower rate of creaming and hence higher stability of the emulsion. This can be understood due to equation 1.2, known as the Stoke law.

$$v = \frac{2a^2(\rho_w - \rho_o)g}{9\eta} \quad (1.2)$$

Where v = velocity (m s^{-1}), a = droplet radius (m), ρ = density of oil or water phase (g cm^{-3}), g = gravitational force (9.81 m s^{-2}) and η = viscosity of continuous phase (Pa s).

As can be seen in equation 1.2, an increase in viscosity of the continuous phase leads to a decrease in the velocity of the emulsion droplets, slowing the rate of creaming and keeping mayonnaise stable for a longer period of time (i.e. increases shelf-life).

Hydrogels are able to encapsulate active components, act as vehicles and deliver them to target areas. They have a high water content and are biocompatible, making them cheap and attractive for this purpose. Another reason hydrogels are desirable materials for encapsulation is that they are degradable and can be tailored to suit specific requirements. A recent study produced spherical and cubic hydrogel particles using a multilayer template approach, where the template was subsequently removed by dissolution. The hydrogel particles were loaded with doxorubicin and could be swollen at neutral conditions or at acidic conditions. Neutral conditions allowed for drug uptake, whereas acidic conditions facilitated the release of the hydrogel particles from the endosomes/lysosomes into the cytosolic space, where the glutathione present breaks down the hydrogel matrix, releasing the encapsulated drug and allowing the smaller polymer chains to be excreted. The doxorubicin loaded hydrogel particles were tested for cytotoxicity, showing 50% and 90% cytotoxicity to HeLa cancer cells after 24 hour and 48 hours, respectively. Finally, spherical hydrogel particles showed a 12% higher initial cytotoxicity (10 hours incubation) showing an effect of shape on the initial release kinetics. This study is a good example to demonstrate the versatility of hydrogels as it produces pH responsive hydrogels, that are degradable and of a controlled shape.⁹³

In this thesis, two types of hydrocolloids have been used; agar-agar and methylcellulose.

1.2.1. Agar-agar

Agar-agar, also known as agar, is a polymer extracted from red seaweed. It is a mixture of two different polymers: agarose and agaropectin.⁹⁴ Agaropectin consists of sulphate ester, pyruvic acid, D-glucuronic acid and agarobiose. Experiments have been performed using optical rotation that showed agaropectin does in fact have a coil-helix transition even though it does not gel.⁹⁵ This lead to the conclusion that the electrostatic interactions between the sulphate groups do not allow gelation to occur in agaropectin, and the gelation of agar is due to agarose; the non-ionic component. Agarose consists of alternating 1,3-linked β -D-galactopyranose and 1,4-linked 3,6-anhydro- α -L-galactopyranose units.⁹⁶ The structure is shown below.

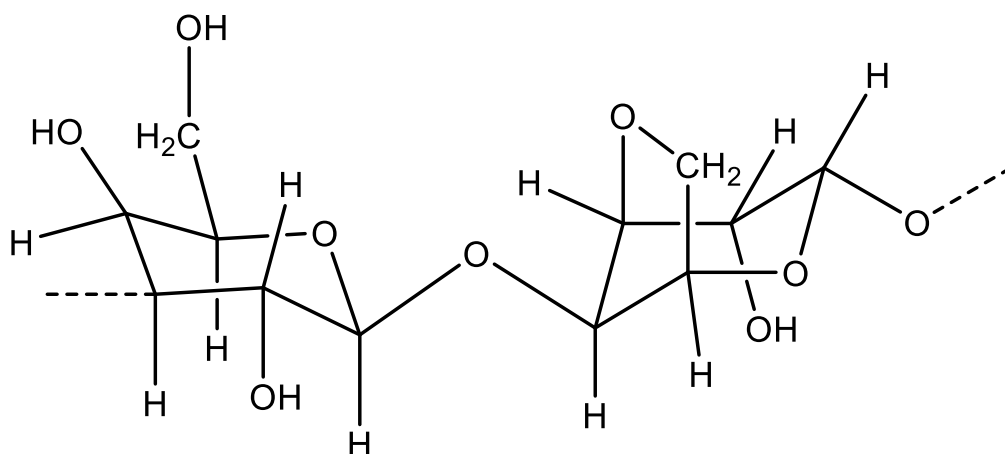


Figure 1.12. The molecular structure of the repeating unit of agarose.

Agar is a non-ionic polymer that forms physical gels i.e. a gel that forms solely from interacting with itself. Agar will hydrate and become disordered coils in water at a temperature close to 100 °C. Upon cooling of this solution, the disordered coils will transition to an ordered double helix structure. In this widely accepted double helix model, the basic unit is the double helix. Each polymer chain (with an estimated average molecular weight of 120 000 g mol⁻¹) forms a left-handed threefold helix with a pitch of 1.90 nm. The two chains of the double helix are related by a 0.95 nm translation along the helix axis. Furthermore, the inner cavity has a diameter of 0.45 nm and is lined with oxygen atoms available for hydrogen bonding. Thus, it was suggested that water molecules participate in hydrogen bonding within the double helix's interior, which contributes to its stability.⁹⁷ There are also oxygen atoms on the outside of the double helix which are available for hydrogen bonding with the bulk water molecules or other helices. This allows for the formation of higher order assemblies which contribute significantly to the elastic properties of the hydrogel.^{97,98}

Agar gels upon cooling at approximately 38 °C and will melt above 85 °C, showing very large thermal gelling hysteresis. The gelling temperature of agar varies with the methoxyl content; as the methoxyl content increases, so does the gelation temperature.⁹⁹ Furthermore, the gelation temperature increases with a decrease in cooling rate.¹⁰⁰ Agar is widely used in cooking due to its large thermal gelling hysteresis. When heating agar hydrogel above 85 °C melting occurs due to increase in

kinetic energy of the polymer chains which in turn causes the aggregates to dissociate.¹⁰¹

Whilst the gelling mechanism is agreed upon, there are a number of unusual gelation behaviours that are exhibited by agar. For example, the gelation temperature of agar is known to be approximately 38 °C, however, it has been shown that a 3.0% w/v solution of agar will gel at 51.5 °C when left for 1000 hours. This leads to the conclusion that gelation is thermodynamically favoured at temperatures above the gelling point, but is kinetically unstable.¹⁰²

Interestingly, low concentrations of agar solution (< 2.0% w/v) were found to have a slightly different gelation pathway to higher concentrations.¹⁰³ When agar is in low concentrations, the solution is found to undergo spinodal demixing into polymer rich and water rich regions. At the polymer rich regions there is increased local concentration, leading to increased aggregation of the polymer chains which causes gelation. Then these polymer rich regions aggregate with each other, trapping large amounts of water inside the polymer matrix. On the other hand, when the concentration of agar is higher than 2.0% gelation occurs simply from a homogenous polymer solution to a gel.

Another phenomenon shown by agar hydrogels is syneresis which is the release of water from the polymer matrix over time. This process causes internal osmotic stress within the hydrogel. It is possible to speed up syneresis by applying pressure to the hydrogel. On the other hand, it is possible to decrease syneresis by increasing the concentration of agar which decreases the pore size in the polymer mesh. Another way to decrease syneresis is by addition of locust bean gum (5-10% by weight of agar).¹⁰¹

More recently, research is being done on agar organogels. This is where the liquid trapped inside the polymer matrix is non-aqueous. An agar organogel has been produced by mixing agar (0.22% w/v) with a glycerol solution (50% w/v in water). The gelling concentrations were determined for different glycerol concentrations by measurements of viscosity of agar solutions. It was found that higher concentrations of glycerol needed higher concentrations of agar for it to gel; with water needing 0.18% agar for gelation to occur and 50% w/v glycerol in water needing 0.22% w/v agar. Furthermore, it was found that the agar organogels had a lower gelation temperature and a lower melting temperature compared to agar hydrogels. Their measured gelation

and melting temperatures for agar hydrogel were 40 °C and 81 °C, respectively, whereas for agar organogels with 50% by volume of glycerol they were 20 °C and 65 °C.¹⁰⁴

1.2.2. Methylcellulose (MC)

MC is a non-ionic polymer and a derivative of cellulose. It is produced by dispersing cellulose in an alkali solution and then reacting with chloromethane.¹⁰⁵ This partially methylates the cellulose by replacing some of the hydroxyl groups with methoxyl groups. The extent of this substitution is known as the degree of substitution (DS) and it controls the polymer's solubility. This is a heterogeneous substitution along the polymer chain and ranges from 0-3, as each of the three hydroxyl groups can be substituted with a methoxyl group. The structure of MC can be seen below in Figure 1.13.

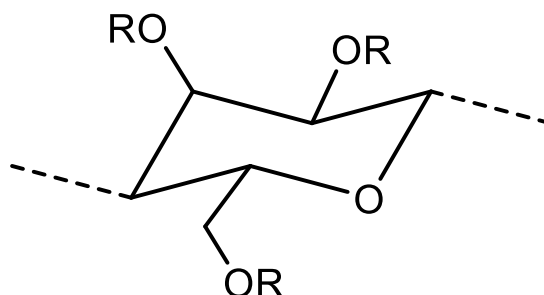


Figure 1.13. Molecular structure of MC. The R constituent is either H or CH₃, depending on the DS.

MC hydrates in cold water and will form a gel upon heating above a certain temperature that is dependent upon the DS and concentration of MC in solution. Currently, the gelation mechanism is not fully understood. Initially, it was suggested that the gelation of MC was due to dehydration upon heating.¹⁰⁶ Later work studied x-ray diffraction (XRD) patterns of MC films and gels and concluded that the cross-linked regions were crystalline and were tri-substituted anhydroglucose units.¹⁰⁷ A more recent suggestion of the gelation mechanism is that the unsubstituted cellulose units dissociate upon initial heating which allows for sections of the polymer chain to separate. After further heating, cage-like water structures that surround the methoxy

substituents are disrupted which allows for an association of the hydrophobic regions. This was followed by phase separation, interpreted as spinodal decomposition, and formation of a turbid gel.¹⁰⁸ Another two-step process was suggested by Kobayashi *et al.* where the first step is hydrophobic association of the highly substituted regions, followed by phase separation induced gelation.¹⁰⁹ Lodge *et al.* have argued for a nucleation and growth mechanism of phase separation due to the gelation temperature being dependent on the heating rate.¹¹⁰ Furthermore, they have utilised cryogenic transmission electron microscopy (cryo-TEM) and small angle neutron scattering (SANS) to reveal a fibrillar structure where each fibre is 15 ± 2 nm and independent of concentration, DS and molecular weight.¹¹¹ Finally, they have shown that the linear and nonlinear viscoelastic response of MC solutions and gels can be described by a filament based model.¹¹²

The hydrophobic methoxyl groups, along with the unsubstituted hydrophilic hydroxyl groups, give the compound its amphiphilic properties. The surface activity of MC has been studied and for concentrations of $1 - 10 \text{ mg L}^{-1}$ the interfacial tension at the air-water interface is reduced from 70 mN m^{-1} to about 55 mN m^{-1} . This effect can be explained by the increasing concentration of amphiphilic molecules packing at the interface. It was found that the surface activity of MC at equilibrium was independent of the molecular weight and was determined by the DS.¹¹³

Current uses of MC are as an emulsion stabiliser and as a thickener in food products.^{114,115} Investigations are also being performed on two-component polymer systems containing MC. One study has shown that a combination of κ -carrageenan and MC will undergo a gel-sol-gel transition with increasing temperature and has been suggested as an entrapment medium for various colloidal particles.¹¹⁶

1.3. Gypsum

Gypsum has been used extensively in this thesis as a scaffold material. Calcium sulphate hemihydrate ($\text{CaSO}_4 \cdot \frac{1}{2}\text{H}_2\text{O}$), also known as plaster of Paris, can come in two forms: α - and β -. These are defined according to their method of preparation i.e. calcium sulphate dihydrate ($\text{CaSO}_4 \cdot 2\text{H}_2\text{O}$), also known as gypsum, can be autoclaved to obtain the α -form (wet method) or calcined to obtain the β -form (dry method).¹¹⁷

No structural differences have been reported between the two forms from XRD studies and it has been suggested that they only differ in the size and arrangement of the crystals.¹¹⁸ The α -hemihydrate consists of well-formed crystals with sharply defined edges and the β -hemihydrate is flaky and made up of small crystals. Their reactivities with water are not identical and the mechanical properties of the hydrated hemihydrates are different, with the α -hemihydrate forming stronger gypsum plasters.¹¹⁹

Gypsum plasters are commonly used in building materials, ceramics and medical industries.¹²⁰ There has been a significant amount of effort placed towards elucidating the processes that occur upon hydration of the hemihydrate. On mixing the hemihydrate with water, the following exothermic reaction occurs:



The hemihydrate has a low solubility in water (6.5 g L^{-1}) and a saturated solution is quickly obtained. The dihydrate has an almost three times lower solubility (2.4 g L^{-1}) and needle-like crystals of the dihydrate nucleate and precipitate which interlock to form a rigid, highly porous material.¹²⁰

To investigate the setting process further, the electrical resistance of the gypsum paste during hardening was monitored and it was found that it involved three separate steps. The first point of interest was a minimum in the resistance between 5-10 minutes (induction period) which is where there is a maximum solubility of Ca^{2+} and SO_4^{2-} ions. After this, there was a large increase in electrical resistance over the next 100 minutes, attributed to the formation of dihydrate needles. Finally, it reached a relatively constant value with only slight increases due to the final drying of the material.

The mechanical properties of gypsum plasters over time were also investigated. Plasters of both the α -form and β -form followed similar trends, however, the α -form was stronger during the whole process of hardening. An initial maximum in fracture stress was obtained after approximately one hour, followed by a decrease. This decrease has been attributed to two different reasons: firstly, a build-up of internal stress due to the growth of dihydrate needles within the hardened paste and secondly, thermal gradients within the material due to the exothermic hydration reaction could

lead to microcracking. A final maximum in fracture stress was found after 15-20 hours that was approximately twice that of the initial maximum. This was explained due to the drying and precipitation of the final dihydrate needles.¹²¹

Gypsum based composites are widely exploited in building materials for their passive fire resistance. Their low thermal conductivity, combined with the large amount of energy required to evaporate the water present in the gypsum makes them ideal barriers for delaying rise in temperatures.¹²²

1.4. Presentation of this thesis

Chapter 2 details the materials used throughout this thesis and describes all experimental methods and instrumentation used for analysis and characterisation.

The experiments investigating the thermal and mechanical properties of porous and hierarchically porous gypsum composites produced using hydrogel templating and viscous trapping techniques are summarised in Chapter 3.

The same methods from Chapter 3 were used to produce porous and hierarchically porous gypsum composites again. However, their acoustical properties are investigated and described in Chapter 4.

In Chapter 5, the first investigations of a household product with hydrogel beads incorporated within are described. Here, soap bars were produced which contained various amounts of hydrogel beads. Their dissolution rates, mechanical properties and release rate of encapsulated active species within the hydrogel beads used are discussed.

The synergistic behaviour between agar and MC when used together to formulate a binary hydrogel was investigated. Their stability to heat treatment, rheological behaviour and structures were studied and the results are presented in Chapter 6.

By exploiting the thermal stability of the binary hydrogels produced in Chapter 6, the production of pancakes with hydrogel beads incorporated within was performed. An investigation into the health benefits of these composites was an enjoyable and fruitful final project. The reader can find the results in Chapter 7.

The summary of the conclusions and suggestions for future work are described in Chapter 8.

1.5. References

- 1 M. Rutkevičius, S. K. Munusami, Z. Watson, A. D. Field, M. Salt, S. D. Stoyanov, J. Petkov, G. H. Mehl and V. N. Paunov, *Mater. Res. Bull.*, 2012, **47**, 980–986.
- 2 A. Feinle, M. S. Elsaesser and N. Hüsing, *Chem. Soc. Rev.*, 2016, **45**, 3377–3399.
- 3 D. Schneider, D. Mehlhorn, P. Zeigermann, J. Kärger and R. Valiullin, *Chem. Soc. Rev.*, 2016, **45**, 3439–3467.
- 4 W. J. Roth, B. Gil, W. Makowski, B. Marszalek and P. Eliasova, *Chem. Soc. Rev.*, 2015, 3400–3438.
- 5 K. A. Cychoz, R. Guillet-Nicolas, J. Garcia-Martinez and M. Thommes, *Chem. Soc. Rev.*, 2017, **46**, 389–414.
- 6 Q. Sun, Z. Dai, X. Meng and F.-S. Xiao, *Chem. Soc. Rev.*, 2015, **44**, 6018–6034.
- 7 C. Z. Yuan, B. Gao, L. F. Shen, S. D. Yang, L. Hao, X. J. Lu, F. Zhang, L. J. Zhang and X. G. Zhang, *Nanoscale*, 2011, **3**, 529–545.
- 8 M. Wang, X. Yu, Z. Wang, Z. Guo and L. Dai, *J. Mater. Chem. A*, 2017, **5**, 9488–9513.
- 9 M.-H. Sun, S.-Z. Huang, L.-H. Chen, Y. Li, X.-Y. Yang, Z.-Y. Yuan and B.-L. Su, *Chem. Soc. Rev.*, 2016, **45**, 3479–3563.
- 10 X.-Y. Yang, L.-H. Chen, Y. Li, J. C. Rooke, C. Sanchez and B.-L. Su, *Chem. Soc. Rev.*, 2017, **46**, 481–558.
- 11 C. M. a Parlett, K. Wilson and A. F. Lee, *Chem. Soc. Rev.*, 2013, **42**, 3876–3893.
- 12 X.-Y. Yang, Y. Li, A. Lemaire, J.-G. Yu and B.-L. Su, *Pure Appl. Chem.*, 2009, **81**, 2265–2307.
- 13 J. Rouquerolt, D. Avnir, C. W. Fairbridge, D. H. Everett, J. H. Haynes, N. Pernicone, J. D. F. Ramsay, K. S. W. Sing and K. K. Unger, *Pure Appl. Chem.*, 1994, **66**, 1739–1758.

- 14 A. Vantomme, A. Léonard, Z. Y. Yuan and B. L. Su, *Colloids Surf., A*, 2007, **300**, 70–78.
- 15 H. K. and Y. D. and H. S. and H. Deping, *J. Phys. D. Appl. Phys.*, 2011, **44**, 365405.
- 16 H. Yu, A. Fisher, D. Cheng and D. Cao, *ACS Appl. Mater. Interfaces*, 2016, **8**, 21431–21439.
- 17 P. Fratzl and R. Weinkamer, *Prog. Mater. Sci.*, 2007, **52**, 1263–1334.
- 18 B.-L. Su, C. Sanchez and X.-Y. Yang, Insights into Hierarchically Structured Porous Materials: From Nanoscience to Catalysis, Separation, Optics, Energy and Life Science, in *Hierarchically Structured Porous Materials*, ed. B.-L. Su, C. Sanchez and X.-Y. Yang, Wiley-VCH Verlag GmbH & Co. KGaA, 2011, ch. 1, pp. 1–27.
- 19 P. Colombo, C. Vakifahmetoglu and S. Costacurta, *J. Mater. Sci.*, 2010, **45**, 5425–5455.
- 20 Ö. Sel and B. M. Smarsly, Hierarchically Structured Porous Materials by Dually Micellar Templating Approach, in *Hierarchically Structured Porous Materials*, ed. B.-L. Su, C. Sanchez and X.-Y. Yang, Wiley-VCH Verlag GmbH & Co. KGaA, 2011, ch. 3, pp. 41–53.
- 21 R. Nagarajan, *Langmuir*, 1985, **1**, 331–341.
- 22 O. Sel, D. Kuang, M. Thommes and B. Smarsly, *Langmuir*, 2006, **22**, 2311–2322.
- 23 G. Widawski, M. Rawiso and B. Francois, *Nature*, 1994, **369**, 387–389.
- 24 A. Zhang, H. Bai and L. Li, *Chem. Rev.*, 2015, **115**, 9801–9868.
- 25 A. Boker, Y. Lin, K. Chiapperini, R. Horowitz, M. Thompson, V. Carreon, T. Xu, C. Abetz, H. Skaff, A. D. Dinsmore, T. Emrick and T. P. Russell, *Nat. Mater.*, 2004, **3**, 302–306.
- 26 M. Srinivasarao, D. Collings, A. Philips and S. Patel, *Science*, 2001, **292**, 79–83.
- 27 L. Qian and H. Zhang, *J. Chem. Technol. Biotechnol.*, 2011, **86**, 172–184.

- 28 H.-W. Kang, Y. Tabata and Y. Ikada, *Biomaterials*, 1999, **20**, 1339–1344.
- 29 M. L. Ferrer, R. Esquembre, I. Ortega, C. R. Mateo and F. del Monte, *Chem. Mater.*, 2006, **18**, 554–559.
- 30 S. Deville, *Adv. Eng. Mater.*, 2008, **10**, 155–169.
- 31 N. D. Petkovich and A. Stein, Colloidal Crystal Templating Approaches to Materials with Hierarchical Porosity, in *Hierarchically Structured Porous Materials*, ed. B.-L. Su, C. Sanchez and X.-Y. Yang, Wiley-VCH Verlag GmbH & Co. KGaA, 2011, ch. 4, pp. 55–129.
- 32 A. Stein, F. Li and N. R. Denny, *Chem. Mater.*, 2008, **20**, 649–666.
- 33 Y. Yin and Y. Xia, *Adv. Mater.*, 2001, **13**, 267–271.
- 34 O. D. Velev, T. A. Jede, R. F. Lobo and A. M. Lenhoff, *Nature*, 1997, **389**, 447–448.
- 35 M. Antonietti, B. Berton, C. Göltner and H.-P. Hentze, *Adv. Mater.*, 1998, **10**, 154–159.
- 36 P. Yang, T. Deng, D. Zhao, P. Feng, D. Pine, B. F. Chmelka, G. M. Whitesides and G. D. Stucky, *Science*, 1998, **282**, 2244–2246.
- 37 B. T. Holland, L. Abrams and A. Stein, *J. Am. Chem. Soc.*, 1999, **121**, 4308–4309.
- 38 O. D. Velev, P. M. Tessier, A. M. Lenhoff and E. W. Kaler, *Nature*, 1999, **401**, 548.
- 39 X. Li, J. Jiang, Y. Wang, X. Nie and F. Qu, *J. Sol-Gel Sci. Technol.*, 2010, **56**, 75–81.
- 40 J. Bibette and F. Leal-Calderon, *Curr. Opin. Colloid Interface Sci.*, 1996, **1**, 746–751.
- 41 B. P. Binks, *Langmuir*, 2017, **33**, 6947–6963.
- 42 B. P. Binks, *Curr. Opin. Colloid Interface Sci.*, 2002, **7**, 21–41.
- 43 L. L. C. Wong, P. M. Baiz Villafranca, A. Menner and A. Bismarck, *Langmuir*, 2013, **29**, 5952–5961.

- 44 S. Huš, M. Kolar and P. Krajnc, *Des. Monomers Polym.*, 2015, **18**, 698–703.
- 45 M. Sušec, S. C. Ligon, J. Stampfl, R. Liska and P. Krajnc, *Macromol. Rapid Commun.*, 2013, **34**, 938–943.
- 46 B. Zhao and M. M. Collinson, *Chem. Mater.*, 2010, **22**, 4312–4319.
- 47 M. Breulmann, S. A. Davis, S. Mann, H. P. Hentze and M. Antonietti, *Adv. Mater.*, 2000, **12**, 502–507.
- 48 L. Meng, X. Zhang, Y. Tang, K. Su and J. Kong, *Sci. Rep.*, 2015, **5**, 7910.
- 49 A. Kumar, F. Ciucci, A. N. Morozovska, S. V Kalinin and S. Jesse, *Nat. Chem.*, 2011, **3**, 707–713.
- 50 Z. Hu, Z. Zhang, Z. Li, M. Dou and F. Wang, *ACS Appl. Mater. Interfaces*, 2017, **9**, 16109–16116.
- 51 J. Tang, R. R. Salunkhe, J. Liu, N. L. Torad, M. Imura, S. Furukawa and Y. Yamauchi, *J. Am. Chem. Soc.*, 2015, **137**, 1572–1580.
- 52 Y. Zhao, Q. Lai, Y. Wang, J. Zhu and Y. Liang, *ACS Appl. Mater. Interfaces*, 2017, **9**, 16178–16186.
- 53 A. Corma and H. García, *Chem. Rev.*, 2003, **103**, 4307–4366.
- 54 J. D. A. Pelletier and J.-M. Basset, *Acc. Chem. Res.*, 2016, **49**, 664–677.
- 55 W. Yan, B. Chen, S. M. Mahurin, S. Dai and S. H. Overbury, *Chem. Commun.*, 2004, 1918–1919.
- 56 Y. Men, H. Gnaser, R. Zapf, V. Hessel, C. Ziegler and G. Kolb, *Appl. Catal. A*, 2004, **277**, 83–90.
- 57 M. R. Avhad and J. M. Marchetti, *Catal. Rev.*, 2016, **58**, 157–208.
- 58 K. Hagedorn, U. Bahnmüller, A. Schachtschneider, M. Frei, W. Li, J. Schmedt auf der Günne and S. Polarz, *ACS Appl. Mater. Interfaces*, 2017, **9**, 11599–11608.
- 59 M. Trueba and S. P. Trasatti, *Eur. J. Inorg. Chem.*, 2005, **2005**, 3393–3403.
- 60 M. Trombetta, G. Busca, S. A. Rossini, V. Piccoli and U. Cornaro, *J. Catal.*,

- 1997, **168**, 334–348.
- 61 A. Zaherian, M. Kazemeini, M. Aghaziarati and S. Alamolhoda, *J. Porous Mater.*, 2013, **20**, 151–157.
- 62 S. Shafiee and E. Topal, *Energy Policy*, 2009, **37**, 181–189.
- 63 R. Zhang, Y. Zhang, K. Zhu, F. Du, Q. Fu, X. Yang, Y. Wang, X. Bie, G. Chen and Y. Wei, *ACS Appl. Mater. Interfaces*, 2014, **6**, 12523–12530.
- 64 Y. Cheng, W. Zhou, K. Feng, H. Zhang, X. Li and H. Zhang, *RSC Adv.*, 2017, **7**, 38415–38423.
- 65 Z.-X. Chi, W. Zhang, X.-S. Wang, F.-Q. Cheng, J.-T. Chen, A.-M. Cao and L.-J. Wan, *J. Mater. Chem. A*, 2014, **2**, 17359–17365.
- 66 J. Yang, J. Wang, Y. Tang, D. Wang, B. Xiao, X. Li, R. Li, G. Liang, T.-K. Sham and X. Sun, *J. Mater. Chem. A*, 2013, **1**, 7306–7311.
- 67 R. P. Schwarzenbach, B. I. Escher, K. Fenner, T. B. Hofstetter, C. A. Johnson, U. von Gunten and B. Wehrli, *Science*, 2006, **313**, 1072–1077.
- 68 M. A. Shannon, P. W. Bohn, M. Elimelech, J. G. Georgiadis, B. J. Marinas and A. M. Mayes, *Nature*, 2008, **452**, 301–310.
- 69 J. Zhang, Z. Meng, J. Liu, C. Schlaich, Z. Yu and X. Deng, *J. Mater. Chem. A*, 2017, 16369–16375.
- 70 L. Li, Z. Liu, Q. Zhang, C. Meng, T. Zhang and J. Zhai, *J. Mater. Chem. A*, 2015, **3**, 1279–1286.
- 71 X. Ge, J. Liu, X. Song, G. Wang, H. Zhang, Y. Zhang and H. Zhao, *Chem. Eng. J.*, 2016, **301**, 139–148.
- 72 W. Chen, R. Parette, J. Zou, F. S. Cannon and B. A. Dempsey, *Water Res.*, 2007, **41**, 1851–1858.
- 73 S. Shevade and R. G. Ford, *Water Res.*, 2004, **38**, 3197–3204.
- 74 Z. Wu, W. Li, P. A. Webley and D. Zhao, *Adv. Mater.*, 2012, **24**, 485–491.
- 75 X. Ge, Y. Ma, X. Song, G. Wang, H. Zhang, Y. Zhang and H. Zhao, *ACS Appl. Mater. Interfaces*, 2017, **9**, 13480–13490.

- 76 L. Nie, K. Deng, S. Yuan, W. Zhang and Q. Tan, *Mater. Lett.*, 2014, **132**, 369–372.
- 77 Q. Zhang, B. Chen, L. Tao, M. Yan, L. Chen and Y. Wei, *RSC Adv.*, 2014, **4**, 32475–32481.
- 78 X. Wu, Y. Han, X. Zhang and C. Lu, *Phys. Chem. Chem. Phys.*, 2017, **19**, 16198–16205.
- 79 J. Du, R. Yue, F. Ren, Z. Yao, F. Jiang, P. Yang and Y. Du, *Gold Bull.*, 2013, **46**, 137–144.
- 80 A. Nsabimana, J. Lai, S. Li, P. Hui, Z. Liu and G. Xu, *Analyst*, 2017, **142**, 478–484.
- 81 J. R. Jones, L. M. Ehrenfried and L. L. Hench, *Biomaterials*, 2006, **27**, 964–973.
- 82 X. Yan, C. Yu, X. Zhou, J. Tang and D. Zhao, *Angew. Chemie Int. Ed.*, 2004, **43**, 5980–5984.
- 83 D. Onna, Y. Minaberry and M. Jobbagy, *J. Mater. Chem. B*, 2015, **3**, 2971–2977.
- 84 M. N. Rahaman, D. E. Day, B. Sonny Bal, Q. Fu, S. B. Jung, L. F. Bonewald and A. P. Tomsia, *Acta Biomater.*, 2011, **7**, 2355–2373.
- 85 M. Xu, D. Zhai, L. Xia, H. Li, S. Chen, B. Fang, J. Chang and C. Wu, *Nanoscale*, 2016, **8**, 13790–13803.
- 86 K.-Y. Chen, W.-J. Liao, S.-M. Kuo, F.-J. Tsai, Y.-S. Chen, C.-Y. Huang and C.-H. Yao, *Biomacromolecules*, 2009, **10**, 1642–1649.
- 87 A. W. Hixson and J. H. Crowell, *Ind. Eng. Chem.*, 1931, **23**, 923–931.
- 88 J. Siepmann and F. Siepmann, *Int. J. Pharm.*, 2013, **453**, 12–24.
- 89 T. Yang, Y. Hu, C. Wang and B. P. Binks, *ACS Appl. Mater. Interfaces*, 2017, **9**, 22950–22958.
- 90 P. J. Flory, *Principles of Polymer Chemistry*, Cornell University Press, Ithaca, NY, 1953.

- 91 K. Almdal, J. Dyre, S. Hvidt and O. Kramer, *Polym. Gels Networks*, 1993, **1**, 5–17.
- 92 G. O. Phillips and P. A. Williams, 1 - Introduction to Food Hydrocolloids, in *Handbook of Hydrocolloids*, ed. G. O. Phillips and P. A. Williams, Woodhead Publishing Limited, Cambridge, 2nd edn., 2009, ch. 1, pp. 1–22.
- 93 B. Xue, V. Kozlovskaya, F. Liu, J. Chen, J. F. Williams, J. Campos-Gomez, M. Saeed and E. Kharlampieva, *ACS Appl. Mater. Interfaces*, 2015, **7**, 13633–13644.
- 94 C. H. Araki, *J. Chem. Soc. Jpn.*, 1937, **58**, 1338–1350.
- 95 I. T. Norton, D. M. Goodall, K. R. J. Austen, E. R. Morris and D. A. Rees, *Biopolymers*, 1986, **25**, 1009–1029.
- 96 C. Araki, *Bull. Chem. Soc. Jpn.*, 1956, **29**, 543–544.
- 97 S. Arnott, A. Fulmer, W. E. Scott, I. C. M. Dea, R. Moorhouse and D. A. Rees, *J. Mol. Biol.*, 1974, **90**, 269–284.
- 98 I. C. M. Dea, A. A. McKinnon and D. A. Rees, *J. Mol. Biol.*, 1972, **68**, 153–172.
- 99 K. B. Guiseley, *Carbohydr. Res.*, 1970, **13**, 247–256.
- 100 K. C. Labropoulos, D. E. Niesz, S. C. Danforth and P. G. Kevrekidis, *Carbohydr. Polym.*, 2002, **50**, 407–415.
- 101 R. Armisén and F. Gaiatas, 4 - Agar, in *Handbook of Hydrocolloids*, ed. G. O. Phillips and P. A. Williams, Woodhead Publishing Limited, Cambridge, 2nd edn., 2009, ch. 4, pp. 82–107.
- 102 M. Leone, F. Sciortino, M. Migliore, S. L. Fornili and M. B. P. Vittorelli, *Biopolymers*, 1987, **26**, 743–761.
- 103 P. L. San Biagio, D. Bulone, A. Emanuele, M. B. Palma-Vittorelli and M. U. Palma, *Food Hydrocoll.*, 1996, **10**, 91–97.
- 104 S. Boral and H. B. Bohidar, *J. Phys. Chem. B*, 2012, **116**, 7113–7121.
- 105 J. C. F. Murray, 25 - Cellulosics, in *Handbook of Hydrocolloids*, ed. G. O.

- Phillips and P. A. Williams, Woodhead Publishing Limited, Cambridge, 2nd edn., 2009, ch. 25, pp. 710–723.
- 106 E. Heymann, *Trans. Faraday Soc.*, 1935, **31**, 846–864.
- 107 T. Kato, M. Yokoyama and A. Takahashi, *Colloid Polym. Sci.*, 1978, **256**, 15–21.
- 108 A. Haque and E. R. Morris, *Carbohydr. Polym.*, 1993, **22**, 161–173.
- 109 K. Kobayashi, C. Huang and T. P. Lodge, *Macromolecules*, 1999, **32**, 7070–7077.
- 110 S. A. Arvidson, J. R. Lott, J. W. McAllister, J. Zhang, F. S. Bates, T. P. Lodge, R. L. Sammler, Y. Li and M. Brackhagen, *Macromolecules*, 2013, **46**, 300–309.
- 111 J. R. Lott, J. W. McAllister, S. A. Arvidson, F. S. Bates and T. P. Lodge, *Biomacromolecules*, 2013, **14**, 2484–2488.
- 112 J. W. McAllister, J. R. Lott, P. W. Schmidt, R. L. Sammler, F. S. Bates and T. P. Lodge, *ACS Macro Lett.*, 2015, **4**, 538–542.
- 113 P. L. Nasatto, F. Pignon, J. L. M. Silveira, M. E. R. Duarte, M. D. Nosedá and M. Rinaudo, *Polymers.*, 2015, **7**, 777–803.
- 114 J. Borreani, M. Espert, A. Salvador, T. Sanz, A. Quiles and I. Hernando, *Food Funct.*, 2017, **8**, 1547–1557.
- 115 D. Saha and S. Bhattacharya, *J. Food Sci. Technol.*, 2010, **47**, 587–597.
- 116 M. Tomšič, F. Prossnigg and O. Glatter, *J. Colloid Interface Sci.*, 2008, **322**, 41–50.
- 117 J. Bensted and S. P. Verma, *Cem. Technol*, 1972, **3**, 67–70.
- 118 H.-J. Kuzel and M. Hauner, *Zement-Kalk-Gips*, 1987, **40**, 628–632.
- 119 M. E. Enayetallah, A. A. Khalil and A. M. Gadalla, *Trans. J. Br. Ceram. Soc.*, 1977, **76**, 95–104.
- 120 A. J. Lewry and J. Williamson, *J. Mater. Sci.*, 1994, **29**, 5279–5284.
- 121 A. J. Lewry and J. Williamson, *J. Mater. Sci.*, 1994, **29**, 5524–5528.

122 Y. W. I. Rahmanian, *Acta Polytech.*, 2009, **49**, 16-20.

2. Experimental

In this chapter, the materials and experimental methods used throughout this research are described.

2.1. Materials

2.1.1. Hydrocolloids

Agar (food grade) was purchased from Special Ingredients. Methylcellulose (MC) (Methocel A4M and Methocel SG A7C, food grade) were gifts from The Dow Chemical Company. MC solution (A4M, 2.0% w/v) has a viscosity of 4000 cPs and MC solution (SG A7C, 2.0% w/v) has a viscosity of 700 cPs. Furthermore, the SG A7C MC forms stronger gels and gelation occurs at lower temperatures. The A4M grade MC is used for the viscous trapping methods described in Chapters 3-4 whilst the SG A7C grade MC is used for everything else.

2.1.2. Matrix materials

These are the materials that are templated with hydrogel beads to produce porous materials (gypsum) or composite materials (soap base, pancake batter). Gypsum is also templated with a viscous hydrocolloid solution (MC) to produce a porous composite material.

2.1.2.1. Gypsum

Gypsum powder ($\text{CaSO}_4 \cdot \frac{1}{2}\text{H}_2\text{O}$, < 3% crystalline silica impurities, Lafarge Prestia) was purchased from Fred Aldous: Art, design and craft supplies.

2.1.2.2. Soap base

A soap base was purchased from a local shop (Hobbycraft) and the main components were sodium stearate, glycerol and water.

2.1.2.3. Bakery ingredients for pancake batter

Plain flour, UK standard medium size eggs, semi-skimmed milk and butter were purchased from a local shop (Tesco).

2.1.3. Water

Water was purified by passing through an Elgastat Prima Reverse Osmosis Unit followed by a Millipore Milli-Q reagent water system consisting of one carbon filter and two ion-exchange filters.

2.1.4. Solvents

The solvents acetone ($\geq 99.8\%$) and ethanol ($\geq 99.8\%$) for cleaning glassware, microscope slides etc. were all analytical grade and purchased from VWR Chemicals. Silicon oil (40 cPs) was purchased from Alfa Aesar.

2.1.5. Other chemicals

Berberine chloride form (BBR, 98%) was purchased from Sigma-Aldrich, methylene blue (MB, high purity) was purchased from Lancaster Synthesis Ltd and poly(sodium 4-styrenesulfonate) (PSS) with a weight average molecular mass (M_w) of ca. 70 000 g mol⁻¹ was purchased from Sigma-Aldrich.

2.2. Characterisation equipment

2.2.1. Microscopy

2.2.1.1. Optical microscopy

Hydrogel beads were dispersed in water and images taken in bright field light using an Olympus BX-51 optical microscope fitted with DP70 CCD camera. The objective used was always 4x and the image analysis software used was Image Pro Plus 6. Size distributions were obtained by measuring 150-300 hydrogel beads from several fields of view using the software ImageJ.

2.2.1.2. *Scanning electron microscopy*

A bench-top Hitachi TM-1000 scanning electron microscope (SEM) was used to visualise the porous gypsum composites, which were left uncoated. It was also used to image the freeze-dried pancake and pancake-hydrogel composites after they were gold coated. These samples were sputter coated using a Polaron model SC7640 fitted with an annular alloy foil (82% Au/18% Pd) sputtering source. The process was performed at 2-4 Pa argon pressure, 1.5 kV and 20 mA to produce a gold coating with thickness of approximately 2 nm which was automatically terminated. The samples were rotated during the sputter coating. A fragment of each sample was stuck to an aluminium SEM stub *via* the use of a double sided adhesive carbon disc.

2.2.1.3. *Cryogenic scanning electron microscopy*

Samples of MC solution (1.0% w/v), agar hydrogel (1.0% w/v) and agar-MC hydrogel (1.0% w/v : 1.0% w/v) were mounted on a copper SEM stub, flash frozen in slush nitrogen (~ -210 °C) then transferred to the preparation stage at -140 °C where they were fractured with a blade that was cooled to the same temperature. Slushing reduces the N₂ temperature by about 14 °C to -210 °C and minimises boiling and the Leidenfrost effect upon sample freezing.¹ The samples were then sublimed at -70°C and 2-4 Pa for 7 mins and transferred onto a cryo-SEM cool stage in the preparation chamber under vacuum. The sample was then fractured and coated with an electro-conductive coating (Pt) by using an integrated sputter coater. Finally, they were transferred into the SEM chamber of a Zeiss Evo 60 Scanning Electron Microscope and visualised at at -140 °C with an accelerating voltage of 15 kV.

2.2.2. **Measurement of thermal conductivity**

Before any measurements, the cartridge heater (6.5 mm diameter, 60 mm height, purchased from RS components) was calibrated by the following procedure: A known mass of water was poured into a double jacketed calorimeter and the heater and a thermocouple (k-type, with a resolution of 0.1 °C) were fully submerged. The calorimeter was sealed with a rubber bung which had space for the heater's wires and thermocouple to connect to a power supply and data logger (HH306A data logger thermometer, purchased from Omega), respectively. A constant current of 160 mA

was supplied to the heater and the measured temperature change over time was used to calculate the power output as follows:

$$Q = \frac{mC_p\Delta T}{t}. \quad (2.1)$$

Here Q is the power output (W), m is the mass of the water (g), C_p is the specific heat capacity of water ($4.184 \text{ J g}^{-1} \text{ K}^{-1}$), ΔT is temperature change of the water (K) and t is time (s). This experiment was performed three times to give an average power output of $2.10 \pm 0.05 \text{ W}$. For testing of the gypsum control sample and the porous gypsum composites, the sample was placed inside a cylindrical water jacket that was open at both ends (inner dimensions were 60 mm diameter and 180 mm length). The samples were moulded in such a way that they fit inside the water jacket and were in contact with the water-cooled ($15 \text{ }^\circ\text{C}$) glass surfaces. The heater was placed in the hole in the centre of the composites which travels the full length of the sample. Three thermocouples were placed in the sample at three different distances from the heater and to a depth of half the sample height. Addition of insulating foam to both ends of the sample was done to minimise any axial heat loss. The heater was then switched on and the sample was heated until it reached steady state. Once steady state was achieved, the temperatures at each location could be used to calculate the thermal conductivity using the following equation:²

$$\kappa = \frac{Q \ln\left(\frac{r_x}{r_1}\right)}{2\pi L \Delta T}. \quad (2.2)$$

Here κ is the thermal conductivity ($\text{W m}^{-1} \text{ K}^{-1}$), r_1 is the distance between the centre of the sample and the closest thermocouple (m), r_x is the distance between the centre of the sample and the thermocouple at location x (m), L is the length of the sample (m) and ΔT is the temperature difference between the thermocouple at location 1 and the thermocouple at location x .

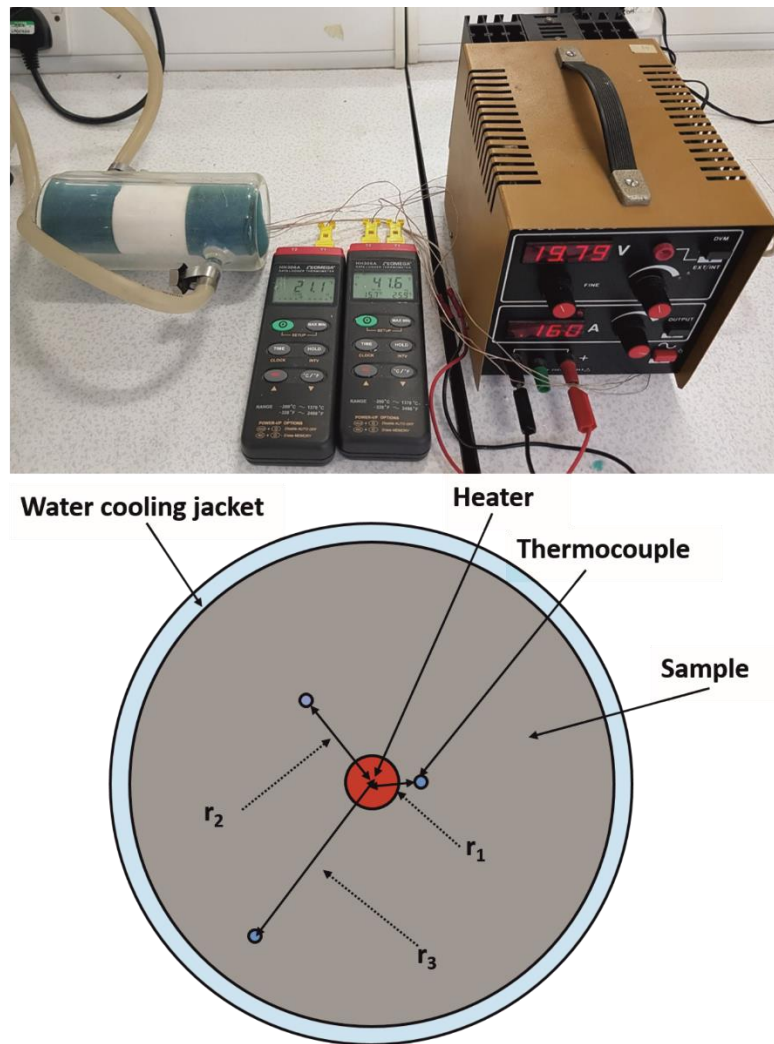


Figure 2.1. The top image shows the radial heat flow experimental setup for measuring the thermal conductivity of the porous gypsum composites. The bottom image shows an illustration of a cross-section of a sample during a measurement.

2.2.3. Acoustical analysis

An impedance tube was designed and produced in-house according to ASTM E2611-09.³ Briefly, a cylindrical aluminium tube with an internal diameter of 76.2 mm and a wall thickness of 12.7 mm was used. The cut off frequency of the tube was 2600 Hz. Four spaces for microphones were made that had a spacing of 50 mm and the distance from the sample to the closest microphone on each side was 65 mm. Anechoic termination in the form of a 400 mm long foam cylinder was placed in the downstream region, topped with a wedge that had an angle of 28° which has been shown to produce the best sound absorbing properties.⁴ In order to allow the full development of plane

waves within the impedance tube, the distance between the sound source and the first microphone was 250 mm. White noise was generated in the upstream tube and a single capacitor microphone (type 4939-L-002 $\frac{1}{4}$ inch free-field microphone with type 2669-L preamplifier, purchased from Bruel & Kjaer (B&K)) was used to measure the sound pressures at four different locations in the impedance tube. The holes that didn't contain the microphone were plugged. Each sample was moulded into dimensions that were a close fit in the sample holder, and petroleum jelly (Vaseline) was used when mounting the sample to stop any sound pressure leakage.⁵ Venting plugs were utilised at each side of the impedance tube that were removed during sample mounting and then replaced during the testing. This prevents any displacement of the sample after mounting due to compression of air when fitting the sample holder into the tube. The procedure utilises a transfer matrix method for the calculation. Sound pressures over time during the experiments were measured at four different locations; two upstream and two downstream of the sample. The data was collected using VirtualBench-Scope 2.6 software. These sound pressures, along with a reference signal from the sound source, were used to calculate four complex transfer functions, which were then used to determine the STL. The full procedure for calculating STL is found in ASTM E2611-09. Each STL spectrum presented is an average of 10 runs.

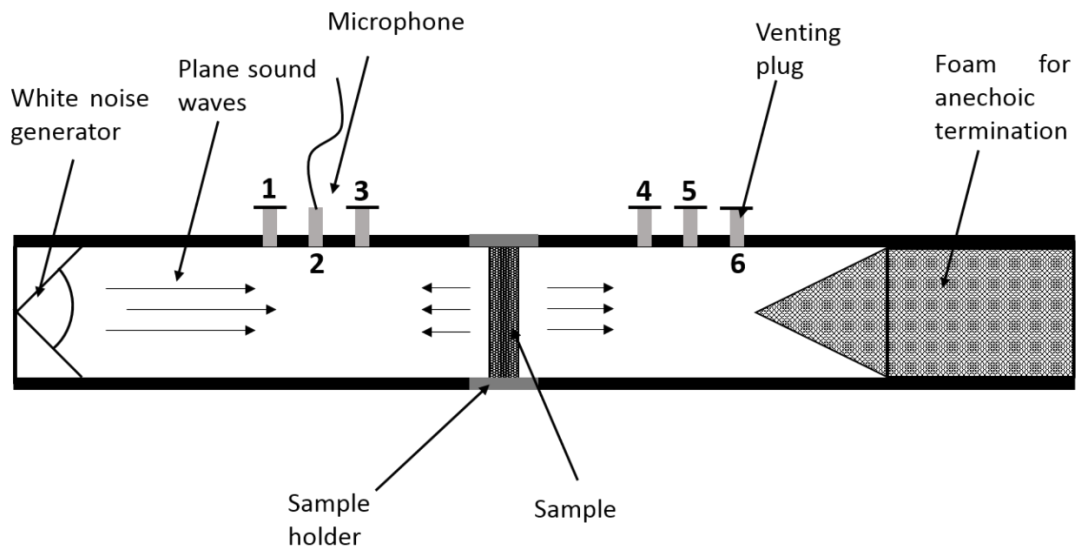


Figure 2.2. Schematic of the impedance tube used for measuring STL. The microphone at position 2 was moved to positions 3, 4 and 5 to obtain sound pressures at four different locations for determination of the complex transfer functions. Positions 1 and 6 were for the venting plugs.

2.2.4. Dissolution rates

An investigation into how the volume percentage of hydrogel beads incorporated within the soap composites affected their dissolution rate compared to the control sample of soap alone was performed. Samples of the same shape and surface area were placed into a sample holder then submerged in water (750 cm³, 30.0 ± 0.2 °C). The holder consisted of a metal wire basket designed in-house to allow maximum exposure of the sample to warm water. Dissolution was encouraged *via* agitation with a magnetic stirrer bar (35 mm length, 6 mm width) rotating on a magnetic stirrer at 600 rpm. The conductance of the solution as a function of time passed since the sample was added to water was measured using a Jenson 4510 Bench Conductivity Meter. Care was taken to have the sample and the probe in the same position in each measurement. The conductance was compared with a calibration curve to elucidate the dissolution rate over a period of 120 seconds.

2.2.5. UV-vis

A Perkin Elmer Lambda Bio-10 UV-Vis spectrometer with UV WinLab v.6.0.4 software was used to determine the absorbance of two different species of interest; MB and BBR. A calibration graph for each species of absorbance at λ_{\max} wavelength versus concentration was produced. This was done by preparing solutions of known concentrations in water and analysing them spectrophotometrically over the wavelength range 200-700 nm. The instrument was configured to subtract the absorbance of the cuvette and water, allowing measurement of only the species of interest. The quartz cuvette used had a path length of 1 cm and contained a maximum volume of 1 cm³. The λ_{\max} wavelengths for MB and BBR were 664 nm and 422 nm, respectively. Upon production of the calibration graphs, solutions of unknown concentration were able to be analysed.

2.2.6. Release rates from soap-hydrogel composites

BBR solution (0.15% w/v) was gelled with agar (either 2.0% w/v or 8.0% w/v). MB solution was mixed with PSS solution so that the overall concentrations were 0.01 M MB and either 0.1% or 0.25% w/v PSS, respectively. This solution was gelled using agar (2.0% w/v). The resulting hydrogels were then blended for either 10 seconds or

300 seconds to produce slurries of large or small beads. Then, the soap-hydrogel composites were prepared with 50% volume percentage of hydrogel beads. The composites were immersed in water (200 cm³, 30.0 ± 0.2 °C) whilst being agitated with a magnetic stirrer bar at 600 rpm. Aliquots from the surrounding solution were taken at certain time intervals and their UV-visible spectra measured to obtain the release rate, with the utmost care to take each sample from the same position each time. The effect of the hydrogel bead size, agar concentration in the hydrogel and the concentration of an oppositely charged polyelectrolyte (PSS) on the release rate of encapsulated compounds was investigated.

2.2.7. Rheology

All rheological measurements were performed using a Bohlin CVO 120 rheometer (Malvern Instruments) with a 20 mm diameter parallel plate geometry and a gap size of 2200 µm. Temperature control was done with the use of a Peltier plate. Oscillatory tests were performed and the storage modulus at 25 °C, 40 °C, 55 °C, 70 °C and 85 °C was measured at increasing shear stress from 1 - 100 Pa. The frequency used was always 1 Hz. At each temperature, the sample was equilibrated for 30 seconds prior to being measured. To prevent evaporation of water from the agar and agar-MC hydrogels during testing, a thin layer of low viscosity silicone oil (40 cPs) was added to their surface.

2.2.8. Calorimetry

2.2.8.1. Differential scanning calorimetry

DSC measurements were carried out on agar-MC hydrogel (1.0% w/v - 1.0% w/v) using a NETZSCH DSC 214 *Polyma* differential scanning calorimeter. The hydrogel sample of approximately 100 mg was placed into a medium pressure steel crucible and sealed. An equal mass of water was used as a reference. The sample was heated from 10 °C to 100 °C with a heating rate of 2 °C / min then cooled from 100 °C to 10 °C at the same rate.

2.2.8.2. Bomb calorimetry

Samples of approximately equal mass and shape were cut from each composite and their mass recorded. They were then placed in open polypropylene tubes and frozen in liquid nitrogen for 15 minutes. Subsequently, the tube was covered with a tissue, transferred to a freeze drier and dried for 72 hours (-84 °C, 1.6 Pa). The masses of the dried samples were recorded. They were ground to a fine powder and pellets of roughly 1 g mass were pressed. A 1341 Plain Jacket Bomb Calorimeter (Parr Instruments Company) was used for all measurements. Benzoic acid was used as a standard to calculate the calorimeter constant as its heat of combustion is well documented.⁶ A pellet was placed into the crucible. Fuse wire (Ni-Cr) was cut, weighed, then wrapped around the bomb terminals and put into contact with the sample. Water (1.00 cm³) was added to the bomb which was then assembled and pressurised with oxygen (20 atm). The chamber was filled with water (2000 cm³) and the bomb was placed inside. Two electrodes were connected to the bomb, then a lid with a stirrer and digital thermometer of resolution of 0.001 °C (model 6775, Parr Instruments Company) connected was placed on top of the calorimeter and the temperature was measured as a function of time. After equilibration, the samples were ignited. The temperature was continually recorded until it stabilised. The bomb was then removed from the chamber, depressurised and washed for next use. Any remaining fuse wire was weighed. This method was also applied with the pancake and pancake-hydrogel samples.

2.2.9. Temperature stability

2.2.9.1. High temperature

The high temperature stability was investigated by subjecting hydrogel samples of equal mass and surface area to two different high temperature environments. The first test involved placing a sample of agar hydrogel (2.0% w/v) and a sample of agar-MC hydrogel (1.0% w/v : 1.0% w/v) into a furnace at 150 °C for 45 minutes whilst the second involved immersing a sample of each hydrogel into water (200 cm³) and autoclaving at 121 °C (Classic Prestige Medical autoclave, 105 kPa).

2.2.9.2. *Low temperature*

The freeze thaw stability of agar-MC hydrogel (1.0% w/v - 1.0% w/v) was investigated by preparation of three hydrogel samples of equal mass and shape. They were weighed, then frozen in a freezer at -18 °C for 24 hours, then removed from the freezer, placed in a sealed container and thawed at 30 °C using a thermostatic bath for one hour. The samples were reweighed after removal from the released aqueous phase to evaluate the syneresis.

2.2.10. **Mechanical properties**

The porous gypsum composites or soap-hydrogel composites were placed onto a Lloyds LS100 testing apparatus equipped with a 100 kN load cell and a preload of 10 N was applied. They were compressed at a loading rate of 4 mm min⁻¹ and their compressional strength was taken as the force applied at point of structural failure, normalised with the cross-sectional area of the sample. Young's modulus was obtained from the gradient of the linear elastic region of the stress/strain plots.

The hydrogel samples tested in Chapter 6 were tested using a Mark-10 ESM303 compression testing apparatus with a loading cell of 500 N. They were compressed between two parallel plates at room temperature at a rate of 1.2 mm min⁻¹.

2.2.11. **X-ray diffraction**

A sample of three hydrogel samples (2.0% w/v agar, 2.0% w/v MC and 1.0 - 1.0% w/v agar-MC) were flash-frozen in liquid nitrogen and then freeze-dried for 72 hours at -55 °C and 7 Pa. The dried samples were chopped into a powder and x-ray diffraction (XRD) analysis was performed using a Siemens D5000 X-ray diffractometer with Cu K α radiation (0.151418 nm wavelength) and a 2 θ range between 5° and 80°.

2.3. Methods

2.3.1. Preparation of starting materials

2.3.1.1. Agar hydrogel

To prepare agar hydrogel (1.0% w/v or 2.0% w/v), water was heated to 97 °C using a water bath, followed by addition of the appropriate mass of agar powder. It was homogenised with an Ultra-turrax homogeniser for 15 minutes whilst being covered with aluminium foil to minimise water loss through evaporation. After removal from the water bath and setting at room temperature, the hydrogel was left in the fridge (4 °C) overnight before use.

The hydrogels prepared for the soap-hydrogel composites study (seen in Chapter 5) were prepared in a different way. The appropriate mass of agar powder was added to cold water to produce solutions of 2.0% w/v or 8.0% w/v in a sealable bottle. The bottle was sealed, autoclaved (Classic prestige medical autoclave, 121 °C, 105 kPa) to allow hydration of the agar and then homogenised whilst hot. This was repeated two more times to ensure complete dissolution of the agar. The hydrogel was then left to set at room temperature and placed in a fridge (4 °C) overnight before use.

2.3.1.2. Methylcellulose solution

MC solution (A4M, 0.5% w/v) was prepared by adding the appropriate mass of MC powder to cold water whilst homogenising. To ensure complete hydration of the MC in solution, it was placed in a fridge (4 °C) overnight. It was removed from the fridge and allowed to return to room temperature before use. MC solutions (SG A7C) of different concentrations (1.0% and 2.0% w/v) were prepared using the same method.

2.3.1.3. Agar-methylcellulose hydrogel

To produce the hydrogel that was used for the pancake-hydrogel composites, 500 cm³ of water was heated to 97 °C using a water bath. Agar powder (5.0 g, 1.0% w/v) and MC powder (5.0 g, 1.0% w/v) were added and the solution was homogenised using an Ultra-Turrax homogeniser for 15 minutes whilst being covered with aluminium foil to minimise evaporation. The temperature of the water bath was then decreased to 50 °C whilst the solution was continually agitated. Once the desired temperature was reached,

the solution was removed from the water bath and placed in a fridge (4 °C) overnight for the agar to set and the MC to fully dissolve.

For the rheological studies of this hydrogel, the preparation method was the same but the mixing ratios were different. The following compositions of agar - MC were prepared: 1.75% - 0.25%, 1.5% - 0.5%, 1.25% - 0.75%, 1.0% - 1.0%, and 1.0% - 0.5%. It was poured into cylindrical moulds whilst hot and covered with parafilm to minimise evaporation of water whilst setting at room temperature, then placed in a fridge (4 °C) overnight to ensure full hydration of the MC.

2.3.1.4. Gypsum slurry

Gypsum powder was mixed with water in the mass ratio 1.45:1 to produce a thick aqueous gypsum slurry. This ratio was recommended by the manufacturer to produce the strongest material.

2.3.1.5. Molten soap base

Soap base was cut into small pieces and heated in a thermostatic water bath at 75 °C whilst covered with aluminium foil to minimise evaporation of water. After it had melted, it was used at this temperature.

2.3.1.6. Pancake batter

Pancake batter was prepared using two UK standard medium sized eggs, 110 g plain flour and 300 cm³ semi-skimmed milk. The ingredients were combined with a handheld blender (Goodman's Cuisine Blender).

2.3.2. Preparation of hydrogel beads

2.3.2.1. Agar hydrogel beads

The hydrogel was transferred to a food blender (Tefal Food Processor Minipro, a 500 W blender with 3 stacked blades) and blended at full power. The size distributions of the resulting hydrogel beads were measured as a function of time.

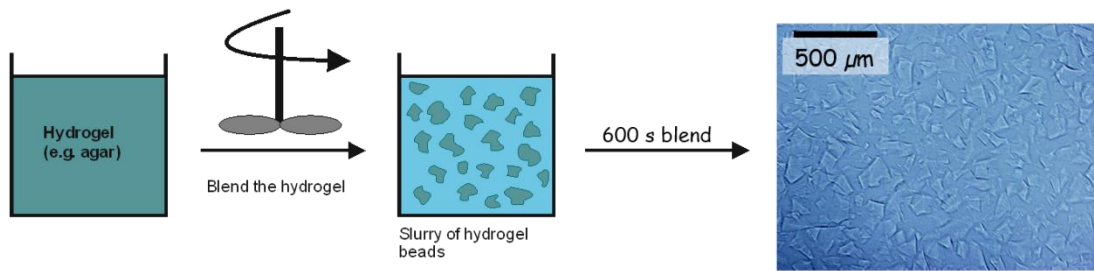


Figure 2.3. Schematic to show the blending of the hydrogel to produce a slurry of hydrogel beads.

Size analysis was done after blending for the following amounts of time: 10 s, 15 s, 30 s, 45 s, 60 s, 90 s, 120 s, 150 s, 300 s and 600 s.

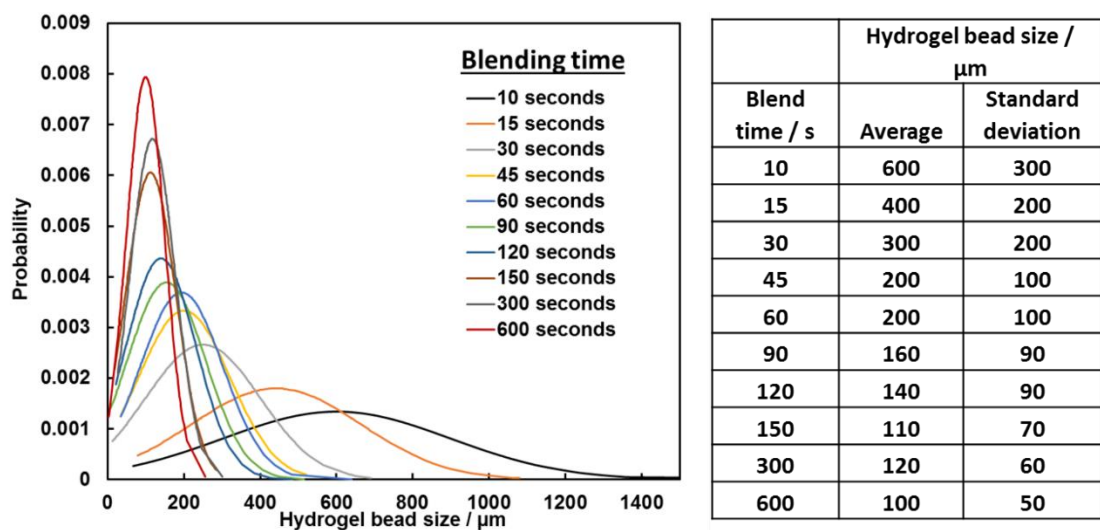


Figure 2.4. Normal distributions of the size of hydrogel beads after different blending times are shown on the left and a table to show the values of the average and standard deviation is shown on the right. A sample size of 150 hydrogel beads was used to obtain each size distribution.

In Chapters 3 and 4, when producing porous gypsum composites, large beads correspond to beads blended for 10 seconds with an average size of $600 \pm 300 \mu\text{m}$ and small beads correspond to beads blended for 600 seconds with an average size of $100 \pm 50 \mu\text{m}$. In Chapter 5, when producing soap-hydrogel composites, large beads

correspond to beads blended for 10 seconds and small beads correspond to beads blended for 300 seconds with an average size of $120 \pm 60 \mu\text{m}$.

2.3.2.2. Agar-methylcellulose hydrogel beads

The hydrogel was transferred to a food blender as described in section 2.3.2.1 and blended for 600 seconds to obtain hydrogel beads with an average size of $100 \pm 30 \mu\text{m}$. These beads were used in Chapter 7.

2.3.3. Hydrogel bead templating to formulate porous gypsum composites

Gypsum slurry was mixed with controlled volume percentages of agar hydrogel beads (either large or small). Five different volume percentages of slurry of hydrogel beads were used during preparation (15%, 30%, 40%, 45% and 60%) as well as a control sample of gypsum alone. For preparation of samples for thermal conductivity testing (Chapter 3), these mixed gypsum/hydrogel bead slurries were poured into a cylindrical mould (inner dimensions were 60 mm height and 60 mm diameter) and a lid was placed on top that had metal cylinders attached. These were to pierce the wet composite samples at the locations for the cartridge heater and thermocouples to fit. This was done to ensure that the placement of the heater and thermocouples would be the same in each sample. After pouring into the mould and placing the lid on, they were allowed to cure at room temperature for one hour. Subsequently, the lid was removed and they were transferred to an oven (40 °C) to dry until they reached a constant mass.

For preparation of samples for acoustical analysis (Chapter 4), the composite slurries were poured into cylindrical moulds (76.2 mm inner diameter and 20 mm height) and allowed to cure at room temperature for one hour. They were then dried the same way.

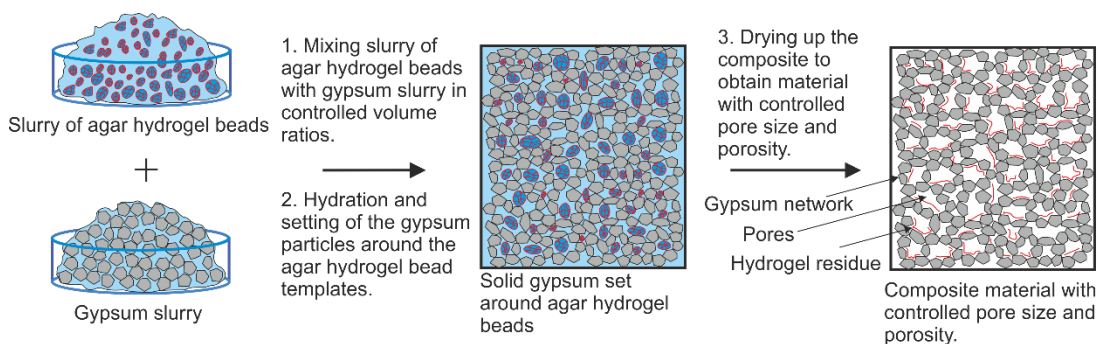


Figure 2.5. Schematic to show the hydrogel beads templating technique to control the porosity and pore size of gypsum composites. Gypsum slurry is mixed with either small hydrogel beads or large hydrogel beads in controlled volume ratios. Subsequent setting of the gypsum and then drying of the composite produces materials with controlled porosity and tuneable microstructures. Note that the composites do not shrink significantly upon during over a wide range of hydrogel volume fractions.

2.3.4. Dual templating with two size hydrogel beads for production of hierarchically porous gypsum composites

Small hydrogel beads were mixed with large hydrogel in controlled volume ratios. This slurry of hydrogel beads was then used to prepare porous gypsum composites using the same method as described in section 2.3.3. Hierarchically porous gypsum composites were produced using 40% or 50% by volume of hydrogel beads. The samples produced with 40% by volume of hydrogel bead slurry were produced with either all large beads, all small beads or large and small beads in a volume ratio of 1:1. The samples produced with 50% by volume of hydrogel bead slurry were produced with either all large beads, all small beads or large and small beads in volume ratios (1:4, 2:3, 3:2 and 4:1).

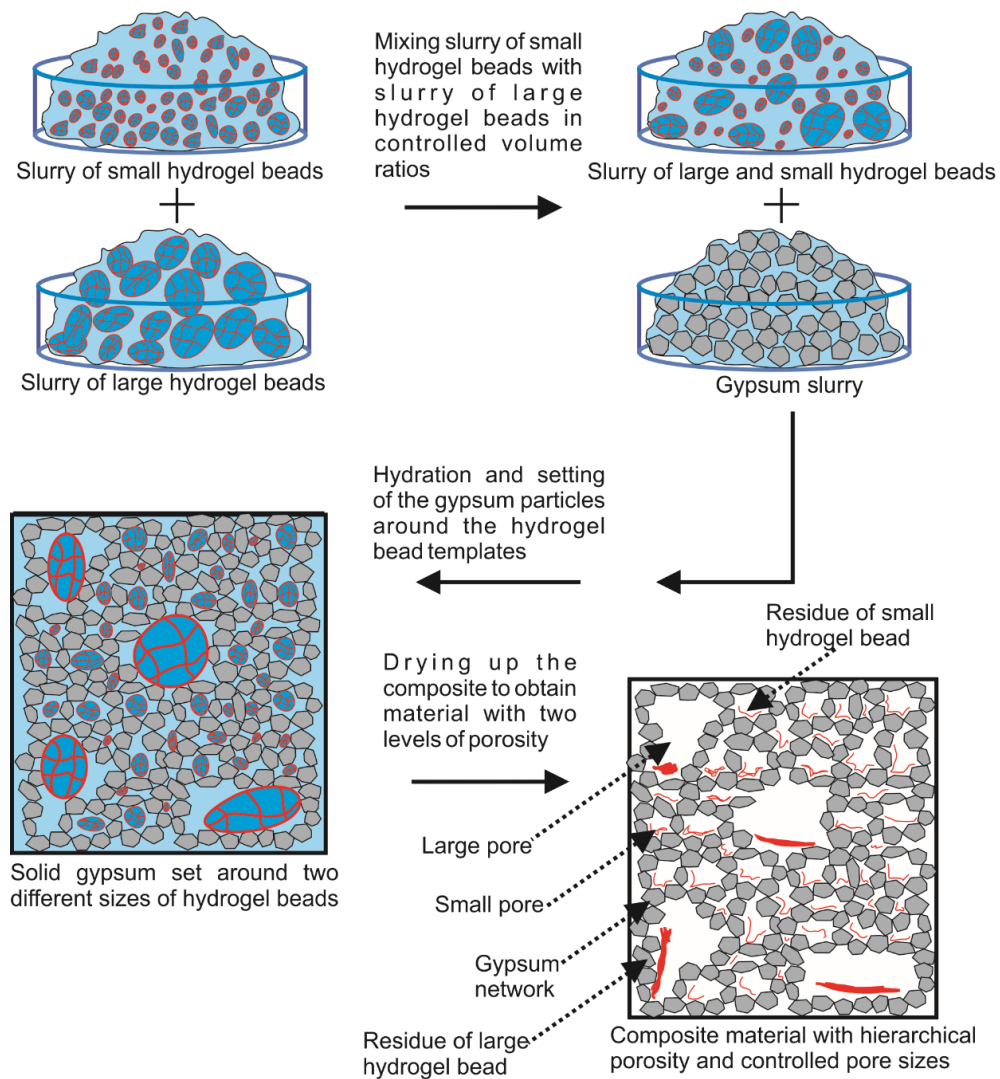


Figure 2.6. A schematic diagram to show the procedure of dual hydrogel bead templating for the fabrication of hierarchically porous gypsum composites. Slurries of large and small hydrogel beads are mixed in controlled volume ratios, then this mixed slurry is mixed with gypsum slurry in controlled volume ratios. Upon curing and drying of these composites, a hierarchically porous structure is obtained with controlled pore size distributions, porosity, and ratio of small pores to large pores.

2.3.5. Viscous trapping to produce porous gypsum composites

Gypsum slurry was mixed with controlled volume percentages of MC solution. Five different volume percentages of MC solution were used for the preparation of these porous composites (15%, 30%, 45%, 50% and 60%). They were poured into moulds

for either thermal conductivity testing of acoustical analysis, allowed to cure for one hour and then dried to a constant mass as described in section 2.3.3.

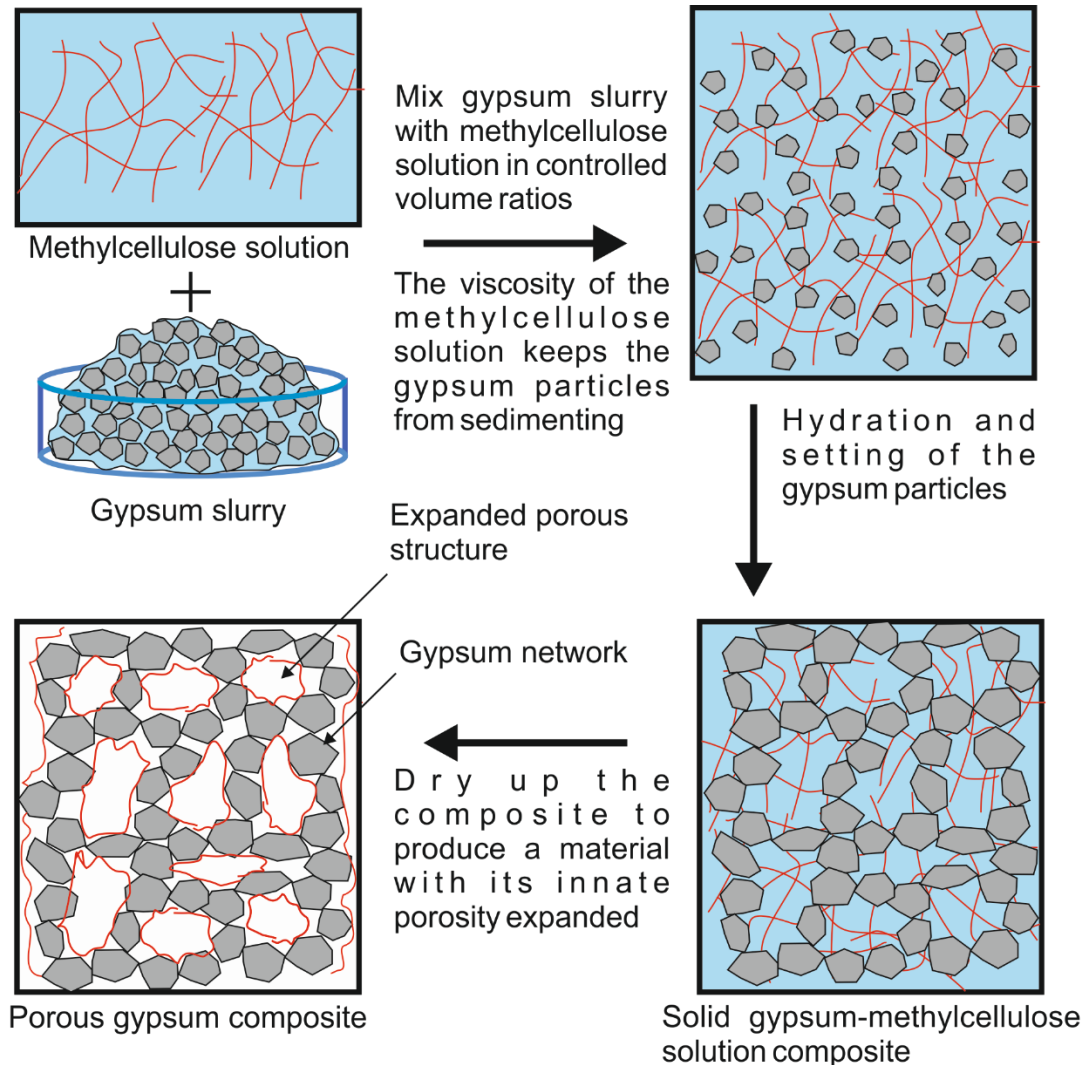


Figure 2.7. Schematic showing the viscous trapping method utilising a viscous MC solution. Gypsum slurry is mixed with a controlled volume percentage of MC solution. This is followed by curing and drying of the composite to produce a porous material with its microstructure expanded by a controlled amount.

2.3.6. Hierarchically porous gypsum composites from a combined viscous trapping and hydrogel bead templating method

MC solution was mixed with slurry of agar hydrogel beads (small or large) in controlled volume ratios. A controlled volume percentage of this mixture (50%) was

then mixed with gypsum slurry and poured into moulds. They were allowed to cure for one hour at room temperature and then dry in an oven until they reached a constant mass. The compositions of gypsum slurry mixed with MC solution and slurry of agar hydrogel beads are illustrated below in table 2.1.

Table 2.1. A table to show the compositions used to prepare hierarchically porous gypsum composites using MC solution and agar hydrogel bead slurry.

Volume of gypsum slurry / %	Volume of MC solution / %	Volume of hydrogel bead slurry / %
50	50	0
50	40	10
50	30	20
50	20	30
50	10	40
50	0	50

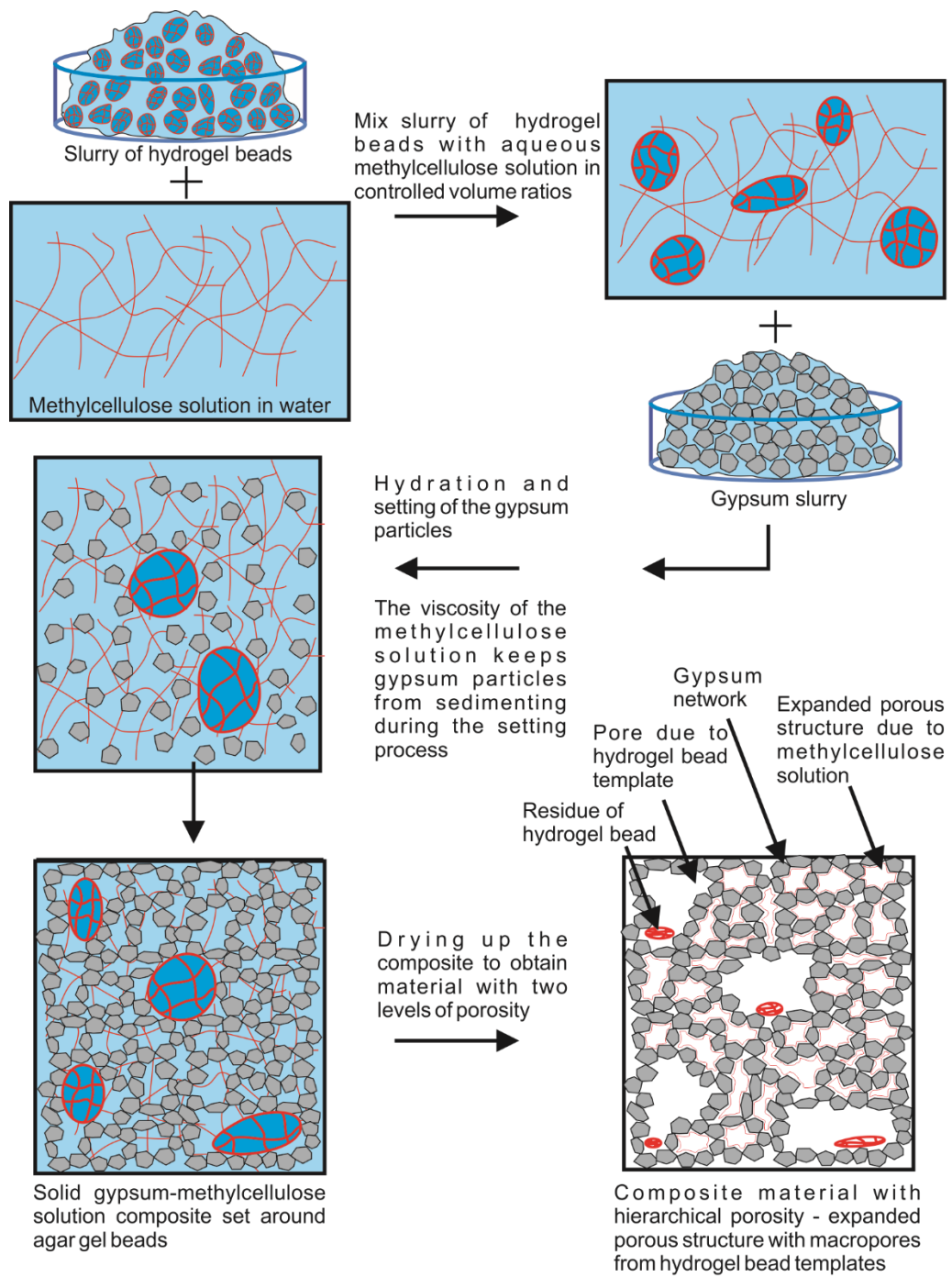


Figure 2.8. A schematic to show a method that combines hydrogel bead templating with viscous trapping that allows control over the porosity and the microstructure on two different length scales (expanded gypsum network and well defined pores due to hydrogel beads).

2.3.7. Formulation of soap-hydrogel composites

Soap was melted at 70 °C and mixed at this temperature with controlled volume percentages of the slurry of agar hydrogel beads (either small or large). Seven different volume percentages of slurry of hydrogel beads were used (5%, 7.5%, 12%, 15%, 25%, 35% and 50%) as well as a control sample of soap alone. The samples prepared for the dissolution studies were then degassed under vacuum in a desiccator and poured into moulds. After setting in a fridge (4 °C) for 1 hour, the samples were removed from the moulds for testing. A schematic to show this procedure is shown below.

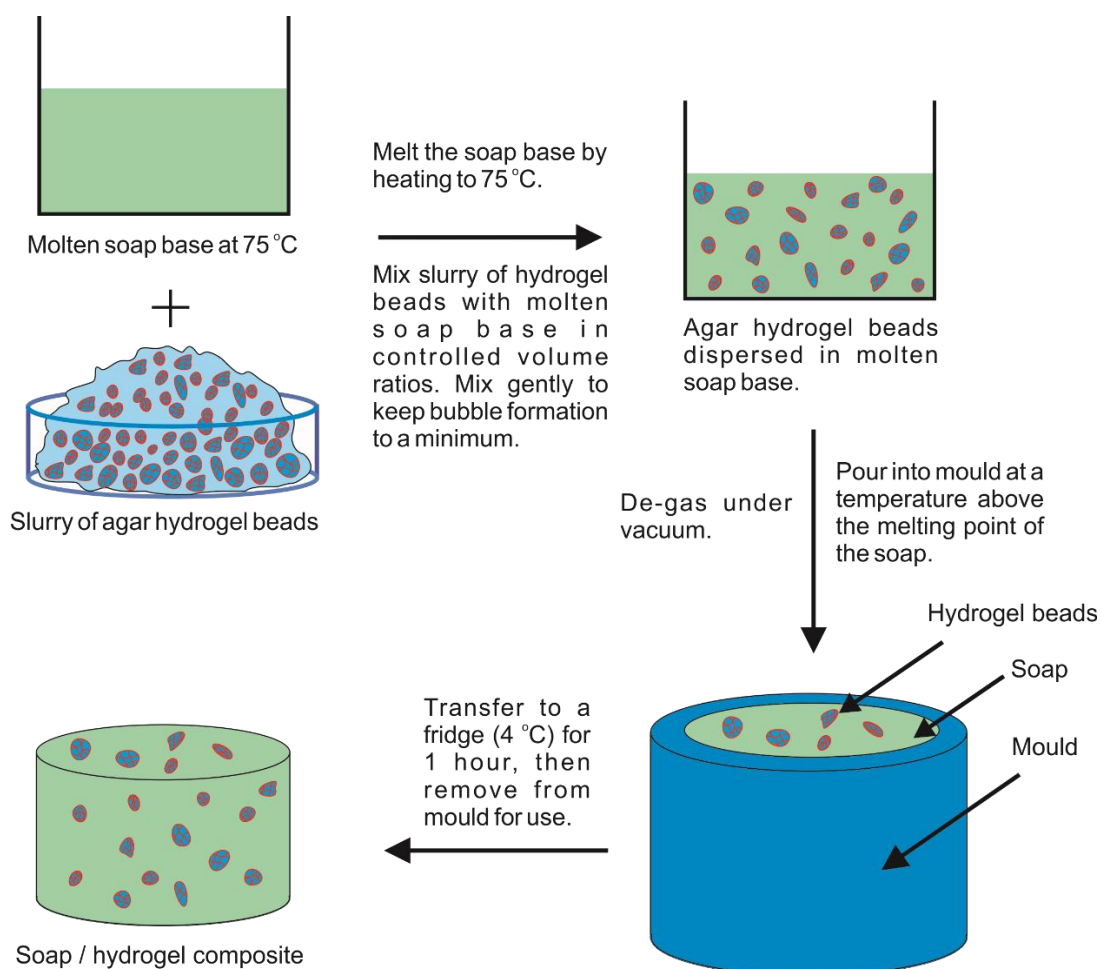


Figure 2.9. Schematic of the formulation of soap-hydrogel beads composites. Slurries of hydrogel beads are mixed with molten soap base in controlled volume ratios. The mixture was de-gassed to remove trapped air bubbles, poured into moulds and then transferred to a fridge (4 °C) for 1 hour to set before further use.

For the composites prepared for the release kinetics studies, molten soap base and slurries of hydrogel beads were mixed gently with a spatula for 15 seconds to limit the formation of air bubbles. After mixing, aliquots were poured into pre-cooled moulds (4 °C), ensuring rapid setting of the composites. This limits the leaking out the aqueous phase from the gel beads into the liquid soap. The samples were set in the fridge (4 °C) for 1 hour before use.

2.3.8. Pancake-hydrogel composites

Various controlled volume percentages of agar-MC hydrogel bead slurry was mixed with pancake batter to an overall volume of 40 cm³. A pan was heated on a hot plate to 170 °C (temperature was monitored using an infrared thermometer with laser target) and then butter (0.3 g) was melted onto the pan. The pancake batter containing hydrogel beads was then poured onto the pan and heated for four minutes on each side. Three different volume percentages of hydrogel bead slurry were used (10%, 17.5% and 25%) as well as a control sample containing only pancake batter.

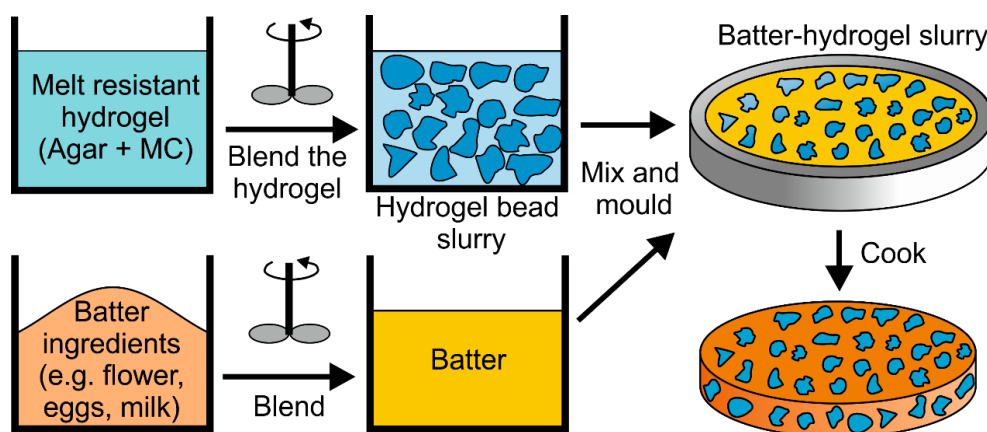


Figure 2.10. Schematic of the process of templating batter with slurry of agar-MC hydrogel beads.

2.4. References

- 1 M. Sansinena, M. V Santos, N. Zaritzky and J. Chirife, *Theriogenology*, 2012, **77**, 1717–1721.
- 2 T. M. Tritt and D. Weston, Measurement Techniques and Considerations for Determining Thermal Conductivity of Bulk Materials, in *Thermal Conductivity: Theory, Properties, and Applications*, ed. T. M. Tritt, Springer US, Boston, MA, 2004, ch. 2.1, pp. 187–203.
- 3 ASTM E2611-09, Standard Test Method for the Measurement of Normal Incidence Sound Transmission of Acoustical Materials Based on the Transfer Matrix Method (2009), <https://www.astm.org/Standards/E2611.htm> (accessed 27/7/2017).
- 4 S. S. Jung, Y. T. Kim and Y. B. Lee, *J. Korean Phys. Soc.*, 2008, **53**, 596–600.
- 5 P. S. Allan, A. Ahmadnia, R. Withnall and J. Silver, *Polym. Test.*, 2012, **31**, 312–321.
- 6 H. A. Gundry and A. R. Meetham, *Trans. Faraday Soc.*, 1958, **54**, 664–670.

3. Microstructure, mechanical and thermal insulating properties of hierarchically porous gypsum composites fabricated by hydrogel templating and viscous trapping techniques

Two techniques have been developed for the preparation of hierarchically porous gypsum composites. The first technique involves templating a mixed slurry of hydrogel beads containing two different size distributions of beads with gypsum slurry. This allows a precise control of the porosity of the hardened composite after the evaporation of the aqueous content of the hydrogel. The second technique relies on a viscous trapping of the gypsum particles in methylcellulose solution during the hardening process. By varying the volume fraction of the hydrogel beads slurry or the methylcellulose solution used during the preparation of the gypsum composite, it is possible to tune both the composite porosity and the pore size distribution. Utilising methylcellulose (MC) solution during the formulation process allows expansion of the innate porosity of gypsum. Furthermore, the volume percentage of methylcellulose solution used determines the porosity of the dried sample. These cheap, facile methods allowed porosities of up to 60% to be obtained with negligible contraction upon drying and to produce hierarchically porous materials with significantly different internal microstructures. An investigation into the composites thermal insulation properties as a function of both their porosity and pore size was performed. Interestingly, it was found that although the thermal conductivity decreased linearly with an increase in the composite porosity, at fixed porosity it was virtually independent of the pore sizes investigated here. Furthermore, the mechanical properties of the porous composites were investigated. It was found that the samples produced with 15 – 45% large hydrogel beads yielded materials with a 60% lower compressional strength and 50% smaller Young's modulus, respectively, compared to those produced with small hydrogel beads or MC solution. On the other hand, the samples produced with small hydrogel beads and MC solution showed very similar mechanical properties. Both methods demonstrate an inexpensive approach for introducing porosity in gypsum

composites which reduces their thermal conductivity, improves their insulation properties and allows economic use of the matrix material whilst controlling their mechanical properties. Such composites allow for tuneable porosity without significantly compromising their strength which could find applications in the building industry as well as structuring of other composites for a variety of consumer products.

3.1. Introduction

In the modern economy, fossil fuels are being consumed at an alarming rate, with estimates that the reserves of oil, gas and coal will be depleted by the year 2040, 2042 and 2112, respectively.¹ The use of these non-renewable energy sources brings with it multiple global issues such as global warming, environmental pollution and climate change. These issues necessitate the development of a sustainable worldwide infrastructure, as well using novel materials to achieve better energy storage and conservation. Progress towards this goal can be achieved through the development of renewable energy sources and the conservation of current energy reserves. Currently, only 14% of the total world's energy demand is supplied by renewable sources,² however, their future potential is outstanding.^{3,4} Therefore, the development of methods to improve energy conservation and in turn increase the efficiency of energy used is crucial. Increasing the thermal efficiency in residential and commercial buildings is a vital step, as these account for a total energy consumption exceeding 40% and for more than 20% of CO₂ emissions.⁵ One way to do this is to decrease the thermal conductivity of commonly used building materials. Gypsum based composites are commonly used in buildings, as dry walls or ceilings. Their relatively low cost and low thermal conductivity are one of the reasons why they are the exploited, as well as their passive fire resistance.⁶ One way to further improve the thermal insulation properties of gypsum and to decrease its thermal conductivity, requires pores to be incorporated within the gypsum network.

Due to air having a significantly lower thermal conductivity than a solid phase, incorporating porosity within a material decreases its thermal conductivity. Heat transfer in a porous material is accomplished through a combination of lattice vibrations in the solid phase, conduction through collisions of gas molecules within the pores, through thermal radiation and, if the pore sizes are sufficiently large,

convection within the pores.⁷ Recently, it has been demonstrated that a cheap, easy and environmentally friendly method of introducing porosity into a material, that also gives a large amount of control over both the porosity and pore size, is using hydrogel bead templates. A hydrogel bead templating technique to produce porous materials has previously been reported.⁸ It involved the use of gellan gum or polyacrylamide hydrogel beads as templates to introduce porosity into a variety of materials. By combining slurries of the matrix material and hydrogel beads in controlled volume ratios, followed by subsequent curing and then drying, porous materials were obtained with a porosity controlled by the volume of hydrogel beads used. Furthermore, the average pore size of the composite was determined by the size of the hydrogel beads used.

Here, this method has been extended further to make hierarchically porous gypsum composites by using agar hydrogel beads of different sizes as the templates. The use of agar hydrogel instead of gellan or polyacrylamide is due to the gelling fraction of agar, agarose, being a non-ionic hydrocolloid that does not interact with calcium ions from the gypsum slurry which allows better control during the formulation of these composites.⁹

A complementary viscous trapping method has been developed for controlling the porosity of gypsum through the use of methylcellulose (MC) solution. Mixing gypsum slurry with a viscous MC solution during the gypsum setting process, stops the sedimentation of the gypsum particles and allows more time for them to hydrate and interconnect into a continuous network. This method allows control over the porosity, but the pore size increases with increasing volume of MC solution used due to it essentially expanding the innate porosity of gypsum. Both methods can also be used to introduce hierarchical porosity in cement, ceramics, food, home and personal care products and other composite materials of similar setting process.

In the current chapter, an investigation into how the thermal conductivity and mechanical properties of the porous gypsum composites vary with porosity and pore size fabricated by these methods has been reported.

3.2. Results

3.2.1. Hydrogel bead size analysis

In order to be able to investigate the effect of pore size on the properties of the porous gypsum composites, it was important to be able to control the size of the hydrogel beads. This was necessary, as the average pore size is dependent on the average size of the hydrogel beads used in the templating process. Average hydrogel bead size was measured after blending for different amounts of time between 10 – 600 seconds and their size distributions were obtained by analysing images of the hydrogel beads dispersed in water.

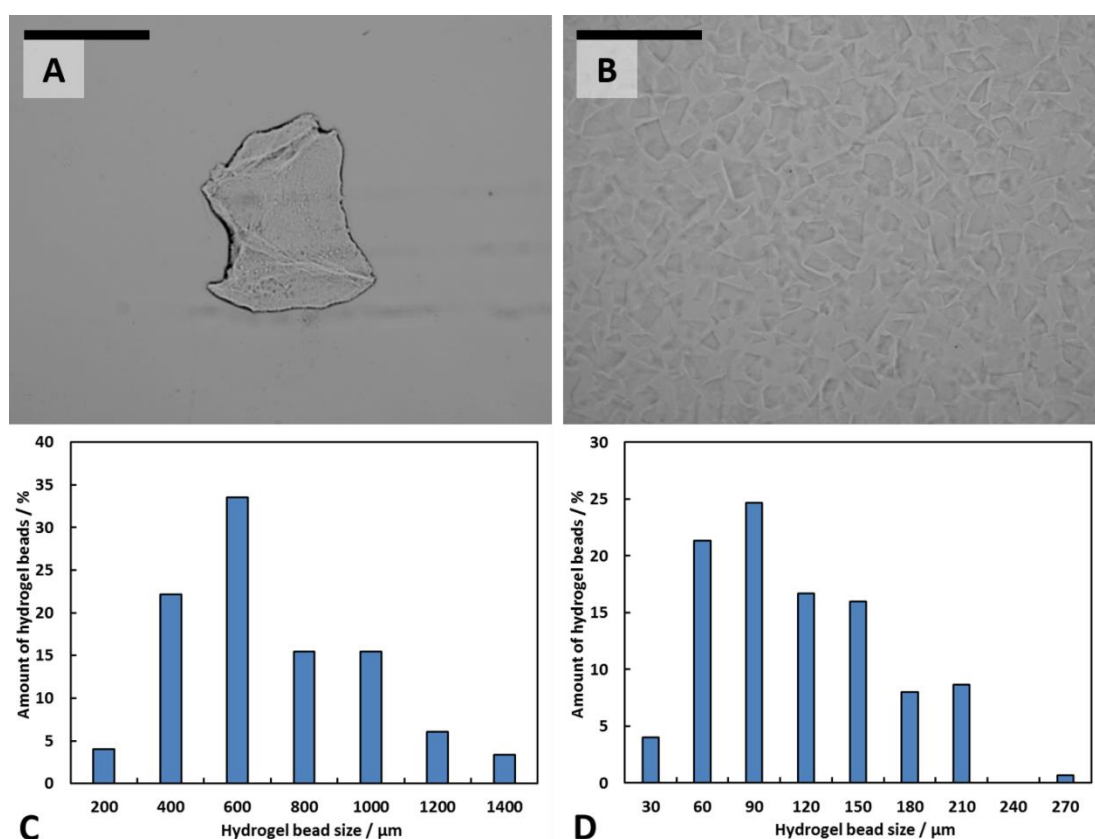


Figure 3.1. (A) and (B) are optical microscopy images of a large agar bead and small agar hydrogel beads, respectively. The scale bars correspond to a distance of 500 μm. (C) and (D) show size distributions produced by sizing an average of 150 large and 150 small beads, respectively. The histograms represent the percentage of the hydrogel beads of various sizes.

The average size of the hydrogel beads varied from $600 \pm 300 \mu\text{m}$ (10 seconds blending) to $100 \pm 50 \mu\text{m}$ (600 seconds blending). These two size distributions of hydrogel beads were used and will be henceforth be referred to as ‘large beads’ and ‘small beads’. Histograms showing their size distribution and optical microscopy images showing their morphology can be seen in Figure 3.1. The hydrogel beads were of irregular shape so they were measured horizontally through their widest section.

3.2.2. Porosity and volume reduction of the composites

After drying of the composites, they were weighed and their dimensions were measured. Images of the samples produced using each method can be seen in Figure 3.2.



Figure 3.2. Photographs of the porous gypsum composites produced using different methods. (A) and (B) show the samples produced using small hydrogel beads and large hydrogel beads, respectively. (C) shows the composites produced using viscous trapping with the aqueous MC solution. The percentages on the images represent the volume of template used during their production.

Their densities and volumes were compared to the gypsum control sample to calculate the porosity and the volume reduction of the porous composites. It is worthwhile to note that gypsum plaster alone is a porous material,¹⁰ so when talking about the porosity of the composites, it is the reduction in density compared to gypsum plaster produced without hydrogel beads or MC solution. It was calculated as follows:

$$\theta = \left(1 - \frac{\rho}{\rho_0}\right) \times 100\%. \quad (3.1)$$

Here θ is the porosity (%), ρ is the density of porous composite (g cm^{-3}) and ρ_0 is the density of gypsum control sample (g cm^{-3}). The volume reduction was calculated as shown in equation 3.2.

$$V_{red} = \left(1 - \frac{V}{V_0}\right) \times 100\%. \quad (3.2)$$

Here V_{red} is the volume reduction (%), V is the volume of porous composite (cm^3) and V_0 is the volume of gypsum control sample (cm^3).

Figure 3.3 shows the porosity and volume reduction of the porous gypsum composites produced using three different methods. It was found that changing the method used to introduce porosity did not impact the volume reduction or the porosity of the samples, and that these properties were solely dependent on the volume of large agar beads, small agar beads or MC solution added. The reduction in volume was insignificant ($< 3\%$) at all the volumes of porogenic agent used, however it was still taken into account when calculating the porosity of the samples.

The use of large or small hydrogel beads to produce the porous composites works by dispersing hydrogel beads within the gypsum slurry which will then harden around the beads. Upon subsequent drying of the samples, evaporation of water from the trapped hydrogel beads will leave voids within the sample that directly reflect the size of the beads used. Note that this method works only when the surrounding matrix allows for the water to leave the system. Furthermore, the porosity is slightly lower than the volume percentage of hydrogel beads added to the gypsum slurry, possibly due to syneresis of water from the hydrogel due to the osmotic pressure mismatch upon mixing with the gypsum slurry. However, this effect is very small.

When using MC solution to control the porosity of the composites, the viscosity of this hydrocolloid solution suspends the gypsum particles during the setting process.

The low solubility gypsum powder ($\text{CaSO}_4 \cdot \frac{1}{2} \text{H}_2\text{O}$) first hydrates in solution to produce $\text{CaSO}_4 \cdot 2\text{H}_2\text{O}$, which has an even lower solubility and so quickly recrystallises and precipitates out in the form of needles and platelets. Interlocking of these structures forms a rigid structure.¹¹ As the volume percentage of the aqueous MC solution increases, the longer it takes for the interlocking to occur and so an increased viscosity of the aqueous phase added was necessary to stop the sedimentation of gypsum particles before the gypsum composite could harden. Drying of the samples essentially leaves gypsum plaster with its (already present) porosity expanded by a controlled amount, dependent on the volume percentage of MC solution initially added.

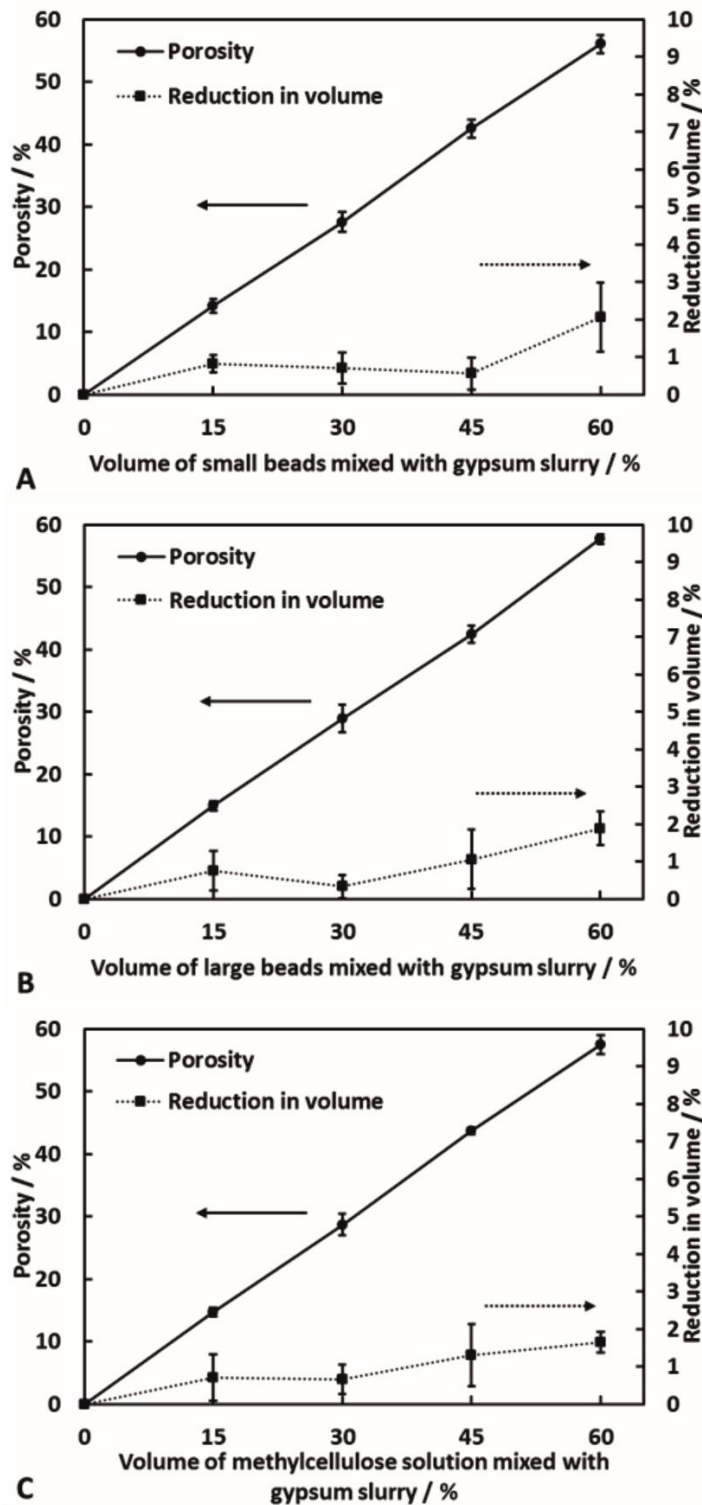


Figure 3.3. Porosity and volume reduction of the porous gypsum composites produced using three different methods. (A) corresponds to the samples produced using small hydrogel beads as a template, (B) corresponds to samples produced using large hydrogel beads as a template and (C) are the values for the composites produced using MC solution. Each result is an average of three samples, with the error bars being the standard deviation.

3.2.3. Thermal conductivity of porous gypsum composites

The samples were measured as described in Chapter 2, section 2.2.2. Each sample contained three thermocouples (tc_1 , tc_2 and tc_3) at increasing distances (r_1 , r_2 and r_3) from the centre of the sample. Upon heating with a cartridge heater in the centre at constant power, the temperature was monitored until steady state was achieved. Once the temperature at each thermocouple had been stable for 30 minutes, steady state was assumed to have been reached. The temperatures at each thermocouple, as well as the thermocouple distances from the centre of the sample, the power output of the heater and the sample geometry could then be used to calculate the thermal conductivity of the composite using the following equation:¹²

$$\kappa = \frac{Q \ln\left(\frac{r_x}{r_1}\right)}{2\pi L \Delta T} \quad (3.3)$$

Where κ is the thermal conductivity of the sample ($\text{W m}^{-1} \text{K}^{-1}$), Q is the power output of the heater (J s^{-1}), r_1 is the distance between the centre of the sample and the closest thermocouple (m), r_x is the distance between the centre of the sample and thermocouple at location x (m), L is the length of the sample (m) and ΔT is the temperature difference between the thermocouple at location 1 and the thermocouple at location x .

Figure 3.4 shows an example of steady state being reached and the steady state temperatures as a function of distance from the centre of the sample.

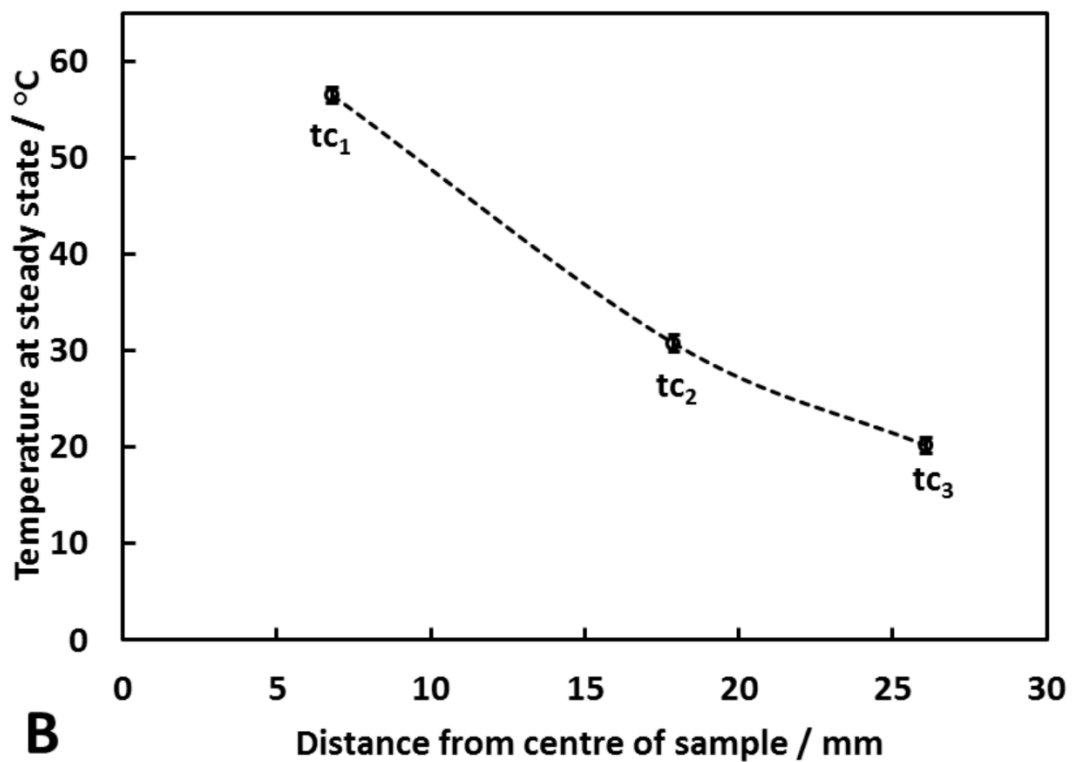
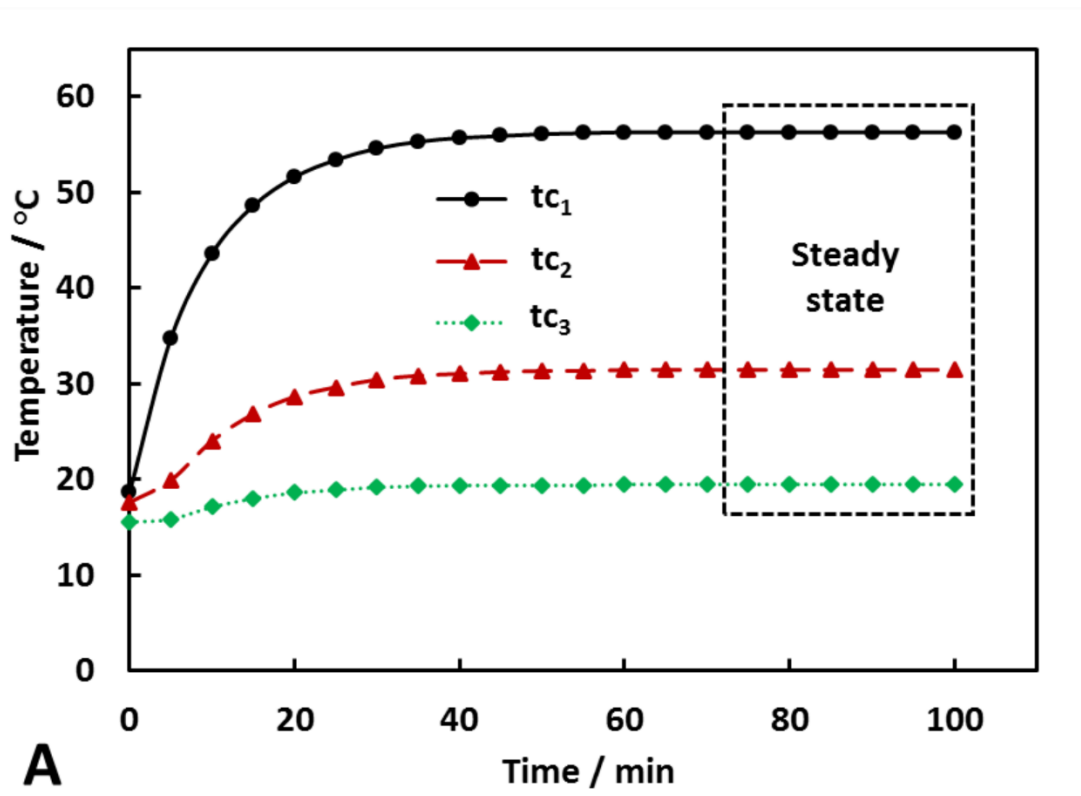


Figure 3.4. (A) shows an example of the temperature change over time and steady state being reached at each thermocouple location and (B) shows an example of the steady state temperatures used for the calculations of thermal conductivity of a sample.

The total thermal conductivity (κ_T) of a porous material is assumed to be due to four different contributions:¹³

$$\kappa_T = \kappa_s + \kappa_g + \kappa_c + \kappa_r. \quad (3.4)$$

Here κ_s is the contribution due to conduction through the solid material, κ_g is the conduction through the gas within the material, κ_c is the convection within the pores and κ_r represents thermal radiation. In the porous composite materials investigated here, there will also be a contribution due to the presence of hydrocolloid residue present within the pores after drying. However, the amount of solid gelling agent (agar or MC) is so small (ca. 0.35 – 3% by mass of agar or ca. 0.09 – 0.75% by mass of MC) that it can be deemed insignificant. Other studies have shown that for heat transfer in closed pore materials with a pore size less than 4 mm and in open pore materials with a pore size less than 2 mm, convection only plays a minor role.^{14,15} Finally, thermal radiation is well known to be negligible for porous materials with relative density greater than 0.2.¹⁶

An investigation into how the variation of the microstructure of the porous gypsum composites affected their thermal conductivities was performed. Three different methods were used to prepare these materials: Large hydrogel beads or small hydrogel beads as templates produced porous gypsum composites with an average pore size that reflected the size of the hydrogel beads used. In the case of gypsum composites fabricated by viscous trapping with MC solution the porous materials did not have fixed pore size as it expanded the innate porosity of the gypsum particle network during setting. Figure 3.5 shows the thermal conductivity of these materials and the reduction in thermal conductivity when compared to the gypsum control sample, which did not have hydrogel beads or MC solution added. The reduction in thermal conductivity was calculated as follows:

$$\kappa_{red} = \left(1 - \frac{\kappa}{\kappa_0}\right) \times 100\%. \quad (3.4)$$

Here κ_{red} is the reduction in thermal conductivity (%), κ is the thermal conductivity of the porous composite ($\text{W m}^{-1} \text{K}^{-1}$) and κ_0 is the thermal conductivity of the gypsum control sample ($\text{W m}^{-1} \text{K}^{-1}$).

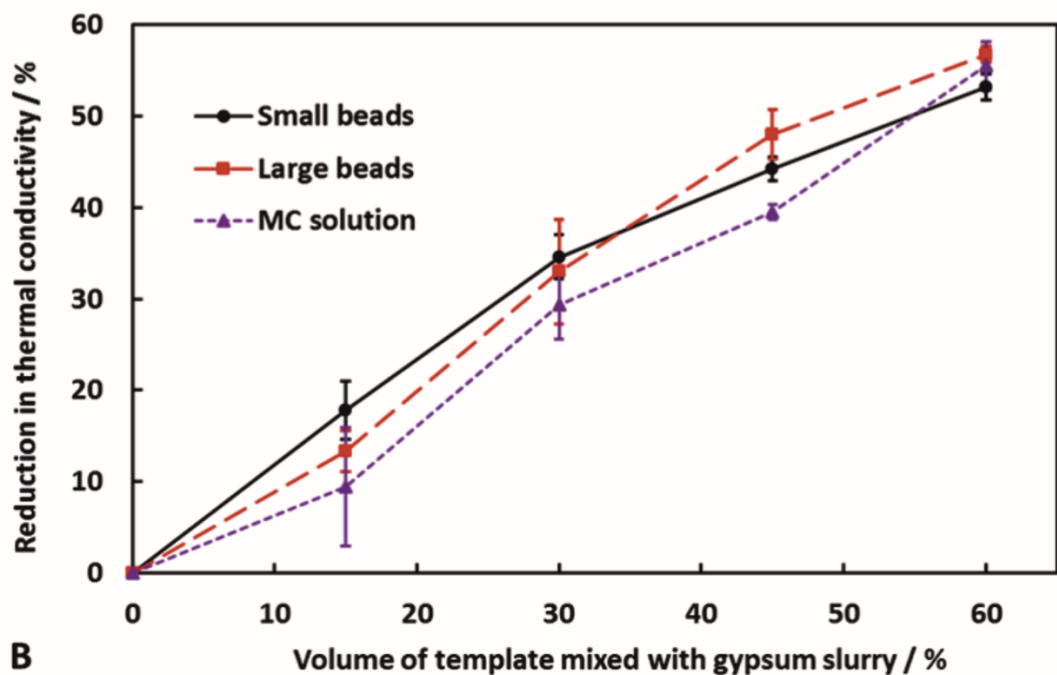
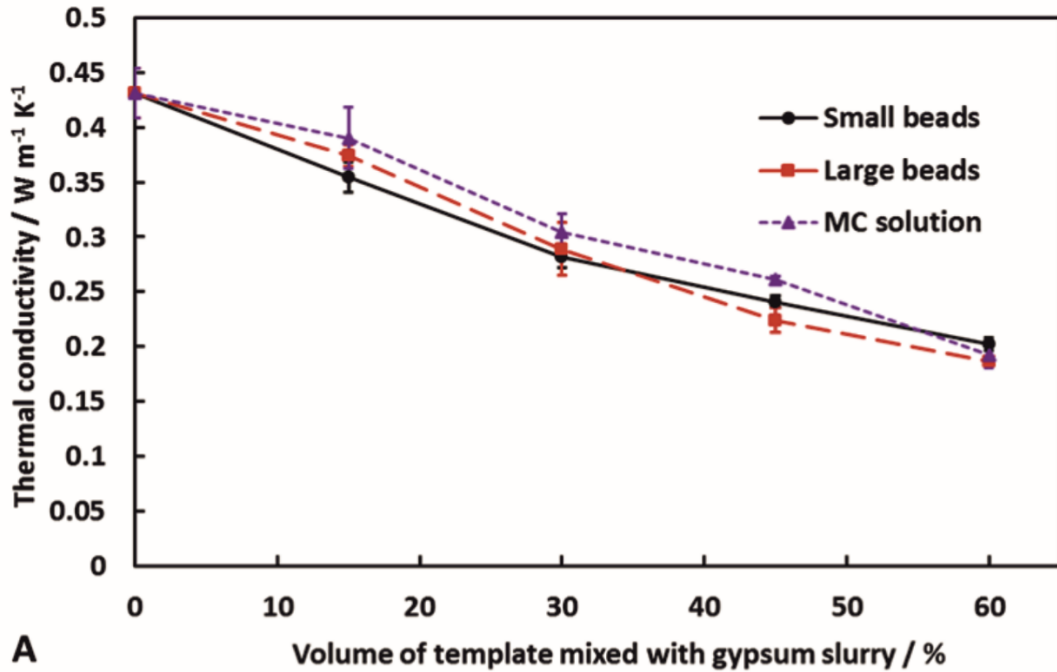


Figure 3.5. (A) shows the thermal conductivity of the porous gypsum composites as a function of the volume of template (large beads, small beads or MC solution) initially mixed with the gypsum slurry. (B) shows the reduction in thermal conductivity when compared to the gypsum control sample as calculated in equation 3.4. Each data point is an average result of three separate samples with the error bars being the standard deviation.

The measured thermal conductivity of gypsum plaster alone was found to be $0.43 \pm 0.02 \text{ W m}^{-1} \text{ K}^{-1}$ which is within the range of other results found in the literature.¹⁷ The thermal conductivity of the porous composites was found to decrease linearly as the volume of template used during formulation was increased. Note that the reduction in thermal conductivity closely reflects the initial volume percentage of template used to prepare the composites *i.e.* when using 30% by volume of template during the formulation process, the composites show a reduction in the thermal conductivity by approximately 30%.

Fitting a simple linear equation to each data set in Figure 3.5(B) allows a reasonable approximation of the reduction in thermal conductivity when adding different volume percentages of template. These are shown in equations 3.5 – 3.7 for composites prepared by using small beads, large beads, and aqueous MC solution, respectively.

$$\kappa_{red} = 0.9599 V_{SB}, \quad (3.5)$$

$$\kappa_{red} = 1.0004 V_{LB}, \quad (3.6)$$

$$\kappa_{red} = 0.9080 V_{MC}. \quad (3.7)$$

Here κ_{red} is the reduction in thermal conductivity (%) and V is the volume of template used to make the porous gypsum composite (%); (SB = small beads, LB = large beads, MC = methylcellulose solution)). The R^2 values were 0.964, 0.986 and 0.988 for the linear fits shown in equations 3.5, 3.6 and 3.7, respectively. Further work would be needed to investigate whether these equations are applicable to other porous materials produced with these templating methods. Furthermore, it was found that the pore size distribution within the porous gypsum composites had no impact on the thermal conductivity when compared at the same overall porosity.

One way to reduce the thermal conductivity of a porous composite material at a fixed porosity involves the reduction of the thermal conductivity of the gas within the pores. This can be done in two ways: by replacing air with a gas of lower thermal conductivity, or by reducing the thermal conductivity of air.¹⁸ The Knudsen effect describes the reduction of the thermal conductivity of a gas within a pore when the pore size is comparable to or smaller than the mean free path of the gas. For air at room temperature, this is approximately 70 nm.¹⁹ The Knudsen equation describes how variation of the pore size affects the thermal conductivity of the air within the pores.²⁰

$$\kappa'_g = \frac{\kappa'_{g0}}{\left(1 + \beta \left(\frac{l_g}{\phi}\right)\right)} \quad (3.8)$$

Here κ'_g is the thermal conductivity of air within the pores, κ'_{g0} is the thermal conductivity of free air ($0.026 \text{ W m}^{-1} \text{ K}^{-1}$), β is a parameter that takes into account the transfer of energy when air molecules collide with a pore boundary (~ 2), l_g is the mean free path of air and ϕ is the average pore diameter. One can explain the lack of effect of the pore sizes on the thermal conductivity from estimates using equation 3.8.

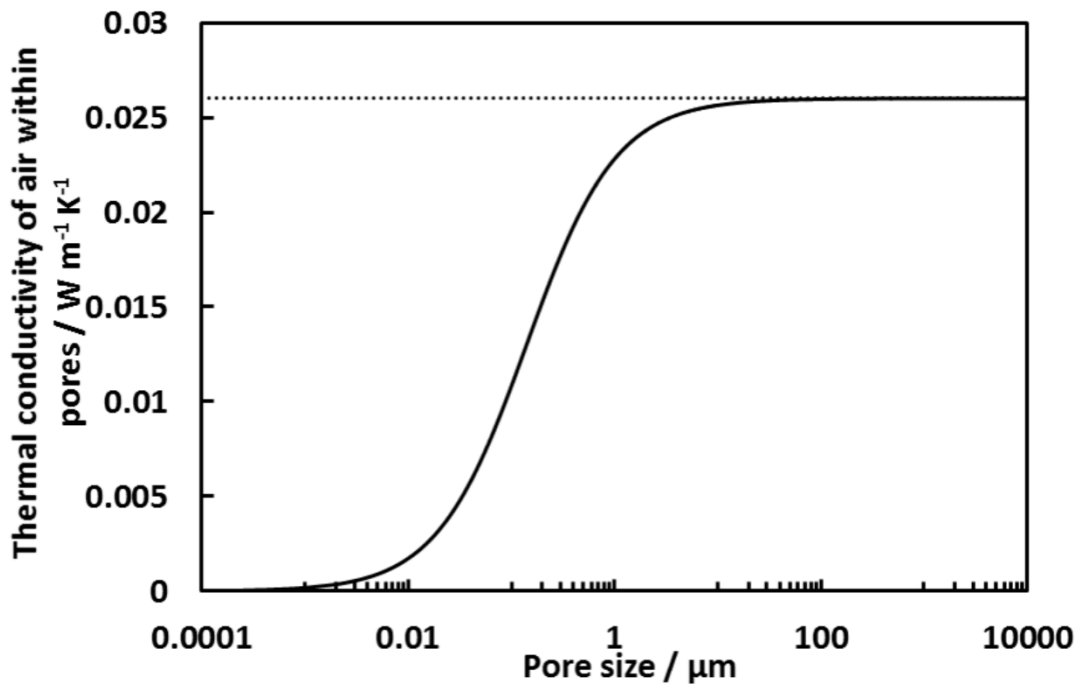


Figure 3.6. The thermal conductivity of air within pores of a material as a function of the pore size. The values were calculated as shown in equation 3.8. The dashed black line is the thermal conductivity of free air ($0.026 \text{ W m}^{-1} \text{ K}^{-1}$).

If, for example, five significantly different pore sizes over the range shown in Figure 3.6 are taken, the linear rule of mixtures (simplest model) can be applied to predict the thermal conductivity of gypsum plaster at each porosity with each pore size.

$$\kappa_{theoretical} = V_p \times \kappa'_g + V_m \times \kappa_m \quad (3.9)$$

Here $\kappa_{theoretical}$ is the theoretical value of thermal conductivity of the porous material, κ'_g and κ_m are the thermal conductivities of the air within the pore and of the matrix

material, respectively and V_p and V_m are the volume fractions of pores and matrix material, respectively.

Using gypsum as the matrix material ($\kappa = 0.43 \text{ W m}^{-1} \text{ K}^{-1}$), the theoretical thermal conductivity at five different pore sizes (0.01 μm , 0.1 μm , 1 μm , 10 μm and 100 μm) between porosities of 1-99% can be calculated. Doing this calculation when $\kappa'_g = 0.026 \text{ W m}^{-1} \text{ K}^{-1}$ (thermal conductivity of free air) then allows determination of the theoretical reduction in thermal conductivity at each porosity due to reductions in the thermal conductivity of the gas within pores of different sizes:

$$\kappa_{red(theoretical)} = \left(1 - \frac{\kappa_{xtheoretical}}{\kappa_{ktheoretical}}\right) \times 100\%. \quad (3.10)$$

Where $\kappa_{red(theoretical)}$ is the theoretical reduction in thermal conductivity (%), $\kappa_{xtheoretical}$ is the thermal conductivity of the porous material calculated using the thermal conductivity of air in pores of different sizes ($\text{W m}^{-1} \text{ K}^{-1}$) and $\kappa_{ktheoretical}$ is the thermal conductivity of the porous material calculated using the thermal conductivity of free air ($\text{W m}^{-1} \text{ K}^{-1}$).

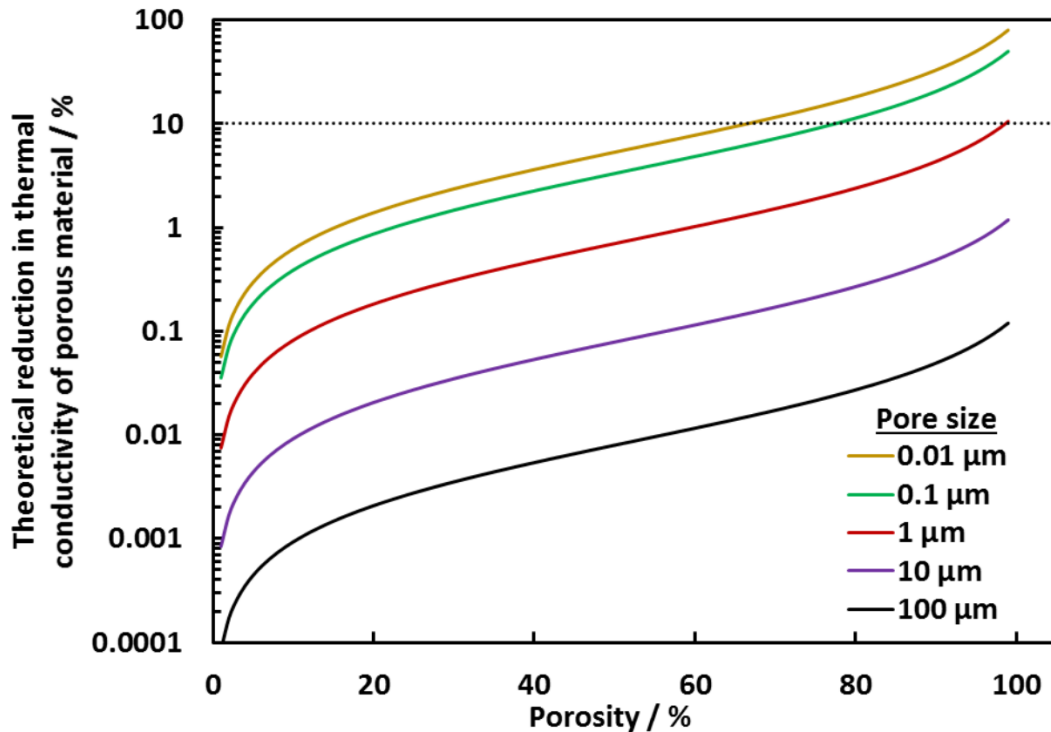


Figure 3.7. The theoretical reduction in thermal conductivity of porous gypsum composites as calculated in equation 3.10 as a function of porosity and pore size. The dashed black line is a guide to the eye showing 10% reduction in thermal conductivity.

As suggested by Figure 3.7, to significantly alter (by $\geq 10\%$) the thermal conductivity of a porous material by controlling the pore size at constant porosity requires a high porosity and submicron size pores. This is not achievable using the hydrogel bead templating technique.

3.2.4. Mechanical properties

Through the use of three different templating techniques, composite gypsum materials with three very different microstructures have been obtained. An investigation into how the microstructure of the porous gypsum composites affects their mechanical properties was performed. Fresh samples without the holes for thermal conductivity testing were prepared and dried to a constant weight. They were subjected to compression until structural failure which allowed calculation of the compressional strength and Young's modulus. Figure 3.8 shows how they were obtained and the results are presented in Figure 3.9.

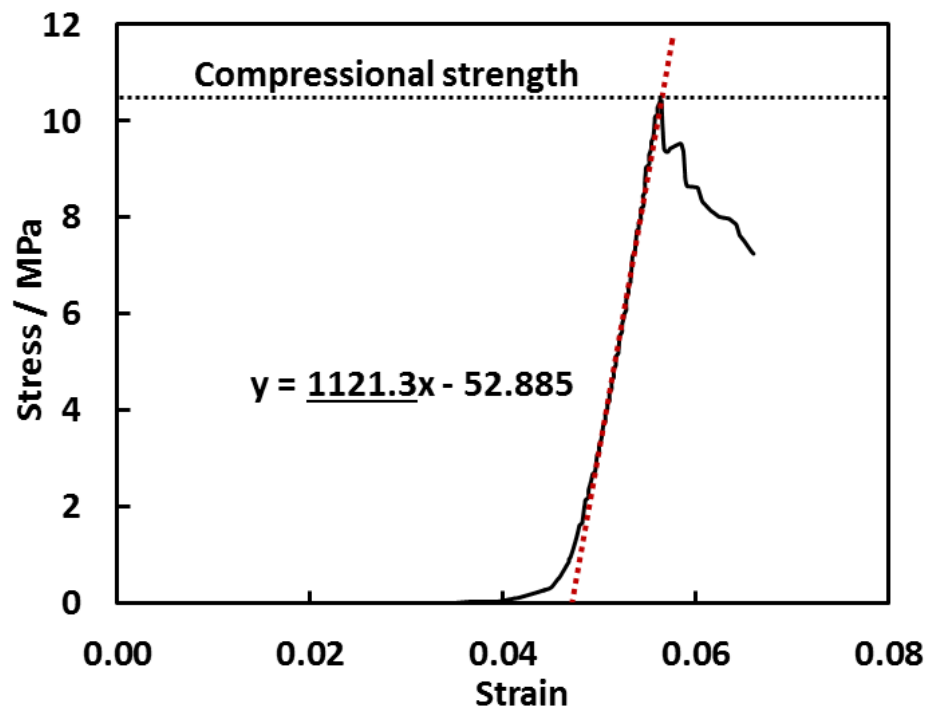


Figure 3.8. An example graph showing stress against strain for a porous gypsum composite. The stress was obtained by normalisation of the force with the cross-sectional area of the sample and the strain was obtained by dividing the displacement by the height of the sample. The compressional strength was taken as the stress at fracture point and the Young's modulus is the gradient of the linear region.

It was found that increasing the size of the hydrogel bead templates used to introduce porosity from 100 μm to 600 μm decreased the compressional strength by approximately 50% when the overall porosity was between 15-45%. When the porosity reached 60%, the compressional strength was independent of the material's microstructure. Likewise, when increasing the template hydrogel bead size, the Young's modulus decreased by approximately 60% for porosity in the range 15-45%. When the porosity reached 60%, however, the average Young's modulus of the porous gypsum composites produced with large hydrogel beads as templates was 80% lower than the ones produced with small hydrogel beads.

The gypsum composites formulated using MC solution had compressional strengths and Young's moduli comparable to the ones produced with small beads. When using either small beads or MC solution to produce the porous gypsum composites, there was a relatively linear decrease of the compressional strength and Young's modulus with the volume percentage of template hydrogel of MC solution used. On the other hand, when using large beads as a template, there was a large initial decrease of approximately 60% in both the compressional strength and Young's modulus when the porosity was increased from 0 to just 15%. At porosities higher than 15% however, a linear decrease was observed. As the thermal conductivity does not vary with pore size on the length scales investigated here, but the mechanical properties do, it is possible to have materials with constant thermal conductivity and controlled mechanical properties by varying the pore size.

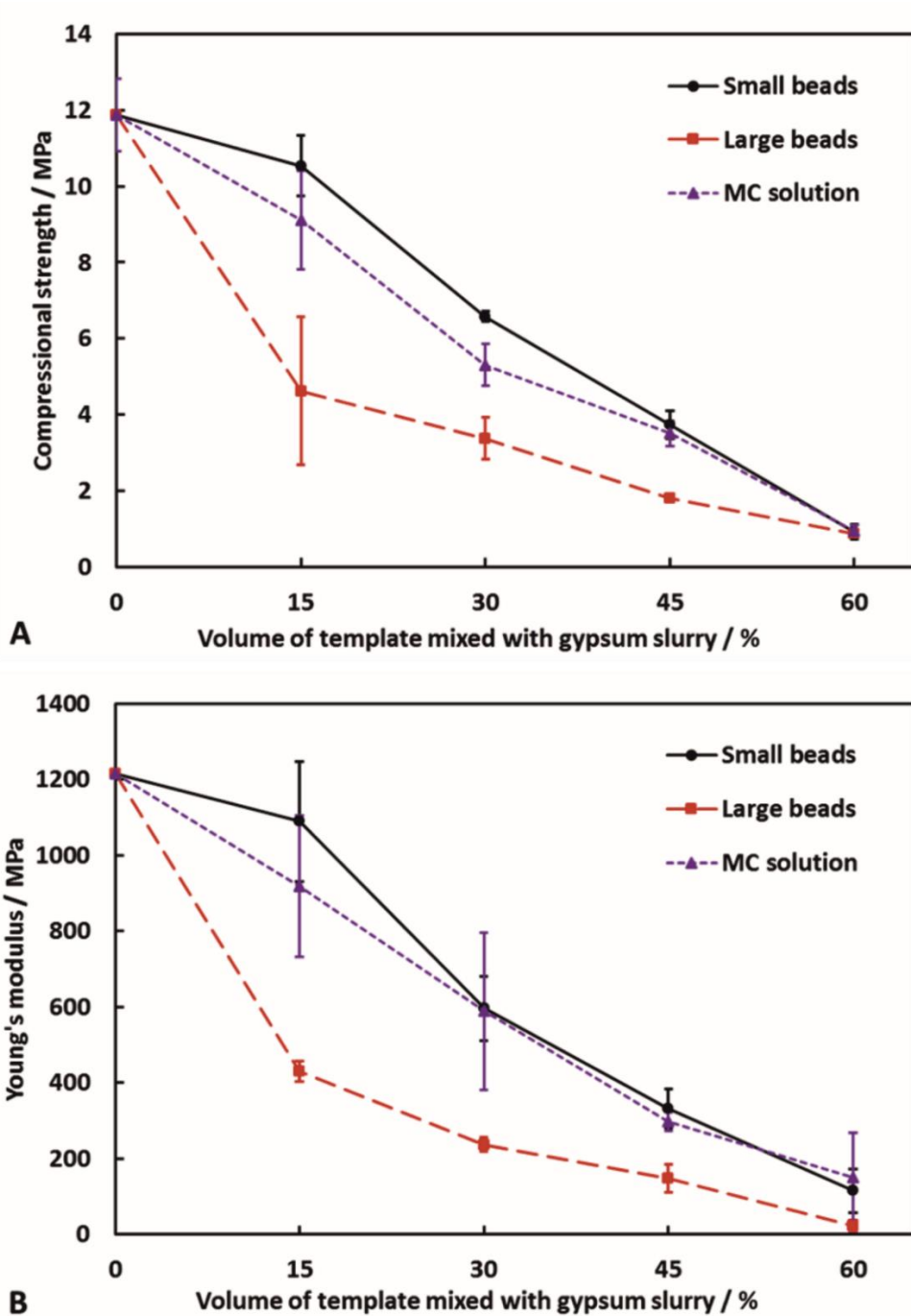


Figure 3.9. The compressional strength and (B) the Young's modulus of the porous gypsum composites as a function of the volume of template (small beads, large beads or MC solution) initially mixed with the gypsum slurry. Each sample was measured at least twice and the average value is shown with the error bars being the standard deviation.

The phenomenon of smaller pores producing materials with enhanced mechanical properties has also been reported by other authors^{21,22} and attributed to a combination

of an increased surface area to volume ratio, sharing of the load between more and smaller pores and a decrease of the moment upon the walls of the small pores.^{22,23}

An investigation into how varying the ratio of large pores to small pores, at constant porosity, affects the mechanical properties of the porous composites was performed. With the overall volume of hydrogel beads kept at a constant 50%, the ratio of large beads to small beads was varied to produce hierarchically porous gypsum composites with controlled pore sizes and controlled ratio of large pores to small pores. Their mechanical properties are presented in Figure 3.10.

The mechanical properties of the hierarchically porous composite materials increase with an increase in the overall volume of small hydrogel beads. This can be explained by Figure 3.9, where the composites produced using small beads had increased mechanical properties when compared to those produced using large beads.

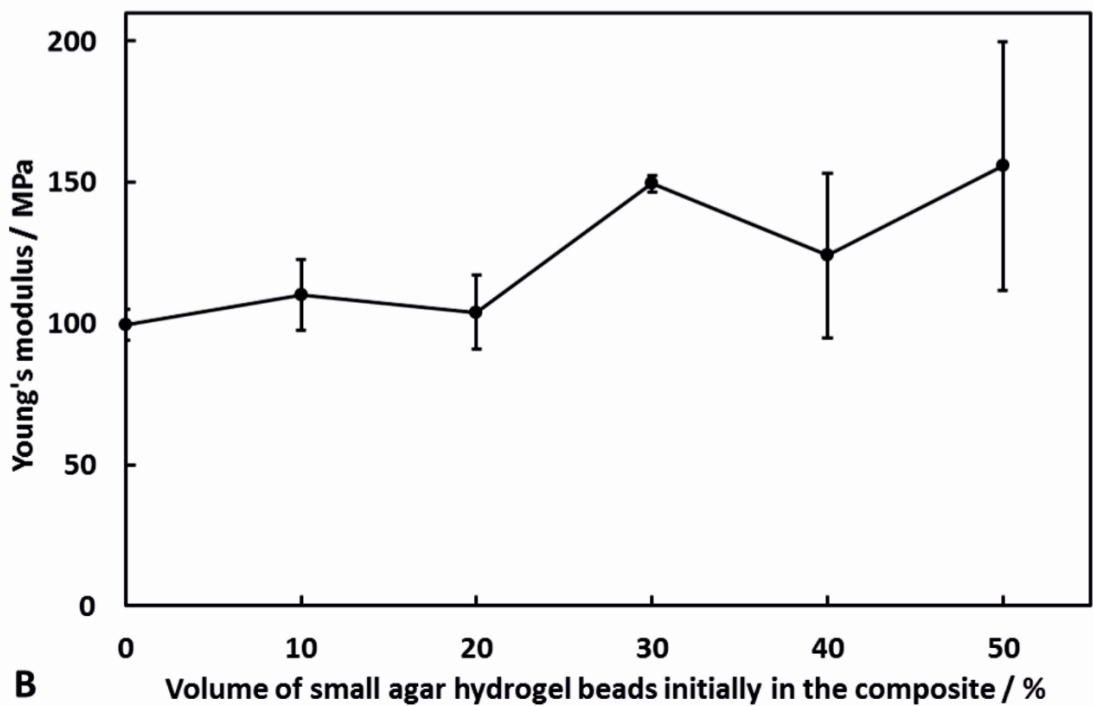
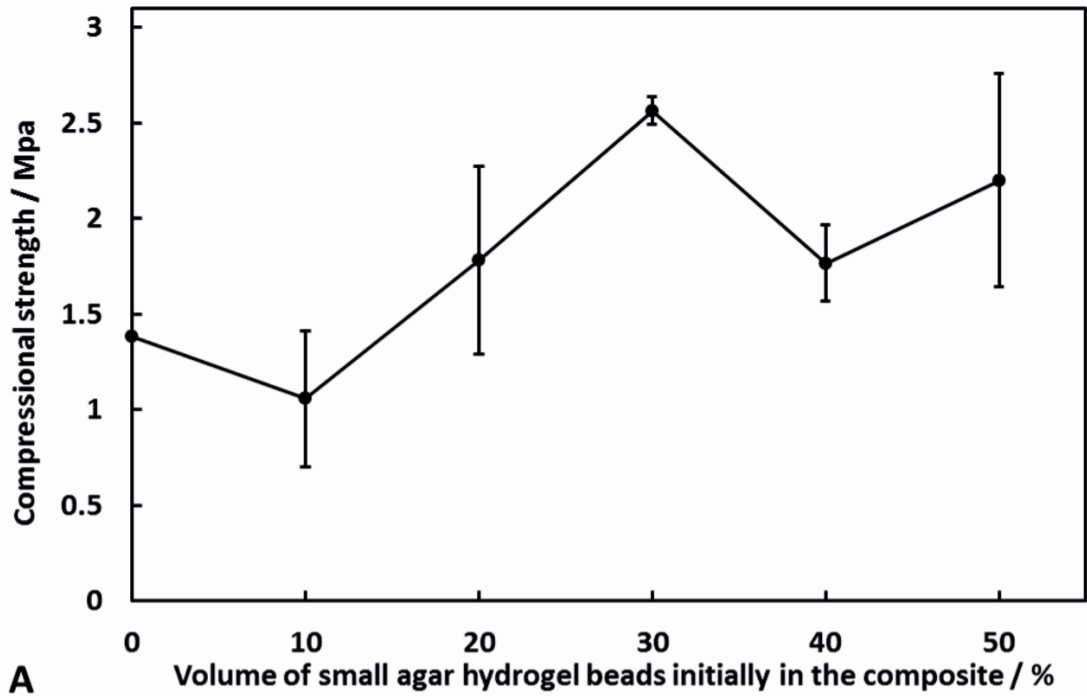


Figure 3.10. Compressive strength (A) and Young's modulus (B) of hierarchically porous gypsum composites. The overall volume of gypsum slurry used was kept constant at 50%. The volume percentage of small hydrogel beads is shown on the x-axis and the volume percentage of large beads is what makes up the rest i.e. when 10% by volume of small hydrogel beads are used, 40% by volume of large beads are used. Each data point is the average of at least two results and the error bars are the standard deviation.

Finally, a study into how varying the ratio of hydrogel beads (large or small) to MC solution, at constant overall volume percentage of template, affected the mechanical properties of the hierarchically porous composites produced was undertaken. The overall volume percentage of gypsum slurry used during production was kept at 50%, while the volume percentages of MC solution and hydrogel beads were varied. The results are shown in Figures 3.11.

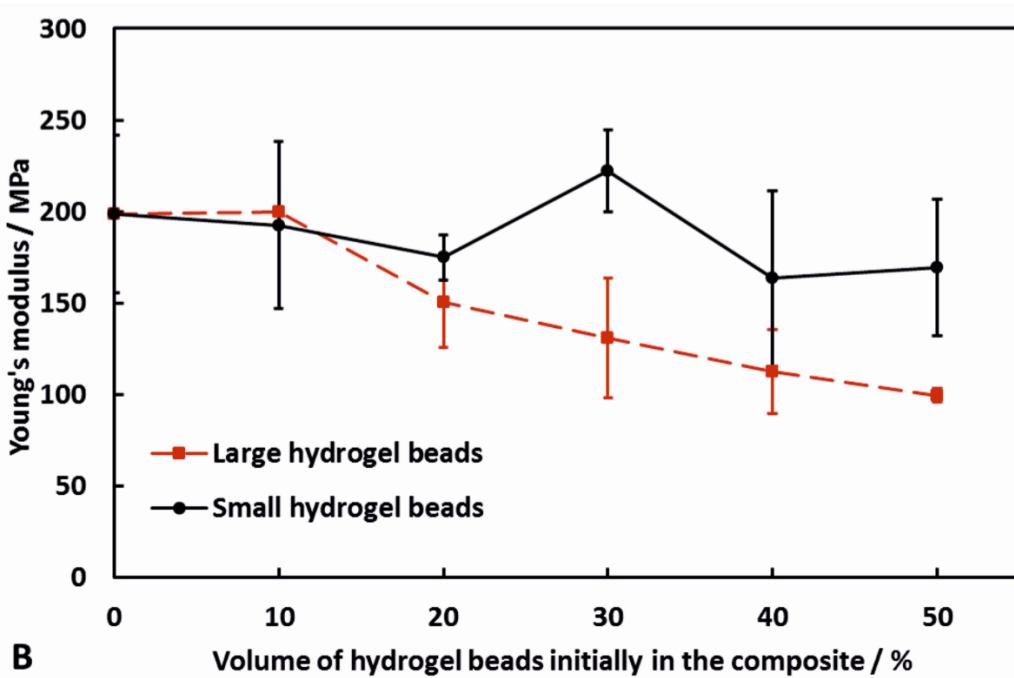
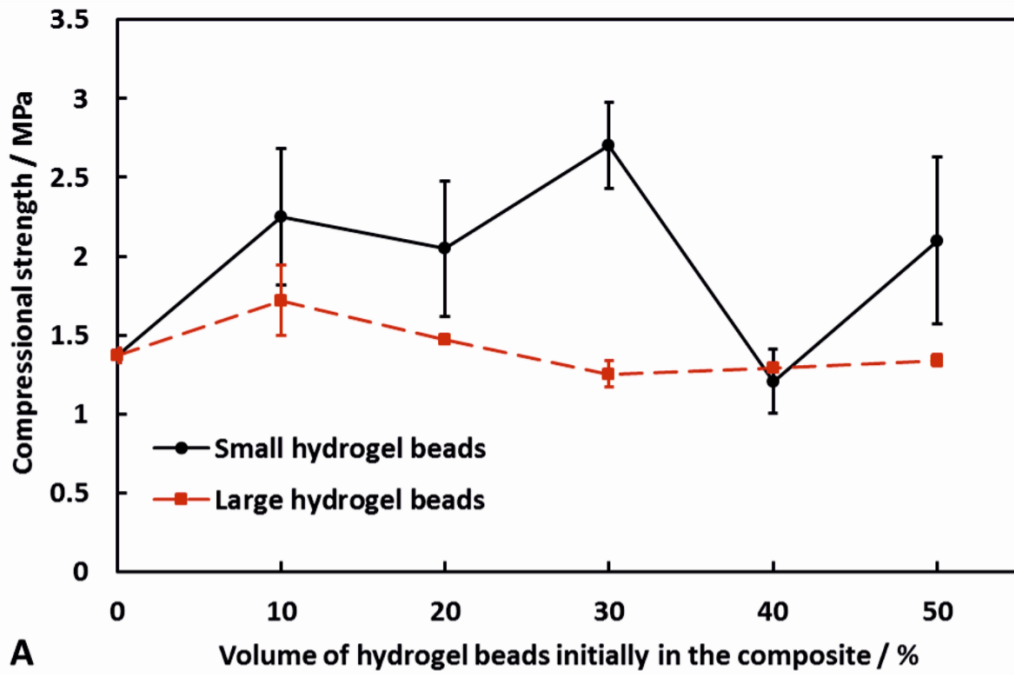


Figure 3.8. Compressive strength (A) and Young's modulus (B) of hierarchically porous gypsum composites produced through a combined approach of viscous trapping with MC solution and hydrogel bead templating. The overall volume percentage of gypsum slurry was kept constant at 50%. The volume percentage of hydrogel beads is shown on the x-axis and volume percentage of MC solution is what makes up the rest i.e. when 10% by volume of hydrogel beads are used, 40% by volume of MC solution is used. Each data point is the average of at least two measurements and the error bars are the standard deviation.

In Figure 3.11, an increase in the compressional strength can be seen when increasing the volume percentage of small hydrogel beads, with a maximum compressional strength when the volume percentages of small beads and MC solution are 30% and 20%, respectively. It has been suggested previously that hierarchically porous materials could have an optimum balance between different sized pores to produce materials with enhanced mechanical properties.²⁴ In Figure 3.11(B), it can be seen that as the volume percentage of large beads compared to MC solution is increased, the Young's modulus decreases. This shows there is scope for tuning a material's mechanical properties at constant porosity by varying the microstructure.

3.2.5. Microstructure analysis

Samples were taken from the gypsum control sample and the porous gypsum composites produced with 60% by volume of the templates and viewed with a benchtop SEM, without coating. They were viewed at reasonable magnifications to observe the differences in the composite microstructures due to the presence of the different templates during the formulation process. Figures 3.12(A-C) show the gypsum control sample at three different magnifications (50x, 250x and 2500x) and Figures 3.12(D-F) show the porous gypsum composites produced with 60% by volume of large beads, small beads and MC solution, respectively.

In Figure 3.12(D) it can be seen that the pores present within the composites produced using large hydrogel beads are of a similar size to the original beads used before their embedding in the gypsum slurry and further drying. Furthermore, it can be observed that upon drying of the composites, the hydrogel residues stay mostly within the sample pores. Again, when using small beads as templates, the pore sizes reflect the size of the beads used, however no visible residues of hydrogel material can be seen within the pores. The larger surface area-to-volume ratio of the small hydrogel beads means that the residue produced upon drying will be much thinner so it could have intercalated in between the surrounding microcrystals among the gypsum network.

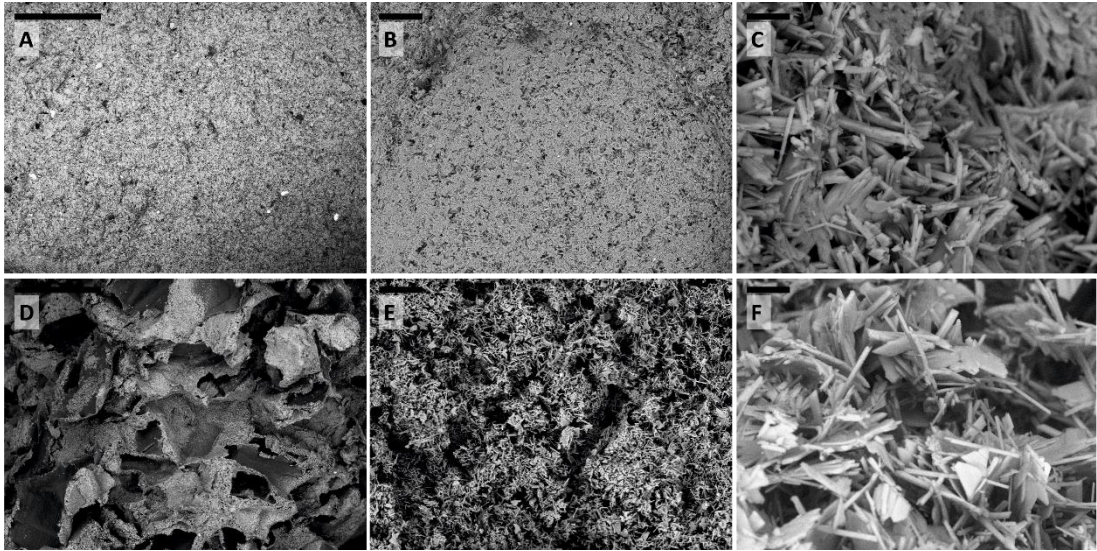


Figure 3.9. (A) – (C) SEM images of the gypsum control sample at three different magnifications. The scale bars are 1000 μm , 100 μm and 10 μm , respectively. (D) – (F) SEM images of the porous gypsum composites produced with 60% by volume of large beads, small beads or MC aqueous solution, respectively. The magnification and scale bars are the same as the image above them.

Figure 3.13(A) and 3.13(B), below, show higher magnifications of the inner pore structures of the composites produced with large and small beads, respectively.

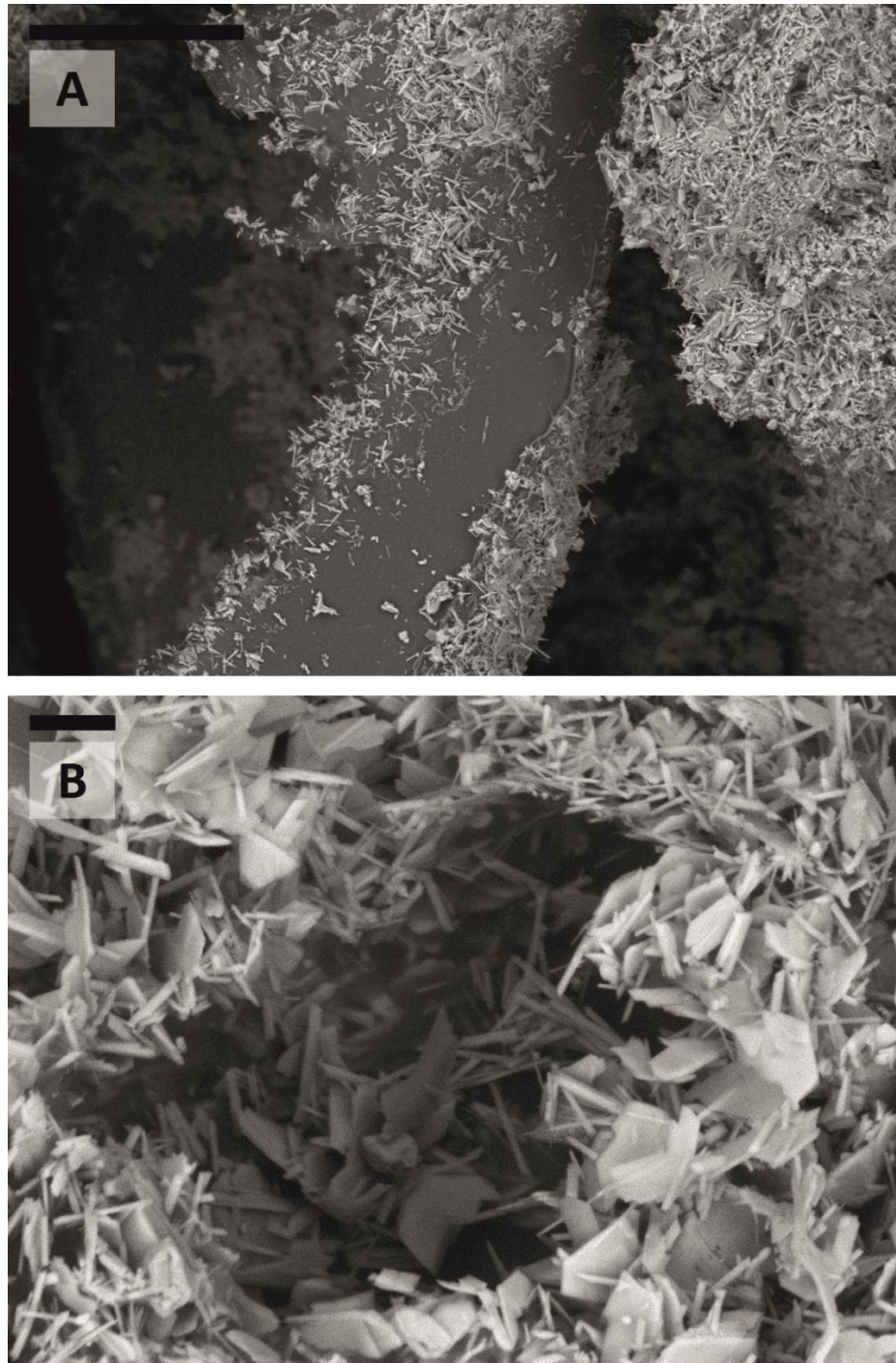


Figure 3.10. The inner pore structures of composites produced using large beads (A) or small beads (B). Note that when using large beads as porosity inducing templates, the gypsum needles and platelets attach to the hydrogel residue upon drying whereas when using small beads, this is not seen. (A) has a magnification of 500x and the scale bar corresponds to a distance of 100 μm . (B) has a magnification of 2000x and the scale bar corresponds to a distance of 10 μm .

Figure 3.13 shows the significantly different microstructures of two composites produced using hydrogel beads of different average size. In Figure 3.13(A), there is evidence of the gypsum crystallite needles and platelets being attached to the hydrogel residues which means that they are separate from the continuous gypsum network. This could possibly contribute to the reduction in mechanical properties when compared to the composites produced using small beads or MC solution, as these structures are not seen within the pores of those samples.

The use of MC solution produced porous composites with an expanded microstructure, as seen through comparison of Figure 3.12(C), Figure 3.12(F) and Figures 3.14(A) and 3.14(B). With the expansion of the gypsum network, the mechanical properties decreased. Similarly to the gypsum composites produced using small hydrogel beads, hydrogel residue was not observed. These differences in the internal pore structures could explain the varying mechanical properties at the same porosity. The composites produced with large hydrogel beads were weaker possibly due to the presence of hydrogel residues within the pores. The needles and platelets attached to the residues will not be contributing to the mechanical properties of the composites, as they are not part of the continuous gypsum network.

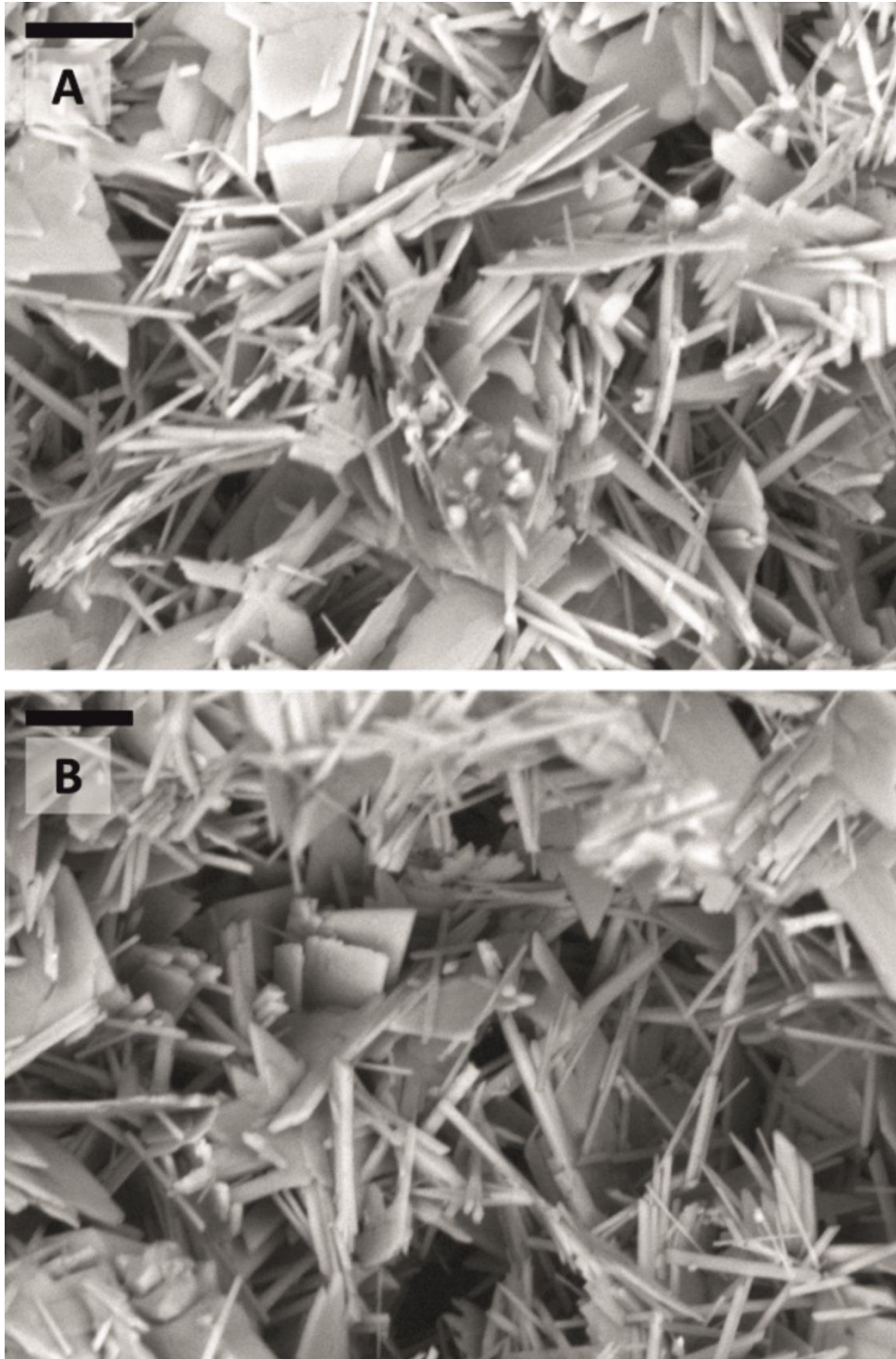


Figure 3.11. SEM images of porous gypsum composites produced with 30% (A) and 60% (B) MC solution. Note the less dense packing of the gypsum needles and platelets when the volume percentage of MC solution is increased. The magnification for both images is 2500x and the scale bars are 10 μm .

Hierarchically porous gypsum composites produced using two different sized hydrogel beads were visualised. The two distinct pore sizes produced as a result of different sized hydrogel beads used is easily seen and is demonstrated in Figure 3.15.

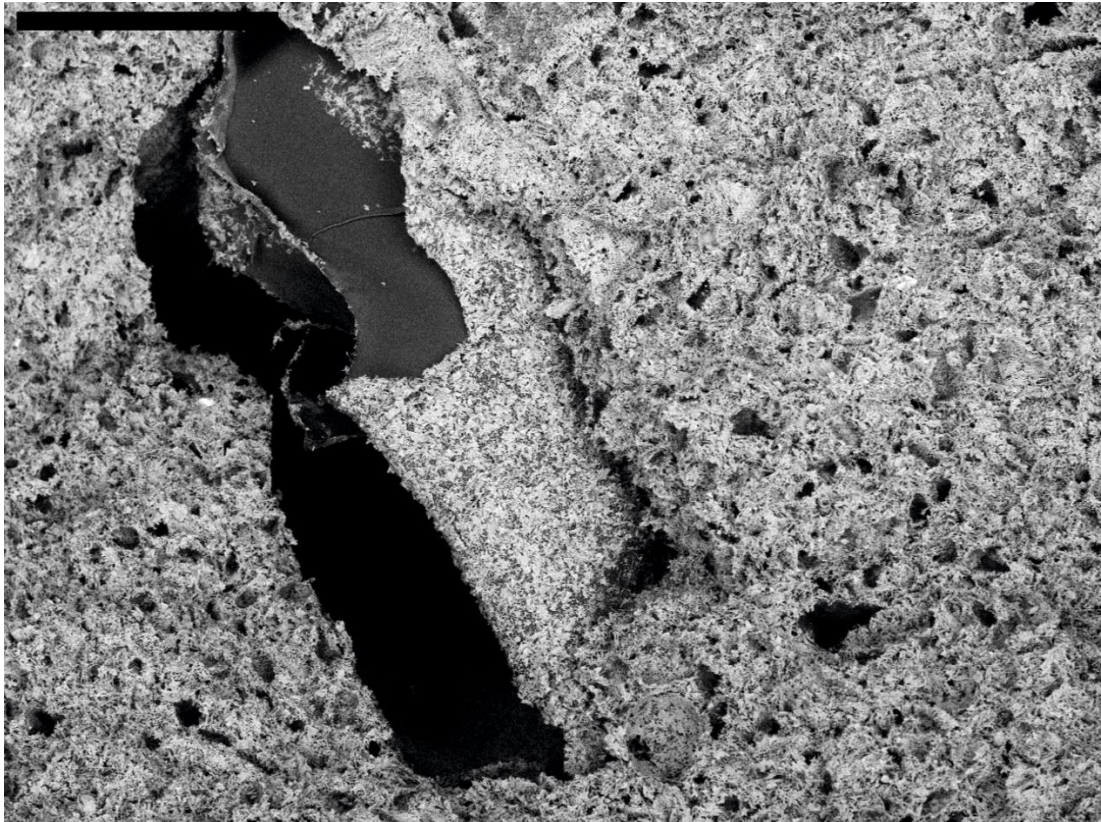


Figure 3.12. SEM image of hierarchically porous gypsum produced using a dual size hydrogel bead templating process. A composite with 50% porosity produced using 30% large beads and 20% small beads is shown. The magnification is 100x and the scale bar corresponds to a distance of 500 μm .

One can observe the hierarchical porosity present in the gypsum composites due to templating with two different size distributions of hydrogel beads. Moreover, hydrogel residues are again present within the large pores, with gypsum needles and platelets attached to them.

Finally, the hierarchically porous gypsum composites fabricated through the use of viscous trapping with MC solution and hydrogel templating with different sized beads were visualised. It was possible to observe evidence of both mechanisms of controlling the porosity.

The difference in how closely packed the gypsum particles are packed can be seen in Figure 3.16. With an increase in the volume percentage of MC solution used to produce the porous composites, the needles and platelets are less tightly packed.

Combining these methods to produce hierarchically porous materials gives scope for the preparation of a range of materials with well-defined, controllable microstructures.

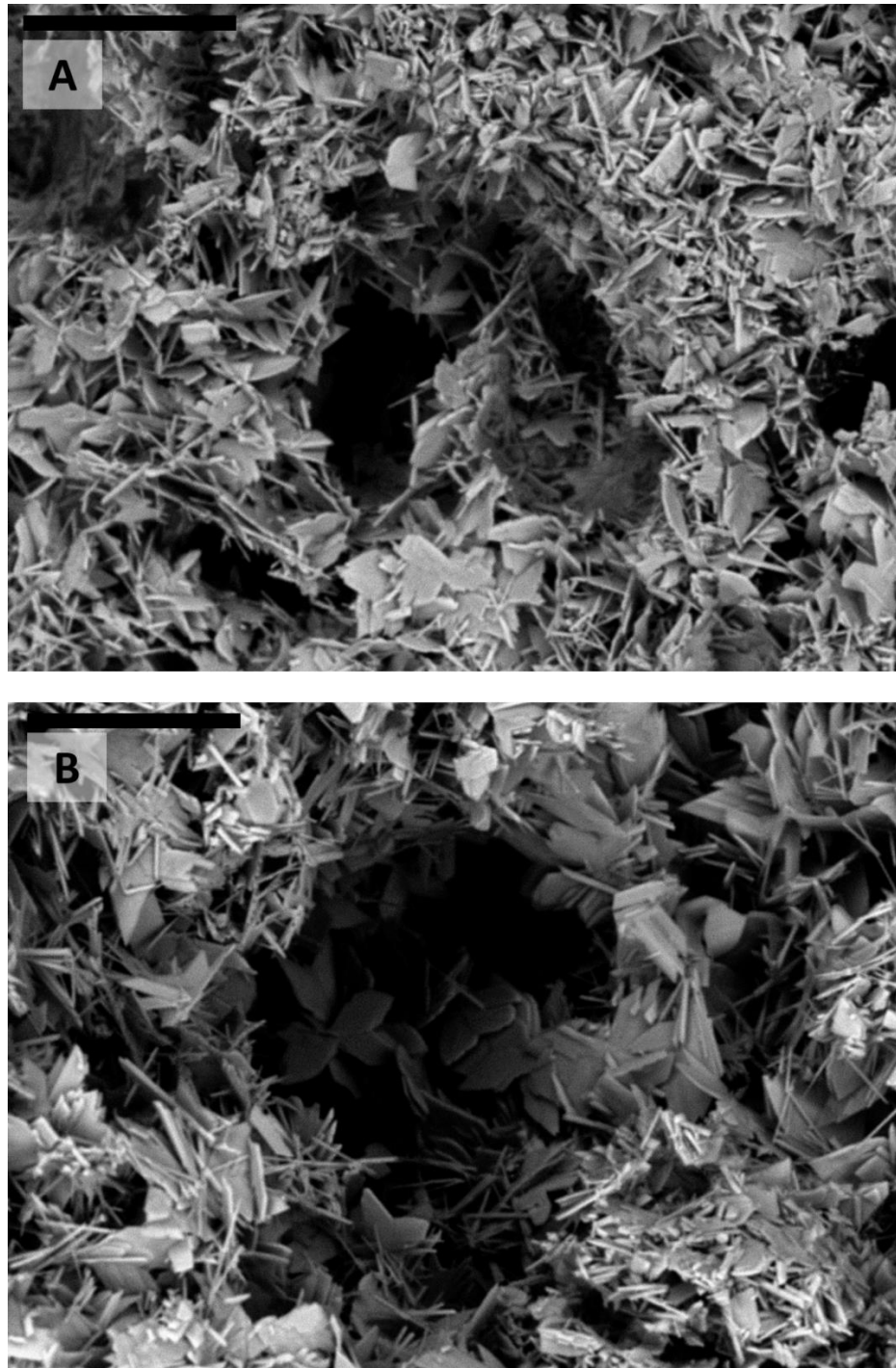


Figure 3.13. SEM images of hierarchically porous gypsum composites produced using a combination of MC solution and small hydrogel beads. (A) was produced with 10% MC solution and 40% small hydrogel beads and (B) was produced with 40% MC solution and 10% small hydrogel beads.

3.3. Conclusions

A hydrogel bead templating technique has been used to produce porous gypsum composites with a controllable porosity, pore size and microstructure. Preparation of agar hydrogel beads of two different average size distributions ($600 \pm 300 \mu\text{m}$ or $100 \pm 50 \mu\text{m}$) was achieved by blending agar hydrogel for different amounts of time. This allowed the use of these as templates to produce hierarchically porous materials with a pore size distribution that reflects the size of the hydrogel beads used. An alternative viscous trapping method was also developed to produce porous gypsum composites which utilises a viscous MC aqueous solution which suspended gypsum particles in solution during the setting process. This produced gypsum composites with an expanded innate porosity without a controlled pore size, but with a porosity directly reflected by the volume of MC solution used during the material formulation. These methods allowed the introduction of up to 60% porosity with negligible volume reductions.

Through the use of a radial heat flow setup, a value of the thermal conductivity of gypsum plaster ($0.43 \pm 0.02 \text{ W m}^{-1} \text{ K}^{-1}$) was obtained which is similar to values found in the literature. Then an investigation into how the porosity and microstructure of the composites affected their thermal conductivities was performed. Increasing their porosity showed a linear decrease in their thermal conductivities. Furthermore, it was found that at the pore sizes and porosities studies here, the thermal conductivity was independent of the microstructure. This was due to the pore sizes not being small enough to reduce the thermal conductivity of the air within them.

On the other hand, the Young's modulus and compressional strength were strongly dependent on the microstructure of the gypsum composites. A large decrease in the mechanical properties of the composites produced using large hydrogel beads was found when comparing to the samples produced by templating small hydrogel beads or MC solution, which had very similar mechanical properties to each other. This decrease in mechanical properties when using large hydrogel beads as templates was attributed to the fact that they leave residues upon drying. Gypsum needles and platelets attach to the residue and therefore do not contribute to the overall mechanical properties of the porous composite. Through the use of SEM, the different microstructures of the composites produced using the three different templates were studied. It was clearly seen that the pore size was dependent on the size of the hydrogel

beads used during the sample preparation. An expansion of the gypsum network due to a smaller amount of gypsum particles being suspended in MC solution in the same overall volume during the setting process was observed. Finally, it was found that materials with a controllable thermal conductivity can be produced by varying the porosity of the composites, then the mechanical properties could be tuned by changing the pore size at a constant porosity.

This chapter describes methods of preparing porous and hierarchically porous gypsum composites not previously seen in the literature. It develops on the hydrogel templating technique previously reported⁸ by offering extra levels of control; either by using hydrogel bead slurries with two different size distributions to introduce tuneable hierarchical porosity into the dried composites or by utilisation of a viscous MC solution to suspend the gypsum particles during the setting process. Furthermore, it is the first time the thermal conductivity of such porous composites have been reported.

3.4. References

- 1 S. Shafiee and E. Topal, *Energy Policy*, 2009, **37**, 181–189.
- 2 E. Cuce, P. M. Cuce, C. J. Wood and S. B. Riffat, *Renew. Sustain. Energy Rev.*, 2014, **34**, 273–299.
- 3 M. A. Hasan and K. Sumathy, *Renewable Sustainable Energy Rev.*, 2010, **14**, 1845–1859.
- 4 N. L. Panwar, S. C. Kaushik and S. Kothari, *Renew. Sustain. Energy Rev.*, 2011, **15**, 1513–1524.
- 5 P. Nejat, F. Jomehzadeh, M. M. Taheri, M. Gohari and M. Z. Abd. Majid, *Renew. Sustain. Energy Rev.*, 2015, **43**, 843–862.
- 6 Y. W. I. Rahmanian, *Acta Polytech.*, 2009, **49**, 16–20.
- 7 D. S. Smith, A. Alzina, J. Bourret, B. Nait-Ali, F. Pennec, N. Tessier-Doyen, K. Otsu, H. Matsubara, P. Elser and U. T. Gonzenbach, *J. Mater. Res.*, 2013, **28**, 2260–2272.
- 8 M. Rutkevičius, S. K. Munusami, Z. Watson, A. D. Field, M. Salt, S. D. Stoyanov, J. Petkov, G. H. Mehl and V. N. Paunov, *Mater. Res. Bull.*, 2012, **47**, 980–986.
- 9 K. C. Labropoulos, D. E. Niesz, S. C. Danforth and P. G. Kevrekidis, *Carbohydr. Polym.*, 2002, **50**, 393–406.
- 10 A. J. Lewry and J. Williamson, *J. Mater. Sci.*, 1994, **29**, 5524–5528.
- 11 A. J. Lewry and J. Williamson, *J. Mater. Sci.*, 1994, **29**, 5279–5284.
- 12 T. M. Tritt and D. Weston, Measurement Techniques for Determining Thermal Conductivity, in *Thermal Conductivity: Theory, Properties, and Applications*, ed. T. M. Tritt, Springer US, Boston, MA, 2004, ch. 2.1, pp. 187–203.
- 13 B. Notario, J. Pinto and M. A. Rodriguez-Perez, *Prog. Mater. Sci.*, 2016, **78**, 93–139.
- 14 D. K. Hale, *J. Mater. Sci.*, 1976, **11**, 2105–2141.
- 15 M. Alvarez-Lainez, M. A. Rodriguez-Perez and J. A. DE Saja, *J. Polym. Sci.*

- Part B Polym. Phys.*, 2008, **46**, 212–221.
- 16 E. Solórzano, M. A. Rodríguez-Perez, J. Lázaro and J. A. de Saja, *Adv. Eng. Mater.*, 2009, **11**, 818–824.
- 17 G. Thomas, *Fire Mater.*, 2002, **26**, 37–45.
- 18 B. Notario, J. Pinto, E. Solorzano, J. A. De Saja, M. Dumon and M. A. Rodríguez-Perez, *Polym. (United Kingdom)*, 2015, **56**, 57–67.
- 19 S. Jennings, *J. Aerosol Sci.*, 1988, **19**, 159–166.
- 20 X. Lu, R. Caps, J. Fricke, C. T. Alviso and R. W. Pekala, *J. Non. Cryst. Solids*, 1995, **188**, 226–234.
- 21 M. Rutkevičius, Z. Austin, B. Chalk, G. H. Mehl, Q. Qin, P. A. Rubini, S. D. Stoyanov and V. N. Paunov, *J. Mater. Sci.*, 2015, **50**, 3495–3503.
- 22 Z. Li, L. Yang, Y. Li, Y. Yang, C. Zhou, Y. Ding, J. Zhao and Y. Li, *Mater. Des.*, 2013, **45**, 52–55.
- 23 Z. G. Xu, J. W. Fu, T. J. Luo and Y. S. Yang, *Mater. Des.*, 2012, **34**, 40–44.
- 24 L. L. C. Wong, P. M. Baiz Villafranca, A. Menner and A. Bismarck, *Langmuir*, 2013, **29**, 5952–5961.

4. Sound transmission loss of hierarchically porous composites produced by hydrogel templating and viscous trapping techniques

In the previous chapter, the preparation of porous and hierarchically porous gypsum composites through the use of hydrogel bead templating or viscous trapping has been discussed. The hydrogel bead templating technique allows for control over the porosity, pore sizes and also the ratio of pore sizes at a constant porosity whereas the viscous trapping technique allows control over the porosity only. In this chapter, the sound transmission loss of these porous and hierarchically porous composites has been studied. It was found that the ones produced by the viscous trapping method had a lower sound transmission loss over the frequency range investigated as the overall porosity was increased. The effect of the composite pore size at a constant porosity on the sound transmission loss was demonstrated. The experiments showed that porous composites with large pores showed increased sound transmission loss at lower sound frequencies. As the frequency increased, the difference between their sound transmission loss (STL) spectra decreased and at the higher frequency range (>2420 Hz), the composites with smaller pores began to perform better. The hierarchically porous composite had an intermediate STL spectrum, suggesting a way for tailoring the hierarchically porous structure at constant porosity to achieve desired sound insulating properties at certain frequencies.

4.1. Introduction

Noise pollution is becoming a major problem due to the rapidly increasing population leading to people living in close proximity with each other. The use of machinery to automate or assist many processes as society advances also contributes to exposing noise to undefended ears.¹ Severe health hazards have been attributed to noise pollution such as ischemic heart disease, hypertension, hearing loss and depression.²⁻⁴ These issues have necessitated the investigation into both sound absorption and sound insulation properties of a variety of materials. Foams with an open porous structure have been used extensively for sound absorption.⁵ It has been shown that

introducing open porosity into a material will increase its sound absorption coefficient, especially at higher frequencies.⁶⁻⁹

Sound absorption and sound insulation are significantly different acoustical concepts. Sound absorption accounts for the sound energy loss due to viscous friction and thermal effects within the material while sound insulation is the partial prevention of the transmission of sound waves through the material.¹⁰⁻¹² Due to mass and stiffness laws, porous materials alone are less used for sound insulation. They are, however, used as centre pieces between two dense, stiff materials in a sandwich-type structure.^{13,14} Composite materials have been studied for their sound insulating properties, often being a material with a filler encased within.¹⁵ A recent study showed that the addition of mica platelets to poly(vinyl chloride) (PVC) foams affected the transmission of sound through the composite. During formation of the PVC foam, when the pore density became high enough, an ordering of the mica along the walls of the pore occurred, significantly increasing the sound insulating properties of the composite.¹⁶

In general, there have been two methods to define sound insulating properties. The first method required two adjacent rooms; one where sound was generated and transmitted through a wall containing the sample under investigation and a second room where the sound power was measured. The sound power was also measured in the first room, thereby allowing the STL to be calculated.¹⁷ Although conceptually simple, this method suffers from multiple drawbacks, such as it being time consuming, expensive and requiring a large sample. The second method uses a four microphone impedance tube that has been developed for the measurement of STL. It is cheap, allows rapid measurements and the sample only needs to be as wide as the tube (generally not more than 10 cm).¹⁸

Hydrogels are 3D hydrophilic, polymeric networks that have the ability to be swollen with large amounts of water. Their properties are also highly tailorable by varying polymer concentration, concentration of cross-linking agents, or by combining two or more polymers into a hybrid hydrogel with new properties. They have been exploited in areas such as porogenic materials,¹⁹ drug delivery and wound dressings,²⁰ tissue engineering²¹ and food structuring.^{22,23}

Recently, a hydrogel bead templating technique has been described as a cheap, easy and environmentally friendly method for fabrication of a variety of porous materials with precise control of the porosity and the pore size.¹⁹ It involved chopping hydrogels to hydrogel beads of desired size which are then used as template for structuring other materials. Slurry of these beads was then mixed with templating material (e.g. cement, gypsum, clay, resin, etc.) before curing. After solidification of the surrounding matrix around the templates, the material is dried and the water is evaporated from the hydrogel bead templates, thus leaving pores in its place that reflected the size of the beads used. The porosity reflects the volume percentage of the hydrogel beads used. This only worked when water is able to leave the system through open pores.

Here, the same templating methods as described in Chapter 3 to produce porous and hierarchically porous gypsum composites have been utilised. MC solution has been used to fabricate porous gypsum composites with varying porosity and the hydrogel bead templating technique has been used to prepare gypsum composites with a constant porosity (40%) with different pore size distributions; controlled by varying the size distributions of the hydrogel bead templates or by mixing slurries of hydrogel beads with two different size distributions.

In this chapter, an investigation into how the sound transmission loss and the mechanical properties of gypsum composites of hierarchical porosity fabricated using these methods vary with the pores volume fraction and size distribution has been performed.

4.2. Results

4.2.1. Size distributions of hydrogel beads

In order to investigate the effect of the pore size on the sound insulating properties of porous gypsum, control over the size distributions of the hydrogel bead templates used during the fabrication of the porous gypsum composites was required. This was important as the average size of the hydrogel bead templates used determines the average size of the pores in the dried composites. The agar hydrogel was blended for different durations between 10 – 600 seconds and their size distributions were obtained by analysing optical images of hydrogel beads dispersed in water. Visualising the hydrogel beads in water will still give an accurate representation of their sizes as it is

known that agar hydrogel does not swell when dispersed in water.²⁴ It was found that blending for 10 seconds produced hydrogel beads with an average size of $600 \pm 300 \mu\text{m}$ while after blending for 600 seconds, hydrogel beads with an average size of $100 \pm 50 \mu\text{m}$ could be obtained. In the further experiments these two size distributions of hydrogel beads will be referred to as 'large beads' and 'small beads', respectively. As the shape of the beads was irregular due to their preparation method, they were measured horizontally through the widest section. The cumulative hydrogel bead size distributions after blending for 10 or 600 seconds, along with optical microscopy images showing their morphology are presented in Figure 4.1.

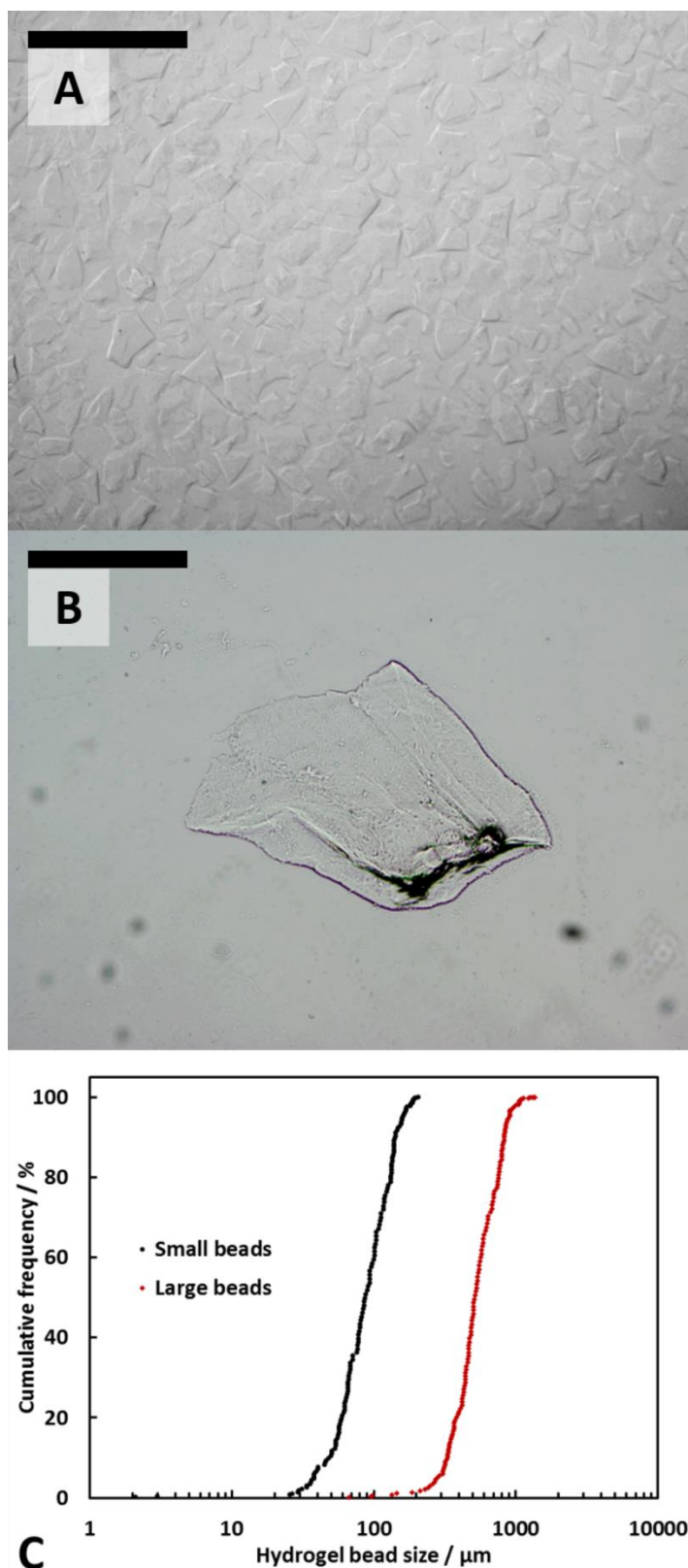


Figure 4.1. (A) and (B) Optical microscopy images showing the size and morphology of the agar hydrogel beads produced by blending 2% agar hydrogel for 600 seconds and 10 seconds, respectively. The scale bars represent a distance of 500 μm. (C) The percentage cumulative size distribution for both the small and large hydrogel beads.

4.2.2. Porous gypsum composites

After the composites were dried to a constant mass, they were weighed and their dimensions were measured. The volume and density of each sample was compared to a gypsum control sample that was produced without any hydrogel beads or MC solution. This allowed for calculation of the porosity and the reduction in volume of the porous gypsum composites. As hardened gypsum plaster itself is a porous material,²⁵ the porosity reported is, in fact, the reduction in density when compared to the gypsum control sample. It was calculated using the following equation:

$$\theta = \left(1 - \frac{\rho}{\rho_0}\right) \times 100\%. \quad (4.1)$$

Here θ is the porosity (%), ρ is the density of the porous gypsum composite (g cm^{-3}) and ρ_0 is the density of the gypsum control sample (g cm^{-3}).

The reduction in sample volume V_{red} (%) upon drying of the gypsum-hydrogel composite was calculated as follows:

$$V_{red} = \left(1 - \frac{V}{V_0}\right) \times 100\%. \quad (4.2)$$

Here V is the volume of the porous gypsum composite (cm^3) and V_0 is the volume of the gypsum control sample (cm^3).

Figure 4.2(A) shows the porosity and the reduction in volume of the porous gypsum composites produced using different volume percentages of MC solution after drying. The composites produced by the hydrogel templating technique all were done with the same volume percentage of hydrogel beads, only the volume ratio of large to small beads was varied. Figure 4.2(B) shows that the porosity and reduction in volume is not significantly influenced by the variation in size of the hydrogel beads used. In Figure 4.2A one can see that the porosity is directly controlled by the volume percentage of MC solution used during the sample formulation. When using 50% by volume of MC solution, the porosity of the gypsum composite after drying is approximately 50%. Furthermore, the reduction in volume is not significant (<4%) for all porous composites.

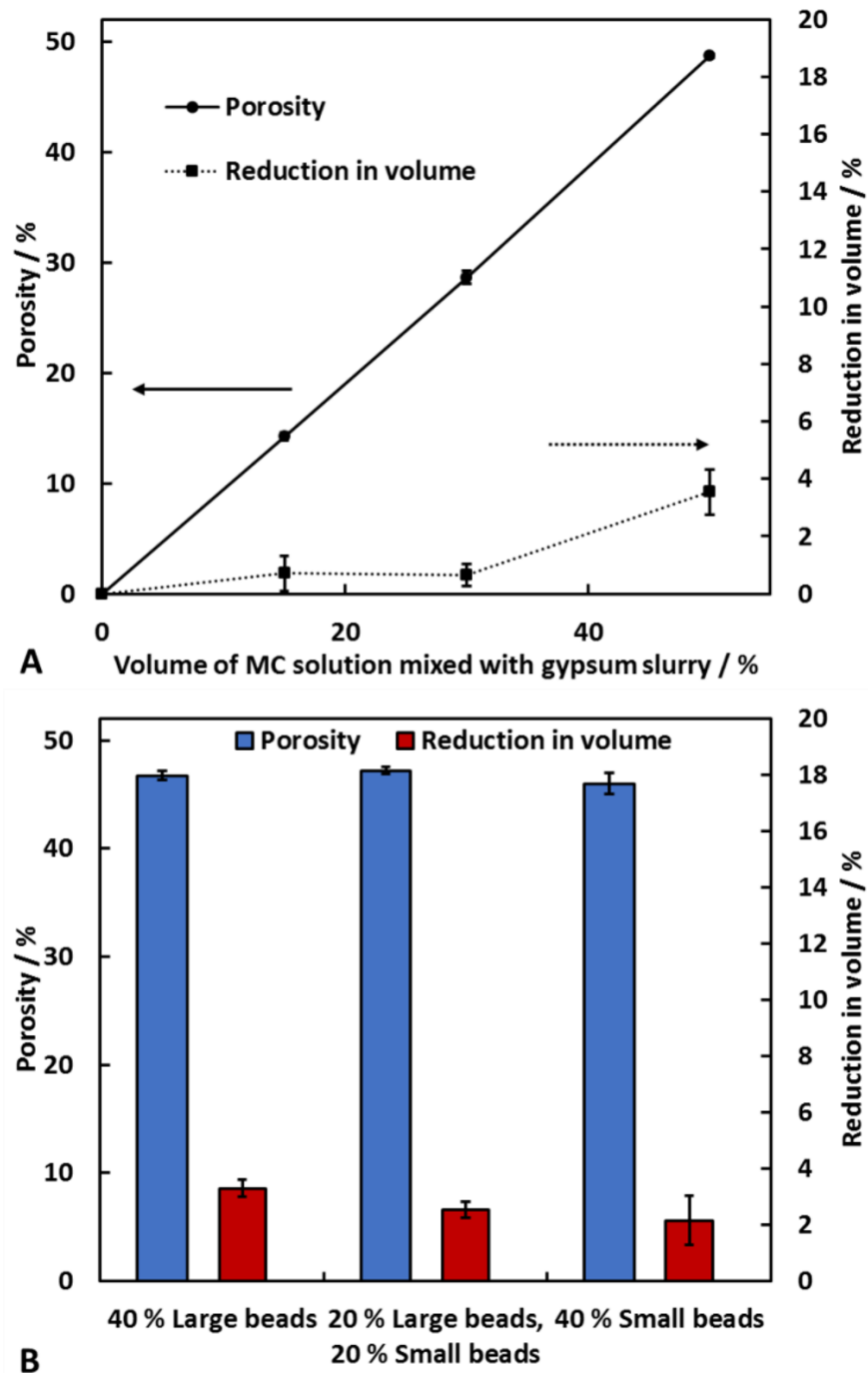


Figure 4.2. (A) The porosity and the volume reduction for the porous gypsum composites produced using different volume percentages of MC solution with the viscous trapping method. The porosity and volume reduction for the sample produced using the hydrogel beads templating method can be seen in (B). Here, a constant volume percentage of hydrogel beads was used (40%), however, the porous gypsum composites were produced with either only large beads, only small beads or a combination of them both mixed in a volume ratio of 1:1. Each data point is an average of at least two samples, with the error bars being the standard deviation.

The porosity and reduction in volume for the porous and hierarchically porous gypsum composites produced using hydrogel beads is shown in Figure 4.2B. This shows that at constant overall volume percentage of hydrogel beads, the size distribution of the beads or the volume ratio of large beads to small beads has no effect on the porosity. Again, the volume reductions are insignificant.

When using slurry of hydrogel beads to produce the porous gypsum, the method works by dispersing hydrogel beads in gypsum slurry which will then set around them. Upon drying of the composites, the evaporation of water from the hydrogel beads will leave pores that reflect the size and morphology of the hydrogel beads used. This is only possible when water is able to leave the system through the surrounding matrix.

Through the use of the viscous MC solution, the innate porosity of gypsum plaster can be expanded by a controlled amount, based on the volume percentage of MC solution used. It does so by suspending the gypsum particles in the viscous solution during the hardening process. Upon hydration of the gypsum, it becomes much less soluble causing it to recrystallise and precipitate out into needle and platelet structures.²⁶ Interlocking of these structures causes the hardening of the gypsum paste. When mixing MC solution with the hydrated gypsum slurry, the suspension of gypsum particles will be less concentrated and so the interlocking and hardening process will take longer. The viscosity of the aqueous MC solution stops the sedimentation of the gypsum particles out of solution whilst the continuous network forms and interlocks. After subsequent drying of the sample, it essentially leaves a porous composite material due to the controlled expansion of the gypsum network. Similar porous composites can also be made with cement and many other ceramic materials using both methods described above. Here, the acoustic properties of porous and hierarchically porous gypsum composites have been focussed on.

4.2.3. Acoustic properties of the porous composites

The fraction of air-born sound power incident on a material that is transmitted through and radiated on the opposite side in a specified frequency band is known as the sound (power) transmission coefficient, τ :

$$\tau = \frac{W_t}{W_i}. \quad (4.3)$$

Here W_t and W_i are the transmitted and incident sound powers, respectively. Furthermore, sound transmission loss (STL) in a specified frequency band is expressed in decibels and can be described mathematically by the following equation:

$$STL = 10 \log_{10} \left(\frac{W_i}{W_t} \right) = 10 \log_{10} \left(\frac{1}{\tau} \right). \quad (4.4)$$

However, it is more practical to measure sound pressure rather than sound power. As the power imparted at a detector by sound is proportional to the square of the pressure, the STL can also be written as:

$$STL = 10 \log_{10} \left(\frac{P_i}{P_t} \right)^2 = 20 \log_{10} \left(\frac{P_i}{P_t} \right), \quad (4.5)$$

where P_i and P_t are the incident and transmitted sound pressures, respectively.

Each STL measurement was taken as an average of ten sound pressure data sets at each microphone position. As the samples were geometrically symmetric, the one-load method described in ASTM E2611-09 was employed along with anechoic termination in the downstream tube. The STL was measured over the frequency range 70-2500 Hz.

Figure 4.3(A) shows the STL spectra of the porous gypsum composites produced using MC solution, along with the gypsum control sample whereas Figure 4.3(B) shows the STL at specific sound frequencies as a function of the volume percentage of MC solution used during sample formulation. In general, the STL is lower for the porous gypsum composites than it is for the gypsum control sample (of no added porosity). This is due to the surface density decreasing with increasing volume percentage of MC solution used during preparation, which allows more sound waves to propagate into and through the material. The reduction in reflected sound pressure due to this effect will therefore increase the transmitted sound pressure due to the law of conservation of energy:

$$E_i = E_r + E_a + E_t. \quad (4.6)$$

Here E_i , E_r , E_a and E_t are the incident, reflected, absorbed and transmitted sound energies, respectively. Figure 4.3(B) shows for almost all volume percentages of MC that the STL increases as the frequency increases from 500 – 2000 Hz, then it decreases slightly again at 2000-2500 Hz.

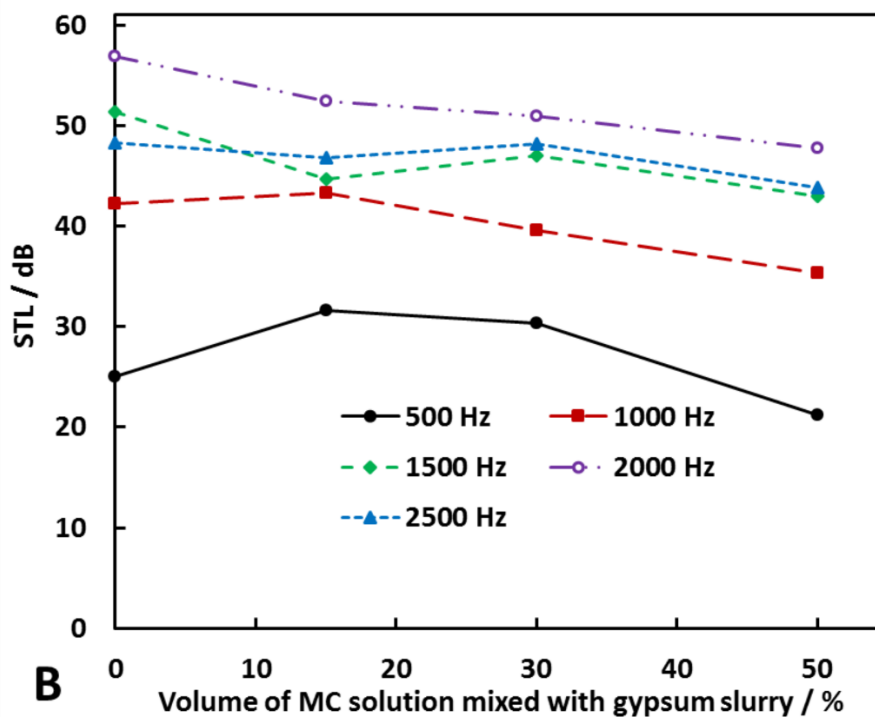
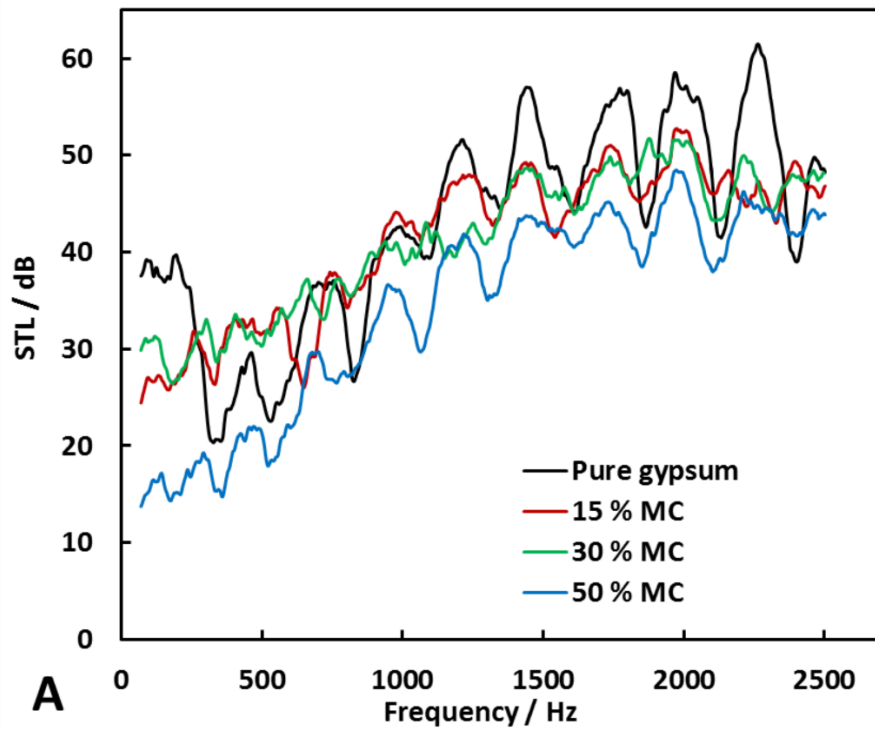


Figure 4.3. The STL spectra for the gypsum control sample, along with the porous gypsum composites produced with different volume percentages of MC solution (A) and the STL values at specific frequencies as a function of the volume percentage of MC solution used during their preparation (B). Each spectrum was taken from an average of 10 experiments.

It was possible to vary the internal microstructure of the hierarchically porous gypsum composites produced using a hydrogel bead templating technique. Depending on the size of hydrogel beads used in the formulation stage, the dried composite contained pores with a similar size distribution to them. Porous gypsum composites with three different microstructures and hierarchy were produced; one with large pores, one with small pores, and one that contained a mix of large and small pores in a 1:1 volume ratio. Figure 4.4(A) shows the results for the composites produced with either large or small pores. Note that the composite produced with 40% large hydrogel beads had a higher overall STL than the one produced with 40% small beads. This was more noticeable at lower frequencies and the difference between them decreased as the frequency increased. The difference between the two spectra was calculated as follows:

$$\Delta STL = STL_{SB} - STL_{LB}. \quad (4.7)$$

Here ΔSTL is the change in STL (dB), STL_{SB} is the STL of the composite produced with 40% small hydrogel beads and STL_{LB} is the STL of the composite produced with 40% large hydrogel beads. This calculation was performed at each frequency and the results were presented in Figure 4.4(B). At low frequencies, the difference is significant, but as the frequency increases, the difference gets closer to zero. Furthermore, at the highest measured frequencies, the composites formulated with small hydrogel beads showed a higher STL. The best-fit line on Figure 4.4(B) has a positive gradient and crosses zero on the y-axis at a frequency of approximately 2420 Hz. The data also shows a Pearson's product moment correlation coefficient of 0.34 which describes a medium positive correlation. This all suggests that at higher frequencies (>2420 Hz), composites produced with small hydrogel beads could be better for sound insulation. Future work could involve development of an impedance tube with a smaller diameter, which would allow higher frequency STL testing.

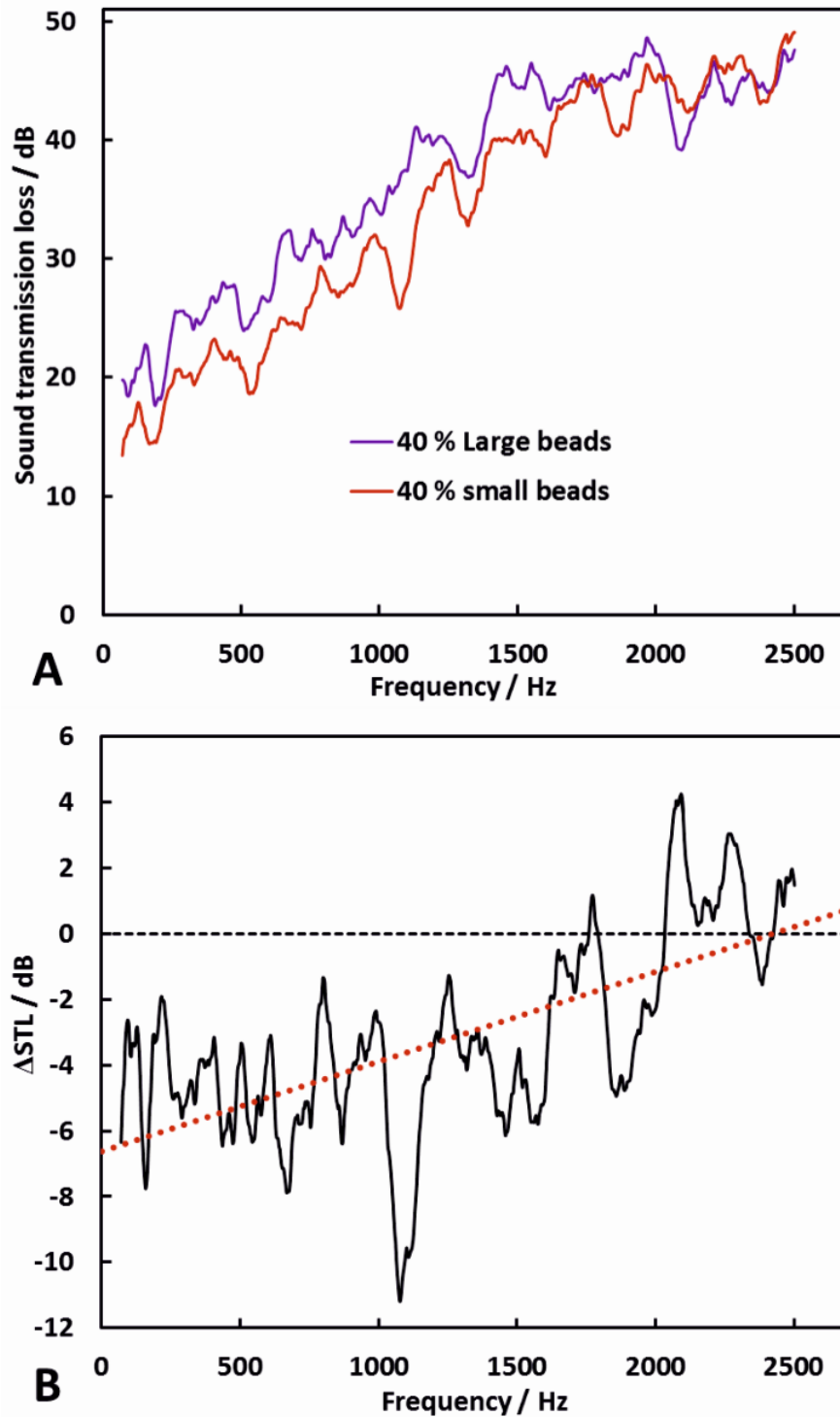


Figure 4.4. STL spectra of porous gypsum composites produced with 40% by volume of small or large beads (A) mixed with gypsum slurry followed by drying. (B) shows the difference between the STL spectra for composites produced with small beads and those with large beads was calculated as seen in equation 5. The dotted red line is a linear best-fit and the dashed black line shows the location of zero on the y-axis. Both are there to guide the eye.

The hierarchically porous composite produced with a combination of large and small beads was also tested. It was seen that the STL spectrum lays between the spectra of the composites produced with only large beads and only small beads. This suggests possible tuning of sound insulating materials by varying the ratio of large to small pores in a material at constant overall porosity. The mean STL over the full frequency range was highest for the composites produced with large hydrogel beads and lowest for the ones produced with small beads, with the mixed size distribution of gel beads having an intermediate mean STL (see Figures 4.5(A) and 4.5(B)). Figure 4.5(C) shows how the STL at specific frequencies varies as the microstructure is varied. It can be seen that as the volume percentage of small beads in the overall volume percentage of hydrogel beads increases, the STL decreases at all frequencies apart from 2500 Hz, where it increases.

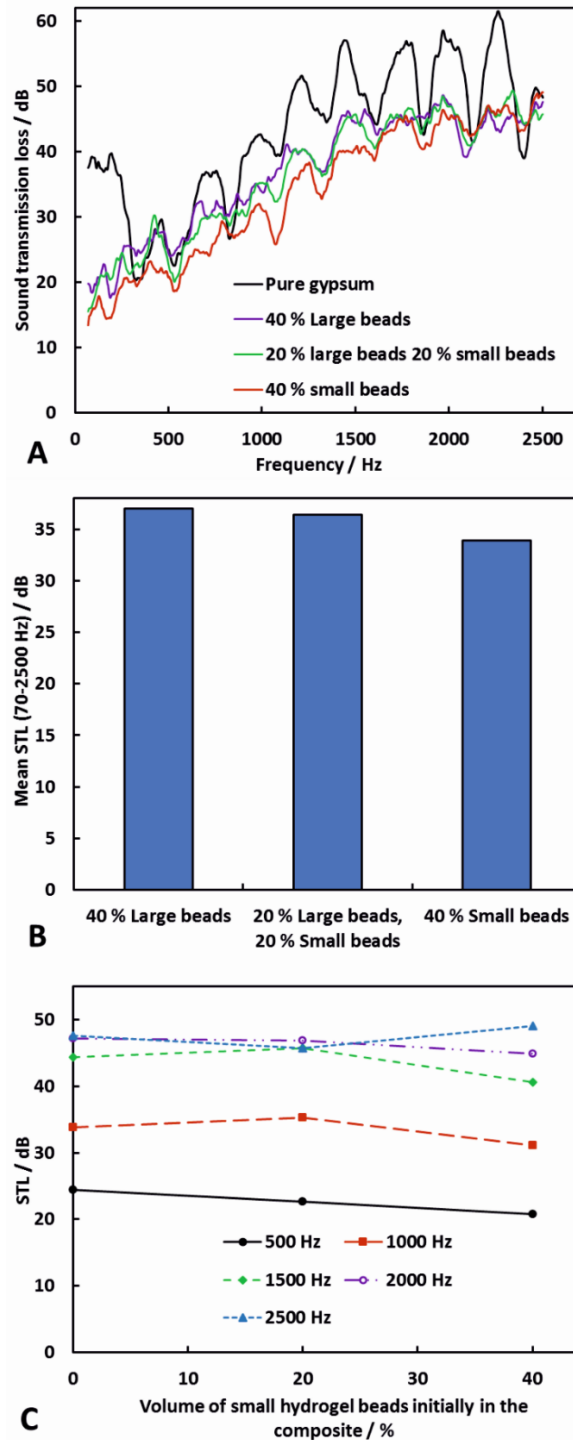


Figure 4.5. (A) The STL spectra obtained from porous gypsum composites produced with 40% large beads, 40% small beads or 20% large and 20% small beads and gypsum slurry by the hydrogel bead templating method. (B) The average STL for each sample over the whole frequency range; (C) The STL at specific frequencies as a function of the volume percentage of small beads used to make the composites (the rest being large beads to make up the overall volume percentage of hydrogel beads used during the formulation to 40%).

4.2.4. Mechanical properties

The mechanical properties of the porous gypsum composites produced by the viscous trapping method using different volume percentages of MC solution were investigated. Fresh samples were prepared and dried to a constant mass. They were then subjected to compression until structural failure which allowed calculation of Young's modulus and the compressional strength, as shown in Figures 4.6(A) and 4.6(B). The mechanical properties of the porous and hierarchically porous gypsum composites produced with 40% by volume of hydrogel beads (small, large or a combination of the two) were also studied. The results are presented in Figures 4.7(A) and 4.7(B). A linear relationship between both the compressional strength and Young's modulus with the volume percentage of MC solution used during formulation (i.e. porosity) was seen. When the porosity was approximately 50%, the reduction in the compressional strength was 88% and the reduction in Young's modulus was 84%.

The average compressional strength and Young's modulus for the porous gypsum composites produced with large beads was 10% lower and 45% lower, respectively, than the ones produced with small beads alone. Other authors have also reported that materials with smaller pores have increased mechanical properties.^{9,27} The hierarchically porous sample has an intermediate Young's modulus, but a slightly higher compressional strength than either of the materials with pores on a single length scale. It has been suggested previously that hierarchically structured porous materials could, at certain ratios of large pores to small pores, produce materials with enhanced mechanical properties.²⁸ This shows that it may be possible to tailor the mechanical properties of hierarchically porous gypsum composites by varying the ratio of large pores to small pores.

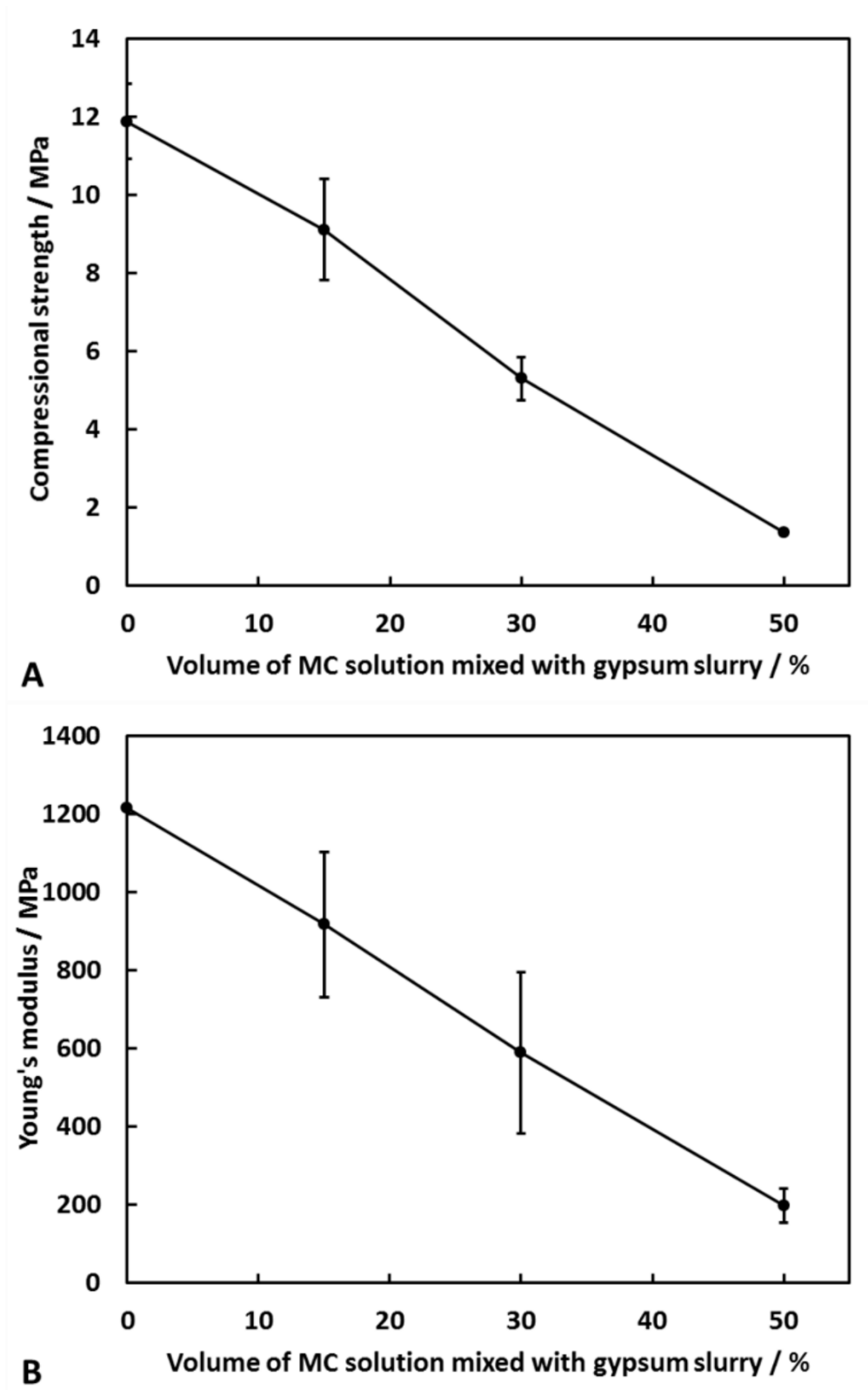


Figure 4.6. Compressive strength (A) and Young's modulus (B) for the porous gypsum composites formulated with different volume percentages of MC solution by the viscous trapping method. Each value is an average of at least two repeats and the error bars represent the standard deviation.

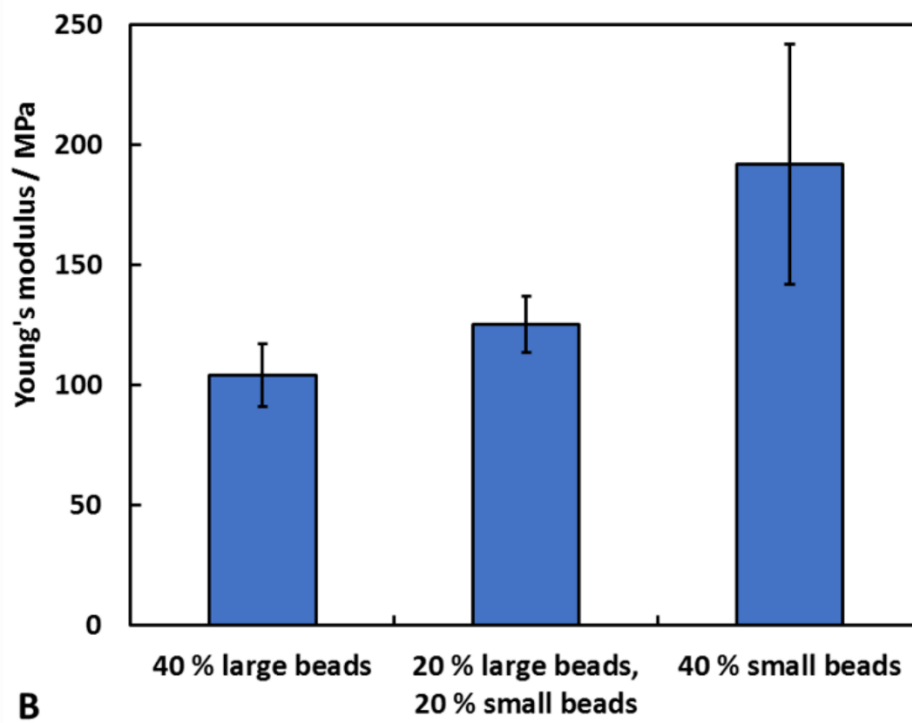
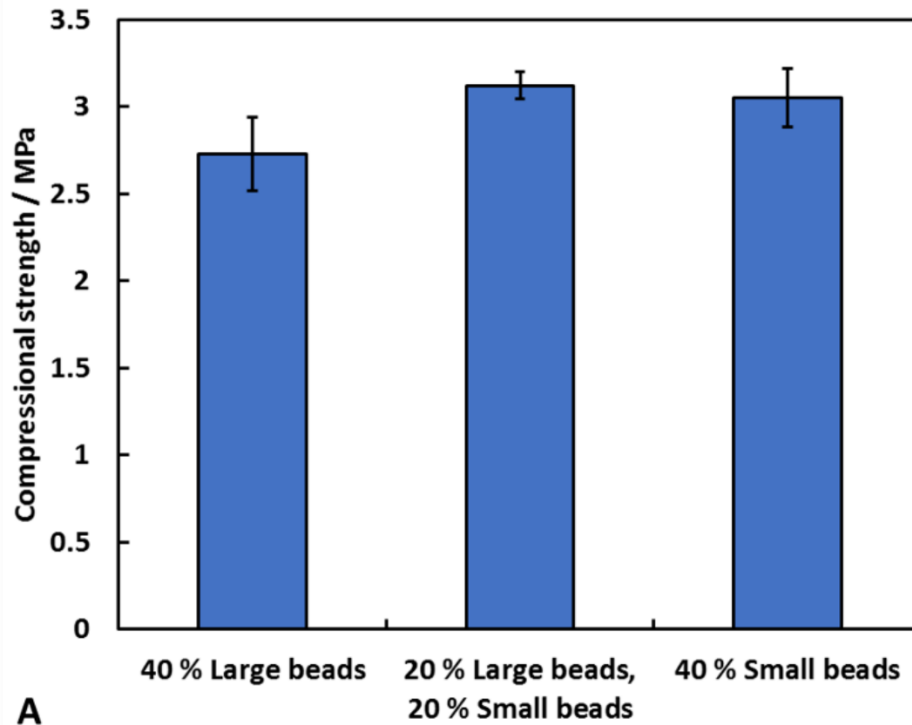


Figure 4.7. Compressional strength (A) and Young's modulus (B) for porous and hierarchically porous gypsum composites produced using 40% by volume of hydrogel beads with the hydrogel bead templating method. The ratio of large-to-small beads was varied to change the microstructure, whilst maintaining the same porosity. Each data point is an average of at least two samples and the error bars are the standard deviation.

4.2.5. Microstructure analysis

Specimens were taken from each porous sample and viewed without conductive coating with a benchtop SEM. The magnifications used were suitable for visualising the microstructural differences between each sample. Figures 4.8(A) – 4.8(C) show the variation in microstructure for samples prepared by the hydrogel bead templating method using large beads, small beads, or a combination of the two. As seen in Figure 4.8, the size of the pores reflect the size of the hydrogel bead templates used during the formulation process. Furthermore, one can see the residues left over in the pores by the dried hydrogel that made the large beads, whereas these are not observed in the small pores, made by the small beads. This is likely due to the larger surface area to volume ratio of the small beads leading to thinner residues which will be prone to intercalating with the surrounding gypsum matrix. The residues left by the large hydrogel beads could increase the sound insulating properties, as it has been shown previously that filler material that lines pores can significantly increase the STL.

Figures 4.9(A) – 4.9(D) show the expansion of the innate porosity of gypsum samples prepared by using the viscous trapping method with MC solution. Through the use of the viscous MC solution, highly porous gypsum composites with an expanded particle network could be obtained. This expansion, however, lead to significant deterioration of the material mechanical properties as well as decreasing its sound insulation properties. The decrease in density of the material allows for easier transmission of sound waves through it, thereby decreasing the STL. Furthermore, dried MC residue within the porous composites at such resolution was not observed.

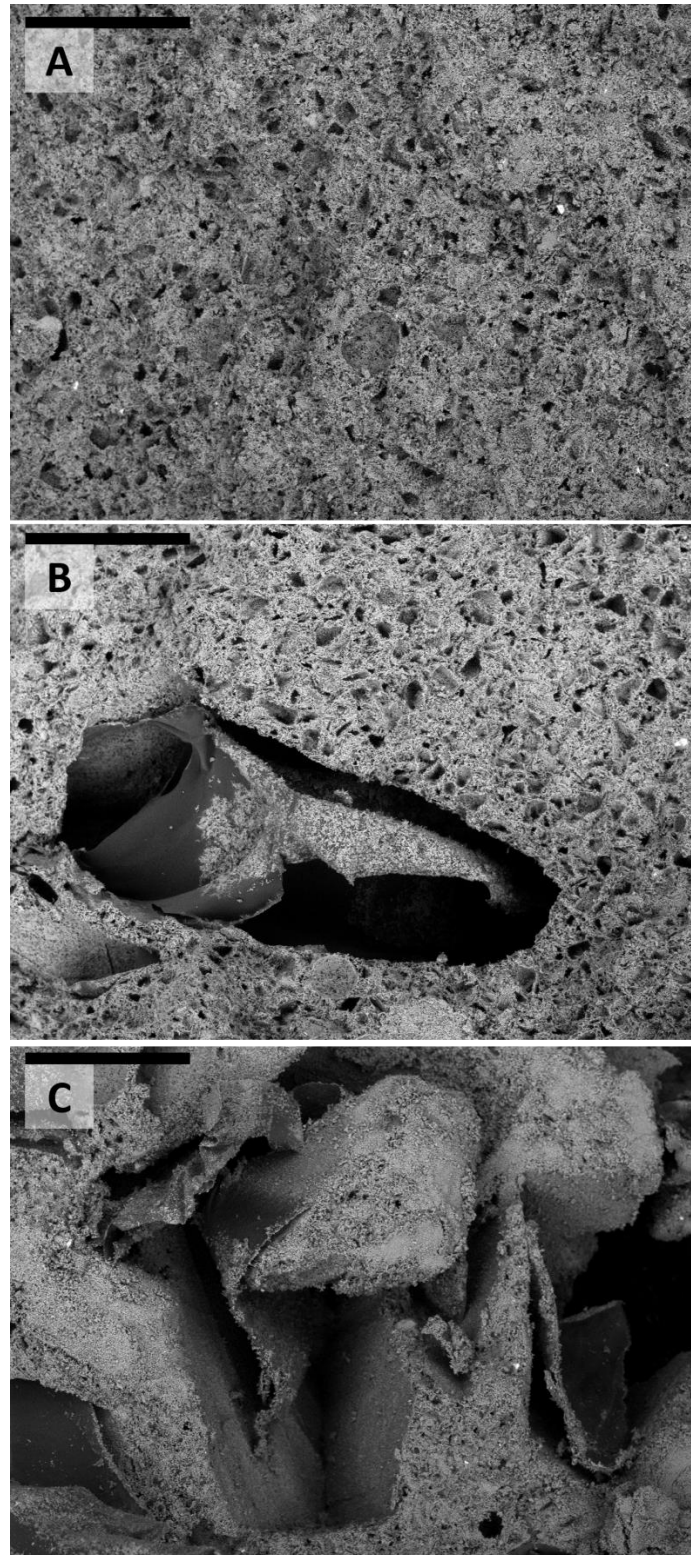


Figure 4.8. SEM images of porous and hierarchically porous gypsum composites produced by the hydrogel bead templating method. Each composite had an overall porosity of 40%, but were produced using either small beads (A), small and large beads in a 1:1 volume ratio (B) or large beads (C). Note the dried hydrogel residue left by the large beads. The scale bars are all 500 μm .

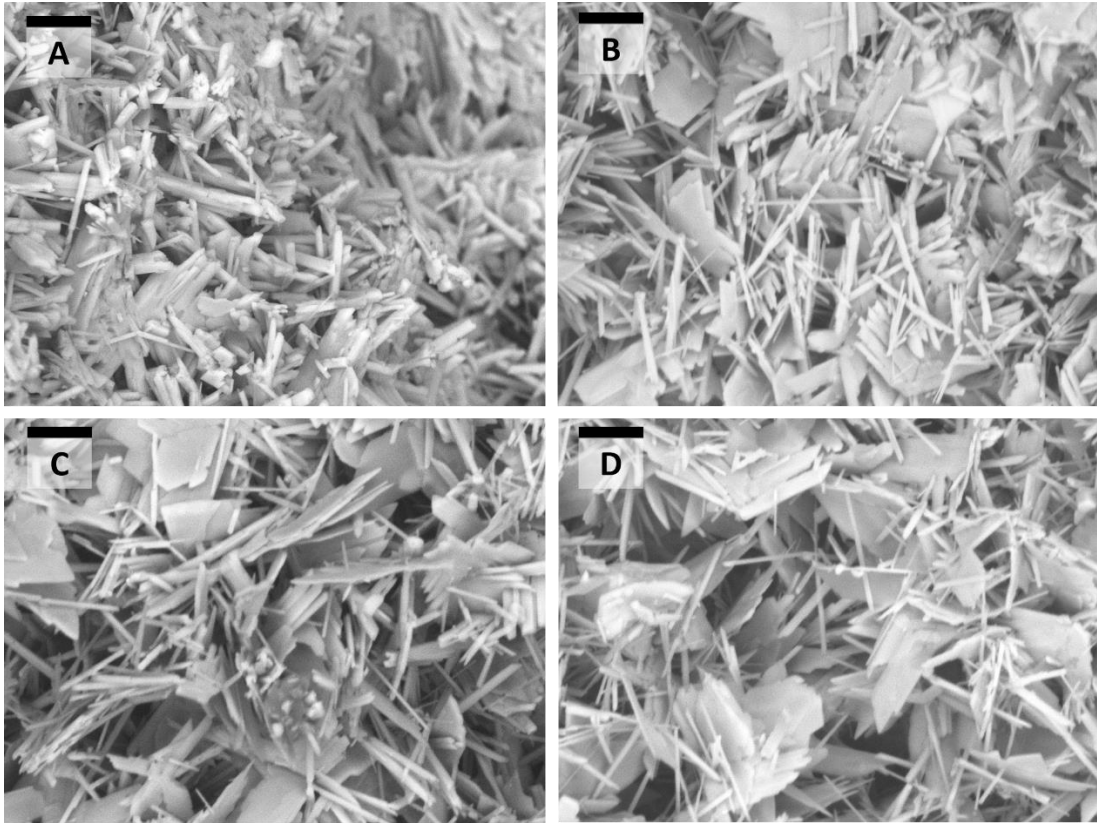


Figure 4.9. SEM images of porous gypsum composites produced using 0% (A), 15% (B), 30% (C) and 50% (D) by volume of MC solution. Note the less dense packing of the gypsum needles and platelets as the volume percentage of MC solution used during formulation increases. All scale bars are 10 μm .

4.3. Conclusions

Two different methods to produce hierarchically porous composites with simultaneous control over the overall porosity and the hierarchical microstructure have been utilised: (i) A hydrogel bead templating technique was used to obtain hierarchically porous gypsum composites. Depending on the volume percentage of hydrogel bead slurry and the size distribution of the beads, both the porosity and the pore size could be controlled. Materials of tuneable hierarchical porosity were produced by mixing slurries of large beads with small beads in controlled volume ratios, then using this “bimodal” slurry of beads as porosity inducing templates by further mixing with gypsum slurry followed by setting and drying. (ii) The second method involved viscous trapping of gypsum particles with MC solution which essentially dilutes the aqueous gypsum slurry but prevents its sedimentation due to gravity during the setting

process. The viscosity of MC solution stops sedimentation of the hydrated gypsum particles whilst the gypsum network forms, which leaves a porous gypsum composite with porosity expanded by a controlled amount, based on the volume percentage of MC solution.

The sound transmission loss (STL) of porous gypsum composites produced using these two methods were studied. It was found that the porous composites formulated using MC solution had a decreased STL with increasing porosity, which can be explained the interaction between the acoustic air flow and the frame of the porous material. This predicts that the STL decreases with increasing porosity of the sample (i.e. higher porosity has less resistance to the acoustic air flow). An investigation into how the pore size affected the STL of porous gypsum composites was performed. STL spectra of porous gypsum composites were produced by the hydrogel templating method with small beads or large beads at a constant porosity (40%) were obtained. It was found that at lower frequencies, the porous composites made with large beads have a higher STL. However, the difference between them decreases as the frequency increases. The data suggests that at frequencies above 2420 Hz, the porous composite produced with small hydrogel beads may have a higher STL, however this would need further testing. The STL spectrum of hierarchically porous gypsum composite with 40% porosity made by templating a mixed slurry of both large and small pores in a 1:1 volume ratio was also obtained. In this case the STL spectrum was in between the ones for the porous composites produced with only large or only small beads. This suggests there could be a possibility for tuning the STL of hierarchically porous materials at constant porosity through careful control of their microstructures.

The mechanical properties of the porous gypsum composites were also studied. A linear relationship was observed between the overall porosity and the compressional strength or Young's modulus for the porous composites produced using the viscous trapping method with MC solution. When using hydrogel beads to introduce porosity into the gypsum matrix, it was found that small beads (and hence small pores) produced materials with increased mechanical properties. One possible explanation is that in the composites produced using large beads the dried hydrogel residue resides inside the pores. As they are not part of the continuous gypsum network, they do not contribute to the overall strength of the composite. Porous composites made with small beads get their hydrogel residue intercalated within gypsum particles network which

increases their overall compressional strength. The hierarchically porous gypsum composites showed an intermediate Young's modulus and an increased compressional strength.

This chapter further investigates the acoustical properties of porous composites produced by hydrogel templating techniques. Previous work has investigated the sound absorption coefficient as a function of porosity and pore size.^{8,9} Here, the sound transmission loss of the porous gypsum composites has been studied at various porosities, pore sizes and hierarchical porosities at the same porosity. It has been shown that it may be possible to tune the sound transmission loss at constant porosity by changing the microstructure. Investigation of the material's microstructure allowed for the suggestion of a possible reason for this.

4.4. References

- 1 W. Passchier-Vermeer and W. F. Passchier, *Environ. Health Perspect.*, 2000, **108**, 123–131.
- 2 S. A. Stansfeld and M. P. Matheson, *Br. Med. Bull.*, 2003, **68**, 243–257.
- 3 M. N. Mead, *Environ. Health Perspect.*, 2007, **115**, A536–A537.
- 4 F. Godlee, *Br. Med. J.*, 1992, **304**, 110–113.
- 5 S. Ghaffari Mosanenzadeh, H. E. Naguib, C. B. Park and N. Atalla, *J. Mater. Sci.*, 2015, **50**, 1248–1256.
- 6 M. E. Delany and E. N. Bazley, *Appl. Acoust.*, 1970, **3**, 105–116.
- 7 M. R. F. Kidner and C. H. Hansen, *Int. J. Acoust. Vib.*, 2008, **13**, 112–119.
- 8 M. Rutkevičius, G. H. Mehl, V. N. Paunov, Q. Qin, P. A. Rubini, S. D. Stoyanov and J. Petkov, *J. Mater. Res.*, 2013, **28**, 2409–2414.
- 9 M. Rutkevičius, Z. Austin, B. Chalk, G. H. Mehl, Q. Qin, P. A. Rubini, S. D. Stoyanov and V. N. Paunov, *J. Mater. Sci.*, 2015, **50**, 3495–3503.
- 10 J. Legault and N. Atalla, *J. Sound Vib.*, 2009, **324**, 712–732.
- 11 C. M. Wu and M. H. Chou, *Compos. Sci. Technol.*, 2016, **127**, 127–133.
- 12 H. Meng, X. H. Yang, S. W. Ren, F. X. Xin and T. J. Lu, *Compos. Sci. Technol.*, 2016, **127**, 158–168.
- 13 Z. Li and M. J. Crocker, *J. Sound Vib.*, 2006, **294**, 473–485.
- 14 T. Han, X. Wang, Y. Xiong, J. Li, S. Guo and G. Chen, *Compos. Part A Appl. Sci. Manuf.*, 2015, **78**, 27–34.
- 15 J.-C. Lee, Y.-S. Hong, R.-G. Nan, M.-K. Jang, C. S. Lee, S.-H. Ahn and Y.-J. Kang, *J. Mech. Sci. Technol.*, 2009, **22**, 1468.
- 16 L. Xu, T. Han, J. Li, Y. Xiong and S. Guo, *Compos. Sci. Technol.*, 2017, **145**, 78–88.
- 17 A. R. Barnard and M. D. Rao, presented in part at The 2004 National Conference on Noise Control Engineering, Baltimore, July, 2004.

- 18 ASTM E2611-09, Standard Test Method for the Measurement of Normal Incidence Sound Transmission of Acoustical Materials Based on the Transfer Matrix Method (2009), <https://www.astm.org/Standards/E2611.htm> (accessed 27/7/2017).
- 19 M. Rutkevičius, S. K. Munusami, Z. Watson, A. D. Field, M. Salt, S. D. Stoyanov, J. Petkov, G. H. Mehl and V. N. Paunov, *Mater. Res. Bull.*, 2012, **47**, 980–986.
- 20 M. Constantin, S.-M. Bucatariu, F. Doroftei and G. Fundueanu, *Carbohydr. Polym.*, 2017, **157**, 493–502.
- 21 L. Zhang, K. Li, W. Xiao, L. Zheng, Y. Xiao, H. Fan and X. Zhang, *Carbohydr. Polym.*, 2011, **84**, 118–125.
- 22 M. Rutkevičius, G. H. Mehl, J. T. Petkov, S. D. Stoyanov and V. N. Paunov, *J. Mater. Chem. B*, 2015, **3**, 82–89.
- 23 B. R. Thompson, T. S. Horozov, S. D. Stoyanov, V. N. Paunov, *Food Funct.*, 2017, DOI: 10.1039/c7fo00867h.
- 24 A. Hayashi and T. Kanzaki, *Food Hydrocolloids*, 1987, **1**, 317–325.
- 25 A. J. Lewry and J. Williamson, *J. Mater. Sci.*, 1994, **29**, 5524–5528.
- 26 A. J. Lewry and J. Williamson, *J. Mater. Sci.*, 1994, **29**, 5279–5284.
- 27 Z. Li, L. Yang, Y. Li, Y. Yang, C. Zhou, Y. Ding, J. Zhao and Y. Li, *Mater. Des.*, 2013, **45**, 52–55.
- 28 L. L. C. Wong, P. M. Baiz Villafranca, A. Menner and A. Bismarck, *Langmuir*, 2013, **29**, 5952–5961.

5. Pressure responsive soap-hydrogel bead composites for controlled dissolution and release rate of actives

A method was designed for the preparation of soap-hydrogel composites by incorporating hydrogel beads within a soap matrix. Agar hydrogels were prepared and blended into a slurry of hydrogel beads of desired size, which were mixed with molten soap base with controlled volume percentages of each phase. Upon cooling, the combined suspension of hydrogel beads in molten soap was set into a composite of soap matrix with hydrogel beads within. It was demonstrated that it is possible to increase the dissolution rate of these composites by increasing the volume percentage of hydrogel beads used during preparation. When using 50% by volume of hydrogel beads to prepare the composites, a dissolution rate approximately 2.5 times higher than the soap control sample without hydrogel beads was achieved. It was also found that the dissolution rate was not dependent on the size of the hydrogel beads investigated here. The release rates of species encapsulated within the hydrogel beads used to prepare the composites were investigated and found that they can be controlled in three different ways: varying the hydrogel beads size, using different concentrations of the gelling polymer used to make the hydrogel and also by co-encapsulating an oppositely charged polyelectrolyte to the active encapsulated species investigated. It was found that the composite's compressional strength decreased with increasing the volume percentage of hydrogel beads incorporated within the composite. Syneresis of water from the soap-hydrogel bead composites occurred upon compression. Interestingly, the Young's modulus showed a maximum when 7.5% by volume of hydrogel beads were used for composite preparation. These fast-dissolving soap-hydrogel composites contain significantly less raw materials and would reduce the pollution of waste water with surface active component. It can be envisaged that these soap-hydrogel composites could improve the sustainability of the soap-producing industry and may find their application within the hotel business, where they could reduce costs and waste of the millions of partially used soap bars discarded every day.

5.1. Introduction

The use of soap products is considered essential for modern life when it comes to personal hygiene and disease prevention. For example, one of the leading causes of child death around the world is diarrhoeal disease, with estimates that more than 2.2 million lives are lost each year due to these infections.¹ Handwashing is a preventative measure that may substantially reduce the chances of contracting diarrhoeal diseases. It has been shown that handwashing with soap and water reduces bacteria present on hands to 8% which is almost three times lower than handwashing with water alone.² Therefore, this necessitates cheap and easy worldwide access to soap products.

The Global Soap Project organisation has estimated that 2.6 million bars of soap are discarded each day by the hotel industry in the U.S. alone. This occurs due to hotel guests using only a fraction of their soap bars before they leave, followed by the hotels discarding these partially used bars to replace them with fresh ones for their next guests. Not only is this wasteful, it also incurs unnecessary costs. Furthermore, discarding such large amounts of soap is detrimental to the environment. Many surface active components are harmful to aquatic life, pollute water and can endanger human health.^{3,4} The development of methods to decrease the production costs of soap is a crucial step towards making it more readily accessible worldwide; which in turn could reduce mortality rates due to certain bacterial infections, especially in developing countries.

Hydrogels are 3D hydrophilic, polymeric networks that can be considerably swollen with water. They are largely biocompatible and are aqueous based which has made them useful in various areas such as porogenic materials,⁵ drug delivery and wound dressing,⁶ tissue engineering⁷ and food structuring.^{8,9} Porous materials fabricated from hydrogel templating of cement composites have been explored as sound absorbing materials.^{10,11} Here, the incorporation of hydrogel beads within soap has been explored as a method to reduce costs, increase sustainability of the sourced materials and decrease pollution of waste waters with surface active materials. Agar has been used as a gelling agent, which is derived from natural sources and consists of both agarose and agaropectin, to produce the hydrogels. It is insoluble in cold water, however it hydrates at temperatures close to the boiling point of water. At such temperatures, the polymer chains adopt a random coil conformation. Upon cooling, the agarose chains

form double helixes which then self-assemble into a three-dimensional network with water within.¹² Once set, the hydrogel would not melt at temperatures below 85 °C,¹³ which is a higher melting point than many conventional soaps. Upon chopping the hydrogel with a blender, slurries of hydrogel beads were obtained. These slurries of hydrogel beads have been mixed with molten soap at a temperature below the melting point of the hydrogel but above the soap melting point to obtain soap-hydrogel composites with a controllable composition. The produced soap-hydrogel composites show an increase in their dissolution rate depending on the hydrogel bead content. The presence of hydrogel beads within the composites also allows for control over a range of their properties. For example, one can change the size of the hydrogel beads or the concentration of the gelling polymer to control the release rate of active species encapsulated within the beads. Furthermore, the release rate of an encapsulated species can be also controlled by co-encapsulating different amounts of oppositely charged polyelectrolyte which is expected to delay their diffusion out of the beads during the composite dissolution.

Investigation of the mechanical properties of the produced composites showed that their compressional strength decreased with increasing volume percentage of hydrogel beads used in the composite preparation. The Young's modulus of the composites, however, displayed a maximum when small amounts of hydrogel beads were incorporated within the soap matrix. An unusual behaviour of the composites was observed when they underwent compression; syneresis of water occurred. This suggests that they could be useful for designing a washing action in areas where clean water is not readily available. It is also expected that this effect can be beneficial for better consumer perception when washing with such a composite soap bar.

The use of such soap-hydrogel composites can be foreseen in the hotel industry, where millions of barely used soap bars are discarded each day. The reduced amount of surface active species present in them would lead to a decrease in pollution of waste water. Finally, the decreased cost due to a reduction in raw materials required for production could make them attractive for businesses and more affordable for developing countries.

5.2. Results

5.2.1. Hydrogel bead size analysis

The size of the hydrogel beads has been controlled by varying the blending time of the hydrogel. The hydrogel beads were then dispersed in water, viewed under optical microscopy and their size distributions measured using ImageJ software. It was found that after blending the hydrogel for 10 seconds, the beads produced had an average size of $600 \pm 300 \mu\text{m}$, whereas after blending for 300 seconds, beads with an average size of $120 \pm 60 \mu\text{m}$ were obtained. The cumulative distributions of the average size of large and small beads can be seen in Figure 5.1. Hydrogel beads of irregular shape were produced due to the preparation method used, therefore they were measured horizontally through the widest section to determine their average size.

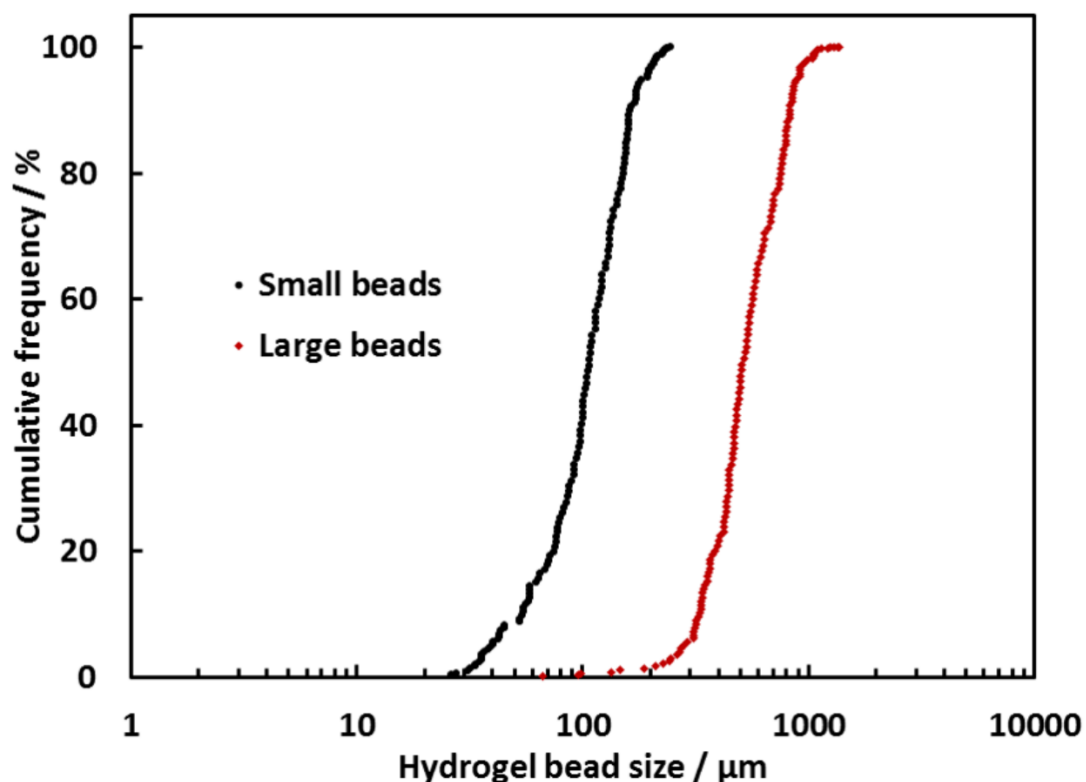


Figure 5.1. Percentage cumulative distribution of agar hydrogel (2.0% w/v) bead sizes for small beads produced by blending for 300 seconds and for large beads produced by blending for 10 seconds.

5.2.2. Dissolution rate of the soap-hydrogel composites

An investigation into the kinetics of dissolution of the soap-hydrogel composites was performed by submerging the sample into a fixed volume of water whilst stirring with a magnetic stirrer. The solution conductance was recorded after 120 seconds and used to calculate the dissolution rate by comparing with a calibration curve. There was a linear dependence of soap concentration and the solution conductance. It can be seen that the composites produced with greater volume percentage of hydrogel slurry had increased dissolution rates and therefore would be faster acting soaps. When the volume of hydrogel beads slurry incorporated within the soap matrix was 50%, the dissolution rate increased by approximately 2.5 times.

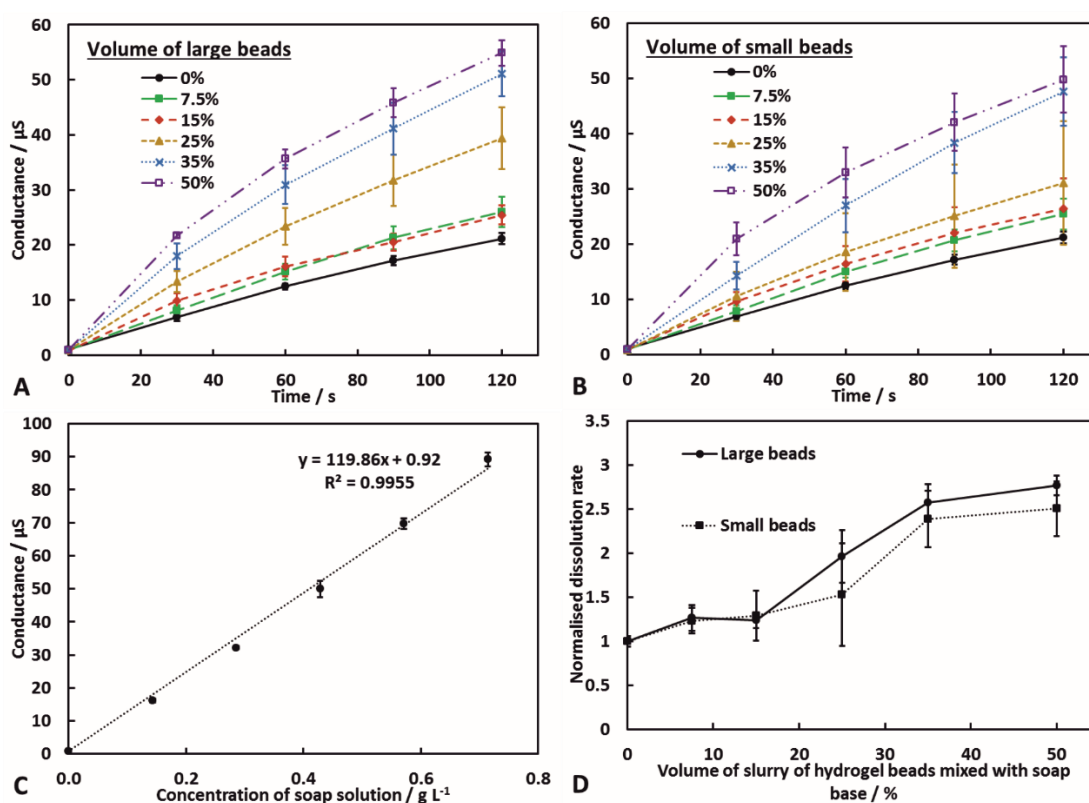


Figure 5.2. (A) and (B) The change in conductance over time when dissolving soap and soap hydrogel composites in water (750 cm^3 , $30 \pm 0.2 \text{ }^\circ\text{C}$). (C) The conductance versus the dissolved mass of soap under the same conditions. (D) The dissolution rate of the soap hydrogel composites after normalising with the dissolution rate of a control sample of soap alone. Each data point represents an average of three separate samples and the error bars are the standard deviation.

This is possibly due to the hydrogel beads being removed from the surface of the composites due to the drag forces acting upon them. Upon the detachment of the hydrogel beads, the surface area of the soap that is exposed to the water will increase which in turn will increase the surface area. In addition, the soap near the hydrogel beads could be partially hydrated within the composite and could dissolve faster. A schematic to illustrate this process is shown in Figure 5.3.

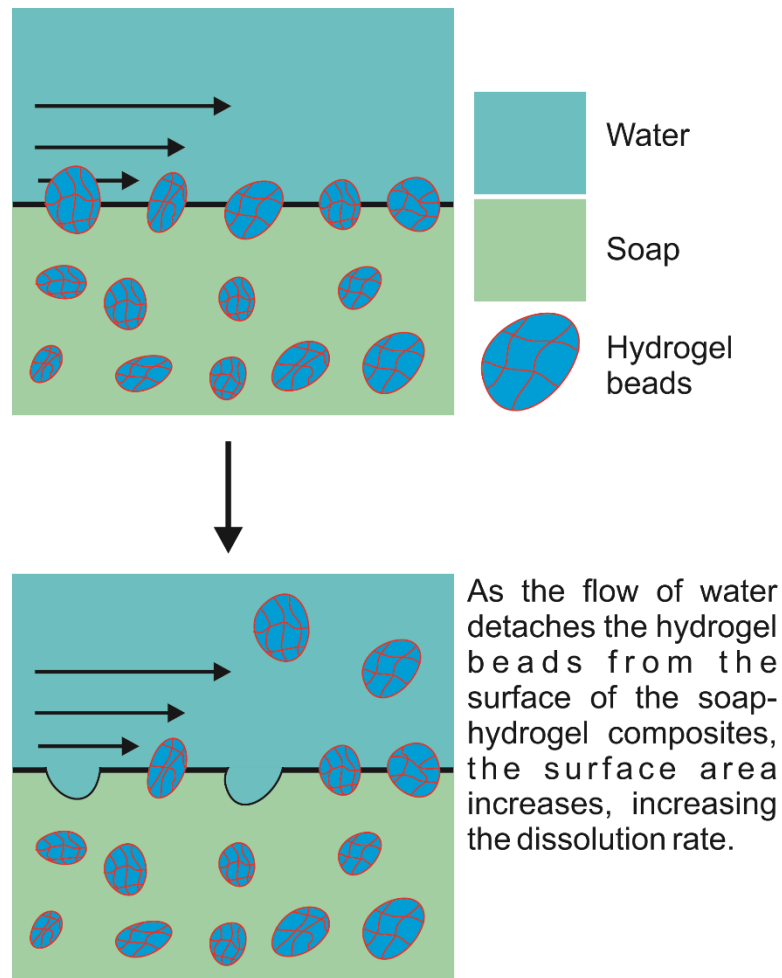


Figure 5.3. A schematic explaining the increase of the sample dissolution rate with increasing volume percentage of slurry of hydrogel beads incorporated within the soap-hydrogel composite. As the flow detaches hydrogel beads from the surface of the dissolving soap-hydrogel composites, the sample surface area increases which increases further the dissolution rate. Large beads experience larger drag force at the composite surface.

5.2.3. Controlling the release rate of active species from the soap-hydrogel composites

5.2.3.1. Role of hydrogel bead size on the release rate of berberine

The effect of the average size of the hydrogel beads used on the release rate of BBR encapsulated within the beads has been investigated. Soap hydrogel beads composites containing 50% by volume of large or small hydrogel beads with berberine encapsulated within them were prepared and investigated. Upon dissolution of the composites, aliquots were taken and their UV-visible spectra was measured to determine the amount of BBR released. The results are shown below in Figure 5.4.

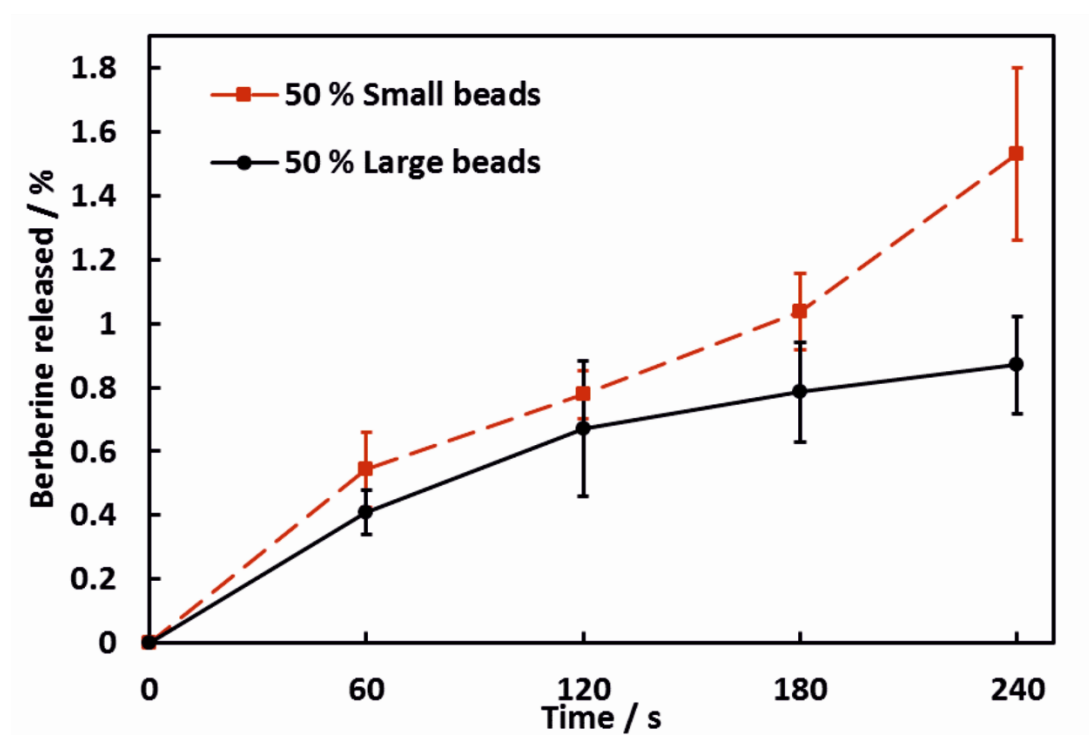


Figure 5.4. Release rate of BBR when dissolving soap hydrogel composites in water (200 cm³). 50% by volume of agar (2.0% w/v) hydrogel beads were incorporated in the composites and the initial concentration of BBR in the hydrogel beads was 0.15% w/v. Each data point is an average of three results and the error bars are the standard deviation.

The soap-hydrogel composites produced using small hydrogel beads showed up to approximately a twice as fast release rate of BRB after 240 seconds, when compared to the soap composites produced with large hydrogel beads. This can be attributed to

a larger surface area to volume ratio of the small beads compared to large beads and decreased diffusion path lengths and increased BBR concentration gradients when using small beads.¹⁴⁻²⁰

5.2.3.2. Role of agar concentration on the release rate of berberine

An investigation into how the concentration of the non-ionic polymer used to prepare the hydrogel beads affected the release rate of actives from the soap-hydrogel composites was performed. This was done by encapsulating BBR within hydrogel beads of different size distributions and different concentrations of agar and using them to prepare the soap-hydrogel composites. Aliquots of the dissolution medium were taken during dissolution process and their UV-visible spectra measured and used to determine the release rate of BBR. For both large and small beads, increasing the concentration of agar used to prepare the hydrogel beads causes a decrease in the release rate of BBR from the soap-hydrogel composites. This is likely due to the higher concentration of agar forming a denser polymer network with reduced porosity and increased stiffness which hinders the diffusion transport of BBR molecules encapsulated within the hydrogel beads.²¹

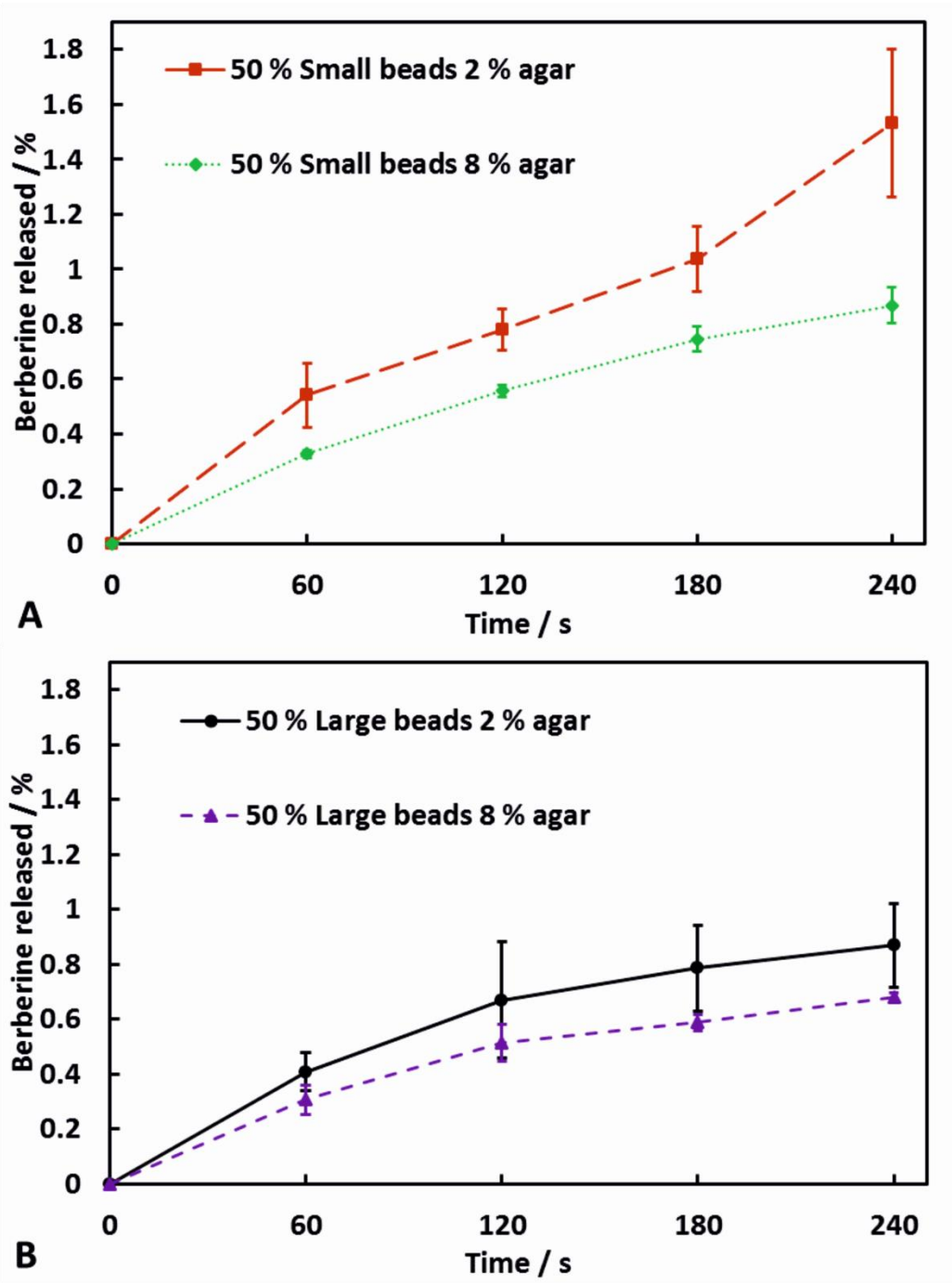


Figure 5.5. The release rate of BBR from soap-hydrogel composites when dissolving in water (200 cm³). The composites were produced using either small (A) or large (B) hydrogel beads prepared with different concentrations of agar (2.0% or 8.0% w/v). 50% by volume of hydrogel beads were incorporated within the composites and the initial concentration of BBR in the hydrogel beads was 0.15% w/v. Each data point is an average of three measurements and the error bars represent the standard deviation.

5.2.3.3. *Effect of polyelectrolyte co-encapsulation on the release rate of methylene blue*

Another method used to control the release rate of molecules encapsulated within the soap-hydrogel composites was to encapsulate a polyelectrolyte that has an opposite charge to the encapsulated active ingredient. PSS, a negatively charged polyelectrolyte, was utilised at two different concentrations; one being not in excess and the other being in excess of the cationic active, MB.

From Figure 5.6, one can see how the release rates depend on the concentration of PSS encapsulated within the hydrogel beads. When small beads were used to prepare the composites, the initial amounts of MB released were independent of the PSS concentration. For times greater than 30 seconds, the composites containing excess PSS showed a slower release rate than those with PSS not in excess. For the composites produced using large hydrogel beads, the effect was seen instantly. The possible reasons for the reduction in the release rate of MB when PSS was in excess are two-fold: firstly, the presence of the polyelectrolyte reduces the free volume within the hydrogel beads, hindering transport of the MB molecules and secondly, there will be ionic attractions between negatively charged PSS and positively charged MB.

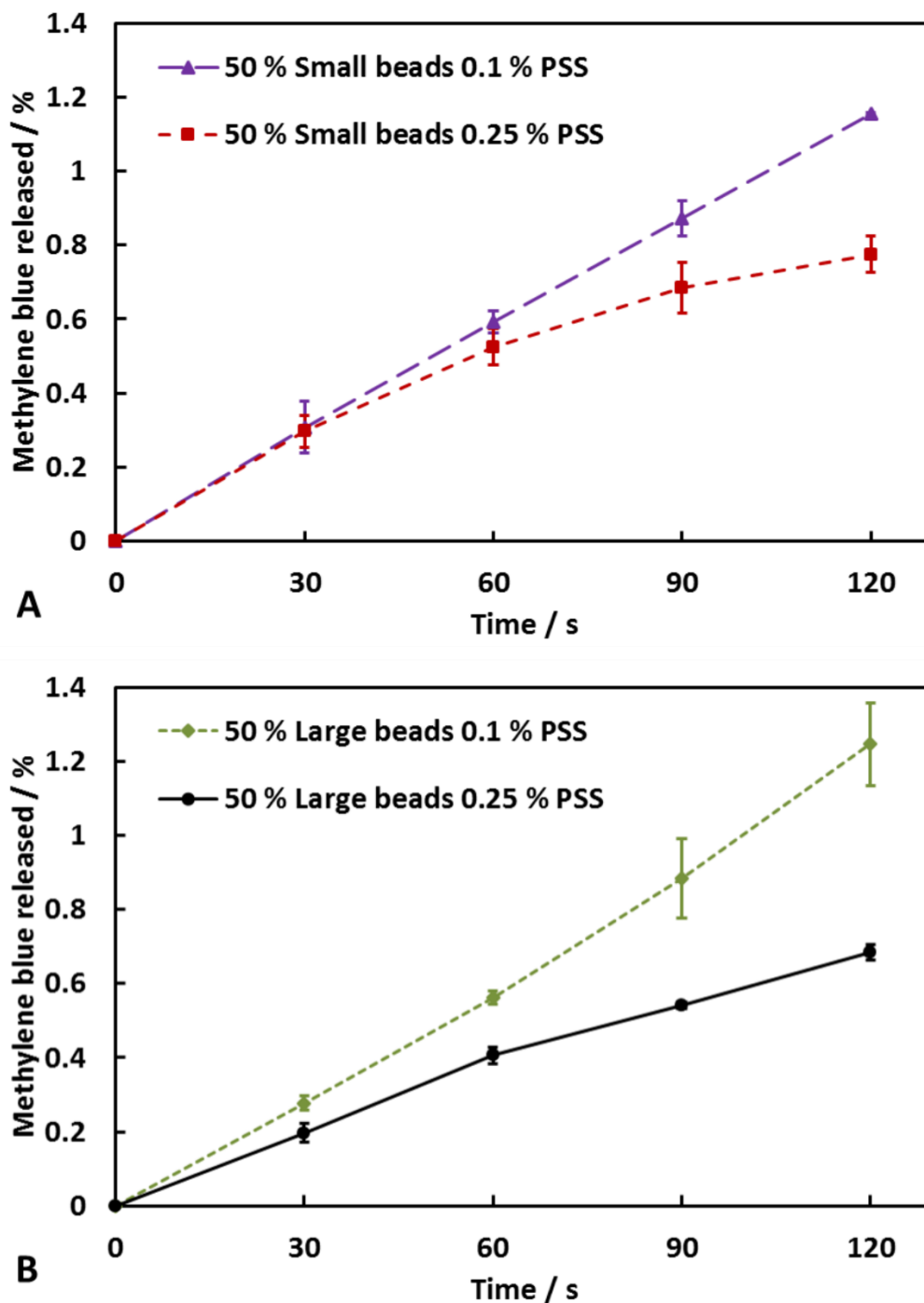


Figure 5.6. The release rate of MB from soap-hydrogel composites when dissolving in water (200 cm³). The composites were produced using either small (A) or large (B) hydrogel beads prepared with agar (2.0% w/v). 50% by volume of hydrogel beads loaded with 0.01 M MB and PSS (0.1% or 0.25% w/v) were incorporated within the composites. Each data point is an average of three results and the error bars represent the standard deviation.

5.2.4. Mechanical properties of soap-hydrogel composites

The effect of size and concentration of hydrogel bead slurry on the mechanical properties of the soap-hydrogel composites was investigated by testing at least three samples of each type at room temperature. The samples were subjected to compression and the force at structural failure was used to calculate the compressional strength, whereas the linear elastic region of the stress/strain curve was used to determine the Young modulus. The results are shown in Figures 5.7(A) and 5.7(B). It was found that the increase of the volume percentage of hydrogel beads incorporated within the composites decreases their compressional strengths. There was no significant effect of changing the size of the hydrogel beads up to 50% volume percentage of beads. The Young modulus however, shows unexpected values that are greater than the soap control sample when the composites contained 5% or 7.5% by volume of hydrogel beads (small or large). At higher volume percentages of beads, the Young modulus is less than the soap control sample and decreases with increasing the volume percentage of hydrogel beads. One possible reason for the initial increase in the Young modulus is that upon compression, the aqueous phase within the hydrogel beads has nowhere to go and so reinforces the composite. The large error bars could be due to the random distribution and arrangement of the beads within the composite. At higher volume percentage of beads, however, due to their partial formation of a network within the composite, water can be released from the beads upon compression and redistributed along the beads network which can dissipate energy and does not correspond to elastic deformation.

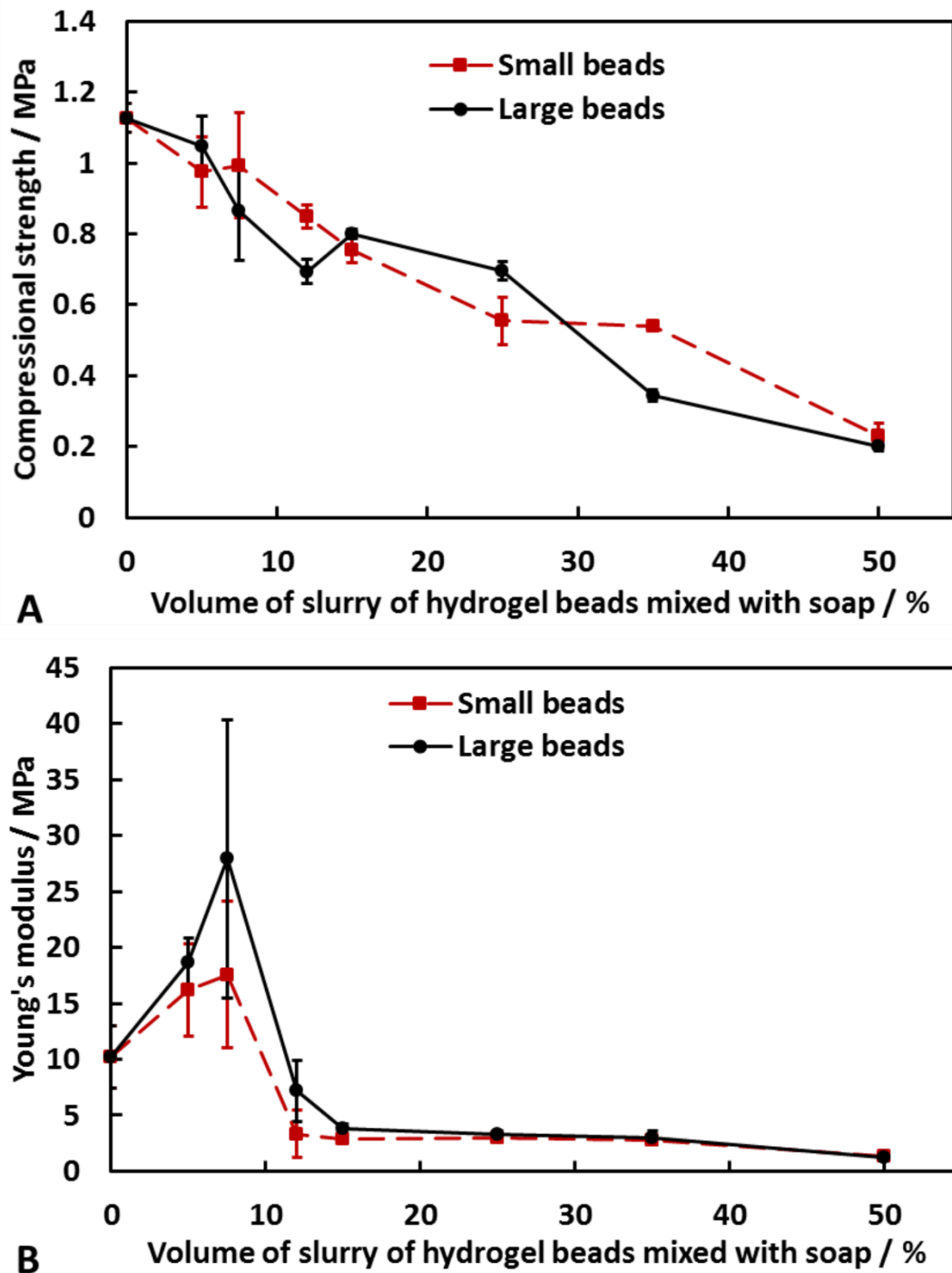


Figure 5.7. The compressional strength (A) and Young's modulus (B) of soap and soap-hydrogel beads composites as a function of the volume of hydrogel beads (either small or large) incorporated within the composites.

An argument in favour of this explanation was revealed during the compression tests, where syneresis of water from the composites produced with beads of either size was

observed. This effect is shown in Figure 5.8 and furthermore, it gives scope for the production of these composites with rather unusual rheological response compared to classic soap bars.

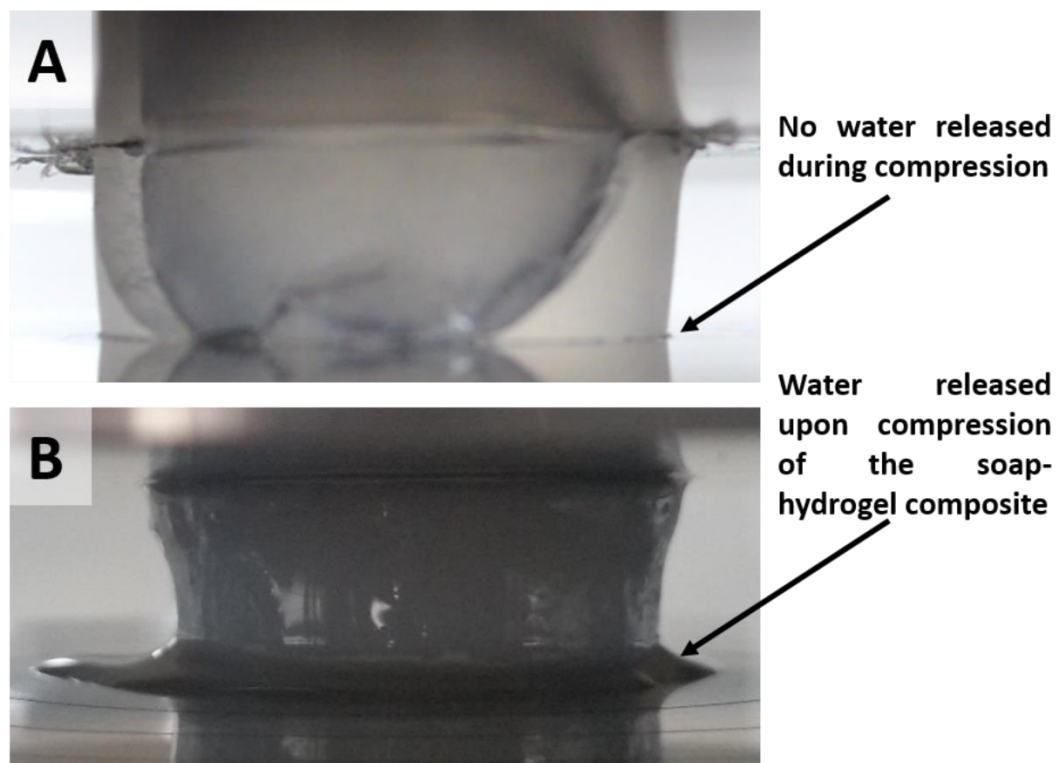


Figure 5.8. Digital camera images of soap (A) and a soap hydrogel composite produced with 50% by volume of small hydrogel beads (B) during compression. Note that the released water can be seen at the base of the composite. This effect is also seen when large hydrogel beads are used.

5.2. Conclusions

Novel soap-hydrogel composites have been formulated where hydrogel beads are encased within the soap matrix. These composites have a reduced cost, could reduce pollution with surface active materials and require less raw materials which improves the sustainability. Agar, a non-ionic hydrogel with a high melting point, was utilised for the preparation of these composites. Upon chopping the hydrogel to beads of a desired size with a blender, controlled volume percentages of slurry of beads were mixed with molten soap. This mixture was then poured into a mould and allowed to harden before use. It was found that the soap dissolution rate increased with the

volume percentage of hydrogel beads incorporated in the composite. The dissolution rate of composites with 50% by volume of hydrogel beads was 2.5 times faster than the soap control sample. This has been attributed to an increase in the surface area of the soap bar exposed to water as hydrogel beads are detached from the surface of the composite.

The release rate of species encapsulated within the hydrogel beads used in the composites was also investigated. It was found that the release rate of BBR could be increased by almost 100% by changing the size of hydrogel beads used from $600 \pm 300 \mu\text{m}$ to $120 \pm 60 \mu\text{m}$. The increase in surface area to volume ratio of smaller hydrogel beads, along with decreased diffusion path lengths and increased concentration gradients of BBR when using small hydrogel beads seem plausible explanation for the observed difference in the release rates. It was also possible to control the release rate of the encapsulated active by changing the agar concentration in the hydrogel. As the concentration of agar increased, the release rate decreased due to the formation of a denser polymer network, hindering the transport of the diffusing molecules. Another method to control the release rate of species of interest (MB) was to co-encapsulate an oppositely charged polyelectrolyte to attract the species. The release rate of MB decreased with the concentration of the polyelectrolyte which could be attributed to ionic attraction between the polyelectrolyte and the diffusing MB molecules, as well as to the polyelectrolyte decreasing the free volume within the hydrogel beads, thus hindering the MB molecule transport.

The mechanical properties of the composites were investigated and found that the compressional strength decreased linearly with an increase in the volume percentage of hydrogel beads in the composite irrespective of the hydrogel bead size. The composites also showed a compression driven syneresis of water, suggesting that they could exercise washing action without running water. The Young modulus showed a significant increase when 5% or 7.5% by volume of hydrogel beads were incorporated within the composite. However, at higher volume percentages of beads, it decreased to values below the soap control sample.

It can be envisaged that such soap-hydrogel composites could find a place within the hotel industry, where millions of partially used soap bars are discarded on a daily basis.

5.3. References

- 1 C. Boschi-Pinto, L. Velebit and K. Shibuya, *Bull. World Health Organ.*, 2008, **86**, 710–717.
- 2 M. Burton, E. Cobb, P. Donachie, G. Judah, V. Curtis and W.-P. Schmidt, *Int. J. Environ. Res. Public Health*, 2011, **8**, 97-104.
- 3 T. Ivanković and J. Hrenović, *Arch. Ind. Hyg. Toxicol.*, 2010, **61**, 95–110.
- 4 C. L. Yuan, Z. Z. Xu, M. X. Fan, H. Y. Liu, Y. H. Xie and T. Zhu, *J. Chem. Pharm. Res.*, 2014, **6**, 2233–2237.
- 5 M. Rutkevičius, S. K. Munusami, Z. Watson, A. D. Field, M. Salt, S. D. Stoyanov, J. Petkov, G. H. Mehl and V. N. Paunov, *Mater. Res. Bull.*, 2012, **47**, 980–986.
- 6 M. Constantin, S.-M. Bucatariu, F. Doroftei and G. Fundueanu, *Carbohydr. Polym.*, 2017, **157**, 493–502.
- 7 L. Zhang, K. Li, W. Xiao, L. Zheng, Y. Xiao, H. Fan and X. Zhang, *Carbohydr. Polym.*, 2011, **84**, 118–125.
- 8 M. Rutkevičius, G. H. Mehl, J. T. Petkov, S. D. Stoyanov and V. N. Paunov, *J. Mater. Chem. B*, 2015, **3**, 82–89.
- 9 B. R. Thompson, T. S. Horozov, S. D. Stoyanov, V. N. Paunov, *Food Funct.*, 2017, **70**, 448–455.
- 10 M. Rutkevičius, Z. Austin, B. Chalk, G. H. Mehl, Q. Qin, P. A. Rubini, S. D. Stoyanov and V. N. Paunov, *J. Mater. Sci.*, 2015, **50**, 3495–3503.
- 11 M. Rutkevičius, G. H. Mehl, V. N. Paunov, Q. Qin, P. A. Rubini, S. D. Stoyanov and J. Petkov, *J. Mater. Res.*, 2013, **28**, 2409–2414.
- 12 S. Arnott, A. Fulmer, W. E. Scott, I. C. M. Dea, R. Moorhouse and D. A. Rees, *J. Mol. Biol.*, 1974, **90**, 269–284.
- 13 R. Armisén and F. Gaiatas, 4 - Agar, in *Handbook of Hydrocolloids*, ed. G. O. Phillips, P. A. Williams, Woodhead Publishing Limited, Cambridge, 2nd edn, 2009, ch. 4, pp. 82–107.

- 14 C. Berkland, K. Kim and D. W. Pack, *Pharm. Res.*, 2003, **20**, 1055–1062.
- 15 J. Siepmann and A. Göpferich, *Adv. Drug Deliv. Rev.*, 2001, **48**, 229–247.
- 16 C. Berkland, E. Pollauf, C. Raman, R. Silverman, K. Kim and D. W. Pack, *J. Pharm. Sci.*, 2007, **96**, 1176–1191.
- 17 C. Berkland, K. Kim and D. W. Pack, *J. Control. Release*, 2001, **73**, 59–74.
- 18 C. Berkland, M. J. Kipper, B. Narasimhan, K. Kim and D. W. Pack, *J. Control. Release*, 2004, **94**, 129–141.
- 19 M. Dunne, O. I. Corrigan and Z. Ramtoola, *Biomaterials*, 2000, **21**, 1659–1668.
- 20 D. Klose, F. Siepmann, K. Elkharraz, S. Krenzlin and J. Siepmann, *Int. J. Pharm.*, 2006, **314**, 198–206.
- 21 R. V. Kulkarni, V. Sreedhar, S. Mutalik, C. M. Setty and B. Sa, *Int. J. Biol. Macromol.*, 2010, **47**, 520–527.

6. An ultra melt-resistant hydrogel from food grade carbohydrates

A binary hydrogel system made from two food grade biopolymers, agar and methylcellulose (agar-MC), which does not require addition of salt for gelation to occur and has very unusual rheological and thermal properties is reported. It is found that the storage modulus of the agar-MC hydrogel far exceeds these of hydrogels from the individual components. In addition, the agar-MC hydrogel has enhanced mechanical properties over the temperature range 25-85 °C and a maximum storage modulus at 55 °C when the concentration of methylcellulose was 0.75% w/v or higher. This is explained by a sol-gel phase transition of the methylcellulose upon heating as supported by differential scanning calorimetry (DSC) measurements. Above the melting point of agar, the storage modulus of agar-MC hydrogel decreases but is still an elastic hydrogel with mechanical properties dominated by the MC gelation. By varying the mixing ratio of the two polymers, agar and MC, it was possible to engineer a food grade hydrogel of controlled mechanical properties and thermal response. SEM imaging of flash-frozen and freeze-dried samples revealed that the agar-MC hydrogel contains two different types of heterogeneous regions of distinct microstructures. The binary hydrogel was also tested for its stability towards heat treatment which showed that upon heating to temperatures above 120 °C its structure was retained without melting. The produced highly thermally stable hydrogel shows melt resistance which may find application in high temperature food processing and materials templating. The work in this chapter was published in the RSC journal RSC Advances.¹

6.1. Introduction

Hydrogels are 3D hydrophilic, polymeric networks containing either chemical or physical cross-links with the ability to be considerably swollen with water. Being cheap, aqueous based and largely biocompatible materials, hydrogels have attracted a great amount of attention² due to their alluring properties and have been used in various areas such as tissue engineering,³ drug delivery and wound dressing,⁴ biomedical applications⁵ and food structuring.^{6,7} With the growing number of versatile hydrogel applications there is demand for more specific hydrogel materials of

tailorable properties. Binary hydrogel systems can give properties superior to either of the individual components, with the gelation of one polysaccharide being notably affected by addition of a second polysaccharide.^{8,9} Agar hydrogel alone shows syneresis of water, whereas when combined with locust bean gum, a more elastic hydrogel with reduced syneresis is produced.¹⁰ Gellan can be either low-acyl or high-acyl, depending on the manufacturing process used.¹¹ When low-acyl gellan and high-acyl gellan is mixed in a 1:1 ratio, the deformability of the hydrogel is increased without any loss of strength when compared to a low-acyl gellan hydrogel of the same overall polymer concentration.¹² Agar and κ -carrageenan co-hydrogels were studied at various mixing ratios and it was seen that the gelling temperature decreased, along with forming more deformable but weaker hydrogels.¹³ Xanthan gum forms a viscous solution in water with pseudoplastic flow behaviour but when mixed with locust bean gum in a 1:1 ratio, a large increase in viscosity is seen at low concentrations and gelation occurs at overall polymer concentration as low as 0.3%.¹⁴

Agar consists of both agarose and agaropectin, with the former being the constituent that causes gelation. Agarose is composed of a linear polymer of the disaccharide D-galactose and 3,6-anhydro-L-galactopyranose and is insoluble in cold water but hydrates at temperatures close to the boiling point of water where its molecules have a random coil conformation. Upon cooling the solution to below the gelling temperature, the agarose chains form double helixes, which aggregate to form a three-dimensional structure with water entrapped within the polymer matrix.¹⁵ The gelling temperature of agar is dependent on the methoxyl content, with an increase of methoxyl content showing an increase in gelling temperature.¹⁶ This thermo-reversible hydrogel shows a large thermal gelling hysteresis, gelling around 38 °C and melting around 85 °C.¹⁰ Agar is widely used in the food industry,¹⁷ electrophoresis¹⁸ and as a solid culture media for bacteria.¹⁹

Methylcellulose (MC) is a derivative of cellulose produced by partial methylation of cellulose²⁰ where the degree of substitution (DS) of hydroxyl with methoxyl groups per anhydro-D-glucose unit determines the solubility of the polymer.²¹ MC is insoluble at high temperatures, but hydrates in cold water. After hydration, the viscosity of the MC solution increases with an increase in temperature and forms a gel above a certain temperature that is dependent on the DS and the concentration of MC in solution.^{22–24} The gelation process is attributed to an initial association of the hydrophobic

methylated regions, followed by formation of a turbid gel and phase separation.^{22,24–27} The heat setting nature of MC, along with its thermoreversibility,²⁸ makes it appealing for use in cooking as a thickener or a binder.²⁰

Previous studies have shown that MC-agar solutions have much quicker gelation times compared to MC alone when held at a constant temperature.²⁹ In this paper the formulation of a novel two-component, physically cross-linked hydrogel system comprising of agar and MC that shows enhanced mechanical properties over the temperature range investigated (25 – 85 °C) compared to agar or MC alone has been demonstrated. For example, when the composition of the binary hydrogel is 1.0% w/v – 1.0% w/v it was found that the storage modulus (G') of the hydrogel is largest at 55 °C. This has been attributed to a sol-gel phase transition of the MC in the mixed gel which is also backed up by DSC data. SEM of freeze-dried agar-MC hydrogels has been utilised to investigate their microstructure which shows heterogeneous mixing with formation of agar-rich and MC-rich regions. The agar-MC hydrogels also show stability to various forms of heat treatment by maintaining its structure at temperatures well above the melting point of agar alone, which may find a number of applications in high temperature hydrogel templating or as novel structuring agents in the food industry.

6.2. Results

6.2.1. Rheological properties of agar-MC hydrogels

A two-component hydrogel comprising of agar and MC has been formulated in a ratio of 1:1, with an overall polymer concentration of 2.0% w/v. Its storage modulus was compared with those of agar (1.0% and 2.0% w/v) and MC (1.0% w/v and 2.0% w/v) alone over a range of temperatures. The results shown in Figure 6.1 demonstrate the differences between the storage modulus at varying temperatures and at constant shear stress (20 Pa and 62 Pa, respectively).

From Figures 6.1(A) and 6.1(B), it can be seen that the storage modulus of the agar hydrogels decreases with increasing the temperature between 25 – 85 °C, showing a minimum at 85 °C because the latter is near the melting point of agar.¹⁰

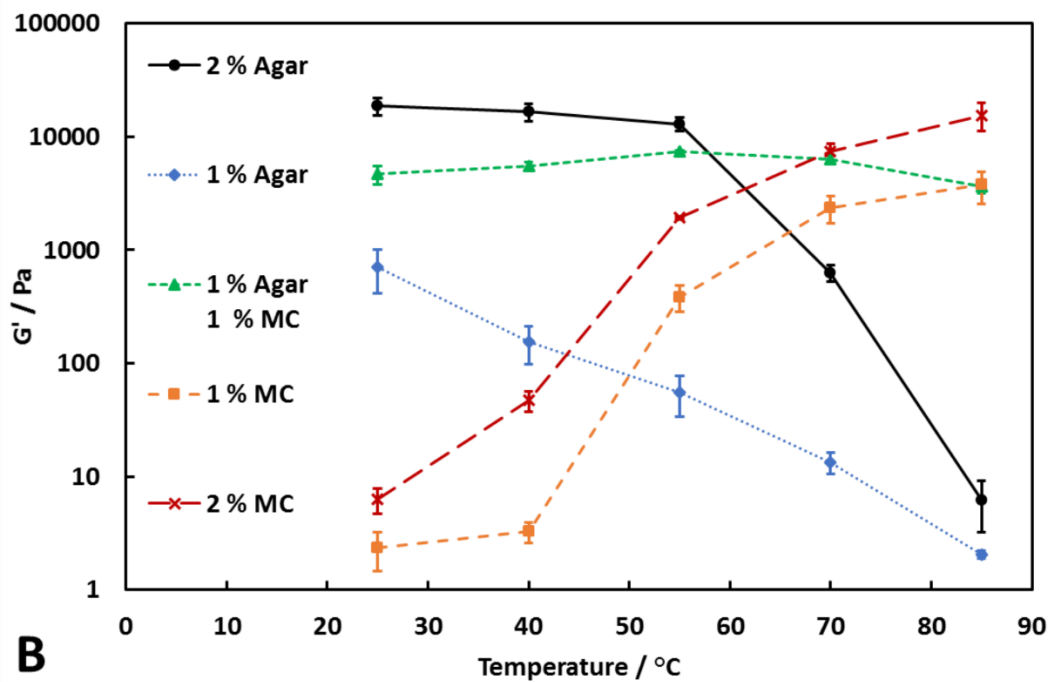
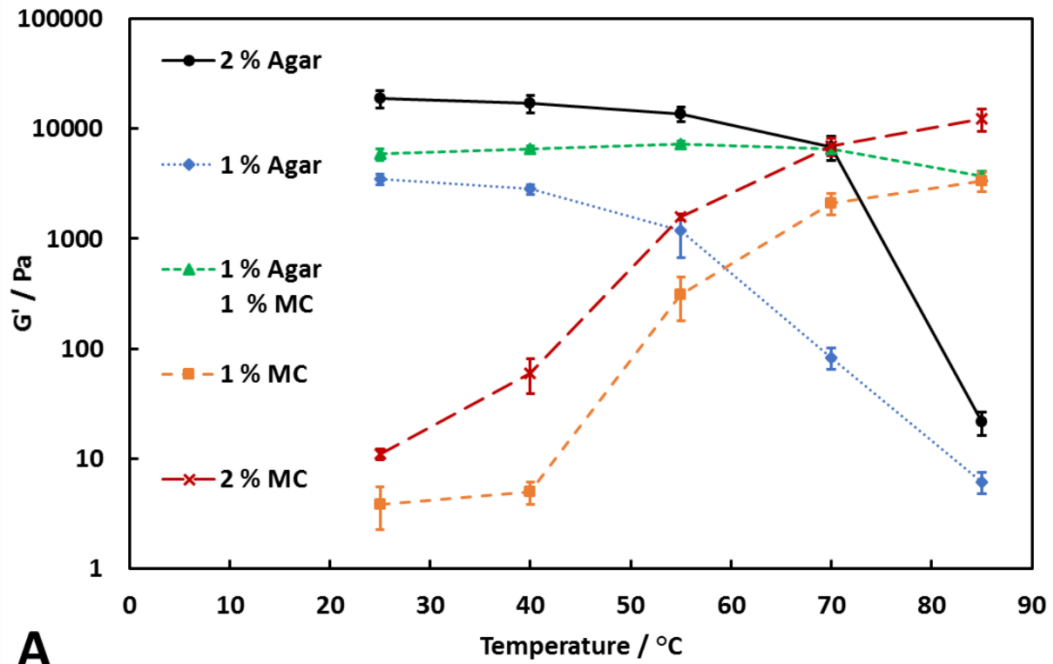


Figure 6.1. The storage modulus of agar hydrogel (1.0% w/v and 2.0% w/v), MC (1.0% w/v and 2.0% w/v) and agar-MC hydrogel (1.0% w/v – 1.0% w/v) as a function of temperature. The shear stresses are (A) 20 Pa and (B) 62 Pa. Note that the y-axes are on log scale. Each sample was measured in triplicate and the error bars are the standard deviation.

As the shear stress was increased, the storage modulus of agar decreased. This was most noticeable at 70 °C, where the increased temperature has started to weaken the hydrogel. The increase in shear stress disturbs the agar polymer network and, combined with the elevated temperature, causes the large decrease in the storage modulus.

MC hydrogels behaved oppositely to agar hydrogels, with the storage modulus increasing with increasing temperature, showing that the MC solution becomes a gel once heated above a certain temperature. For the grade of MC used in these experiments, the gelation temperature was between 40 – 55 °C. It is known that the gelation temperature of MC also varies with the MC concentration²¹⁻²³ but this was not investigated in detail here. Furthermore, at the shear stresses investigated, weakening of the MC hydrogels was not observed. In fact, the storage modulus increased with increased shear stress. However, this is likely due to the hydrogel being held at a temperature above the gelation temperature for a longer period of time, as MC hydrogels continue to increase in strength over time when held above the gelling temperature.²¹

The two-component agar-MC hydrogel showed characteristics of both agar and MC, depending on the temperature. At the lower temperatures, its mechanical properties are dominated by the agar present, and at higher temperatures MC is the polymer contributing to the hydrogel strength. However, even at temperatures below the gelling point of MC, the two-component system shows an almost two-fold increase in storage modulus when compared with 1.0% w/v agar containing no MC, suggesting a synergistic effect between the two polymers. The agar-MC hydrogel samples also showed resistance to an increased shear stress compared to 1.0% w/v agar hydrogel alone. The agar-MC hydrogel has a fairly constant storage modulus upon increasing the temperature from 25°C up to nearly 90 °C with a shallow maximum around 55 °C; this is due to the temperature being above the gelling point of MC. The MC begins to gel, which reinforces the agar hydrogel network, increasing the storage modulus by between 25 – 100% when compared to the same hydrogel at 25 °C. At 70 °C, the agar-MC hydrogel's strength begins to slightly decrease which is likely to be due to the partial weakening of the agar network and by 85 °C the mechanical properties are dominated solely by the MC, showing a very similar storage modulus to 1.0% w/v MC alone.

From Figure 6.2(A), it can be seen that at a shear stress of 20 Pa, the agar-MC hydrogels are significantly stronger than agar alone at 85 °C. At 70 °C, the two-component hydrogels are more resistant to increased shear stress than agar hydrogel alone, even when the concentration of MC is as low as 0.25% w/v, as shown in Figure 6.2(B). However, once the temperature reaches 85 °C, the low concentration of MC is unable to resist the increase in shear stress which results in a large decrease in the storage modulus. On the other hand, when the concentration of MC is 0.5% w/v or higher, the hydrogel can withstand the increase in shear stress due to the formation of a stronger polymer network. From Figures 6.2(A) and 6.2(B), it can be seen that varying the ratio of agar to MC at the same overall polymer concentration significantly changes the storage modulus over the whole temperature range. When the concentration of agar is much higher than MC, the storage modulus at low temperatures is high, but shows a larger decrease when the temperature is increased. As the concentration of agar is decreased and the concentration of MC is increased, the storage modulus of the hydrogel is decreased at low temperatures but increased at high temperatures. When the concentration of MC is high enough, a maximum in the storage modulus vs temperature is seen at 55 °C. By varying the ratio of agar to MC, it is possible to tailor hydrogels with desired mechanical properties over a temperature range.

Figures 6.3(A) and 6.3(B) show that as upon increasing the concentration of MC mixed with agar, the storage modulus of the hydrogel increases at all temperatures compared at agar alone. Furthermore, it can be seen that the addition of MC significantly increases the resistance of the hydrogel to an increase in the shear stress. From Figures 6.3(C) and 6.3(D), the maximum G' at 55 °C can clearly be seen when the concentration of MC is 1.0% w/v. Above 55 °C, G' of the agar-MC hydrogels begin to slightly decrease due to the high temperature starting to disrupt the agar hydrogel network. The data suggests that the MC present reinforces nearly twice the agar polymer network at 1:1 agar-to-MC ratio and makes it much less sensitive to the temperature with this effect being amplified at temperatures above the gelling point of the MC hydrogel.

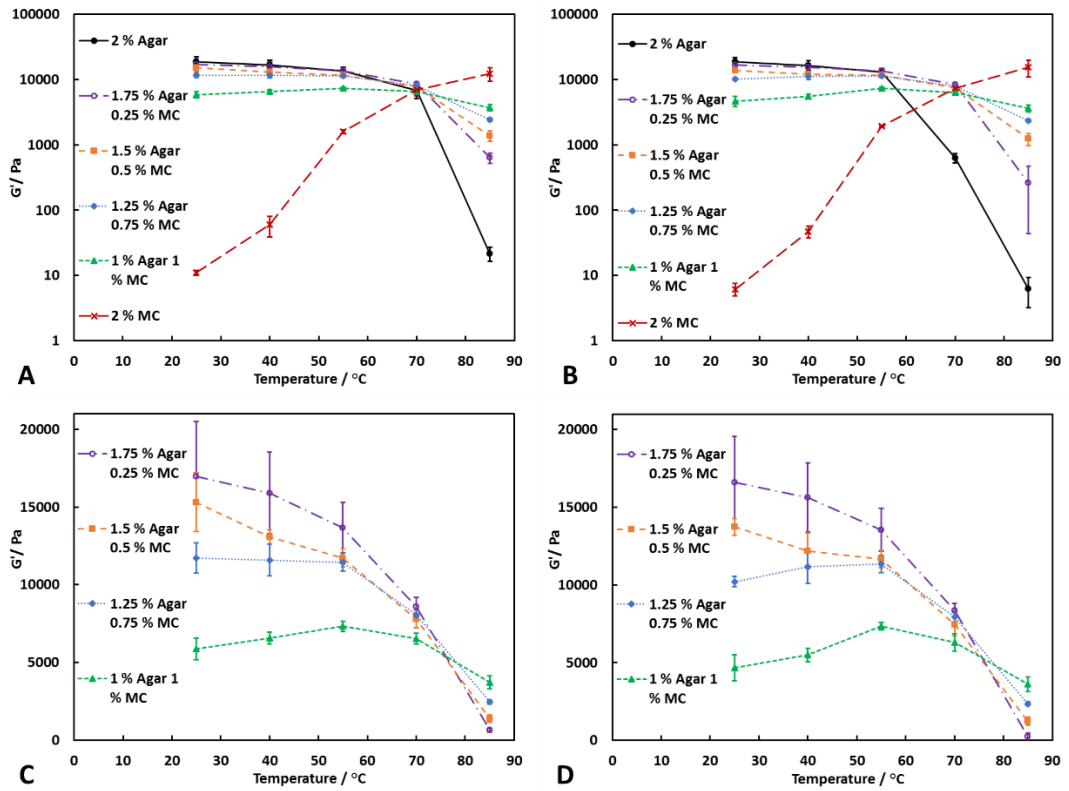


Figure 6.2. The storage modulus as a function of temperature for agar hydrogel (2.0% w/v), MC hydrogel (2.0% w/v) and agar-MC hydrogel with varying compositions of the agar and MC (1.75%:0.25%, 1.5%:0.5%, 1.25%:0.75% and 1.0%:1.0%). The shear stress is kept constant at 20 Pa in (A) and 62 Pa in (B). Note that the y-axes in (A) and (B) are on a log scale. (C) and (D) show only the data for agar-MC hydrogels from (A) and (B), respectively. The y-axis is not on a logarithmic scale to allow easier comparison between the two-component hydrogels. Each sample was measured in triplicate and the error bars are the standard deviation.

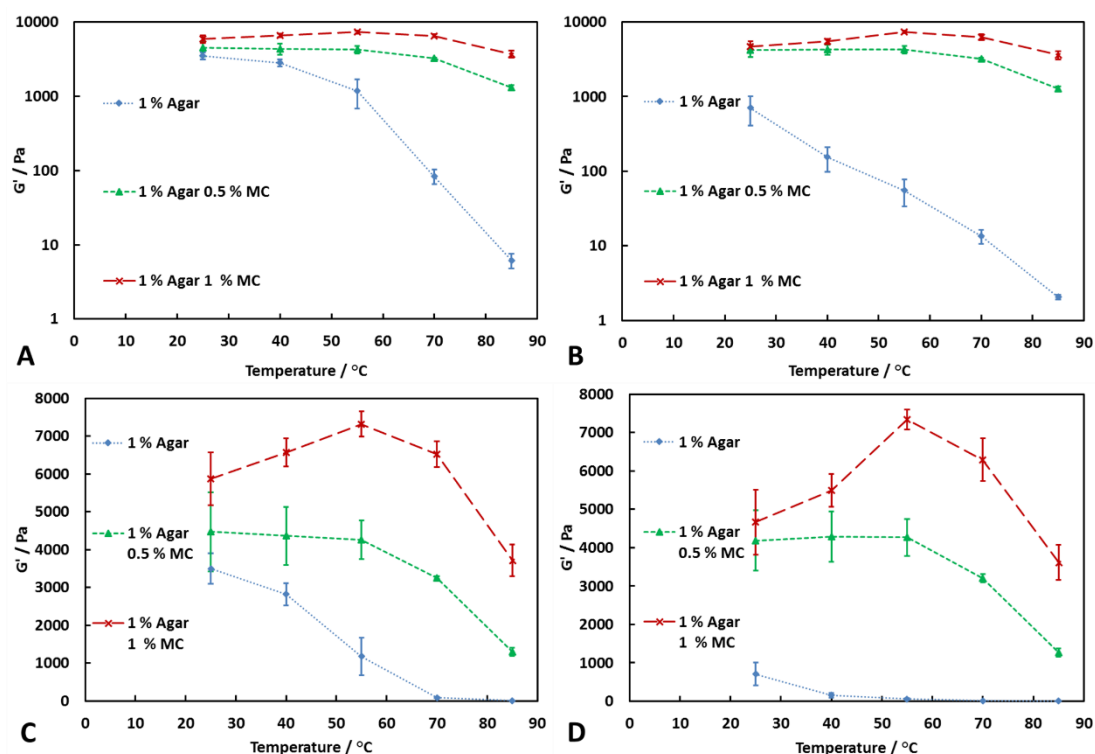


Figure 6.3. The storage modulus of agar-MC hydrogels as a function of temperature at a constant agar concentration of 1.0% w/v and an increasing concentration of MC (0% w/v, 0.5% w/v and 1.0% w/v) in the hydrogel. The shear stress is kept constant at 20 Pa in (A) and at 62 Pa in (B). The y-axis is on the log scale in (A) and (B) while (C) and (D) represent the same data on linear scale to clearly show that the existence of a maximum G' at the 1:1 ratio of agar to MC. Each sample was measured in triplicate and the error bars are the standard deviation.

6.2.2. Uniaxial compression

The mechanical properties of agar and agar-MC hydrogels has been investigated through uniaxial compression testing. The samples were subjected to compression until structural failure which allowed for calculation of the compressional strength and Young's modulus. Figure 6.4 shows that 2.0% w/v agar has a higher compressional strength and Young's modulus at room temperature. At this temperature, agar is the polymer dominating the mechanical properties as the temperature is below that of the gelling point of MC.

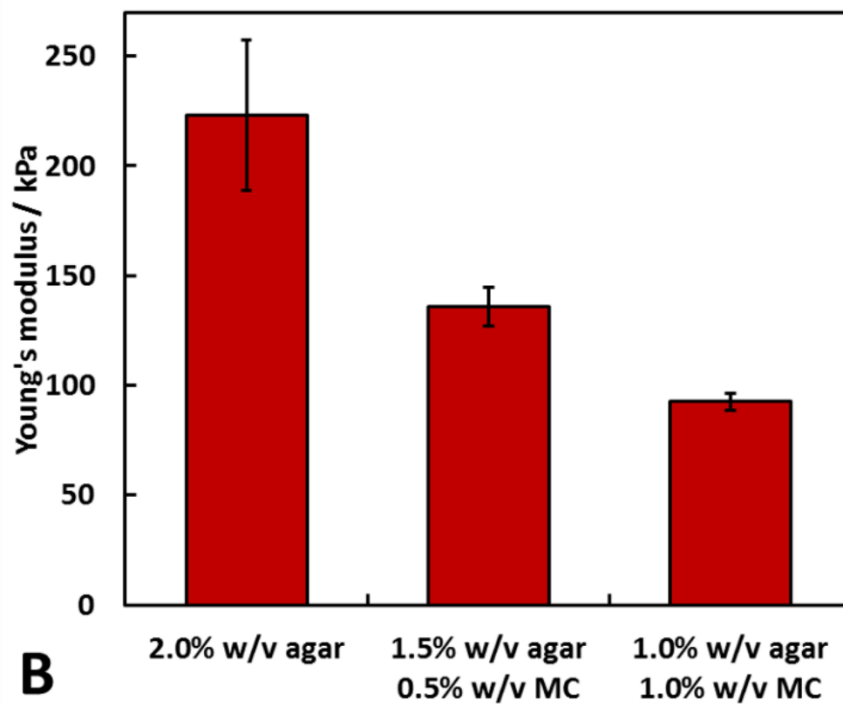
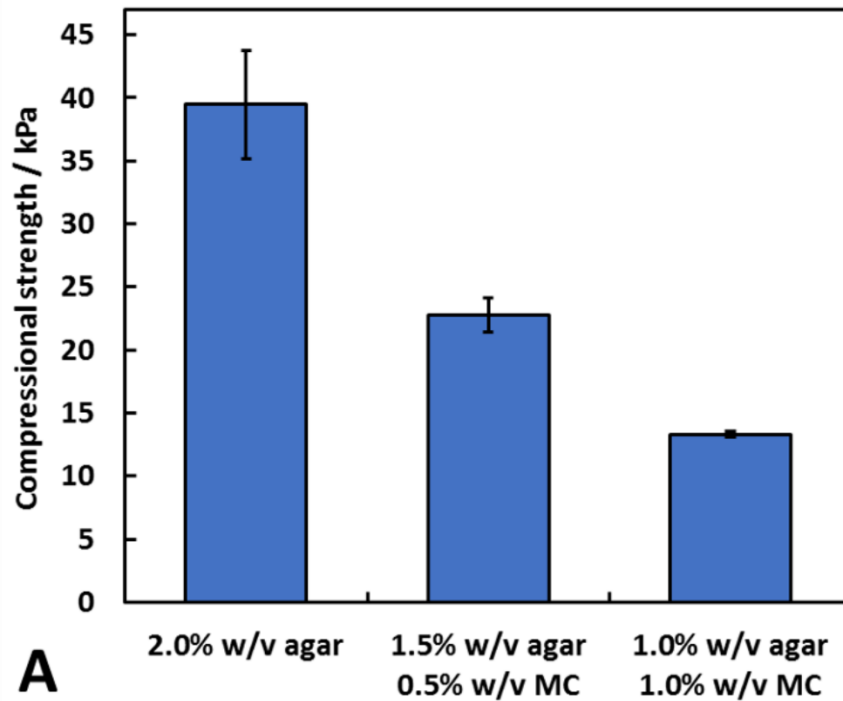


Figure 6.4. Compressional strength (A) and Young's modulus (B) of agar hydrogel (2.0% w/v) and agar-MC hydrogels (1.5 – 0.5% w/v and 1.0 – 1.0% w/v). Each sample was measured at least four times and the average value is shown, with the error bars being the standard deviation.

6.2.3. DSC measurement

Figure 6.5 shows a DSC thermogram for a sample of the agar-MC hydrogel. In the heating curve, two endothermic peaks were observed. The first peak has an onset temperature of 48.0 °C and a peak temperature of 59.4 °C and corresponds to the sol-gel transition of MC. The second peak, which corresponds to the gel-sol transition of agar, has an onset temperature of 71.0 °C and a peak temperature of 83.9 °C. The cooling curve shows a single exothermic peak which corresponds to the sol-gel transition of agar. MC is known to be a thermo-reversible hydrogel;²⁸ however, no peak can be seen showing its gel-sol transition at low temperatures. The endothermic peak due to gelation of MC supports the assumption that, once MC begins to gel, it reinforces the agar hydrogel network, which in turn increases its mechanical properties resulting in the maximum G' seen at 55 °C.

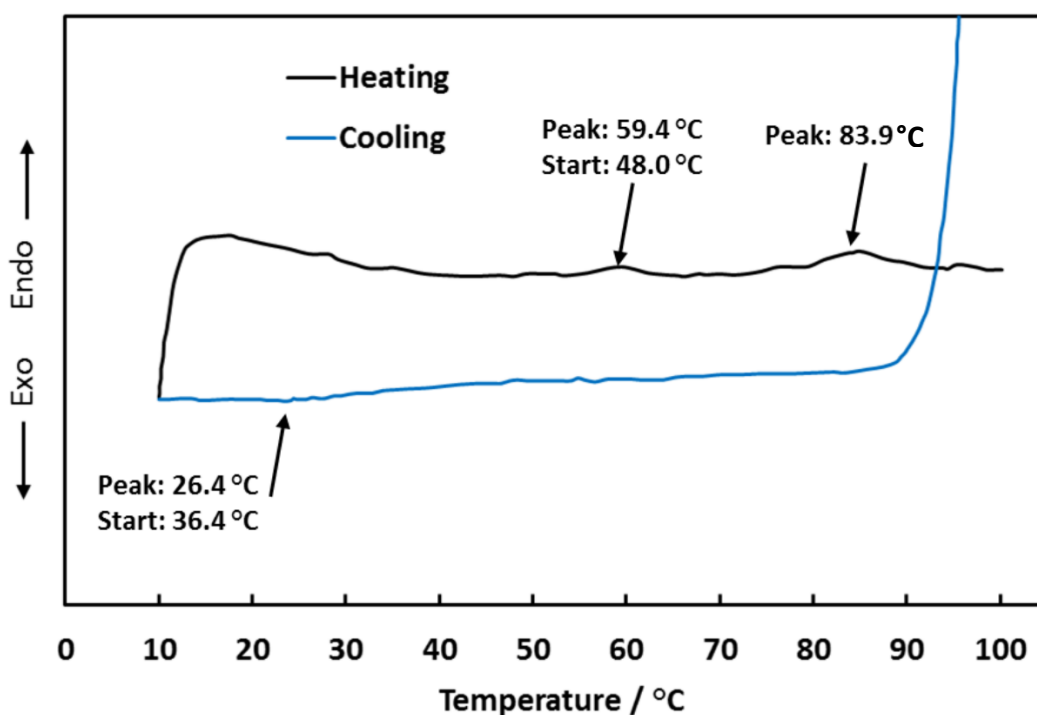


Figure 6.5. DSC thermogram of agar-MC hydrogel (1.0% w/v agar – 1.0% w/v MC, sample mass 102.30 mg). The sample was heated in the range from 10 °C to 100 °C at a heating rate of 2 °C min⁻¹ and then cooled from 100 °C to 10 °C at the same rate. The curves are shifted along the y-axis for clarity.

6.2.4. Thermal stability

The freeze-thaw stability of agar-MC hydrogels was investigated by freezing the hydrogel at -18 °C for 24 hours, followed by subsequent thawing at 30 °C for 1 hour. After freezing, the structure of the sample had changed, and after thawing, there was syneresis of a viscous liquid from the hydrogel. After the sample had thawed, the hydrogel had decreased to $63 \pm 3\%$ of its original mass. This is likely to be due to the ice crystals formed on freezing thus physically disrupting the gel network, leading to a weaker gel upon thawing which enhances the syneresis to occur.

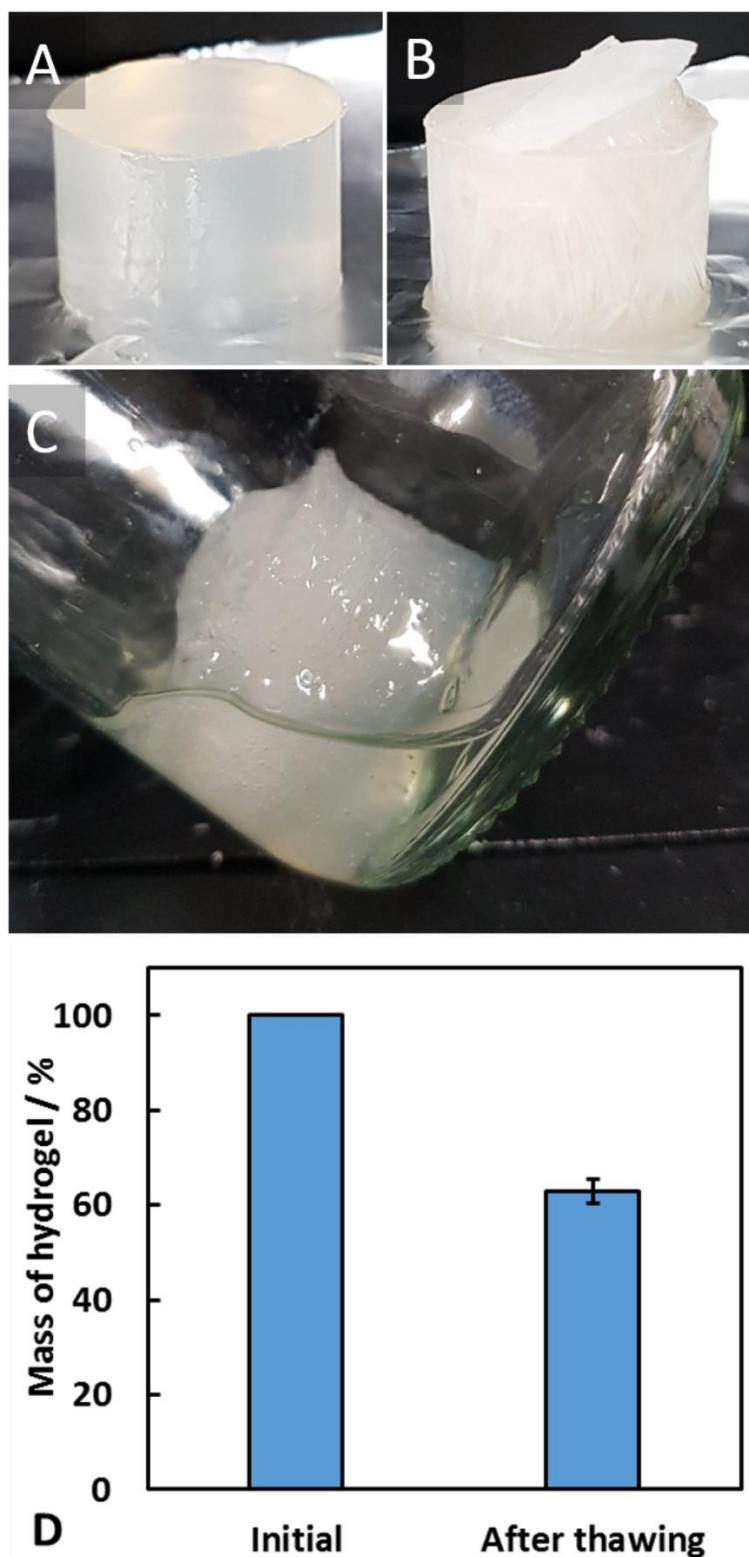


Figure 6.6. (A)-(C) Photographs of the agar-MC hydrogel sample during its freeze-thaw cycle: (A) the hydrogel before freezing, (B) the frozen sample and (C) the sample after it has been thawed. (D) The reduction in mass of the hydrogel after thawing. The experiment was repeated three times (from freshly prepared hydrogel) and an average mass reduction was taken. The error bar is the standard deviation.

The stability of the agar-MC hydrogels was also investigated at high temperatures. The first experiment was to immerse the hydrogel samples in water in a sealed container and then heat them up in an autoclave. The autoclave reaches a temperature of 121 °C (well above the melting point of agar) and operates at an elevated pressure of 105 kPa. The sample was left in the autoclave for a full heating and cooling cycle and then viewed afterwards. The appearance of the agar-MC hydrogel is shown in Figure 6.7, where it is compared to an agar hydrogel sample undergoing the same treatment. Upon removal of the agar-MC sample from the autoclave, it was seen that it retained its shape whereas the agar melted and mixed with the water. This is due to the enhanced hydrogel network of MC formed before the agar network melts, then the agar gel network reforming upon cooling. The agar-MC hydrogel also becomes more turbid which is a characteristic of a sol-gel transition of MC.²¹

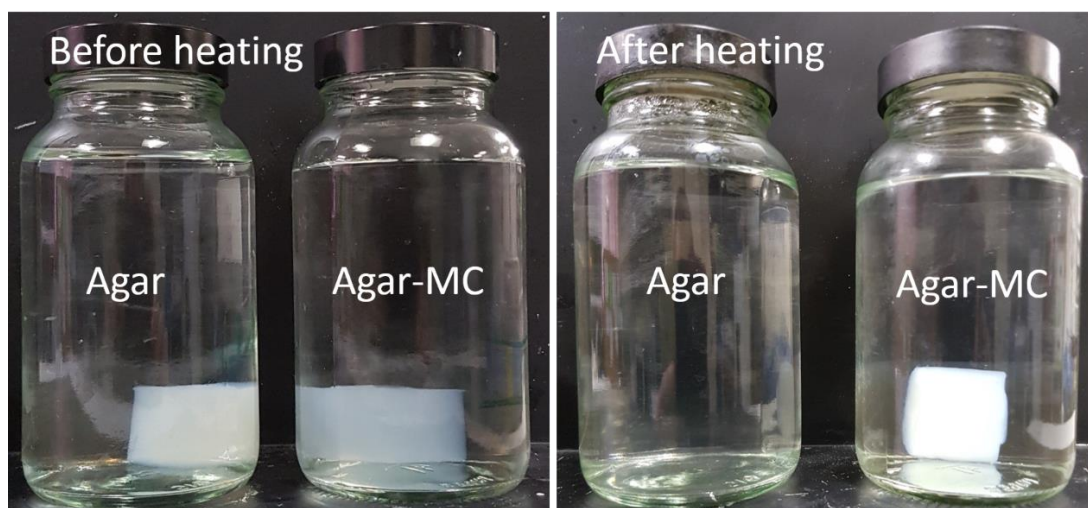


Figure 6.7. The image on the left shows hydrogel samples of agar (2.0% w/v) and agar-MC (1.0% w/v – 1.0% w/v) immersed in water (200 cm³) before heating in the autoclave. The image on the right shows the samples after being heated in an autoclave at 121 °C and cooled down to room temperature.

Samples of agar-MC and agar hydrogels were also heated in a furnace at 150 °C, and their appearances were compared. The samples were left in a furnace for 45 minutes at 150 °C, removed and then compared. Figure 6.8 shows the appearance of the two hydrogel samples before and after heating. The agar-MC hydrogel retained its shape whereas the agar hydrogel melted. Again, an increase in turbidity of the agar-MC

sample is observed due to the gelation of MC. Mass was lost from both samples due to the evaporation of water. However, the fact that the agar-MC sample retained its shape at this high temperature suggests that this two-component hydrogel could be used for high temperature templating.

It could also be used in the development of new food products as it is made from food grade polymers that do not require salts to form a gel, *i.e.* they form physical gels and they keep their structure at the high temperatures used in cooking and high temperature food processing. It is also possible to encapsulate a flavour or taste enhancing compounds in hydrogels, thus making them attractive materials for food product development. Further work will explore some of those possible uses of such agar-MC hydrogels.

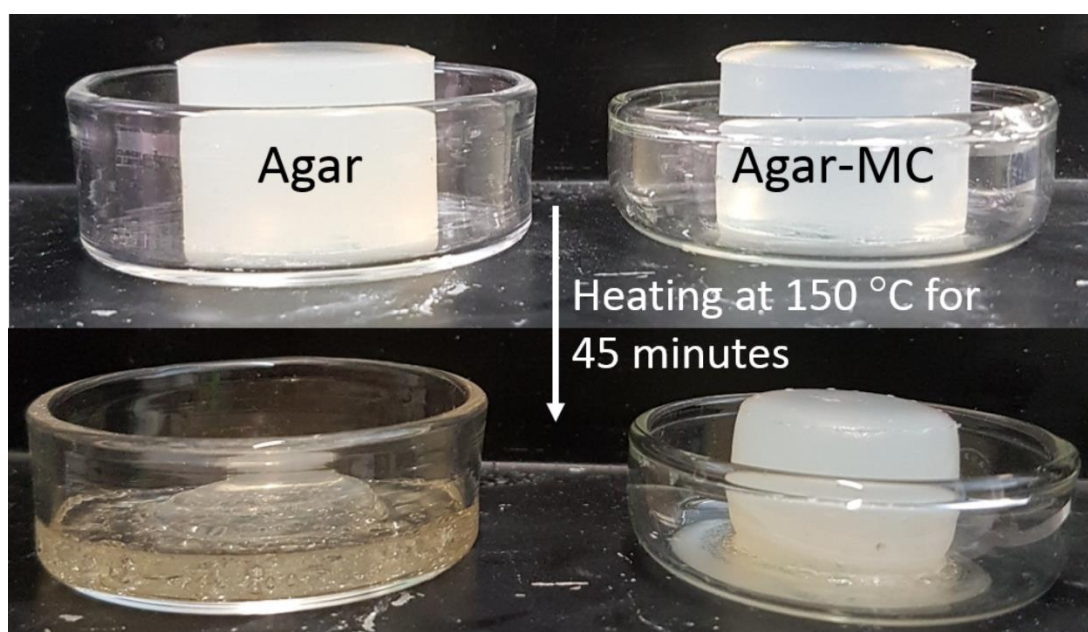


Figure 6.8. This shows the agar hydrogel (2.0% w/v) and the agar-MC hydrogel (1.0% w/v – 1.0% w/v) before (top) and after (bottom) heating in a furnace at 150 °C for 45 minutes.

6.2.5. Hydrogel microstructure analysis

The microstructure of agar hydrogel (2.0% w/v), MC in solution (2.0% w/v) and agar-MC hydrogel (1.0% w/v – 1.0% w/v) was analysed by imaging the flash-frozen and freeze-dried samples by SEM as shown below in Figures 6.9, 6.10 and 6.11-6.13, respectively.

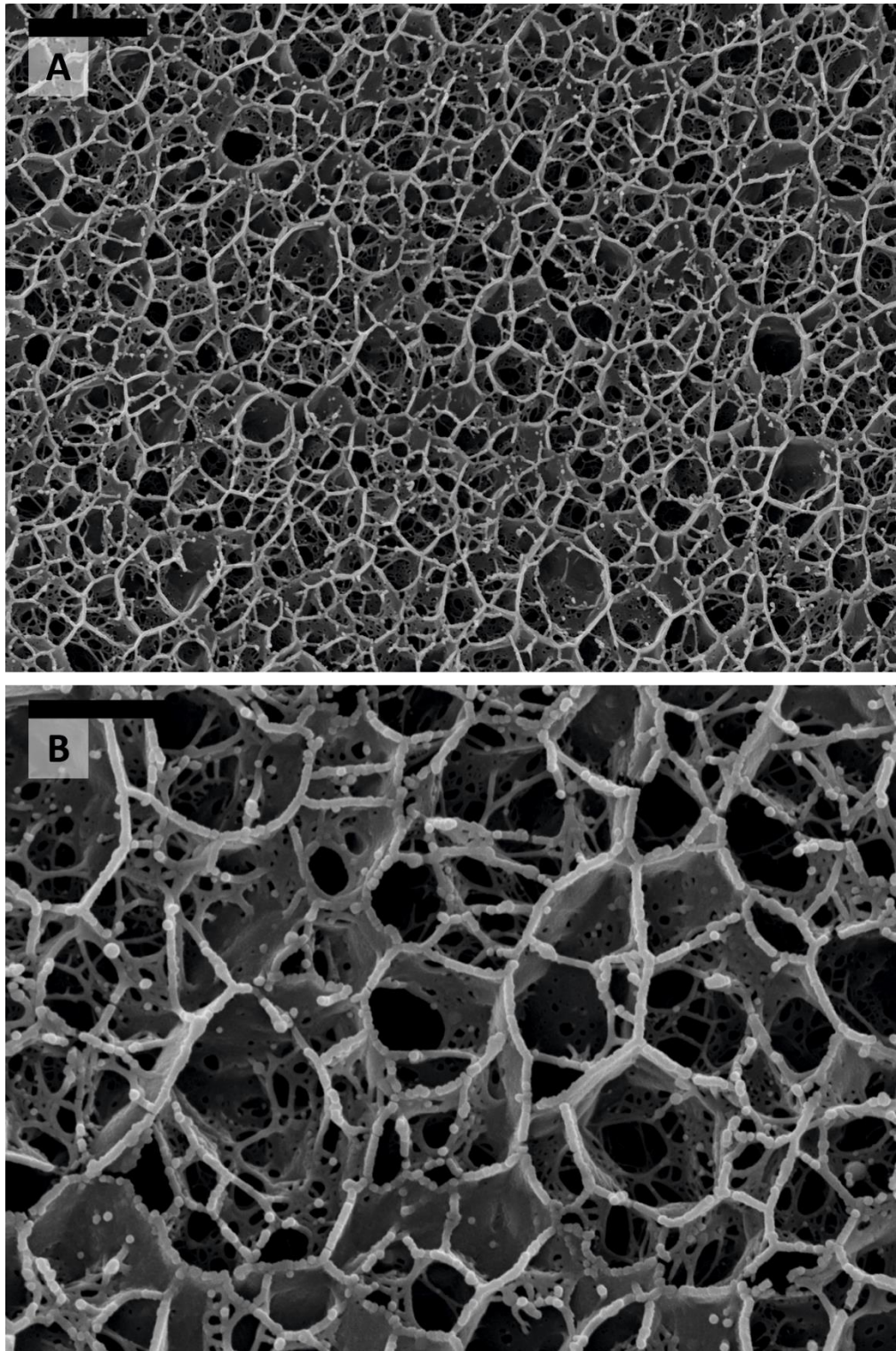


Figure 6.9. SEM images of a flash-frozen and freeze-dried agar (2.0% w/v) hydrogel sample. The sample were imaged after it was flash-frozen in slush nitrogen, fractured by a blade and then the water content sublimed at $-70\text{ }^{\circ}\text{C}$ for 7 minutes. The scale bars correspond to $5\text{ }\mu\text{m}$ and $2\text{ }\mu\text{m}$, respectively.

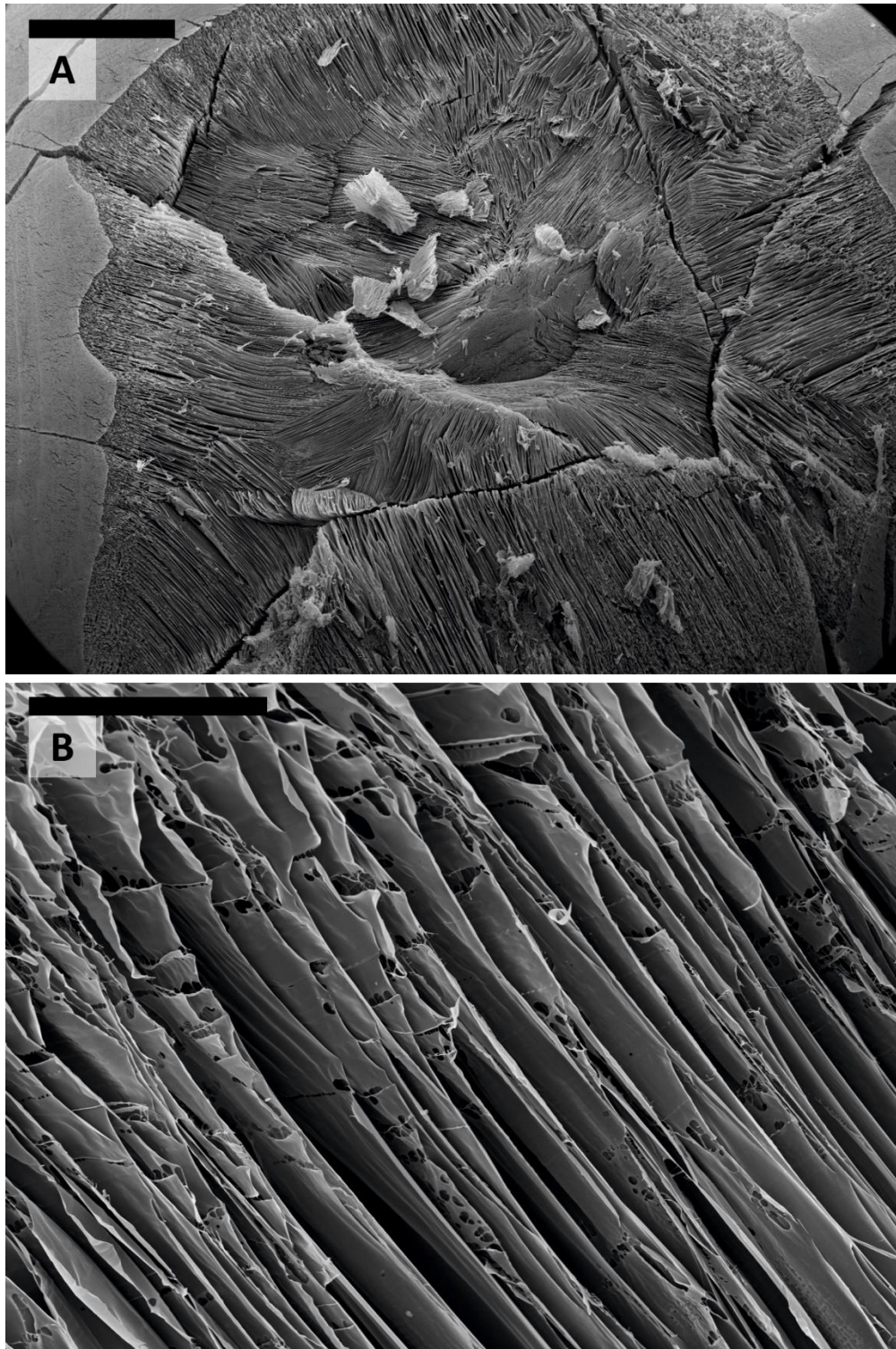


Figure 6.10. SEM images of a flash-frozen and freeze-dried MC (2.0% w/v) solution sample after it was flash-frozen in slush nitrogen, fractured by a blade and then sublimed at $-70\text{ }^{\circ}\text{C}$ for 7 minutes. The smooth parts seen close to the edges of (A) correspond to the surface of the MC droplet that was not fractured. (B) shows the fractured central region of (A) at higher magnification. The scale bars correspond to a distance of 1 mm and $100\text{ }\mu\text{m}$, respectively.

The samples were flash frozen in slush nitrogen and fractured with a blade held at -140 °C. Upon subliming at -70 °C for 7 minutes, the microstructures were revealed.

Figures 6.9(A) and 6.9(B) display the microstructure of the agar hydrogel which shows a pentagonal pore structure as seen in the literature.³⁰ A droplet of MC solution after flash freeze-drying and fracturing is shown in Figures 6.10(A) and 6.10(B). It displays very well ordered layered sheet-like MC structures on a scale larger than 1 mm. The microstructure of the agar-MC hydrogels was then imaged in a very similar way and two distinct structures can be seen within the polymer network in Figures 6.11-6.13. Regions of an agar-like network structure can be clearly seen in Figures 6.11-6.13. Although the network cells look more interconnected than those for agar alone in Figure 6.9, their similarity indicates that those are likely agar-rich regions. Enclosures with a very different structure co-existing with the agar-rich regions are also seen in Figures 6.11(A), 6.12(A) and 6.13(A)-6.13(B). Their structure is more reminiscent of the MC hydrogels as shown in Figures 6.10(A) and 6.10(B) thus indicating that a MC-rich phase is also present in the agar-MC hydrogel.

The sheet-like layered structure is similar to that of MC in Figure 6.10, however the sheets are connected by fibres which are not seen when MC is alone. In some of these regions, there is an interface where the two structures of agar and MC-rich phases meet (Figure 6.12(A)). They appear to be randomly distributed throughout the three-dimensional hydrogel structure, suggesting that the overall microstructure of the agar-MC-hydrogel is defined during the gelation of agar. The latter are likely to fortify the hydrogel which explains its superior mechanical properties compared to those of the agar and MC hydrogels alone.

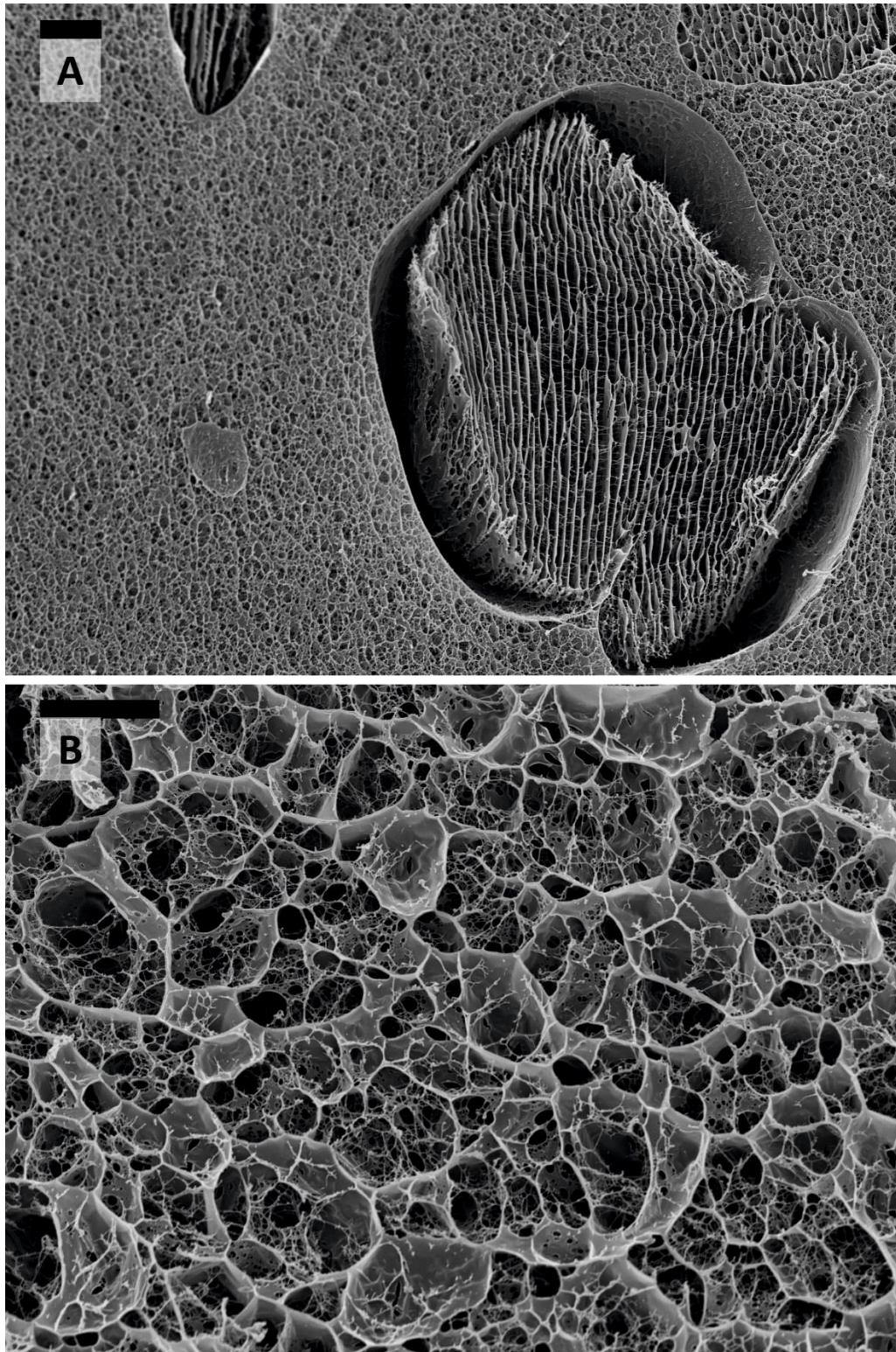


Figure 6.11. SEM images of a freeze-dried sample of agar-MC hydrogel (1.0% w/v – 1.0% w/v) after it was flash-frozen in slush nitrogen, fractured by a blade and then sublimated at $-70\text{ }^{\circ}\text{C}$ for 7 minutes. (A) shows co-existing regions of a MC-like structure surrounded by an agar-like structure. (B) shows the agar-like network at higher magnification. Both scale bars correspond to $10\text{ }\mu\text{m}$.

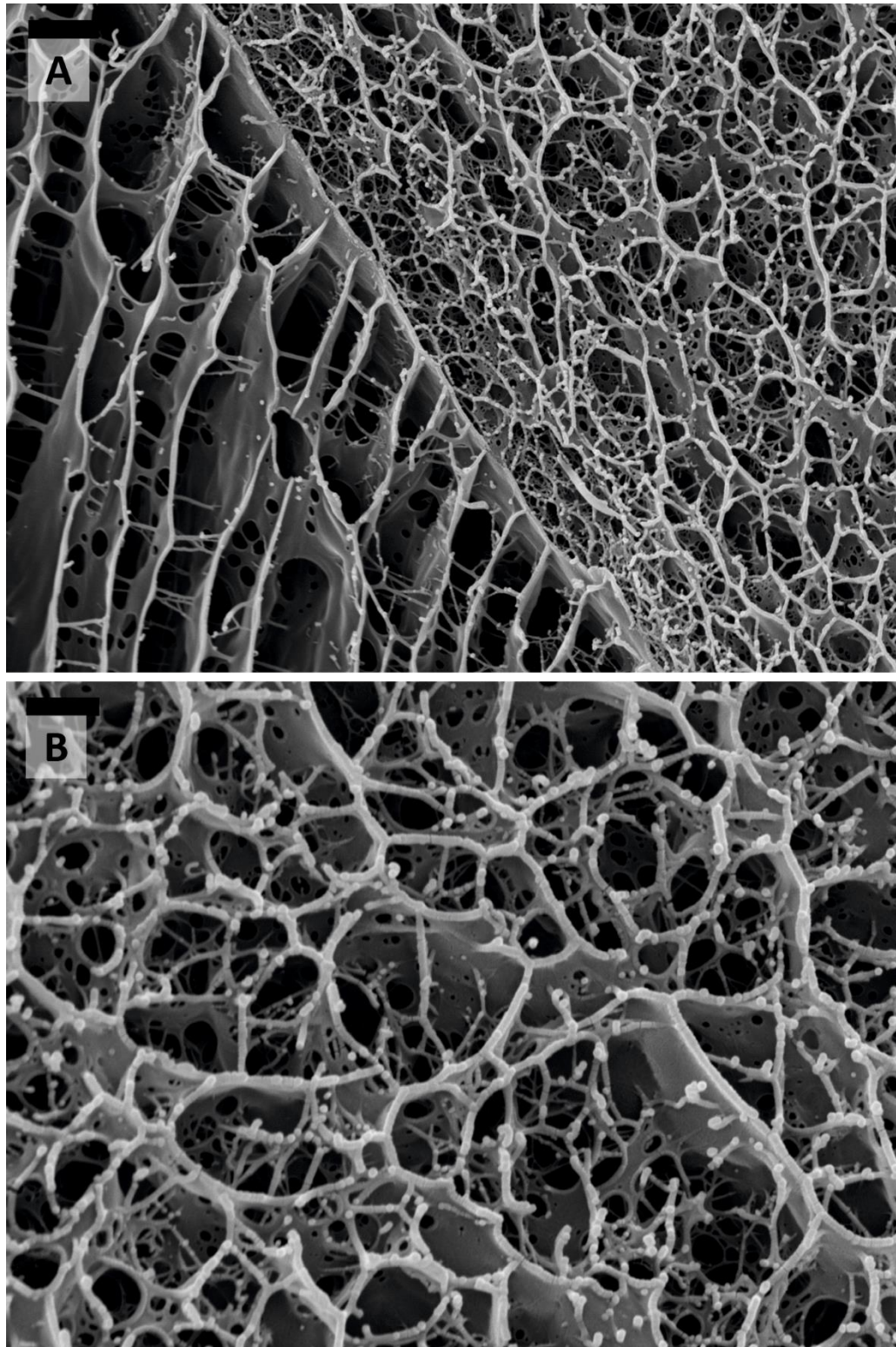


Figure 6.12. SEM images of a freeze-dried samples of agar-MC hydrogel (1.0% w/v – 1.0% w/v) after it was flash-frozen in slush nitrogen, fractured by a blade and then sublimated at $-70\text{ }^{\circ}\text{C}$ for 7 minutes. (A) shows the interface between a MC-like (left) and agar-like (right) structures and (B) shows the agar network at high magnification. The scale bars correspond to $2\text{ }\mu\text{m}$ and $1\text{ }\mu\text{m}$, respectively.

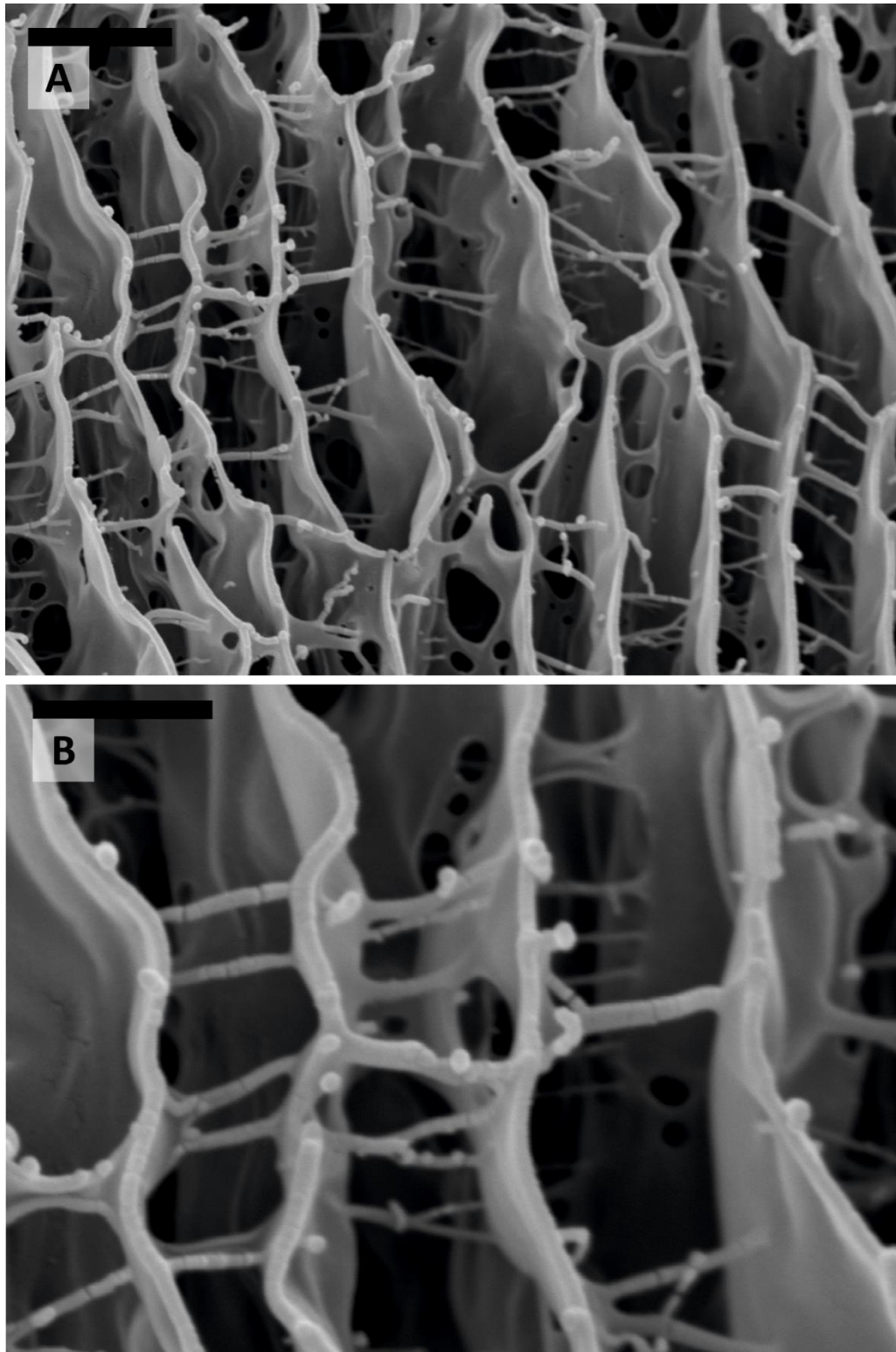


Figure 6.13. SEM images of a freeze-dried samples of agar-MC hydrogel (1.0% w/v – 1.0% w/v) after it was flash-frozen in slush nitrogen, fractured by a blade and then sublimated at $-70\text{ }^{\circ}\text{C}$ for 7 minutes. Both (A) and (B) show the region of MC-like structure at different magnifications. The scale bars correspond to $2\text{ }\mu\text{m}$ and $1\text{ }\mu\text{m}$, respectively.

6.2.6. X-ray diffraction analysis

X-ray diffraction (XRD) patterns of the freeze-dried hydrogel samples (2.0% w/v agar, 2.0% w/v MC and 1.0 – 1.0% w/v agar-MC) were obtained and the results are shown in Figure 6.14. The diffraction pattern for MC is in agreement with other studies in the literature which show have suggested that MC is semi-crystalline.^{31,32} The reduction in the intensity of the MC peaks after addition of agar indicates that agar interferes with the ordering of MC. Other studies have come to the same conclusion when investigating composites of MC and chitosan.³² Analogous XRD patterns have been seen for agar where it was concluded that crystallisation of agar did not occur during gelation.^{33,34}

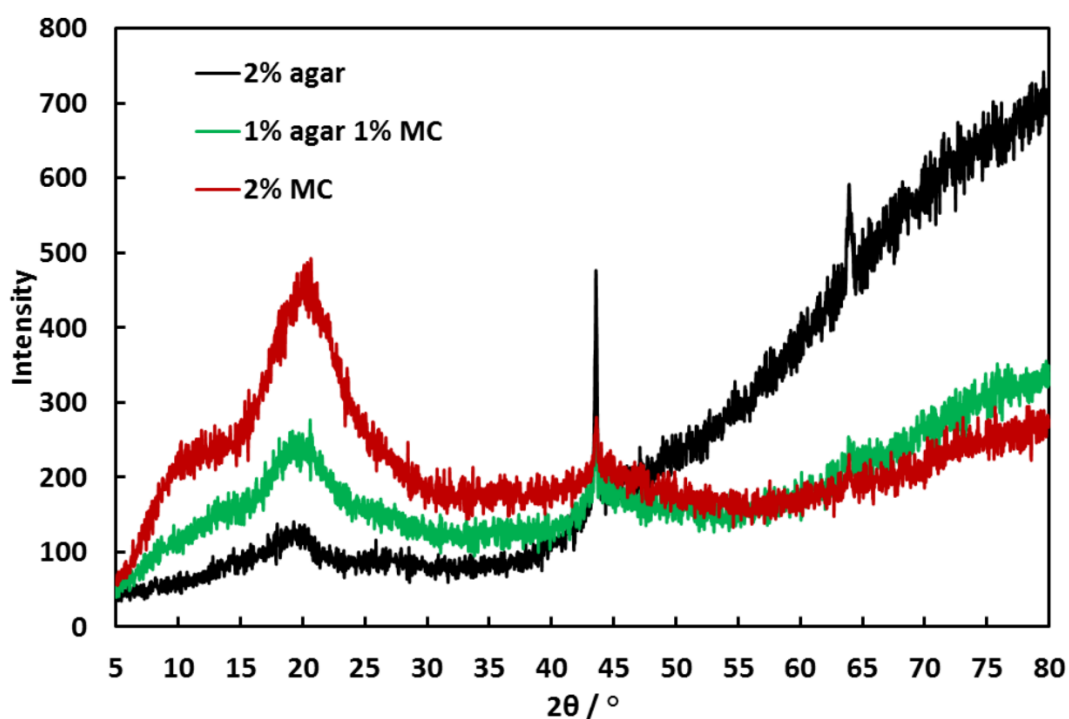


Figure 6.14. XRD patterns of freeze-dried agar hydrogel (2.0% w/v), freeze-dried MC solution (2.0% w/v) and freeze-dried agar-MC hydrogel (1.0 – 1.0% w/v).

6.3. Conclusions

A novel two-component hydrogel consisting of agar and MC with tailorable storage modulus over a range of temperatures has been reported. The agar-MC hydrogels show improved rheological properties over a temperature range of 25-85 °C. The storage modulus of the agar-MC hydrogel goes through a maximum when the temperature is

55 °C due to a sol-gel phase transition of MC present in the mixed hydrogel. Evidence of this transition was seen during DSC measurements. The addition of MC to agar showed an increase in storage modulus at temperatures both below and above the gelling point of MC. At temperatures above the melting point of agar, the mixed gel was still elastic with the rheological properties dominated by MC.

SEM imaging of freeze-dried samples of agar-MC revealed details of their microstructure. The mixed gel showed heterogeneous mixing, with randomly distributed MC-rich regions within an agar-rich continuous network. It was found that the mixed agar-MC gel was stable after being heated above 120 °C. At these temperatures agar alone melts, whereas the agar-MC hydrogel maintains its structure. The high melt-resistance of the two-component agar-MC hydrogels, along with the fact that both components are food grade polymers and do not require a salt for gelation, implies that they could be used in the food industry for baking or in high temperature templating of a range of porous and composite materials.

This chapter is the first report of a temperature insensitive binary hydrogel made from food grade carbohydrates (agar and MC). Previous work in the literature has described the use of addition of small amounts of agar to MC solutions which decreased the gelation time of MC when kept at the same temperature.²⁹ Here, the heat setting nature of MC is exploited to prepare hydrogels that keep their structure and elasticity at temperatures higher than the melting point of agar alone.

6.4. References

- 1 B. R. Thompson, T. S. Horozov, S. D. Stoyanov and V. N. Paunov, *RSC Adv.*, 2017, **7**, 45535–45544.
- 2 J. Kopeček, *Biomaterials*, 2007, **28**, 5185–5192.
- 3 L. Zhang, K. Li, W. Xiao, L. Zheng, Y. Xiao, H. Fan and X. Zhang, *Carbohydr. Polym.*, 2011, **84**, 118–125.
- 4 M. Constantin, S.-M. Bucatariu, F. Doroftei and G. Fundueanu, *Carbohydr. Polym.*, 2017, **157**, 493–502.
- 5 S. Morariu, M. Bercea, M. Teodorescu and M. Avadanei, *Eur. Polym. J.*, 2016, **84**, 313–325.
- 6 M. Rutkevičius, G. H. Mehl, J. T. Petkov, S. D. Stoyanov and V. N. Paunov, *J. Mater. Chem. B*, 2015, **3**, 82–89.
- 7 B. R. Thompson, T. S. Horozov, S. D. Stoyanov and V. N. Paunov, *Food Funct.*, 2017, **8**, 2967–2973.
- 8 J. P. Gong, Y. Katsuyama, T. Kurokawa and Y. Osada, *Adv. Mater.*, 2003, **15**, 1155–1158.
- 9 S. Liu and L. Li, *ACS Appl. Mater. Interfaces*, 2016, **8**, 29749–29758.
- 10 R. Armisén and F. Gaiatas, 4-Agar, in *Handbook of Hydrocolloids*, ed. G. O. Phillips and P. A. Williams, Woodhead Publishing Limited, Cambridge, 2nd edn., 2009, ch.9, pp. 82–107.
- 11 G. Sworn, 9-Gellan gum, in *Handbook of Hydrocolloids*, ed. G. O. Phillips and P. A. Williams, Woodhead Publishing Limited, Cambridge, 2nd edn., 2009, ch.9, pp. 204–227.
- 12 R. Mao, J. Tang and B. G. Swanson, *Carbohydr. Polym.*, 2000, **41**, 331–338.
- 13 M. H. Norziah, S. L. Foo and A. A. Karim, *Food Hydrocolloids*, 2006, **20**, 204–217.
- 14 G. Sworn, in 17-Xanthan gum, in *Food Stabilisers, Thickeners and Gelling Agents*, ed. A. Imeson, Wiley-Blackwell, Hoboken, NJ, 2010, ch. 17, pp. 325–

342.

- 15 S. Arnott, A. Fulmer, W. E. Scott, I. C. M. Dea, R. Moorhouse and D. A. Rees, *J. Mol. Biol.*, 1974, **90**, 269–284.
- 16 K. B. Guiseley, *Carbohydr. Res.*, 1970, **13**, 247–256.
- 17 A. Imeson, 3-Agar, in *Food Stabilisers, Thickeners and Gelling Agents*, ed. A. Imeson, Wiley-Blackwell, Hoboken, NJ, 2010, ch. 3, pp. 31–49.
- 18 P. Serwer, *Electrophoresis*, 1983, **4**, 375–382.
- 19 P. C. Debergh, *Physiol. Plant.*, 1983, **59**, 270–276.
- 20 M. J. Cash and S. J. Caputo, 6-Cellulose derivatives, in *Food Stabilisers, Thickeners and Gelling Agents*, ed. A. Imeson, Wiley-Blackwell, Hoboken, NJ, 2010, ch. 6, pp. 95–115.
- 21 P. L. Nasatto, F. Pignon, J. L. M. Silveira, M. E. R. Duarte, M. D. Nosedá and M. Rinaudo, *Polymers*, 2015, **7**, 777–803.
- 22 L. Li, P. M. Thangamathesvaran, C. Y. Yue, K. C. Tam, X. Hu and Y. C. Lam, *Langmuir*, 2001, **17**, 8062–8068.
- 23 N. Sarkar, *J. Appl. Polym. Sci.*, 1979, **24**, 1073–1087.
- 24 M. Hirrien, C. Chevillard, J. Desbrières, M. A. . Axelos and M. Rinaudo, *Polymer*, 1998, **39**, 6251–6259.
- 25 K. Kobayashi, C.-I. Huang and T. P. Lodge, *Macromolecules*, 1999, **32**, 7070–7077.
- 26 P. L. Nasatto, F. Pignon, J. L. M. Silveira, M. E. R. Duarte, M. D. Nosedá and M. Rinaudo, *Int. J. Polym. Anal. Charact.*, 2015, **20**, 110–118.
- 27 J. R. Lott, J. W. McAllister, S. A. Arvidson, F. S. Bates and T. P. Lodge, *Biomacromolecules*, 2013, **14**, 2484–2488.
- 28 J. Desbrières, M. Hirrien and M. Rinaudo, *Carbohydr. Polym.*, 1998, **37**, 145–152.
- 29 B. C. Martin, E. J. Minner, S. L. Wiseman, R. L. Klank and R. J. Gilbert, *J. Neural Eng.*, 2008, **5**, 221–231.

- 30 A. S. Medin, PhD thesis, Uppsala University, 1995.
- 31 N. Rangelova, L. Radev, S. Nenkova, I. M. Miranda Salvado, M. H. Vas Fernandes and M. Herzog, *Cent. Eur. J. Chem.*, 2011, **9**, 112-118.
- 32 A. Pinottia, M. A. Garcia, M. N. Martino and N. E. Zaritzky, *Food Hydrocolloids*, 2007, **21**, 66-72.
- 33 M. Matsuo, T. Tanaka and L. Ma, *Polymer*, 2002, **43**, 5299-5309.
- 34 Q. Cao, Y. Zhang, W. Chen, X. Meng and B. Liu, *Int. J. Biol. Macromol.*, 2017, DOI: 10.1016/j.ijbiomac.2017.08.134.

7. Structuring and calorie control of bakery products by templating batter with ultra melt-resistant food-grade hydrogel beads

The use of a temperature insensitive, food-grade hydrogel to reduce the caloric density of pancakes that were prepared at temperatures much higher than the boiling point of water has been reported. This cheap, facile method utilises a mixed agar-methylcellulose hydrogel, which was blended to produce a slurry of hydrogel microbeads. The pancake batter was mixed with a controlled volume percentage of slurry of hydrogel beads and cooked. From bomb calorimetry experiments, the composites were found to have a reduced caloric density that reflects the volume percentage of hydrogel beads mixed with the batter. Using this procedure, it was possible to reduce the caloric density of pancakes by up to $23 \pm 3\%$ when the volume percentage of hydrogel beads initially used was 25%. The method is not limited to pancakes and could potentially be applied to various other food products. The structure and morphology of the freeze-dried pancakes and pancake-hydrogel composites were investigated and pores of a similar size to the hydrogel beads were found, confirming that the gel beads maintained their structure during the cooking process. There is scope for further development of this method by the encapsulation of nutritionally beneficial or flavour enhancing ingredients within the hydrogel beads.

The work in this chapter has been published in the RSC journal Food and Function.¹

7.1. Introduction

The rapid incline in cases of obesity is cause for major concern due to the health issues that are attributed to it. Cardiovascular diseases, type 2 diabetes, hypertension and certain cancers are some of the numerous comorbidities associated with this global epidemic.² The impact of obesity is recognised by health organisations, the food industry and consumers alike. A main culprit of excessive weight gain is the over consumption of food with low nutritional benefits and high fat and refined sugar content. This has led to major investment into the development of new, healthier food products.³ A challenge in producing these reformulated, nutritionally beneficial foods

is preserving their physical and sensorial properties whilst maintaining a flavour that will appeal to consumers.

Composite foods, foods comprising of two or more different materials, are widely available. Emulsions, dispersions and emulsion filled gels are all forms of composite foods.⁴ Hydrocolloids are frequently used in their formulation as thickeners, emulsifiers and gelling agents. Xanthan gum is used as a fat replacement in low-fat mayonnaise where its role is to increase the viscosity of the aqueous phase, increasing shelf life.⁵ The techniques in which hydrocolloids can be employed is constantly expanding, with a recent study showing that chia mucilage gel can partially replace vegetable fat in bread and margarine in cakes to reduce fat content and caloric density.⁶

Another way hydrocolloids have been utilised is in the preparation of hollow salt particles. This involves formulation of salt-hydrogel liquid marbles by producing an aerosol of hot liquid gelling agent and passing it through a cold column, which yields hydrogel beads, and then rolling these beads in salt microcrystals. After drying the salt-hydrogel composites, hollow salt particles could be obtained. These salt particles exhibited an increased dissolution rate when compared to table salt, showing they would have an increased perception of saltiness at the same concentration which could lead to a decreased salt intake.^{7,8}

The incorporation of hydrogel beads into food products has previously been employed in the formulation of chocolate-hydrogel composites, through emulsification. When incorporating water droplets alone into chocolate, the mechanical properties will suffer when their volume fraction is too high. This led to gelling agents being added to the aqueous phase. One group utilised gelatine to gel the water droplets, where the hydrogel network within the droplets contributes to the overall strength of the composite.⁹ A drawback of gelatine, however, is that it is derived from animals, making it unsuitable to a large consumer base. Agar, an abundant biopolymer derived from red seaweed, has been used as an alternative to gelatine to produce suspensions of up to 80% w/v aqueous microgel agar particles dispersed within chocolate.¹⁰

Whilst using agar in chocolate formulations is an excellent method to reduce fat content, an issue when using it for the design of other food formulations however, is that it melts at around 85 °C.¹¹

A two-component hydrogel consisting of agar and methylcellulose (MC) has been developed that maintains its structural integrity well above the melting point of agar. This combination of food-grade hydrocolloids maintains the advantage of being derived from nature, does not require salts for gelation and, once gelation has occurred, will not melt at temperatures above 100 °C. This resistance to melting at elevated temperatures allows the incorporation of hydrogel beads of this composition into food products that require high temperatures during preparation. In this chapter, structuring and calorie control by the use of melt-resistant hydrogel beads of agar-MC hydrogel blended in a pancake batter that were cooked at temperatures above 100 °C has been demonstrated. It can easily be applied for a range of bakery products. The caloric density of a control sample of pancakes and pancake-hydrogel bead composites has been measured. The reduction in caloric density of the pancake composites closely reflects the initial volume percentage of hydrogel beads that were incorporated within them. The microstructure of the pancakes and pancake-hydrogel composites have been studied *via* SEM and pores have been seen in the freeze-dried composites consistent with the size of the hydrogel beads, confirming that these elements of the composites maintained their structure during the cooking process.

7.2. Results

7.2.1. Rheology and microstructure of agar-MC hydrogel

The rheological behaviour of the agar-MC hydrogel has been measured as a function of temperature. The two-component 1.0% w/v – 1.0% w/v agar-MC hydrogel showed characteristics of both agar and MC, depending on the temperature range. Figure 7.1 shows that the hydrogel has a fairly constant storage modulus upon increasing the temperature from 25 °C to nearly 90 °C with a maximum around 55 °C which is above the gelling temperature of MC. Note that the agar-MC hydrogels are significantly stronger than agar hydrogel alone at 85 °C.

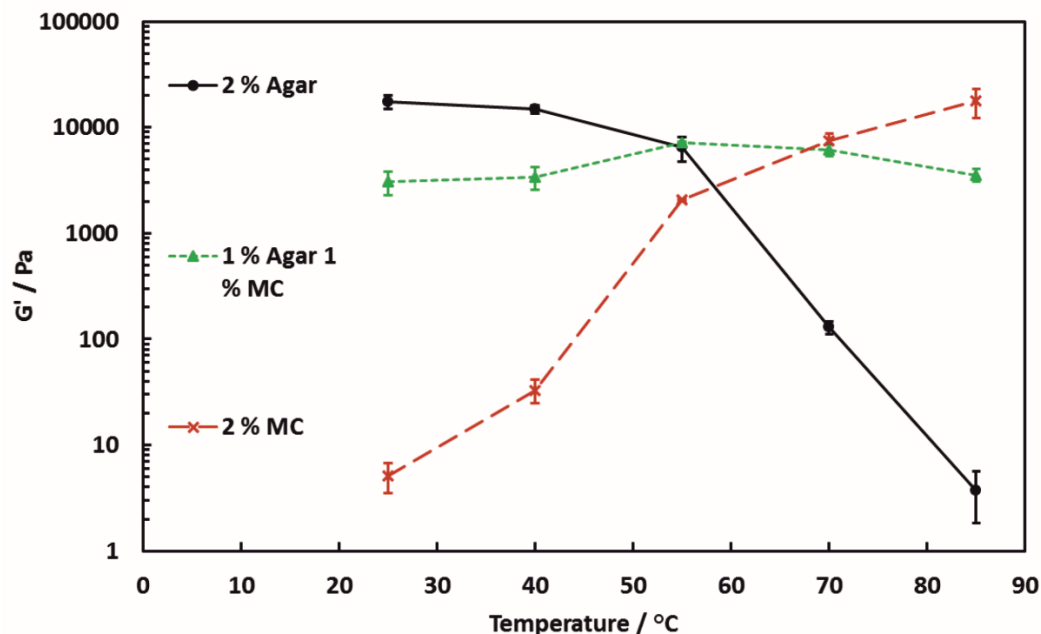


Figure 7.1. The storage modulus of 2.0% w/v agar hydrogel, 2.0% w/v MC solution and 1.0% w/v - 1.0% w/v agar-MC hydrogel as a function of temperature. G' is measured at a shear stress of 100 Pa and averaged over three samples. The error bars represent the standard deviation.

At low temperatures, its rheological behaviour is similar to that of agar hydrogel while at higher temperatures, MC is the polymer dominating the hydrogel rheology. The experiments on thermal stability of agar-MC hydrogels (shown in Chapter 6) show that the hydrogel does not melt even after submerging in water and autoclaving at 121 °C or after heating in an oven at 150 °C for 45 minutes. Figure 7.2 shows SEM images of freeze-dried samples of the melt-resistant hydrogel after flash-freezing and freeze-drying under vacuum. The microstructure of this hydrogel involves two phase regions with agar-like structure (continuous phase) surrounding domains of MC-like structure. Both phases contain network features that look more interlinked than the microstructure of agar or MC hydrogels alone at the same concentration.

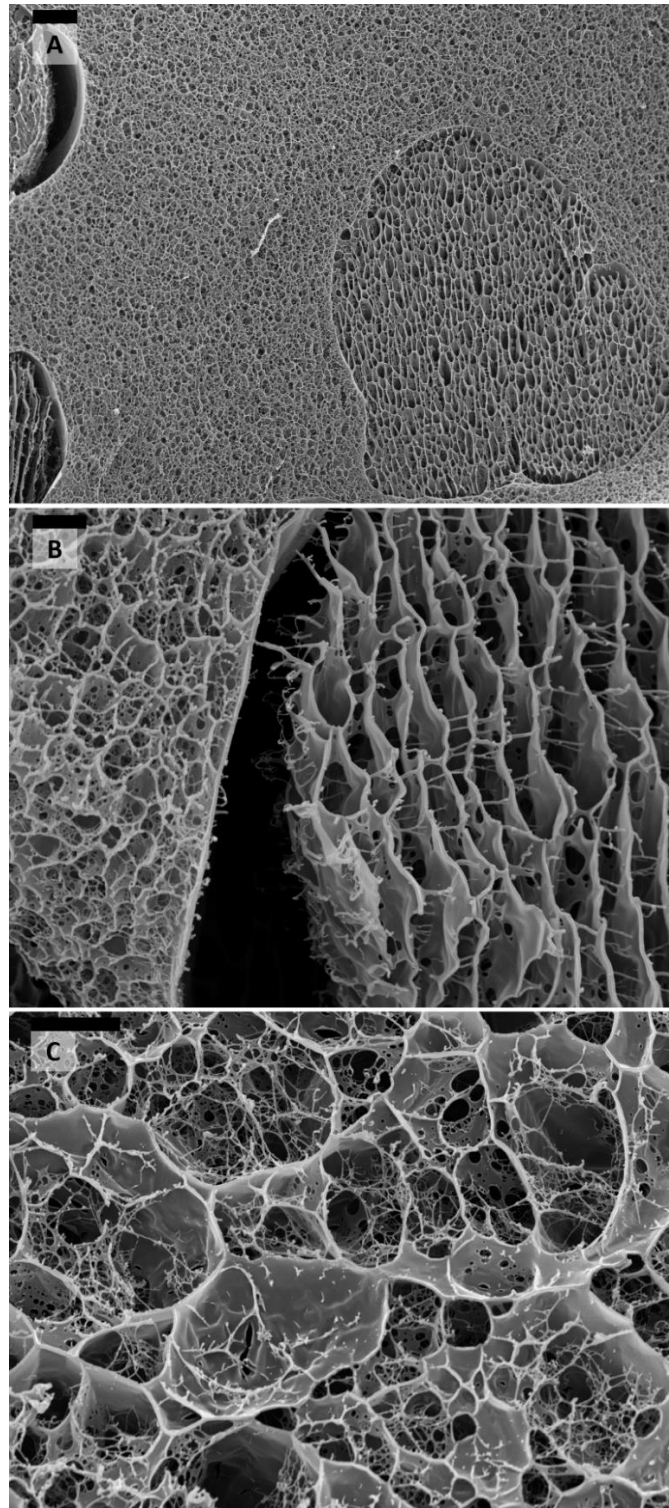


Figure 7.2. SEM images of freeze-dried samples of agar-MC hydrogel (1.0% w/v - 1.0% w/v) after it was flash-frozen in slush nitrogen, fractured and then the water was sublimed at $-70\text{ }^{\circ}\text{C}$ for 7 minutes. (A) and (B) SEM images show co-existing regions of a MC-like structure surrounded by an agar-like structure. (C) is a higher magnification image of the agar-like structure of the melt-resistant hydrogel. The scale bars represent $10\text{ }\mu\text{m}$, $2\text{ }\mu\text{m}$ and $5\text{ }\mu\text{m}$, respectively.

7.2.2. Hydrogel bead size analysis

In order for the hydrogel beads in the pancake-hydrogel composites to be undetectable during consumption, their size must be on the micron scale.¹² Therefore it was important to achieve control over the size of the beads produced. Hydrogel bead size was measured as a function of blending time and their size distribution obtained by analysing microscope images of the gel beads dispersed in water. Due to the irregular shape of the beads, they were measured horizontally through their widest section. After blending for ten minutes, the average size of the beads was $100 \pm 30 \mu\text{m}$ where the standard deviation represents their polydispersity. Their morphology and size distribution can be seen below in Figure 7.3. It was seen that further increasing the blending time showed insignificant reduction in the size distribution of the beads. In future studies, efforts will be made towards reducing the average size and polydispersity of the hydrogel beads with an aim to produce composites with a smoother mouthfeel.

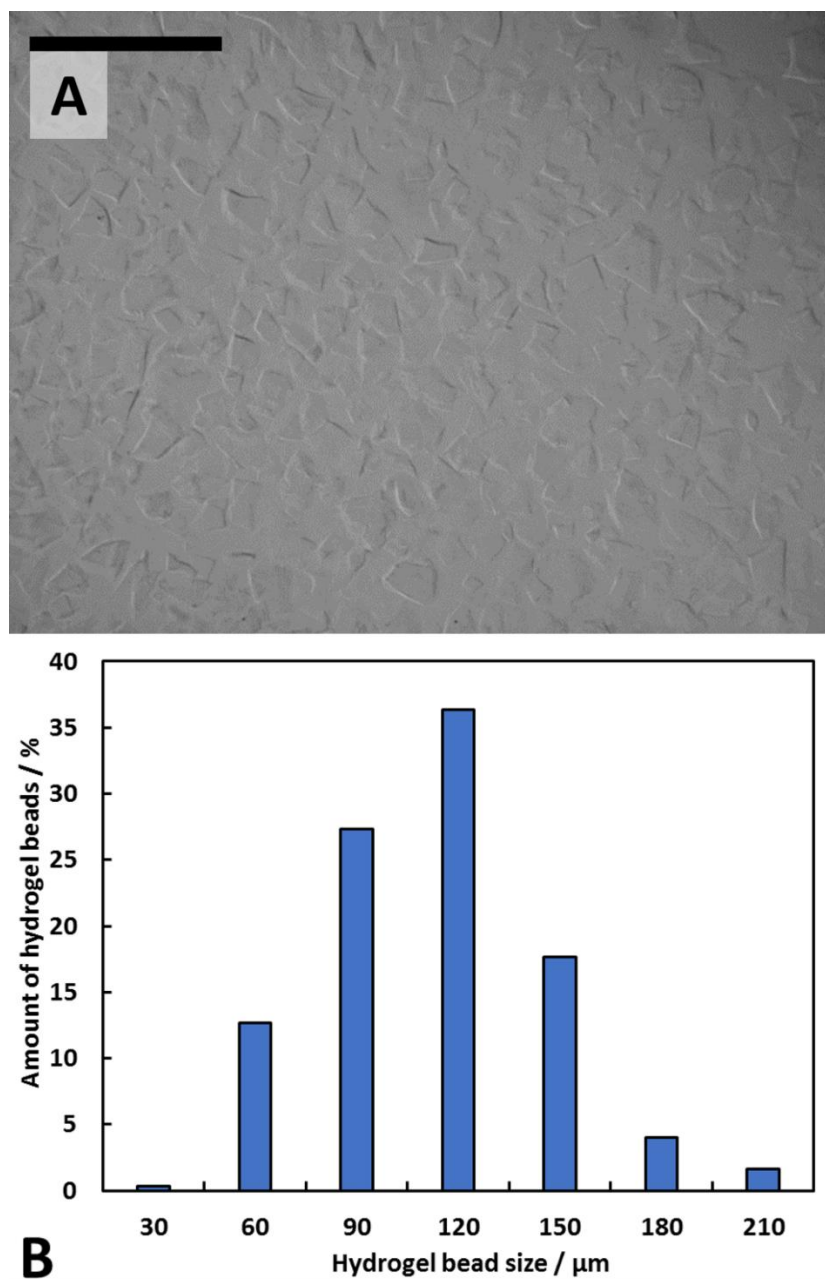


Figure 7.3. (A) is an optical microscopy image of agar-MC hydrogel beads dispersed in water. They were blended at full power with a Tefal food processor Minipro for ten minutes. The scale bar is 500 μm and the magnification was 4x. (B) shows the size distribution diagram of these beads. A sample size of 300 beads within several fields of view was used and their sizes measured using Image J software. The histogram represents the number percentage of the hydrogel beads of various sizes.

7.2.3. Formulation of pancake-hydrogel composites

The mass reduction of the composites after preparation, $R_{m(pre)}$, was calculated using the following formula:

$$R_{m(pre)} = \left(1 - \frac{m_c}{m_0}\right) \times 100\%. \quad (7.1)$$

Here $R_{m(pre)}$ is the mass reduction after preparation (%), m_c is the mass of the pancake-hydrogel composite after cooking and m_0 is the mass of the pancake control sample containing no hydrogel beads.

It is shown in Figure 7.4 that there are some small mass reductions of the composites and this increases with an increase in the volume fraction of hydrogel beads initially present in the pancake batter. The probable causes for this are two-fold: Firstly, hydrogel beads on the surface of the pancake batter are able to lose mass due to evaporation of water. Furthermore, hydrogel syneresis and loss of water from the hydrogel beads into the pancake batter could occur due to an osmotic pressure gradient.

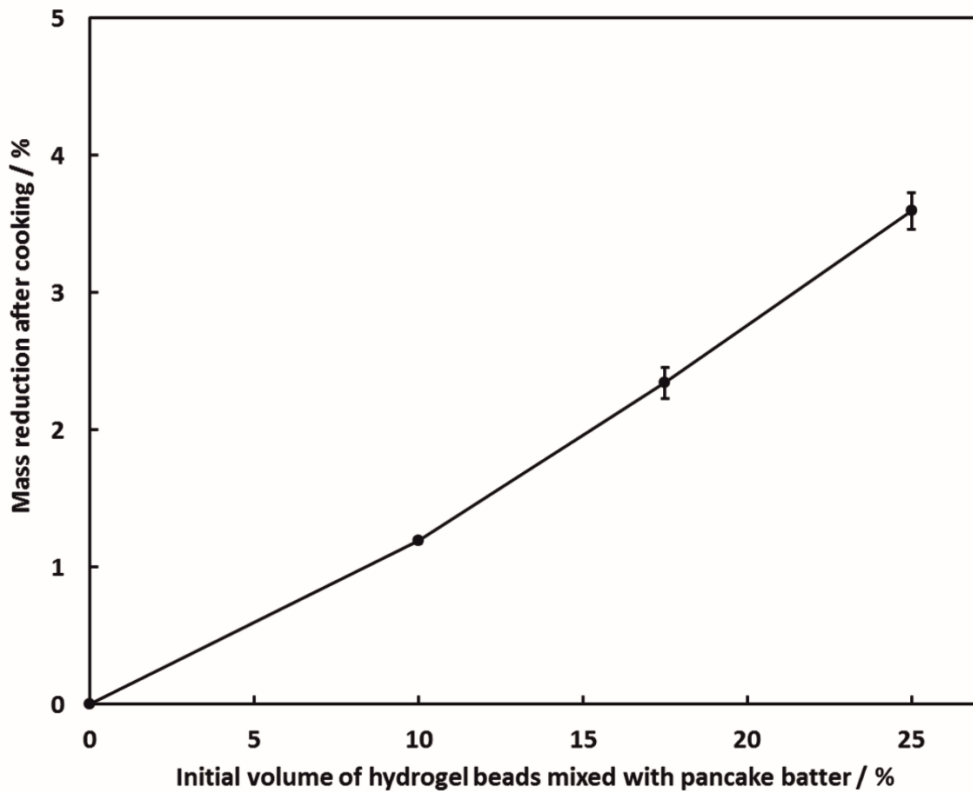


Figure 7.4. Mass reduction of the pancake-hydrogel composites after the cooking process as a function of the initial volume percentage of hydrogel beads in the composite.

The MC present in the hydrogel beads gels upon heating which maintains their structure, whereas if the gel beads were to melt, mass transport through the batter could occur which would lead to further evaporation of water. In Figure 7.5, the appearance of the pancake-hydrogel composites are shown to have a very close likeness to the pancake control sample so they will be as aesthetically appealing to the consumer as regular pancakes that contain no hydrogel beads.



Figure 7.5. A photograph of a pancake (A) and pancake hydrogel composites initially containing (B) 10%, (C) 17.5% and (D) 25% by volume slurry of agar-MC hydrogel beads. They were prepared by mixing a controlled volume percentage of slurry of hydrogel beads with pancake batter, then heated at 170 °C for four minutes on each side.

Before the caloric density of the pancakes and pancake-hydrogel composites could be measured, they needed to be freeze-dried to remove all moisture and allow easy

ignition of the sample inside the bomb. The samples were weighed before and after freeze-drying and their reduction in mass (R_m) calculated:

$$R_m = \left(1 - \frac{m_{dry}}{m_{wet}}\right) \times 100\%. \quad (7.2)$$

Here R_m is the reduction in mass (%), m_{dry} is the mass after freeze drying measured in grams and m_{wet} is the mass of the sample prior to freeze drying measured in grams. The masses before and after freeze drying, along with the overall mass reduction, are shown in Figure 7.6. It was found that with an increase in initial volume fraction of hydrogel beads present in the composite that the overall mass reduction was larger.

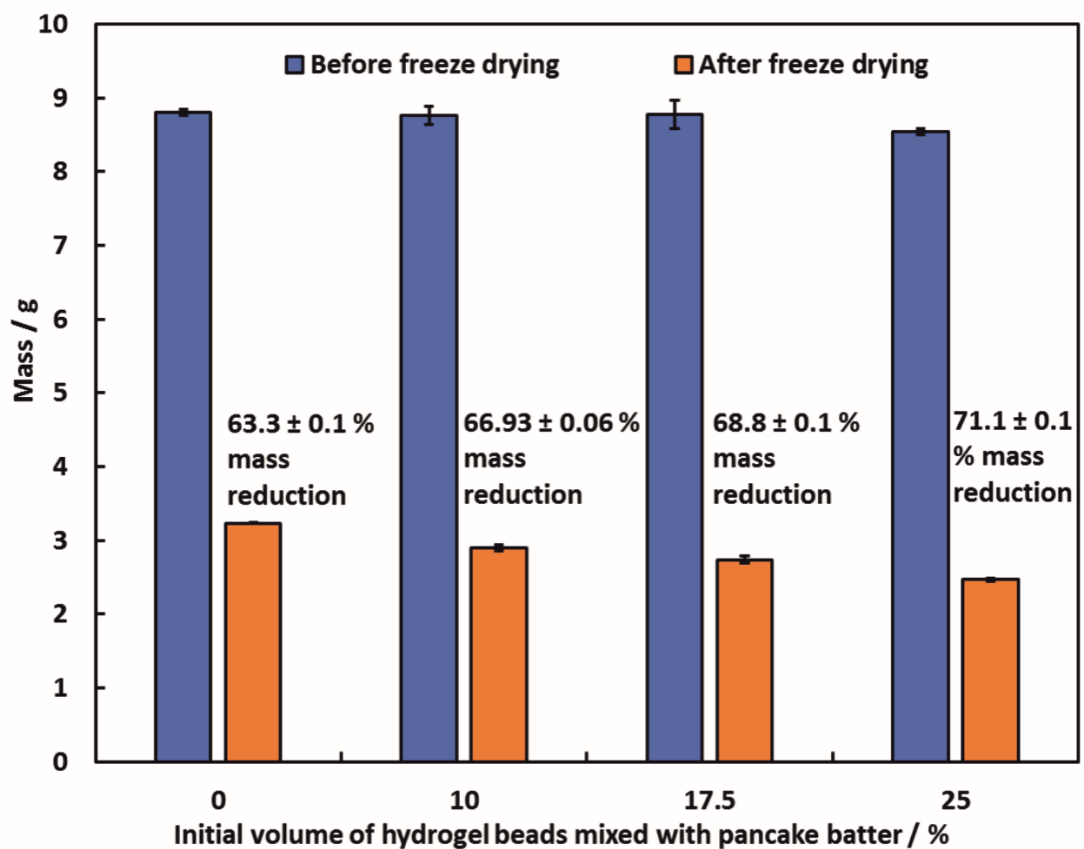


Figure 7.6. The mass of the samples of pancake and pancake-hydrogel composites before and after freeze-drying for 72 hours. The mass reductions were calculated by equation 7.2. They were measured in triplicate and the values are an average with the error bars showing their standard deviation.

Further to this, it was possible to calculate the extra mass lost from the composites compared to the control sample due to the presence of the gel beads. This was done using the following equation:

$$R_{m(gb)} = \frac{R_{m(c)} - R_{m(std)}}{100 - R_{m(std)}} \times 100\%. \quad (7.3)$$

Here $R_{m(gb)}$ is the extra mass reduction due to the presence of gel beads initially in the composite (%), $R_{m(c)}$ is the mass reduction of the composite (%) and $R_{m(std)}$ is the mass reduction of the pancake control sample containing no hydrogel beads (%).

Figure 7.7 shows the percentage mass reduction due to the presence of the hydrogel beads.

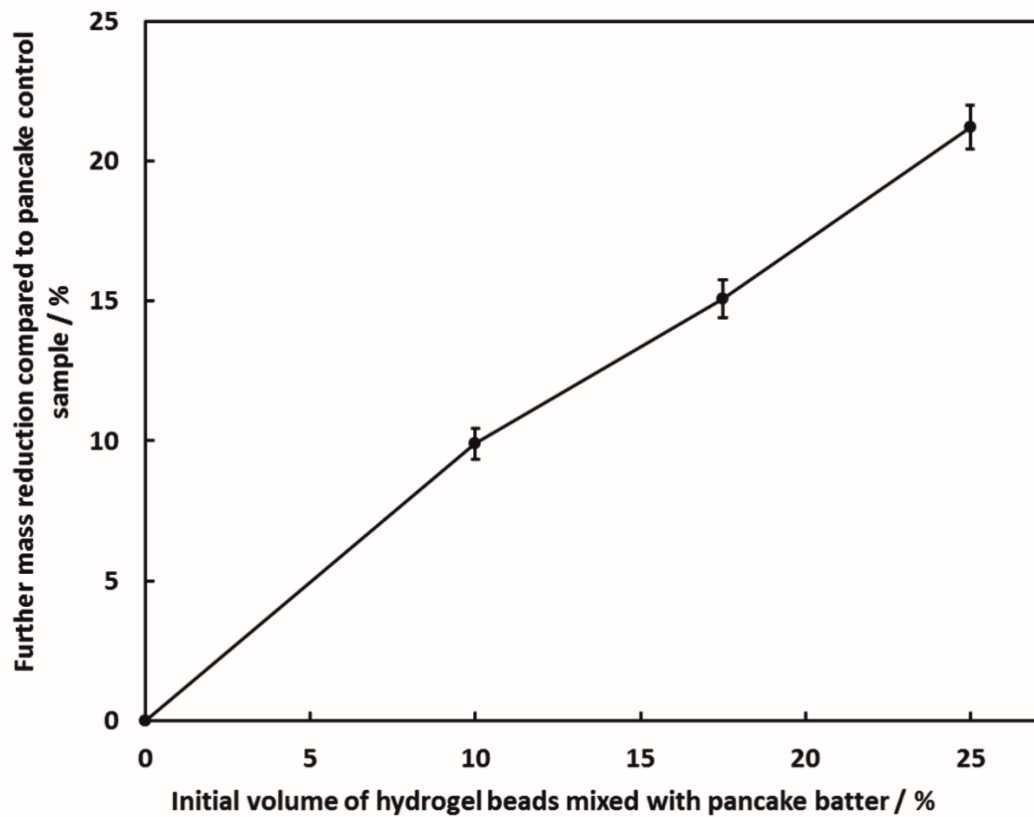


Figure 7.7. This shows the further mass reduction of the pancake-hydrogel composites compared to the pancake control sample due to the presence of hydrogel beads. Each data point is an average of three measurements with the error bars showing the standard deviation.

It can be seen that the further mass reduction closely reflects the initial volume percentage of hydrogel beads present in the composite, being offset by 0.1% when the initial volume of hydrogel beads was 10%, 2.5% when the initial volume was 17.5% and approximately 4% when the initial volume was 25%. This can be attributed to evaporation of water from hydrogel beads at the surface and loss of water from the hydrogel beads due to osmotic effects.

The freeze-dried samples were visualised using a scanning electron microscope. The microstructure of both the control sample and the pancake-hydrogel composites were studied and their images are shown in Figure 7.8. The pancake matrix of the control sample is shown in Figure 7.8(A) whereas Figure 7.8(B) and (C) show the pancake matrix with pores of a similar size to the hydrogel beads that were incorporated within the pancake batter.

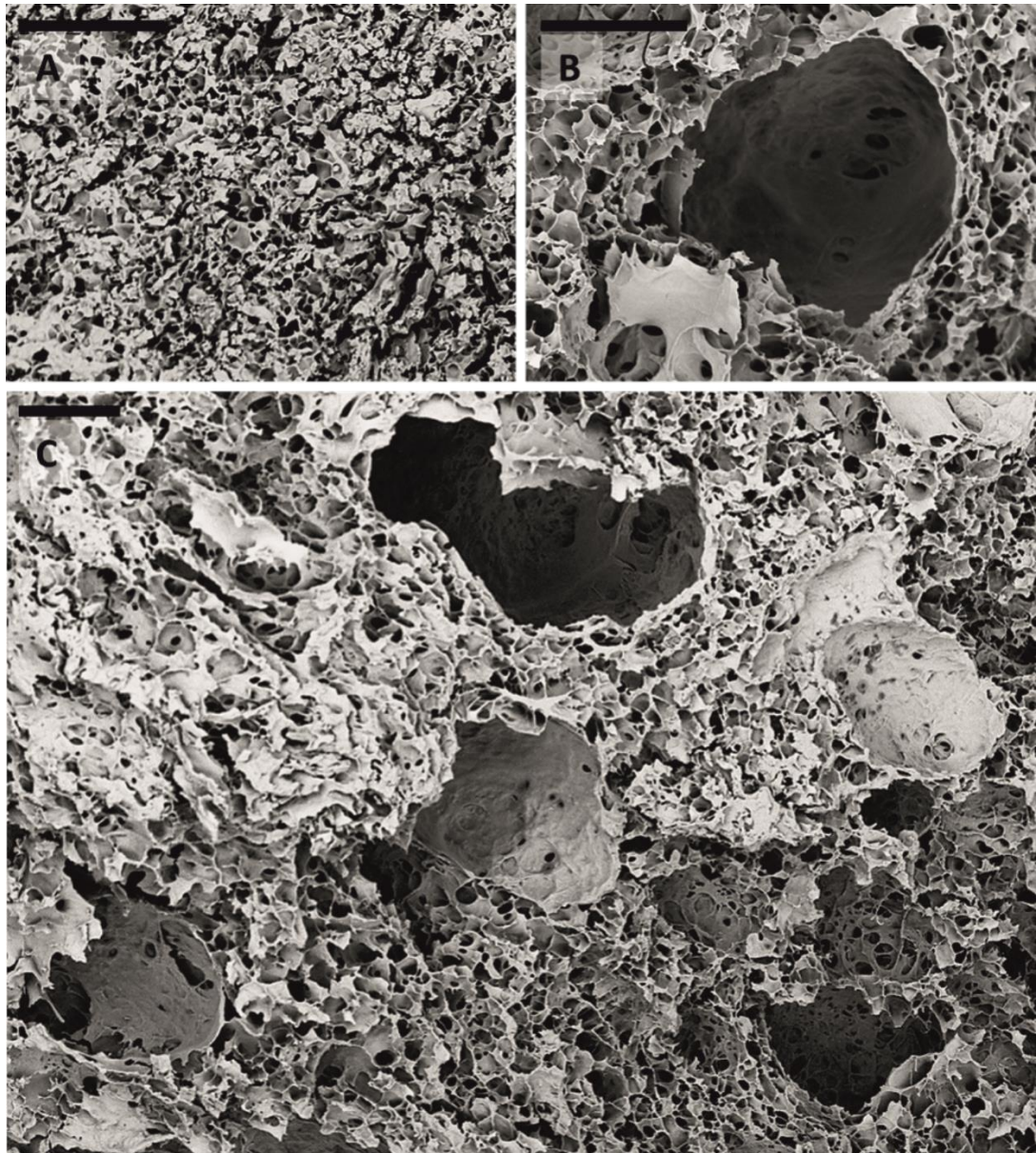


Figure 7.8. SEM images of freeze-dried pancake (A) and pancake-hydrogel composites (B) and (C). The composites were produced with an initial volume percentage of 17.5% of agar-MC hydrogel beads (1.0% w/v - 1.0% w/v). (C) corresponds to a larger field of view than (B). All scale bars are 100 μm .

7.2.4. Caloric density of pancake-hydrogel composites

Calibration of the calorimeter was done using benzoic acid which has an energy of combustion of $(-26\,433 \pm 3) \text{ J g}^{-1}$. This was performed three times to obtain a constant that corresponds to the calorimeter when 2000 g of water was used. Figure 7.9 shows

an example of the measurement of the calorimeter constant when igniting benzoic acid in the bomb.

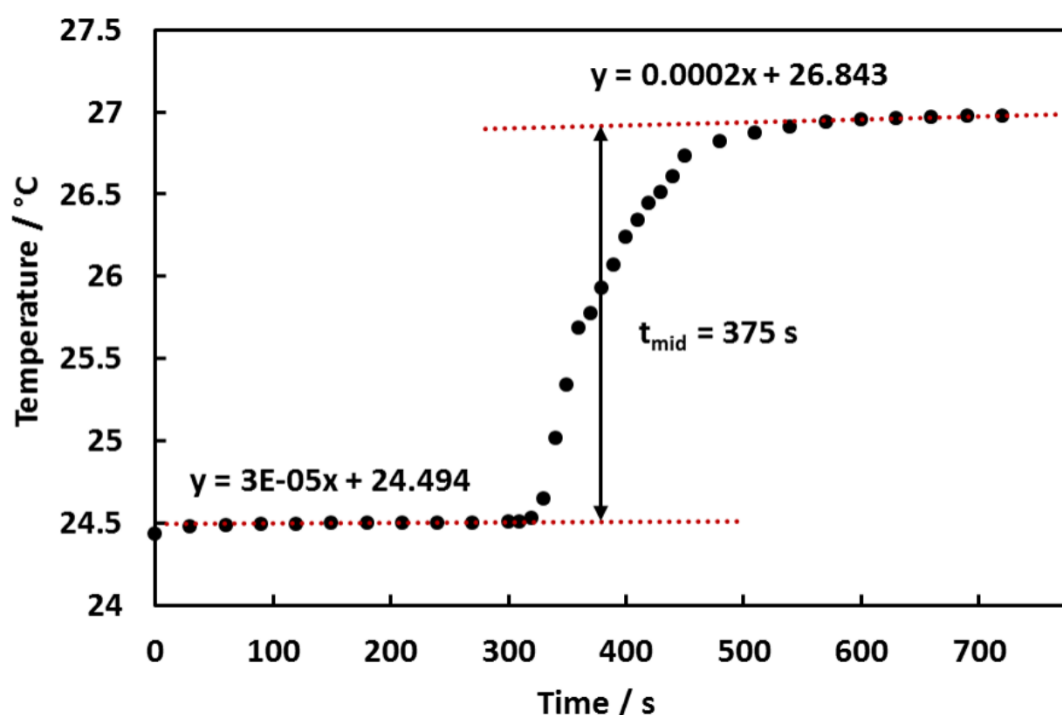


Figure 7.9. An example graph to show the temperature change during the combustion of benzoic acid. The bomb was ignited at 300 seconds.

Using the temperature change at t_{mid} , the calorimeter constant can be calculated:

$$c_v = \frac{m_{\text{benz}} \times \Delta H_{c(\text{benz})} + m_{\text{wire}} \times \Delta H_{c(\text{wire})}}{\Delta T} \quad (7.4)$$

Here c_v is the calorimeter constant (J K^{-1}), m_{benz} is the mass of the benzoic acid pellet used (g), $\Delta H_{c(\text{benz})}$ is the heat of combustion of benzoic acid (J g^{-1}), m_{wire} is the mass of the fuse wire and $\Delta H_{c(\text{wire})}$ is the heat of combustion of the fuse wire (J g^{-1}) and ΔT is the temperature change at t_{mid} (K).

Three calibration measurements were performed and the calorimeter constant was calculated to be $10\,500 \pm 200 \text{ J K}^{-1}$ or, in units more common in the food industry, $2.51 \pm 0.05 \text{ kcal K}^{-1}$.

The freeze-dried samples were ground into a fine powder and pellets of approximately 1 g were pressed. The pancake control sample as well as the pancake-hydrogel composites were measured three times each and the caloric density was calculated:

$$q = \frac{c_v \times \Delta T - m_{wire} \times \Delta H_{c(wire)}}{m_{sample}} \quad (7.5)$$

Here q is the caloric density of the sample under investigation (kcal g^{-1}), c_v is the calorimeter constant calculated previously (kcal K^{-1}), $\Delta H_{c(wire)}$ is the heat of combustion of the fuse wire (kcal g^{-1}) and m_{sample} is the mass of the sample (g) which is the wet mass that is represented by the dry mass of the pellet.

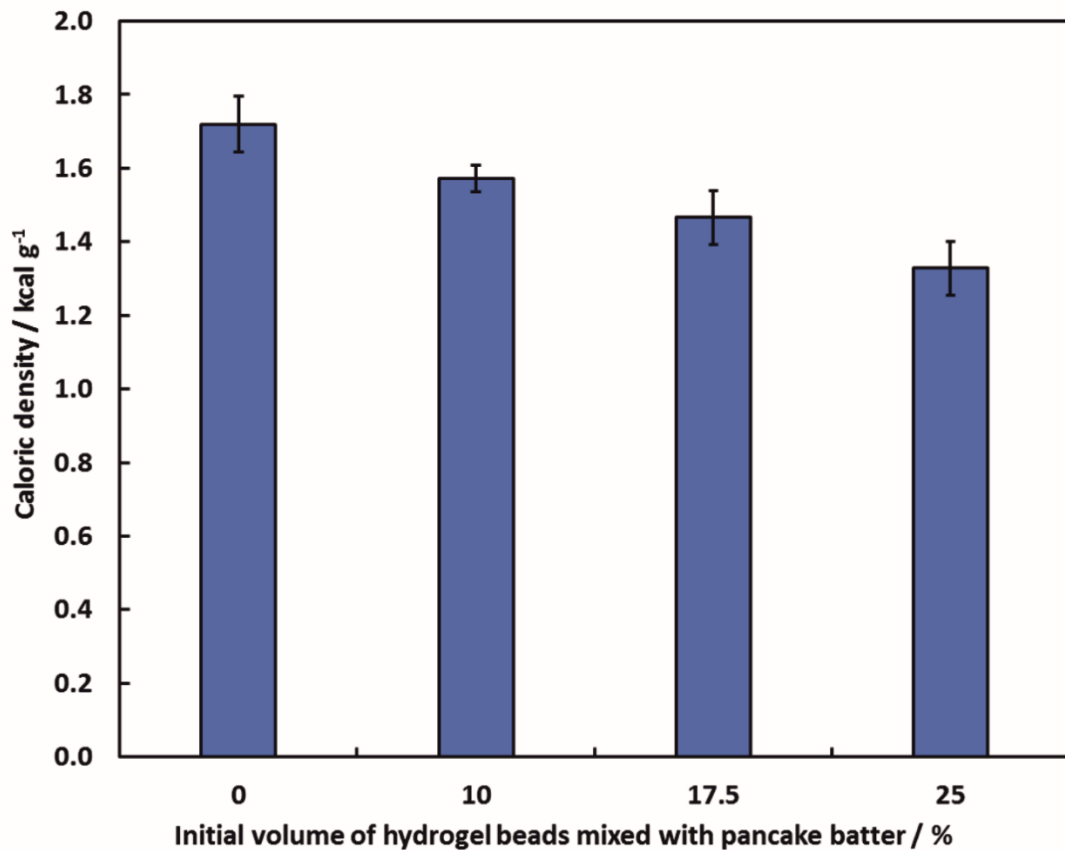


Figure 7.10. The caloric densities of the pancake control sample and the pancake-hydrogel composites containing increasing volume percentages of agar-MC hydrogel beads (1.0% w/v – 1.0% w/v). Each sample was measured three times to obtain an average caloric density, with the error bars showing the standard deviation.

Figure 7.10 shows that the caloric density decreases with increasing volume fraction of hydrogel beads initially in the composite. This is due to the fact that the beads are made from a hydrogel that contains 98% water which contains zero calories. The small amount of biopolymer present is mostly indigestible; it is a soluble dietary fibre known to be a satiety aid.^{13,14} The reduction in caloric density was then calculated using the following equation:

$$q_{red} = \left(1 - \frac{q_c}{q_{std}}\right) \times 100\%. \quad (7.6)$$

Here q_{red} is the reduction in caloric density (%), q_c is the caloric density of the pancake-hydrogel composite (kcal g^{-1}) and q_{std} is the caloric density of the pancake control sample containing no hydrogel beads (kcal g^{-1}).

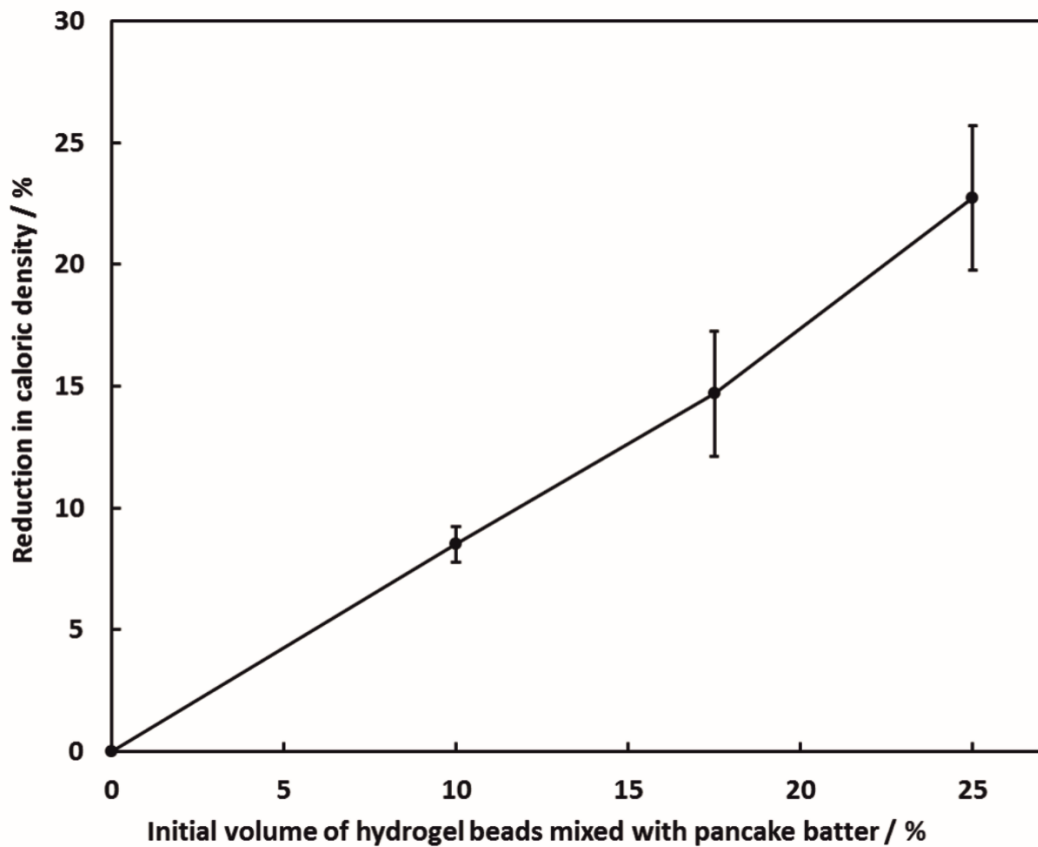


Figure 7.11. The reduction in caloric density of pancake-hydrogel composites compared to the pancake control sample as a function of the initial volume percentage of hydrogel beads mixed with the pancake batter. Each value is an average of three experiments, with the error bars representing the standard deviation.

It can be seen in Figure 7.11 that the caloric density reduction in the pancake-hydrogel composites closely follows the initial volume fraction of hydrogel beads in the composite. The incorporation of water into food decreases the caloric density by increasing the mass of the food whilst not adding any calories. Furthermore, addition of water to food has been shown to significantly increase fullness and suppress appetite in subsequent meals.¹⁵ Here, water has been incorporated into food in the form of hydrogel beads and it is expected that it will have the same beneficial effects. An additional advantage gained from the use of hydrogel beads is the ability to encapsulate flavour or taste enhancing compounds, thereby allowing for a range of flavoured products to be formulated.

7.3. Conclusions

A new method for the reduction of caloric density in bakery products has been designed and it has been demonstrated on pancakes. A highly melt resistant hydrogel consisting of agar and methylcellulose has been utilised. Upon blending of this mixed hydrogel, a slurry of hydrogel microbeads was obtained. Controlled volume percentages of slurry of hydrogel beads were mixed with pancake batter and cooked to produce pancake-hydrogel composites. The caloric densities of the composites were measured and when compared to a pancake control sample, they exhibited a reduction in caloric density comparable to the volume percentage of hydrogel beads initially incorporated within the composite. This method allowed controllable reduction of the caloric density up to $23 \pm 3\%$, when 25% by volume of hydrogel bead slurry was mixed with the pancake batter prior to cooking. The microstructure of freeze-dried pancakes and pancake-hydrogel composites was analysed and the composites showed pores on a similar length scale to the hydrogel beads used, confirming that the hydrogel beads maintained their structure during the high temperature cooking process. It is expected that this strategy is not limited to pancakes, and could find applications in a variety of food products such as waffles, crumpets, muffins, biscuits, cereal bars and many others. This method could be developed further by encapsulation of nutritionally beneficial or flavour enhancing ingredients within the hydrogel beads.

Previous work in literature has shown the possibility of preparing composites of food and hydrogel in an attempt to lower fat and calorie content.^{9,10} Until now, these

methods have been performed on food products prepared at temperatures significantly below the boiling point of water. Here, it has been shown that a melt resistant binary hydrogel consisting of agar and MC can be used to template food products at high temperatures and that the reduction in caloric density can be controlled by varying the volume percentage of hydrogel beads in the formulation.

7.4. References

- 1 B. R. Thompson, T. S. Horozov, S. D. Stoyanov and V. N. Paunov, *Food Funct.*, 2017, **8**, 2967-2973.
- 2 P. Poirier, T. D. Giles, G. A. Bray, Y. Hong, J. S. Stern, F. X. Pi-Sunyer and R. H. Eckel, *Circulation*, 2006, **113**, 898 LP-918.
- 3 E. Scholten, *Food Funct.*, 2017, **8**, 481-497.
- 4 D. Seisun, 1 - Introduction, in *Food Stabilisers, Thickeners and Gelling Agents*, ed. A. Imeson, Wiley-Blackwell, Hoboken, NJ, 2010, ch. 1, pp. 1–10.
- 5 G. O. Phillips and P. A. Williams, 1 - Introduction, in *Handbook of Hydrocolloids*, ed. G. O. Phillips and P. A. Williams, Woodhead Publishing Limited, Cambridge, 2nd edn, 2009, ch. 1, pp. 1–22.
- 6 S. S. Fernandes and M. de las M. Salas-Mellado, *Food Chem.*, 2017, **227**, 237–244.
- 7 M. Rutkevičius, G. H. Mehl, J. T. Petkov, S. D. Stoyanov and V. N. Paunov, *J. Mater. Chem. B*, 2015, **3**, 82–89.
- 8 H. L. Meiselman and B. P. Halpern, *Physiol. Behav.*, 1973, **11**, 713–716.
- 9 J. E. Norton and P. J. Fryer, *J. Food Eng.*, 2012, **113**, 329–336.
- 10 T. S. Skelhon, P. K. A. Olsson, A. R. Morgan and S. A. F. Bon, *Food Funct.*, 2013, **4**, 1314–1321.
- 11 R. Armisén and F. Gaiatas, 4 - Agar, in *Handbook of Hydrocolloids*, ed. G. O. Phillips and P. A. Williams, Woodhead Publishing Limited, Cambridge, 2nd edn, 2009, ch. 4, pp. 82–107.
- 12 Y. Lee, S.-Y. Lee and J. D. Donovan, Chapter 28 - Stability Characterization and Sensory Testing in Food Products Containing Microencapsulants, in *Microencapsulation in the Food Industry*, ed. A. G. Gaonkar, N. Vasisht, A. R. Khare and R. Sobel, Academic Press, Cambridge, 2014, ch. 28, pp. 367–381.
- 13 M. Espinal-Ruiz, F. Parada-Alfonso, L.-P. Restrepo-Sanchez, C.-E. Narvaez-Cuenca and D. J. McClements, *Food Funct.*, 2014, **5**, 3083–3095.

- 14 M. E. Clegg and A. Shafat, *Eur. J. Nutr.*, 2014, **53**, 533–539.
- 15 B. J. Rolls, E. A. Bell and M. L. Thorwart, *Am. J. Clin. Nutr.* , 1999, **70**, 448–455.

8. Summary of the thesis

Hydrogel bead templating has been applied throughout this thesis¹ as a versatile and attractive method for preparation of hierarchically structured composites and porous materials. Cheap, non-toxic and food grade templates which can be applied to a multitude of different materials were used. It has demonstrated that this method offers a significant level of control over the final microstructure of the templated materials. The method involved mixing of an agar hydrogel bead slurry with a slurry of scaffolding material, followed by its subsequent setting and then drying of the composite. Upon drying, the water present in the hydrogel beads evaporates and leaves voids in its place. The size distribution of the hydrogel bead templates and the volume percentage of the hydrogel bead slurry used during composite preparation determines the size distribution of the pores and the overall porosity. Hydrogel bead slurries with different size distributions were used which can be mixed together in controlled volume ratios before the composite preparation which allows for control over the hierarchical porosity of the dried material. A complementary viscous trapping technique has been developed that involves utilising the viscosity of methylcellulose (MC) solution to suspend the particles of the scaffolding material in solution while it develops a sparser network.

Chapter 2 describes the materials and methods used for the preparation of hydrogel bead templates and outlines the protocols for preparation of porous and hierarchically porous gypsum composites. Furthermore, the viscous trapping technique using MC solution to prepare porous gypsum composites is introduced in this chapter. The preparation methods of different hydrogel-based composite materials have also been outlined. All the techniques used for characterisation and analysis of the porous and composite materials are also detailed in this chapter.

In Chapter 3 the preparation of porous and hierarchically porous gypsum composites using the hydrogel bead templating technique and the viscous trapping technique, or a combination of them to make hybrid porous materials has been successfully demonstrated. These methods allow for the preparation of porous gypsum composites with porosities up to 60%, with negligible volume reductions. Through the use of a radial heat flow setup, an investigation into how the porosity and microstructure of the composites affects their thermal conductivity and mechanical properties was

performed. The value of thermal conductivity for the gypsum control sample was $0.43 \text{ W m}^{-1} \text{ K}^{-1}$ which agreed with values in the literature. A linear relationship between thermal conductivity and the composite porosity was obtained which was found independent of the material's microstructure. At constant porosity, the thermal conductivities of the porous composites were not affected by the different pore sizes investigated. The mechanical properties of the porous gypsum composites were sensitive to the microstructure at a constant overall porosity. The porous gypsum composites produced using large hydrogel beads had approximately half the compressional strength and Young's modulus of those produced with small beads or MC solution. Investigation of the microstructure using SEM offered a possible explanation; the composites produced using large hydrogel beads left a shell of dried hydrogel residues in the pores. On these residues were gypsum needles and platelets that were separated from the continuous gypsum network and therefore would not be contributing to the mechanical properties. Finally, it was found that it is possible to produce materials with a controllable thermal conductivity by varying the porosity of the composites and then tune the mechanical properties by changing the pore size at a constant porosity.

In Chapter 4, the same methods for the preparation of porous and hierarchically porous gypsum composites as in Chapter 3 were utilised. However, in this chapter their acoustical properties have been investigated. A four-microphone impedance tube was employed to determine the sound insulation properties (sound transmission loss (STL)) of the composites with different porosities and microstructures. It was found that increasing porosity decreased the sound insulation properties of the material over most of the frequencies (i.e. higher porosity has less resistance to acoustic air flow). However, at 15% and 30% porosity induced by the viscous trapping technique with MC solution, the STL was higher at frequencies around 500 Hz which could be attractive for use in building materials, along with their light weight. It was also revealed that, at a constant porosity (40%), the porous composites produced with large hydrogel beads significantly outperformed the ones produced with small hydrogel beads at frequencies between 75–2000 Hz. The difference between the sound transmission losses of the two materials decreased with increasing frequency until the composite with smaller pores began to perform better at high frequencies (>2420 Hz). The increased performance of the composite with larger pores has been attributed to

the dried hydrogel residue that lines the inside of the pores as it has previously been shown that filler material that lines pores can significantly improve sound insulation properties.² Finally, a hierarchically porous gypsum composite (40% overall porosity) produced with a volume ratio of 1:1 large beads-to-small beads showed intermediate sound transmission loss which suggests there is scope for tuning the sound insulating properties of porous materials by controlling their microstructure.

The first novel example of the hydrogel-based composites are described in Chapter 5. Soap-hydrogel bead composites were prepared by mixing slurry of hydrogel beads with molten soap then allowing it to set. The effect of the hydrogel bead size and volume percentage of hydrogel beads incorporated within the soap matrix on the dissolution rate of the composite was investigated. It was found that it was possible to increase the dissolution rate by 2.5 times when incorporating 50% by volume slurry of hydrogel beads. Interestingly, it was found that the dissolution rate of the soap-hydrogel beads composite was independent of the size of the hydrogel beads used. The release rate of encapsulated species within the hydrogel beads could also be controlled using three different approaches: (i) decreasing the size of the hydrogel beads showed an increase in the release rate, (ii) similar effect was produced by decreasing the concentration of the gelling polymer. (iii) An alternative method was also developed by the co-encapsulation of an oppositely charged polyelectrolyte. This decreased the release rate of the active species and the effect was more significant at higher concentrations of polyelectrolyte. The mechanical properties of these composites were studied and it was found that the compressional strength decreased linearly with increasing volume percentage of hydrogel beads incorporated within the soap and was independent of the hydrogel bead size distribution. Furthermore, compression of the composites encouraged the syneresis of water which suggests that they could be used without running water. The Young's modulus showed a maximum when 5% or 7.5% by volume were mixed with the soap base. However, at higher volume percentages of beads, it decreased to values below that of soap alone. These composites have a reduced cost, could reduce pollution with surface active materials and require less raw materials which improves their sustainability. It can be envisaged that such soap-hydrogel composites could find a place within the hotel industry, where millions of partially used soap bars are discarded on a daily basis.

A binary hydrogel system of unusual properties which was developed and studied was discussed in Chapter 6. It consisted of the two non-ionic, food grade polysaccharides: agar and MC. It does not require salt for gelation and once gelation has occurred, it will not melt at temperatures above 100 °C. This two-component system had improved rheological properties over the temperature range 25–85 °C and showed a maximum storage modulus at 55 °C when the concentration of MC was 0.75% w/v or higher. This has been attributed to a sol-gel phase transition of the MC, evidence of which was seen in differential scanning calorimeter (DSC) measurements. However, addition of MC to agar showed an increase the storage modulus both below and above the gelling point of MC, suggesting a synergism between the two polymers. The binary system maintains its storage modulus at high temperatures (85 °C) whereas agar alone shows a large decrease in its storage modulus with an increase in temperature. It was found that it was possible to tune the rheological behaviour of the material by varying the ratio of agar:MC at a constant polymer concentration. Its stability to heat treatment was tested and it was found that upon heating to temperatures above 120 °C, the hydrogel structure was retained without melting. The microstructure of the mixed gels was revealed by flash-freezing and freeze-drying and visualised with scanning electron microscopy (SEM). It was found to consist of agar-rich and MC-rich regions with a more interconnected network than the individual components.³ The melt resistance of this two-component hydrogel, along with the fact that both components are food grade and do not require salt for gelation, suggests that they could find applications in the food industry for baking or for high temperature templating of a materials.

In Chapter 7, the application of the binary hydrogel system developed in Chapter 6 for food formulations was demonstrated.⁴ A slurry of such melt-resistant hydrogel beads of this composition was obtained and then incorporated within pancake batter at different volume percentages. The advantage of this formulation was that this batter can be cooked without melting its hydrogel bead content. This was then baked at high temperature (170 °C) to produce a pancake-hydrogel bead composite. It was found that it was possible to control the calorie content by varying the volume percentage of hydrogel beads incorporated within the pancake. From bomb calorimetry experiments, it was observed that upon incorporating 25% by volume of hydrogel beads into pancake batter, the calorie content of the cooked product was reduced by $23 \pm 3\%$.

Pores representing the hydrogel beads could be visualised with SEM after freeze-drying the composites, confirming that the gel beads retained their structure during preparation of the composites. This is a promising technique, as flavour enhancing or nutritionally beneficial ingredients could be encapsulated within the hydrogel beads. The method can be applied for the reduction in calorie content of a range of bakery products.

8.1. Future work

The research presented here details a hydrogel bead templating technique. It has been shown to control porosity, pore size, and ratio of large pores to small pores in a hierarchically porous material. It has only been applied to a small amount of different materials in this thesis, however it has potential for use in a multitude of other applications.

The research presented in Chapter 3 could be developed on by testing the thermal conductivity of other materials to investigate if the linear relationship between the reduction in thermal conductivity and volume percentage of hydrogel beads used to prepare the composite is applicable. The combination of hydrogel beads and other scaffolding materials can be further explored in terms of the development of better thermal insulation materials from sustainable resources.

The future work related to sound transmission loss of porous materials described in Chapter 4 would involve testing more hierarchically porous gypsum composites of different pore size distributions to see if it is possible to fine tune the sound insulation properties. Other work could involve investigation of the effect of the hydrogel residue. For example, variation of the concentration of agar would produce dried films with different mechanical properties and possibly obtain composite materials with different sound insulating properties.

The research on soap-hydrogel bead composites presented in Chapter 5 involves controlling the release rates of model active species encapsulated within these systems. It would be useful to see if the release rate of more widely used antimicrobials could be controlled in a similar fashion. Furthermore, investigation of the release rates

during a simulated hand-wash could be performed to see if the composites would perform similarly in a more relevant situation.

The binary hydrogel system consisting of agar and MC described in Chapter 6 should be further explored. A full DSC investigation should be performed which would require a DSC with a micro-sensor. Furthermore, the interconnected regions seen during SEM imaging could be studied by combining SEM with Raman spectroscopy. This could give some insight into the material's melt resistance. The microstructure of the melt-resistant hydrogels at different MC:agar compositions should be explored in more details to investigate the transition from non-crystalline to semi-crystalline structures.

The future work related to the pancake-hydrogel composites in Chapter 7 would involve encapsulation of nutritionally beneficial or flavour enhancing ingredients into the hydrogel beads before preparation of the pancake-hydrogel composites. Furthermore, these hydrogel beads could be applied to other bakery products such as biscuits, muffins, waffles and breakfast bars.

8.2. References

- 1 M. Rutkevičius, S. K. Munusami, Z. Watson, A. D. Field, M. Salt, S. D. Stoyanov, J. Petkov, G. H. Mehl and V. N. Paunov, *Mater. Res. Bull.*, 2012, **47**, 980–986.
- 2 L. Xu, T. Han, J. Li, Y. Xiong and S. Guo, *Compos. Sci. Technol.*, 2017, **145**, 78–88.
- 3 B. R. Thompson, T. S. Horozov, S. D. Stoyanov, V. N. Paunov, *RSC Adv.*, 2017, **7**, 45535-45544.
- 4 B. R. Thompson, T. S. Horozov, S. D. Stoyanov, V. N. Paunov, *Food. Funct.*, 2017, **8**, 2967-2973.